Evaluation and Retrofit of Non-Capacity Designed Braced Frames

Daniel A Sloat.

A thesis

submitted in partial fulfillment of the

requirements for the degree of

Master of Science in Civil Engineering

University of Washington

2014

Committee:

Charles W. Roeder

Dawn E. Lehman

Jeffrey W. Berman

Program Authorized to Offer Degree:

Civil and Environmental Engineering

University of Washington

Abstract

Evaluation and Retrofit of Non-Capacity Designed Braced Frames

Daniel A. Sloat

Chair of Supervisory Committee:
Dr. Charles W. Roeder.
Department of Civil and Environmental Engineering

Concentrically braced frames (CBFs) are lateral-load resisting systems that consist of diagonal braces which are framed concentrically with the intersection of either beam-to-column connections or opposing braces. Since the early 1990s, seismic design of special concentrically braced frames (SCBFs) has placed stringent design and detailing requirements on the braces, gusset plates and related connections. By contrast, CBFs designed before the early 1990's were designed to much less restrictive specifications than SCBFs. There are few tests of these older CBFs, resulting in uncertainty about their performance and about viable retrofit options. Older CBFs are common in current infrastructure, so the uncertainty in their performance poses a substantial risk. This research project seeks to address this uncertainty. A series of tests have been undertaken to investigate the response of both existing and retrofitted older CBFs. The experimental data from these tests is used to validate evaluation approaches for older CBFs and can be used for future development of numerical models. The retrofitted systems demonstrate practical methods to increase system ductility and improve seismic performance by mitigating damage. Finally, tools to aid in the seismic evaluation and retrofit of CBFs per ASCE 41 are proposed.

Acknowledgement

I would like to thank all of the individuals who have helped to make this possible. My three advisors, Charles Roeder, Dawn Lehman, and Jeff Berman, have provided not only funding for me to pursue this research, but also the guidance and resources necessary to complete the work presented here. Vince Chaijaroen, the lab technician, provided crucial assistance in assembling the test setup and data acquisition systems. The various lab assistants who worked on the frames tested were essential.

Thank you also to Molly Johnson, my partner in the lab, who provided much-needed assistance throughout the fabrication, analysis, and writing processes. Andy Sen and Ryan Ballard, the other graduate students on our project, have also been a great help.

I would also like to thank my wife for being understanding and supportive of the challenges associated with this project. My parents deserve great thanks for putting me in a position to achieve my academic goals as well. Finally, a thank you to my friends and family not mentioned here, for providing support and guidance.

Table of Contents

Table of Figures

Table of Tables

Chapter 1: Introduction

1.1 Background

Braced frames are a common lateral load resisting systems in structures. The lateral load is primarily resisted by diagonal braces, such as those shown in Figure 1.1. In seismic design, the brace also acts as the energy dissipating element in the system, and it typically undergoes substantial inelastic deformations due to tensile yielding and compressive buckling.

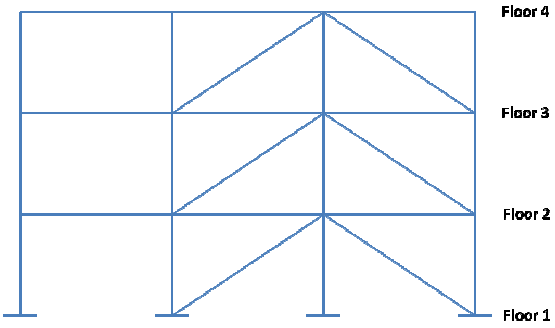

Figure 1.1 Example of a Structure Containing Braced Frames

These systems have been widely used in a variety of building applications for many decades. Their high elastic stiffness and relatively low cost make them a valuable structural system. When properly designed, braced frames can also exhibit substantial ductility. Modern braced frames designed for applications in regions of moderate to high seismicity are typically Special Concentrically Braced Frames (SCBFs). Special detailing requirements for connections, as well as limits on brace and framing member geometry, have been created based on prior braced frame research to ensure ductile braced frame performance. For example, the connection components must be designed to resist the expected brace capacity, and the brace must meet local and global slenderness limits. These requirements have largely been developed between 1988 and the present.

Prior to 1988, braced frame design requirements were substantially less restrictive, as shown in Table 1.1. All members and connections were designed for the reduced seismic loads, rather than the expected brace capacity. As a result, many existing structures designed to these requirements may not exhibit desirable behavior in a seismic event. These systems are more vulnerable to premature brace fracture and connection fracture, among other shortcomings. Existing braced frame structures that do not meet modern SCBF criteria shall be referred to herein as Non-Seismic Concentrically Braced Frames (NCBFs). NCBFs pose a significant

concern in current infrastructure, as they are both prevalent and susceptible to substantial damage or collapse.

Table 1.1 Comparison of Modern and Older Braced Frame Design

Component	**Pre-1988 Braced Frames**	**Modern SCBFs**
Brace Slenderness	No Limit	KL/r < 100
Brace Compactness	No Limit	Seismically Compact
Framing Member Compactness	No Limit	Seismically Compact
Brace End Rotation Clearance	No Limit	Required
Brace Connection Design	Design for Seismic Loads	Design for Expected Brace Capacity
Framing Member Design	Design for Seismic Loads	Design for Expected Brace Capacity

Compared to the extensive research conducted on the performance of modern SCBF systems, comparatively little information is currently available on the expected performance of NCBFs. Figure 1.2 and Figure 1.3 show examples of an SCBF and NCBF connection detail, respectively. Both of these connection details were tested in the UW structures lab. Their performance is shown in Figure 1.4 and Figure 1.5. These plots demonstrate the substantial difference in performance between NCBF and SCBF systems that leads to concern with NCBF seismic performance. Despite having the same design lateral load, the NCBF system exhibited a much lower lateral load resistance, and experienced connection fracture at a low drift level.

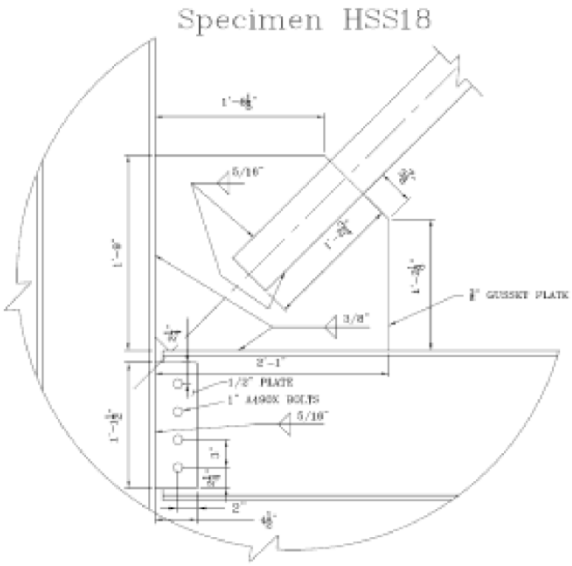

Figure 1.2 SCBF Connection Detail (Powell 2010)

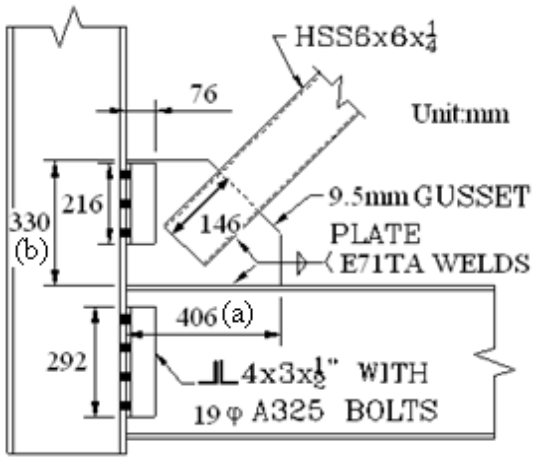

Figure 1.3 NCBF Connection Detail (Hsiao 2012)

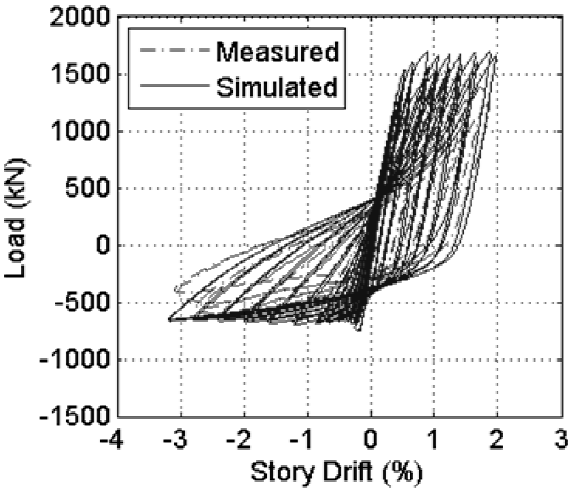

Figure 1.4 SCBF Load-Drift Response

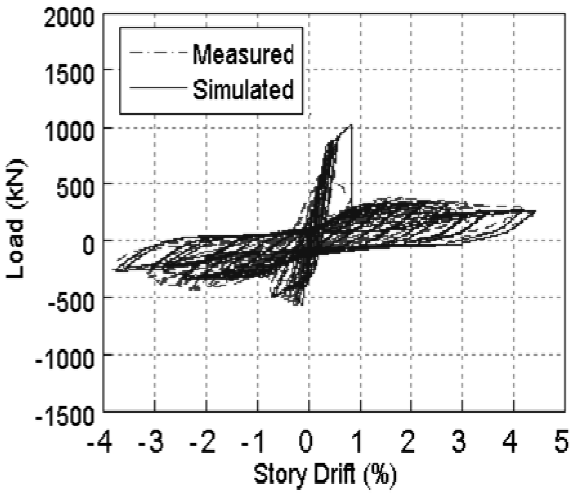

Figure 1.5 NCBF Load-Drift Response

1.2 Project Objectives

The research presented in this thesis is a component of a larger research effort at UW and partner universities to evaluate NCBFs. This research includes additional testing at the University of Washington (Johnson, 2014), two-story braced frame testing at NCREE Taiwan (Sen, 2014), and two-story brace frame testing at UC Berkeley, as well as extensive analytical modeling. The primary objectives of this research are:

- Evaluate the seismic response of NCBF structures at various performance levels
- Establish strength and deformation limits for NCBFs based on failure modes
- Investigate cost-effective methods for seismic rehabilitation of NCBFs
- Establish engineering models for seismic evaluation and retrofit of NCBFs

1.3 Document Overview

The research presented in this thesis provides a starting point for attaining the project objectives stated above. The specific objectives for the research presented in this thesis are:

- Determine typical characteristics of existing NCBF systems and identify vulnerabilities
- Evaluate the performance of common NCBF systems using large-scale experiments
- Evaluate the effectiveness of various retrofits at improving the performance of NCBF systems using large-scale experiments
- Develop recommendations for evaluation and retrofit of NCBFs based on the experimental results

The following chapters of this thesis describe how these objectives were achieved. An infrastructure review was conducted, and six large-scale specimens were tested at UW in 2013-2014. Chapter 2 provides a review of previous work on SCBFs and NCBFs. It also describes the procedure and results of an infrastructure review, which was conducted on existing NCBF structures to evaluate the typical characteristics of NCBFs, as well as the range of expected deficiencies in these systems. Chapter 3 describes the motivation and design basis for each of the specimens tested. Chapter 4 illustrates the experimental setup used at UW, as well as the instrumentation and methodology used to gather information during the tests. Chapter 5 describes the behavior of each specimen and provides nomenclature for discussing their performance. Chapter 6 provides an analysis of the data collected for each specimen with discussion of the impact that this data has on understanding the system performance. Chapter 7 outlines a framework for evaluation and retrofit that can be used to categorize NCBF and retrofit behavior. Chapter 8 provides conclusions based on the previous chapters and makes recommendations for future work. Appendix A provides additional information on the buildings and connections from the infrastructure review, as well as the results for each of the frames analyzed . Appendix B provides instrumentation for each of the specimens. Appendix C describes the experimental setup in detail. Appendix D provides additional supporting plots for data analysis.

Chapter 2: Literature Review & Existing Buildings Survey

2.1 Introduction

The behavior of SCBF systems is well understood as a result of extensive research conducted over previous decades. Section 2.2 describes some of the research that has led to modern SCBF design, the criteria that define desirable SCBF performance, and the direction of future SCBF improvement.

By comparison, the behavior of NCBF systems is poorly understood. Section 2.3 describes the limited research that has been conducted on NCBF systems. Because there is insufficient knowledge not only of how NCBF systems perform, but also of the types of systems and deficiencies that exist in NCBF systems, an infrastructure review was conducted to elucidate these concepts. It is described in Sections 2.3-2.7. The results of this study informed the design of a series of NCBF test specimens, which are described in Chapter 3.

2.2 Evolution of SCBF Design

As discussed in the introduction, modern CBFs designed for regions of moderate and high seismicity are typically designed as SCBFs. SCBF design contrasts significantly with braced frame design for seismic loads prior to 1988. The design of braced frames prior to 1988 did not have in place many of the modern design requirements that are intended to ensure desirable seismic performance of the system. Table 1.1 contrasts some characteristics of modern and older braced frame design. Restrictions on brace slenderness, brace and framing member compactness, and connection strength and geometry have been added since 1988 with the intention of improving system performance. Some of the research leading to these changes will be discussed in the remainder of this section. A more detailed discussion of the history of braced frame design can be found in Powell (2010).

The first objective of modern SCBF design is to ensure structural safety with good inelastic deformation capacity, with the brace strength as the governing limit state for the system. The connections and framing components are designed meet or exceed the demands resulting from the expected capacity of the brace in both tension and compression. The capacity based design approach is to ensure ductile behavior in the system after yielding by concentrating damage in the brace, which behaves in a ductile manner and whose behavior is well understood.

In order to ensure the connections are capable of developing the brace capacity, a number of design checks have been developed for connection components based on previous research. A summary of common modern design checks is given in Table 2.1, and definitions of the variables used in this table are given in

Table 2.2

Table 2.1 Common SCBF Limit States (AISC 2010)

Limit State	**Equation**	**Resistance Factor (ϕ)**
Net Section Fracture	$P_n = \phi R_t F_u A_e$	0.75
Brace Block Shear	$P_n = \phi(U_{bs} A_{nt} R_t F_u + 0.6\min(A_{nv} R_t F_u, A_{gv} R_y F_y))$	0.75
Whitmore Yielding	$P_n = \phi R_y F_y B_w t_p$	0.9
Whitmore Fracture	$P_n = \phi R_t F_u B_w t_p$	0.75
Gusset Plate Buckling	$P_n = \phi B_w t_p F_{cr}$	0.9
Weld Fracture	$P_n = \phi 0.6 F_{EXX} N_w L_c (0.707 W_2)(1+0.5\sin(\theta)^{1.5})$	0.75
Weld Base Metal Shear	$P_n = \phi 0.6 F_y t_p L_c$	0.75
Bolt Bearing	$P_n = \phi F_{up} t_p \min(1.5 L_{cb}, 3 d_b)$	0.9
Bolt Shear	$P_n = \phi F_{nv} A_b$	0.75

Table 2.2 Definitions of Variables for Limit State Equations

Variable	**Description**
R_t	Ratio of Expected to Actual Ultimate Tensile Strength
F_u	Ultimate Tensile Strength
A_e	Effective Net Area
U_{BS}	Loading Uniformity Factor
A_{nt}	Net Area in Tension
A_{nv}	Net Area in Shear
A_{gv}	Gross Area in Shear
R_y	Ratio of Expected to Actual Yield Strength
F_y	Design Yield Strength
B_w	Whitmore Width
t_p	Plate Thickness
F_{cr}	Critical Buckling Stress
F_{EXX}	Design Electrode Strength
N_w	Number of Welds
L_c	Connection Length
W_2	Weld Throat Size
L_{cb}	Clear Distance Between Bolt Hole and Nearest Plate Edge
d_b	Bolt Diameter
A_b	Bolt Cross-Sectional Area
F_{nv}	Bolt Shear Capacity

One of the first developments in braced frame connection analysis was the Whitmore section, which is described in detail in Section 2.5.5. It gives an estimate of the area of the gusset plate that is effective in resisting the brace force in tension (Whitmore 1952). Insufficient strength in the Whitmore section could cause excessive yielding in the gusset plate, potentially leading to tearing or fracture. In compression, the Whitmore section serves as a basis for evaluating the gusset plate buckling capacity. Methods outlined by Thornton (1984) developed checks for gusset plate buckling capacity, which are detailed in Section 2.5.6.

Astaneh, et al. (1986) further elucidated important limit states for braced frame connections with a series of double-angle brace buckling tests. Their test setup is shown in Figure 2.1. The braces were connected to gusset plates, which were fastened to beams only. The beam-to-column connections were idealized pins.

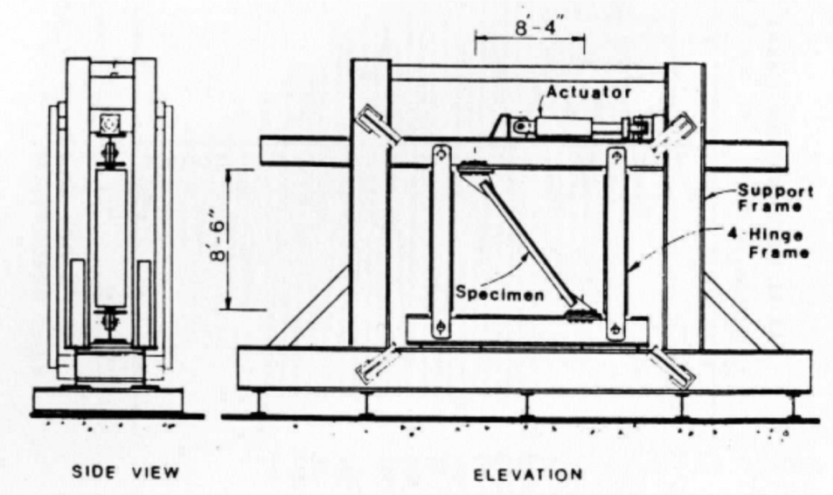

Figure 2.1 Typical Experimental Setup (Astaneh et al 1986)

These tests demonstrated undesirable connection failure modes and equations and methods to prevent them were derived. Several of the specimens suffered block shear failures of the braces, resulting in non-ductile system performance. Along with results from tests by Bjorhovde and Chakrabarti (1985), the research by Ateaneh et al (1986) improved understanding of block shear for braces. Several specimens in their program suffered from tearing of the gusset plates. They identified that a folding region in the plate was necessary to allow the gusset plate to bend to accommodate the brace end rotation due to out of plane buckling. This resulted in the brace end clearance recommendation for SCBF systems in the current AISC Seismic Provisions (AISC 2010b), referred to as The Provisions herein. The frequent connection failures in specimens tested during this region brought attention to the inadequacy of designing the braced frame connections for the seismic forces. In order to ensure that the connections were capable of developing the

brace capacity, the capacity based design approach was adopted. This approach was first introduced in the 1991 UBC, and was further developed in the 1997 AISC Seismic Provisions.

In addition to designing the connections for the strength of the brace, modern design imposes restrictions on the design of the brace itself to help ensure ductile performance. Numerous studies, including Liu and Goel (1988), Shaback and Brown (2003), Tremblay (2002), and Popov, Zayas, and Mahin (1985) have addressed the factors contributing to brace performance. All three studies concluded that brace fracture life was highly dependent on the width-to-thickness ratio of the brace walls. HSS braces with width-to-thickness ratios greater than 25 tend to form plastic hinges almost immediately following global buckling of the brace (Liu and Goel 1988). HSS braces with width-to-thickness ratios less than 12 tend to be able to undergo numerous large deformation cycles after buckling before fracture occurs (Shaback and Brown 2003). These results have led to the seismic compactness requirements for braces used in modern design (AISC 2010b). Additionally, braces with lower slenderness ratios typically have improved fracture life, as demonstrated by Tremblay (2002).

Recent research has suggested additional criteria that could increase the ductility of SCBF systems. Roeder et al (2011) suggested a Balanced Design Procedure, which revises some of the current standards on SCBF design with the intent of improving performance. These recommendations resulted from many tests conducted on single-story and multi-story braced frame systems and significant numerical modeling. The single story test setup, shown in Figure 2.2, is the same experimental setup used for the tests presented in the body of this thesis and is described in more detail in Chapter 4. It was developed by Johnson (2005) and modified by Powell (2010).

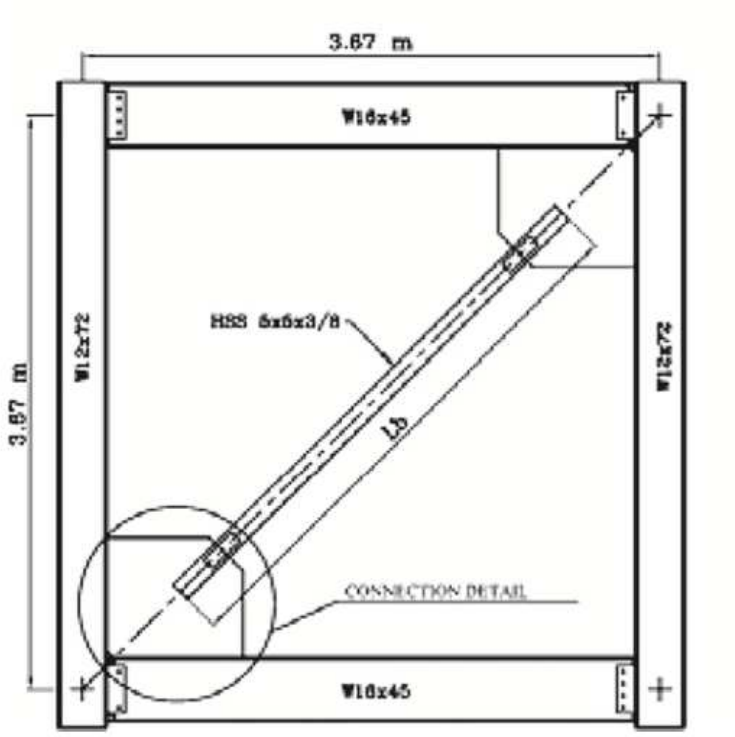

Figure 2.2 Single Story Test Setup (Roeder et al 2011)

The balanced design procedure recommends a more economical elliptical clearance model instead of the $2t_p$ gusset plate clearance requirement, as shown in Figure 2.3. Additionally, the procedure provides balance factors, which replace the resistance factors typically applied to connection limit states. These balance factors are intended to maximize system yielding, which leads to more ductile behavior, while preventing undesirable failure modes. Finally, the method revises the procedure used for design of gusset plate welds, recommending they be sized to develop the expected tensile capacity of the gusset plate rather than the force delivered by the expected brace capacity. This is intended to prevent undesirable weld tearing and fracture, as the gusset plate yields when accommodating the brace out-of-plane deformation.

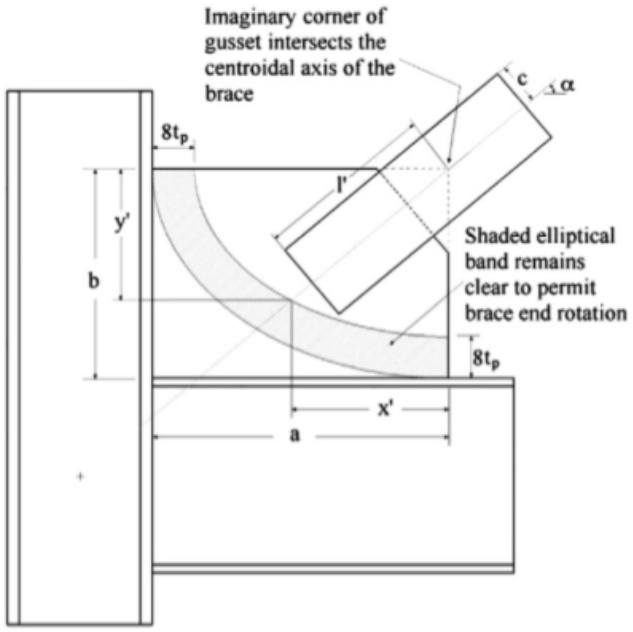

Figure 2.3 Brace End Elliptical Clearance (Roeder et al 2011)

Example connection details for a typical SCBF and a balanced design procedure SCBF are given in Figure 2.4 and Figure 2.5, respectively. These specimens were tested in previous research at UW by Powell (2010) and Johnson (2005). Both frames exhibited desirable seismic performance, including retention of lateral load capacity after brace buckling, extensive deformations after yielding, and brace fracture as the controlling limit state, as shown in Figure 2.6 and Figure 2.7. The load-drift histories for the specimens are given in Figure 2.8 and Figure 2.9.

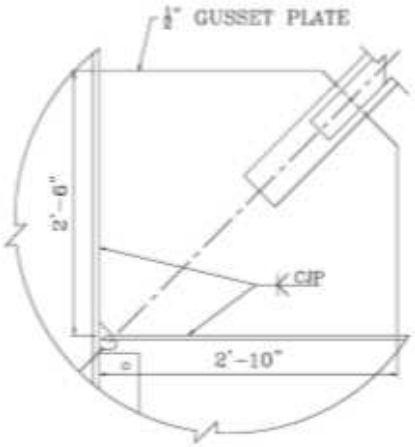

Figure 2.4 SCBF Connection Detail (Powell 2010)

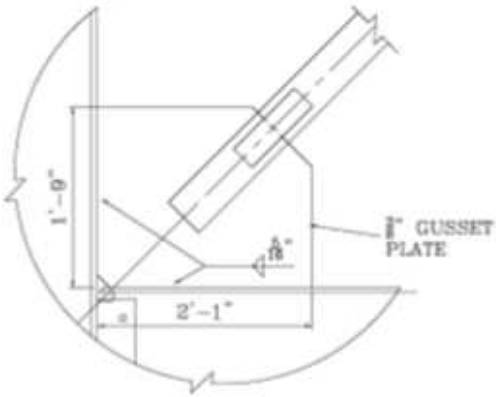

Figure 2.5 BDP SCBF Load-Drift Response (Johnson 2005)

Figure 2.6 HSS18 Brace Cupping (Powell 2010)

Figure 2.7 HSS18 Brace Fracture (Powell 2010)

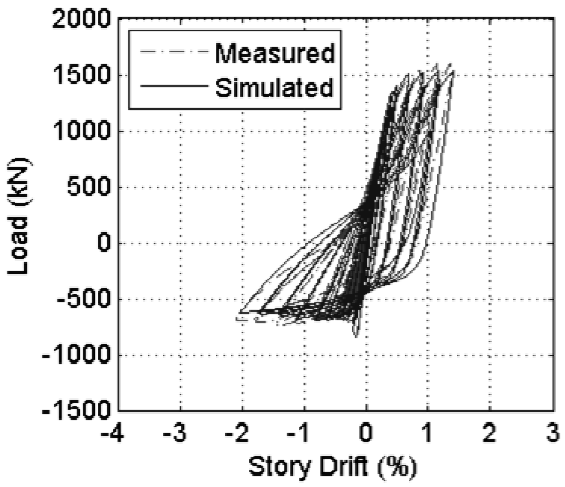

Figure 2.8 SCBF Load-Drift Response (Powell 2010)

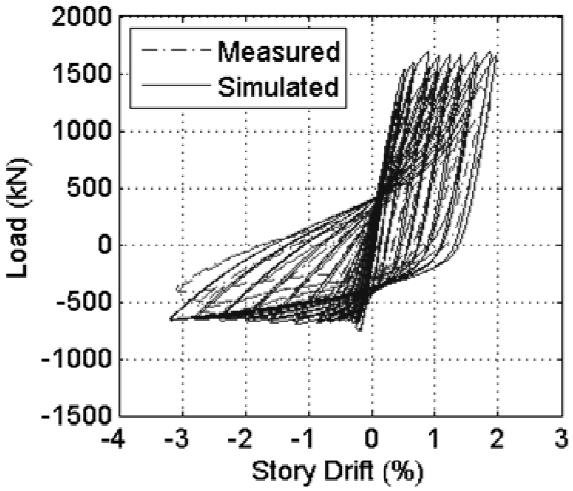

Figure 2.9 BDP SCBF Load-Drift Response (Johnson 2005)

2.3 Motivation for Infrastructure Review

Although a wealth of information is now available on the performance of SCBF systems, almost no system level experimental data exists for NCBF systems. A single pilot test was conducted at UW to evaluate the performance of a typical NCBF from the 1980s (Hsiao et al, 2012). The connection detail tested is shown in Figure 2.10, and the experimental setup is shown in Figure 2.2.. A non-compact, rectangular HSS brace was welded to a gusset plate, which was welded to the beam flange. The beam web and gusset plate were attached to the column flange via bolted double-angles. The connection met 1980s design requirements, but not modern design standards. It suffered brace-gusset weld fracture at less than 1% drift, followed by a series of other connection failures. This specimen demonstrated the severity of deficiency that can be found in NCBF systems.

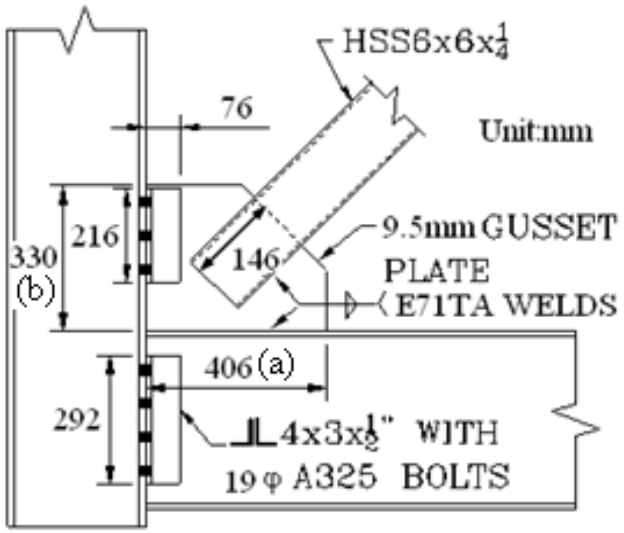

Figure 2.10 NCBF Connection Detail (Hsiao et al 2012)

Hsiao et al (2012) also conducted numerical modeling in OpenSEES to predict the performance of both NCBF and SCBF systems. This model utilized a force-based fracture model for the NCBF connection to predict the brittle connection failure. The experimental and analytical results for an SCBF specimen are shown in Figure 2.11, and the NCBF specimen is shown in Figure 2.12. Despite being designed for the same lateral load as the SCBF specimen, the NCBF specimen was able to resist much smaller loads due to connection failure. The NCBF specimen also achieved a much smaller drift range prior to fracture. The residual strength after connection fracture shown for the NCBF was due to residual moment frame action.

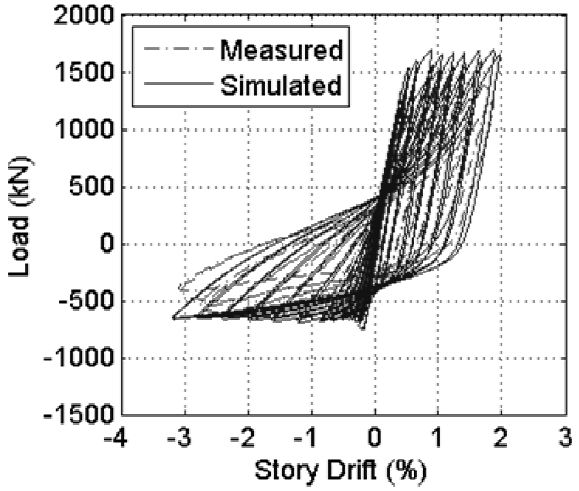

Figure 2.11 SCBF Load-Drift Response

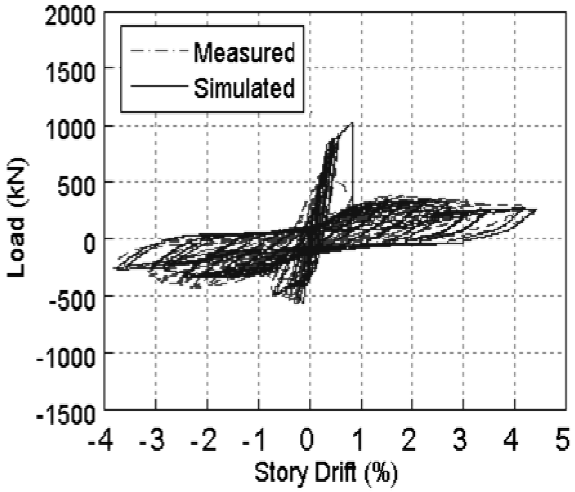

Figure 2.12 NCBF Load-Drift Response

The analytical model was applied to a variety of multi-story building models using various bracing configurations. These structures were subjected to ground motions which were scaled to the 2% in 50 year and 10% in 50 year design spectra used in US practice. The results of this analysis are summarized in Figure 2.13 and Figure 2.14. The NCBF model suffered brace or connection fracture in all cases in the 10/50 and 2/50 events, while the SCBF systems suffered brace or connection fracture only occasionally in the 2/50 event and not at all in the 10/50 event. The NCBF system also had a higher risk of collapse at both hazard levels. These results emphasize the vulnerability of NCBF systems to damage in small seismic events and to collapse in large seismic events.

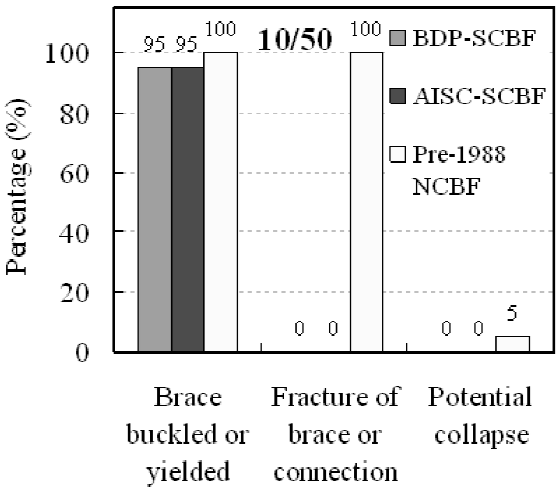

Figure 2.13 Braced Frame Performance in 10/50 Event

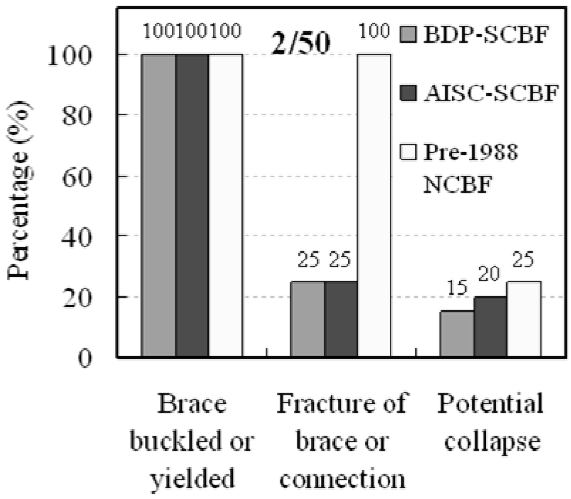

Figure 2.14 Braced Frame Performance in 2/50 Event

Structures containing NCBF systems may be vulnerable to damage or collapse because of their shortcomings relative to modern frames, but the extent of this vulnerability is relatively unknown due in part to the variability in NCBF configurations and details. A survey of existing structures containing NCBFs was conducted to:

- Evaluate the compliance of NCBFs against modern SCBF design criteria
- Determine the common configurations for NCBF connections and systems
- Provide a basis for a series of experiments on single-story and multi-story NCBFs

2.4 Infrastructure Review

Thirteen frames from twelve buildings from regions of high seismicity were analyzed. The drawings for these buildings were acquired from design firms that designed, evaluated, or retrofitted them. Both the names of the providing firms and the names of the original design firms remain anonymous throughout this document. Each building was given an alias that incorporated the design year, the height, and the location. The frame used within that building was also given an alias that incorporated its location on the drawings, as shown in Table 2.3 for building 83CA3A.

Table 2.3 NCBF Building and Frame Naming Convention

Building Information					Frame Information					
Year	State	Stories	Extra Term For Similar Structures	Separator	Gridline in Which the Frame Lays	Separator	First Perpendicular Gridline	Second Perpendicular Gridline	Separator	Floor of Frame
83	CA	3	A	--	P	-	14	15	-	3

Table 2.5 gives a summary of the characteristics of each of the buildings surveyed. These characteristics will be discussed in detail in the remainder of this section.

Table 2.4 NCBF Building and Frame Naming Convention

Building	Date	State	Type	Floors	Braces	Configurations	Connection Types
83CA3A	Oct-83	CA	Corporate HQ	3	HSS, W	Single Diagonal, Chevron	Bolted Shear Tab
82TN4A	Nov-82	TN	Corporate HQ	3,5	HSS, Pipe	Single Diagonal, Chevron	Shared Gusset
88CA3A	Jan-88	CA	Research	2,3	HSS, Pipe	Single Diagonal, Chevron	Shared Gusset
80CA4A	Sep-80	CA	Office	4	HSS, W	Chevron, Single Diagonal	Beam Only
80WA8A	Jun-80	WA	Hospital	8	Angles	X-Bracing, Single Diagonal	Fully Welded, Bolted Shear Tab, Bolted End Plate
86WA3A	Apr-86	WA	Hospital	3	HSS	Chevron, Single Diagonal	Welded Shear Tab
88UT1A	Oct-88	UT	Retail	1	Angles	X-Bracing	Bolted End Plate
83CA2A	May-83	CA	Office	2	HSS	Chevron	Fully Welded
74CA6A	Jul-74	CA	Hospital	6	W	X-Bracing, Single Diagonal	Double Gusset Plate
82OR9A	Jun-82	OR	Hospital	9	W	Single Diagonal, Multi-Story X	Double Gusset Plate
92WA2A	Feb-92	WA	School	2,3	HSS	Chevron	Welded Shear Tab
86CA4A	Aug-86	CA	Office	4	HSS	Chevron	Bolted Double Angle

The geographic distribution of buildings is shown in Figure 2.15. Building heights range from one to nine stories, with most of the buildings in the two to four story range, as shown in Figure 2.16. This is believed to be representative of the types of buildings (low to mid rise) for which concentrically braced frames were typically used at the time. A variety of building functions were included in the set, with office buildings and medical facilities being most prominent, as shown in Figure 2.17. This variety suggests that CBFs were popular in a wide range of building applications. The majority of the structures analyzed are from the 1980's, which may be indicative of the higher popularity of CBFs in the 1980's than in previous decades, though the high availability of newer drawings in comparison to older ones is also a likely contributing factor. Building ages are shown in Figure 2.18. Care was taken to acquire drawings for buildings designed by a variety of structural engineering firms in order to avoid biasing results toward the practices of a particular designer. Figure 2.19 shows the distribution of structures by designer. The names of the design firms have been replaced with numbers to preserve their anonymity.

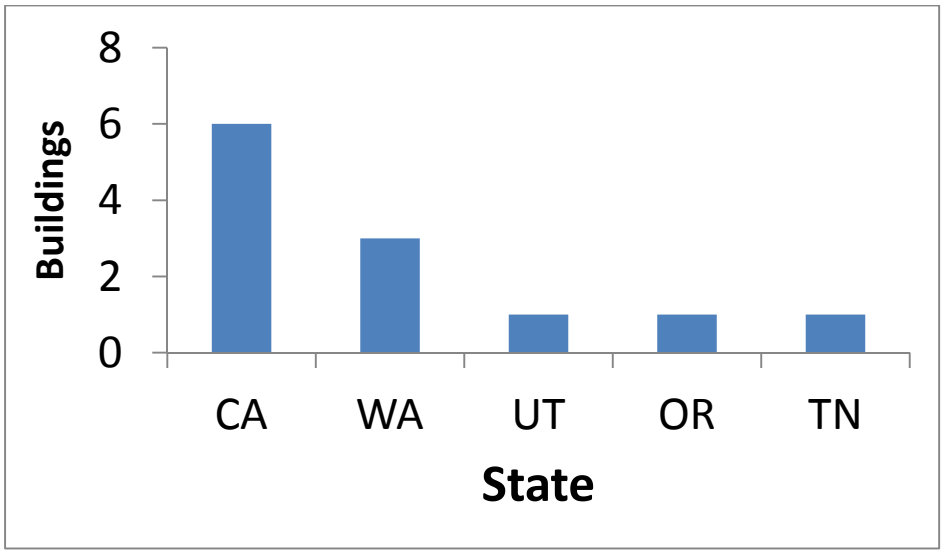

Figure 2.15 Suveyed Buildings by State

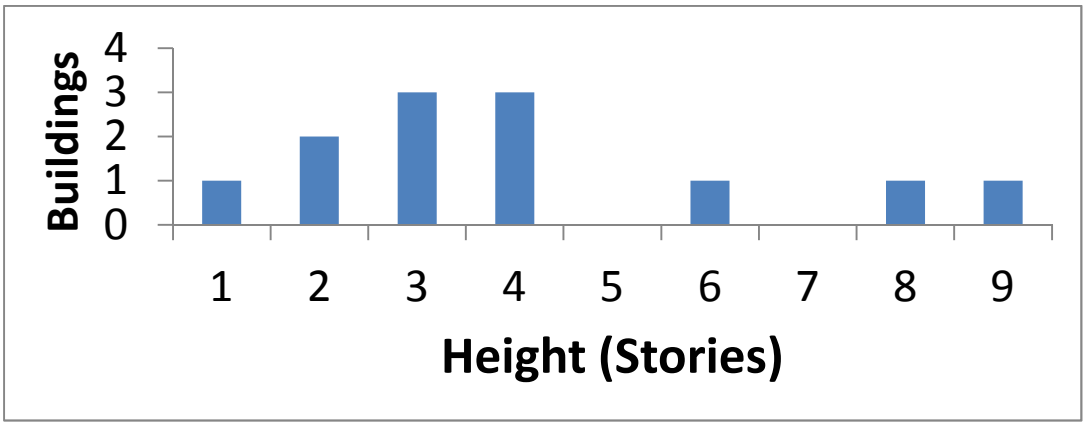

Figure 2.16 Surveyed Buildings by Height

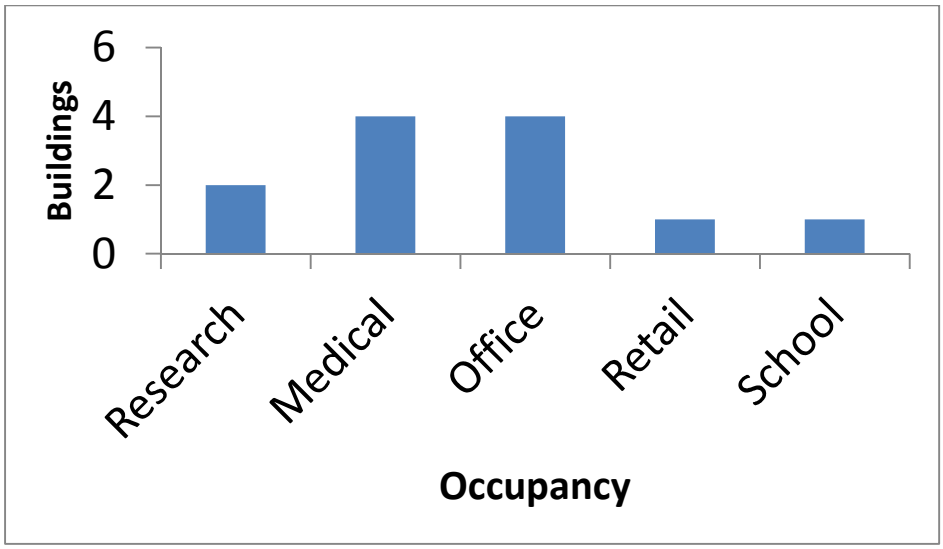

Figure 2.17 Surveyed Buildings by Occupancy Type

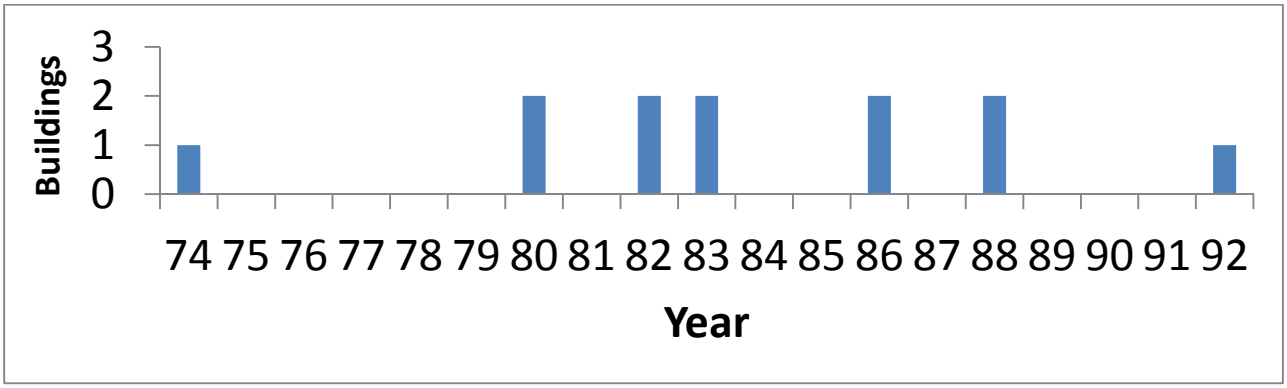

Figure 2.18 Surveyed Buildings by Construction Year

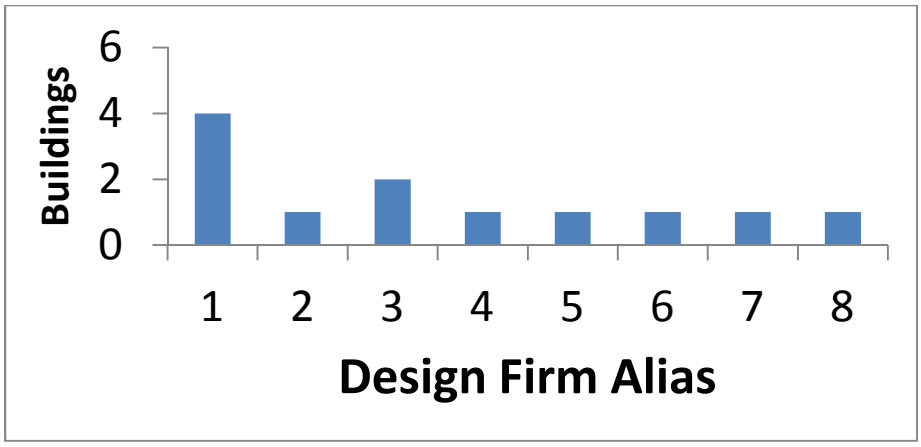

Figure 2.19 Surveyed Buildings by Design Firm

The infrastructure review also revealed several trends in design, displayed in Figure 2.20 and Figure 2.21. It is important to note than many buildings used multiple types of braces and bracing configurations, so the total percentages shown add to more than 100%. By far the most common type of brace was square HSS, which were found in over 70% of buildings. Wide flange sections were the next most common, and some pipe and angle braces were also observed. The most common brace configuration was chevrons, which were present in 70% of buildings. All of the buildings using chevrons were less than five stories tall. Single diagonal braces, as shown in Figure 1.1, were present in half of the analyzed buildings. This was the predominant system in taller buildings. X-bracing was less common, though it was also more popular in taller structures. An example of X-bracing can be found on the first story of the frame in Figure 2.22. About half of the buildings had some type of vertical discontinuity. Typically, these were areas where braced frames were not stacked vertically, but were diagonally adjacent, as shown in Figure 2.22. These types of configurations raise additional concerns about their ability to transfer seismic forces to adjacent bays.

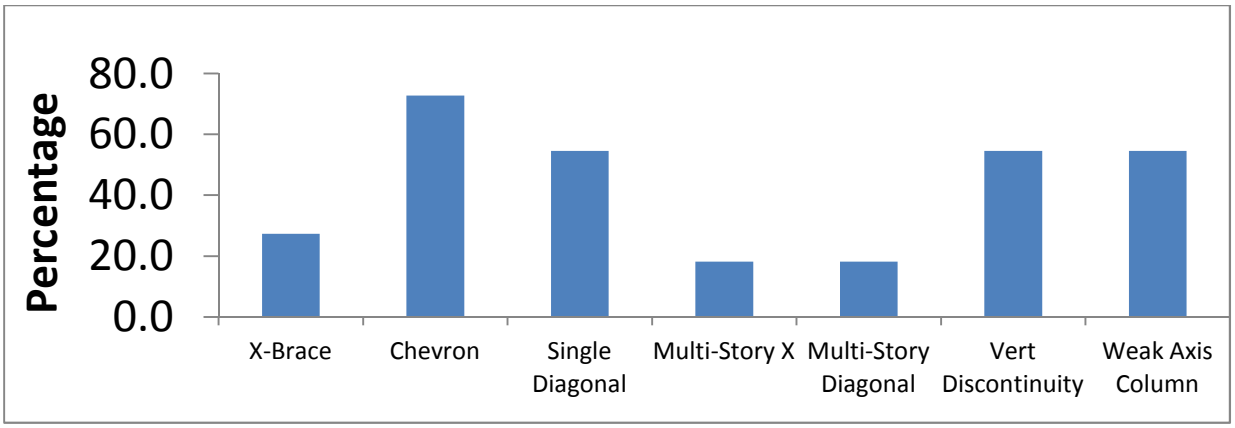

Figure 2.20 Brace Configurations in Surveyed Buildings

\

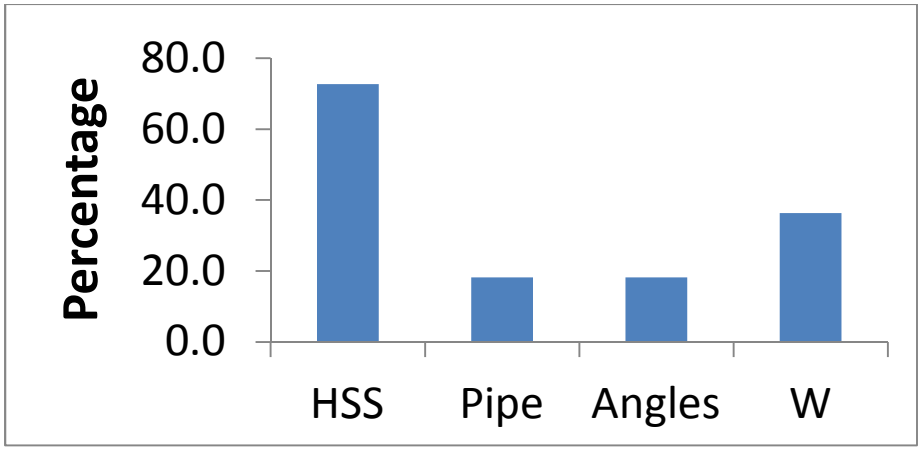

Figure 2.21 Brace Types in Surveyed Buildings

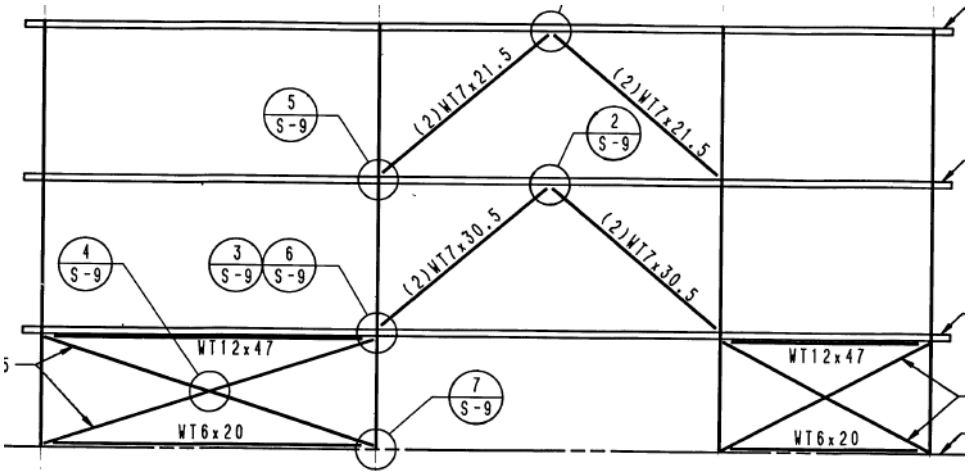

Figure 2.22 Example of Vertical Discontinuity from Building Survey

Brace to gusset plate connections were reasonably uniform between buildings in the infrastructure review. HSS and pipe braces were slotted and fillet welded to the gusset plate in all instances, as seen in

Figure 2.23. Net section reinforcement was not provided on at the net section for any of the braces. This is significant because brace net section fracture, which cover plates are designed to prevent, is a non-ductile and undesirable failure mode in braced frames. Angle brace sections were all bolted via single lines of bolts to the gusset plate, as seen in

Figure 2.24. The most common gusset plate to beam connection was fillet or complete joint penetration welds between the gusset plate and the beam flange, as seen in

Figure 2.23. In some instances, the beam flange was coped on one side, and the gusset plate was bolted to the beam web, as shown in Figure 2.25.

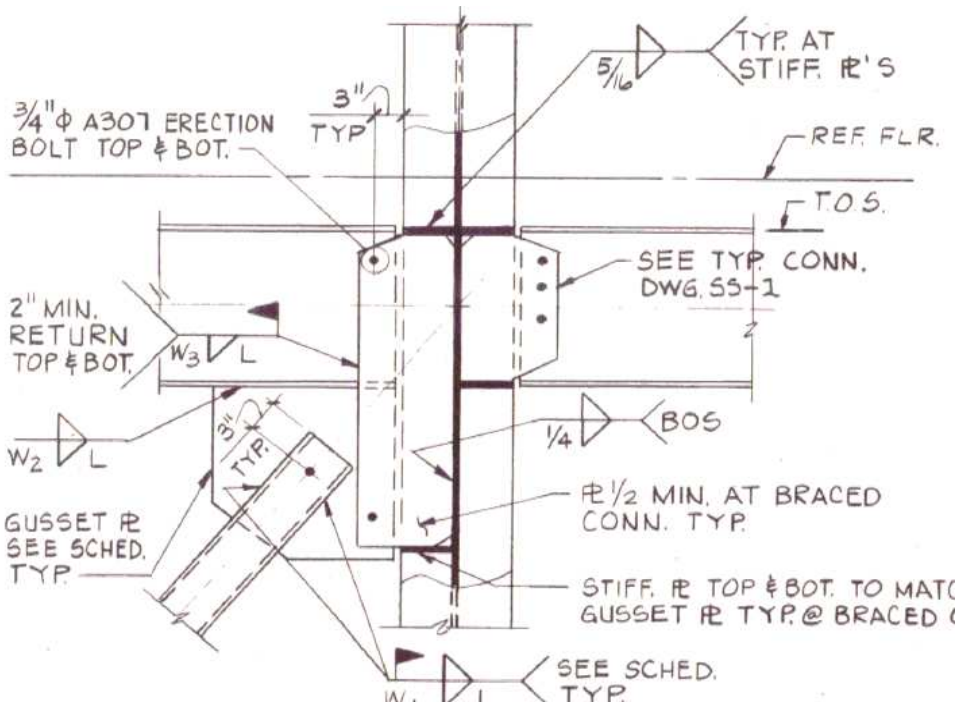

Figure 2.23 NCBF Detail - Welded Shear Tab

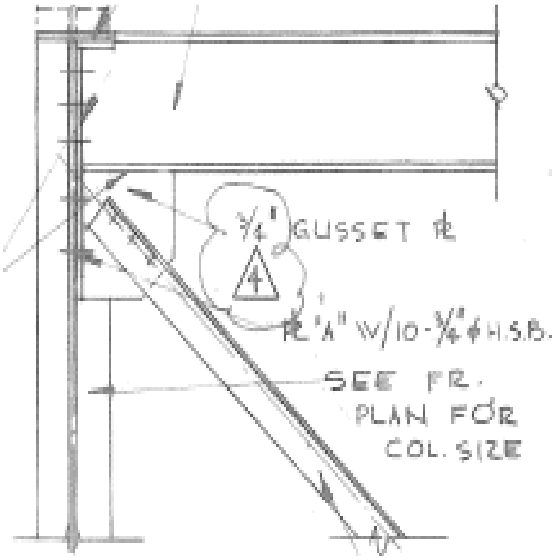

Figure 2.24 NCBF Detail - Bolted End Plate

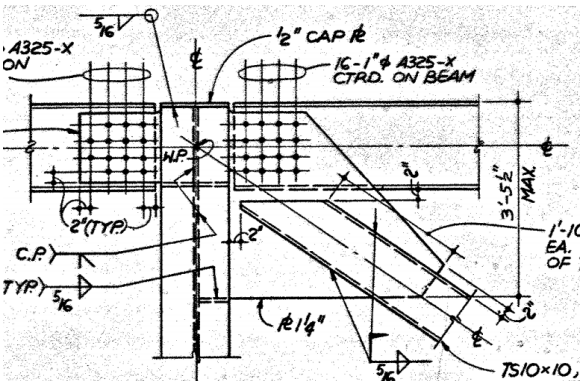

Figure 2.25 NCBF Detail - Shared Gusset Plate

Many gusset plates were welded directly to either the column flange or web. Others were bolted or welded to a shear tab, which was then welded to the column web, as in

Figure 2.23. Most of the shear tabs were also bolted or welded to the beam and served as the beam to column connection as well. Some gussets plates were welded to end plates, which were either bolted or welded to the column flange, as shown in

Figure 2.24. As with the shear tabs, these plates typically also served as the beam to column connection. In cases where the gusset plate and beam were not connected to the column by a shared shear tab or plate, they were typically welded directly to the column. Materials were consistent for most of the buildings investigated. Table 2.5 lists commonly observed materials specifications:

Table 2.5 Typical NCBF Material Properties

Gusset and Wide Flange Steel	A36
HSS Steel	A500
Pipe Steel	A53
High Strength Bolts	A325s, A325x
Weld Metal	Fexx = 70 ksi
Concrete Slab	F’c = 3 ksi

2.5 Connection Analysis

The connection capacities were evaluated and compared to the demands from the expected brace tensile and buckling capacities. For this analysis, R_y and R_t, the ratios between design and expected stresses, were applied to the demand from brace yielding and buckling and to other brace failure modes, but were not applied to failure modes for other connection components. This is consistent with the design requirements for modern SCBFs given in the Provisions. Resistance factors were not applied for any failure modes in order to better simulate the expected performance of the system. Additionally, the out-of-plane displacements and moments from brace buckling were not considered, but braces were checked against AISC requirements for end rotation clearance. All braced frames were assumed to act as trusses, so it was reasonable to assume that the vertical brace force was transmitted directly to the column, while the horizontal brace force was transmitted directly to the beam in the evaluation. In cases where this load path assumption resulted in an unbalanced moment on the gusset plate, the moment demand was assumed to distribute evenly between the gusset-to-beam connection and the gusset-to-column connection. Below, the key limit states that were evaluated for each frame are described

2.5.1 Brace Yielding

Brace tensile yielding is the controlling demand for most of the connection components. The expected yield capacity of the brace was calculated using Equation (2.3-1), where R_y is the ratio of expected to nominal yield stress of the brace material for the brace, A_g is the gross area, and F_y is the design yield stress.

$$P_u = R_y F_y A_g \tag{2.3-1}$$

2.5.2 Brace Buckling

For some limit states, brace compressive strength was the controlling demand. To calculate the buckling strength, the true length of the brace was used with an effective length factor, K, of 1. Unless restraint was provided against weak-axis buckling, it was assumed that buckling would occur on the weak axis. Brace compressive strength was calculated from Equation (2.3-2), which is taken from Section F2.3 of the Provisions. The critical buckling stress, F_{cr}, is found from Equation (2.3-3) and the Euler buckling stress, F_{em} from Equation (2.3-4), both of which are found in Section E3 of the AISC Specifications (2010), referred to herein as the Specifications. *KL/r* is the brace slenderness ratio and *E* is the Young's Modulus

$$P_u = 1.1F_{cr}A_g \tag{2.3-2}$$

$$F_{cr} = 0.877F_e \quad for\frac{KL}{r} \geq 4.71\sqrt{\frac{E}{R_yF_y}}\ and\ F_{cr} = 0.658^{\frac{R_yF_y}{F_e}}R_yF_y \quad Otherwise, \tag{2.3-3}$$

$$F_e = \frac{\pi^2 E}{\left(\frac{KL}{r}\right)^2} \tag{2.3-4}$$

2.5.3 Brace Net Section Fracture

The brace capacity for net section fracture at the brace-to-gusset connection was calculated using Equation (2-3.5) and Equation (2-3.6) from Section D2 of the Specifications. R_t is the ultimate stress ratio, F_u is the design ultimate strength of the steel, and A_e is the effective net area. The net area, A_N, is the gross area minus the area removed for brace slots or holes. Shear lag factors were calculated from Table D3.1 of the specifications.

$$R_u = R_tF_uA_e \tag{2.3-5}$$

$$A_e = A_NU \tag{2.3-6}$$

2.5.4 Block Shear

Block shear was checked for both the brace and gusset plate at the brace-to-gusset connection. Additionally, bolted gusset plates and shear tabs were checked for block shear. Capacity can be determined from Equation (2.3-7) for the brace and Equation (2.3-8) for other components. These equations are from the Specifications. section J4.3. Note that R_y and R_t were only included for block shear of the brace and the reduction coefficient, U_{bs}, is taken as 1 in all cases.A_{NT} is the net area of the failure plane in tension, A_{NV} is the net area in shear, and A_{GV} is the gross area in shear. Other variables were defined in previous sections.

$$R_u = U_{bs}A_{nt}R_tF_u + 0.6\min\left(A_{nv}R_tF_u, A_{gv}R_yF_y\right) \tag{2.3-7}$$

$$R_u = U_{bs}A_{nt}F_u + 0.6\min\left(A_{nv}F_u, A_{gv}F_y\right) \tag{2.3-8}$$

2.5.5 Whitmore Yielding

The Whitmore section is defined by a line which extends perpendicular from the brace at its end a distance of $L_c \tan(30)$ in each direction, where L_c is the brace-gusset splice length. The Whitmore section is illustrated in Figure 2.26. The Whitmore area is the length of this section multiplied by the thickness of the gusset plate. In instances where the Whitmore section extended into the beam or column, the thickness of the beam or column web was used for that portion of the section. Contribution from the flanges of the beam and column were ignored, per AISC recommendation. If part of the section extended past a free edge of the gusset, the section was terminated at that edge. Capacity can be determined from Equation (2.3-9), where F_y is the yield stress, t_p is the gusset plate (or beam) thickness, and B_w is the Whitmore width.

$$R_u = F_y t_p B_w \tag{2.3-9}$$

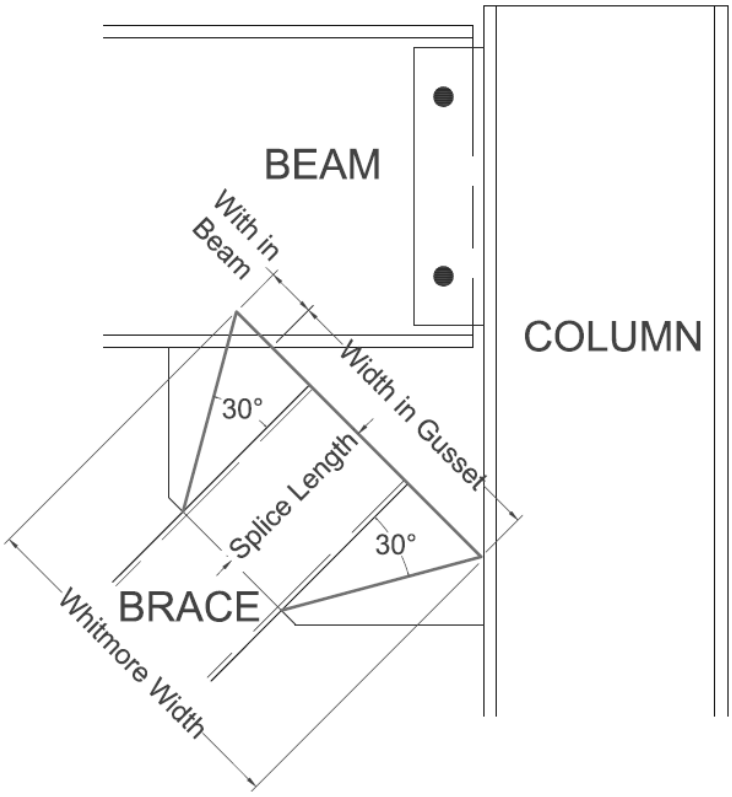

Figure 2.26 Whitmore Width Illustration

2.5.6 Gusset Plate Buckling

Gusset plate effective length factors 0.65 and 1 were used for corner connections and chevron midspan connections, respectively. The clear gusset length was calculated using the Thornton Method. Three lengths, labeled L_1, L_2, and L_3 in Figure 2.27, are averaged to give the equivalent buckling length, as stated in Equation (2.3-10). These lengths are taken as the distance parallel to the brace to the beam of column flange from the ends and center of the Whitmore section. In instances where a portion of the Whitmore section was within the beam or column, the length was recorded as a negative value. For calculating the area, radius of gyration, and inertia of the gusset, the properties of the Whitmore section were used, with effects of the beam and column flanges ignored. Equation (2.3-11) from the Specification Section E3 was used to calculate the buckling capacity. The critical buckling stress and Euler buckling stress were computed from Equation (2.3-12) and Equation (2.3-4).

$$L = \frac{L_1 + L_2 + L_3}{3} \tag{2.3-10}$$

$$R_u = F_{cr} A_g \tag{2.3-11}$$

$$F_{cr} = 0.877F_e \quad for \frac{KL}{r} \geq 4.71\sqrt{\frac{E}{F_y}} \; and \; F_{cr} = 0.658^{\frac{F_y}{F_e}} F_y \quad Otherwise, \tag{2.3-12}$$

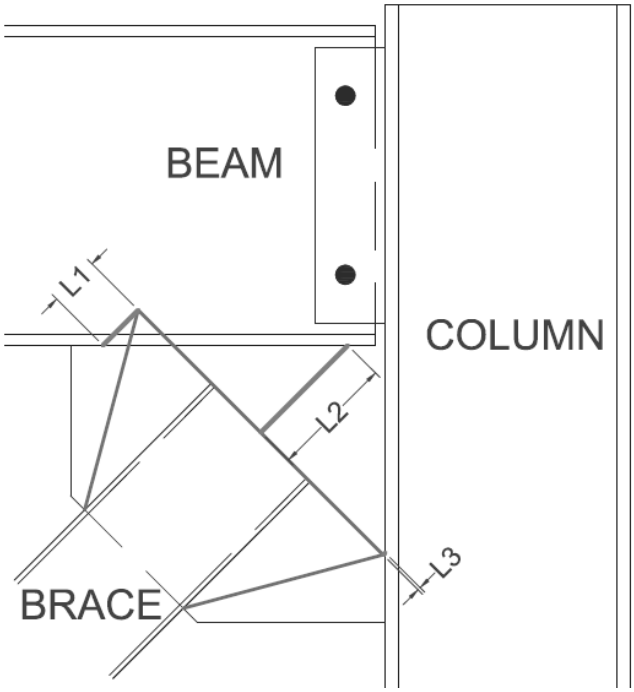

Figure 2.27 Gusset Plate Buckling Lengths

2.5.7 Weld Fracture

Weld capacity was evaluated based on the maximum stress expected on the weld, including effects from forces and moments. Inertia of welds was determined using the inertia of a rectangular cross section, with width equal to the weld throat and height equal to the weld length. In instances where multiple welds acted together, the parallel axis theorem was used. The maximum stress from moment was typically at one end of the weld, and was calculated using Equation (2.3-13), where *M* is the applied moment, *y* is the distance to the extreme fiber from the neutral axis, and *I* is the section inertia.

$$\sigma_m = \frac{My}{I} \tag{2.3-13}$$

Applied forces were assumed to be distributed uniformly over the weld, as shown in Equation (2.3-14), where *P* is the applied load and *A* is the weld area, equal to the throat times the length.

$$\sigma_v = \frac{P}{A} \tag{2.3-14}$$

From shear and moment stresses, the maximum stress on the weld can be calculated from Equation (2.3-15). Since the shear stress is uniformly distributed, the maximum total stress will occur where the bending stress is largest.

$$\sigma_{max} = \sqrt{\left(\sigma_{my} + \sigma_{vy}\right)^2 + (\sigma_{mx} + \sigma_{vx})^2} \tag{2.3-15}$$

The weld stress capacity can then be computed from Equation (2.3-16). F_{EXX} is the filler metal classification strength and θ_F is the angle of the maximum stress relative to the weld axis, which can be computed from Equation (2.3-17) from section J2.4 of the AISC Specifications. The DCR for the weld was calculated from the ratio of the maximum total stress and the weld stress capacity.

$$\sigma_u = 0.6F_{EXX}(1 + 0.5sin(\theta_F)^{1.5}) \tag{2.3-16}$$

$$\theta_T = \text{atan}\left(\frac{\sigma_{my} + \sigma_{vy}}{\sigma_{mx} + \sigma_{vx}}\right) \tag{2.3-17}$$

2.5.8 Base Metal Yielding

For larger welds and complete joint penetration welds, there is a potential for shear yielding of the weld base metal. In most cases, the gusset plate was the thinnest component, so it was checked for yielding. Many gusset to beam and gusset to column connections, particularly those with complete joint penetration welds, were susceptible to shear yielding. Base metal capacity in shear was calculated from Equation (2.3-18) from Section J2.4 of the AISC Specifications,

$$R_u = 0.6F_y t_p L_c \tag{2.3-18}$$

2.5.9 Bolt Shear

Bolts were assumed not to carry moment when possible, because welds are stiffer than bolts and therefore more likely to carry moment demands. Bolt tension and prying were not considered. The bolt force distribution was assumed to be elastic, rather than using the instantaneous center of rotation. Equation (2.3-19) was used to evaluate bolt capacity. F_{nv} is the bolt shear stress capacity from AISC Specification Table J3.2, d_b is the bolt diameter, and N_b is the number of bolts resisting shear.

$$R_u = \pi \left(\frac{d_b}{2}\right)^2 F_{nv} N_b \tag{2.3-19}$$

2.5.10 Bolt Bearing

The bearing capacity of elements connected by bolts was evaluated using Equation (2.3-20) from AISC Specifications Section J3.10. L_{cb} is the clear distance between the edge of the bolt hole and the next bolt hole or plate edge in the direction of loading. d_b is the bolt diameter.

$$R_u = \sum F_u t_p \min\left(1.5L_{cb}, 3d_b\right) \tag{2.3-20}$$

2.6 System Analysis

Framing members (beams and columns) were also checked for their ability to develop the capacity of the braces in the framing system. Frames in adjacent bays were included in the analysis, frames in other bays were not, as shown in Figure 2.28

In chevron configurations, the beam was treated as continuous over the mid-span connection. Four load cases were investigated for each frame, as listed in Table 2.6 and illustrated in Figure 2.29. Horizontal load was applied at each floor. The magnitude of the load was calculated to develop the full tensile and

compressive capacity of all braces in the system. For frames with one column at the exterior wall of a structure, the load was applied to the side of the frame at the interior of the structure. For all other frames, half of the load was applied at each side of the frame, assuming an even load distribution from the diaphragm.

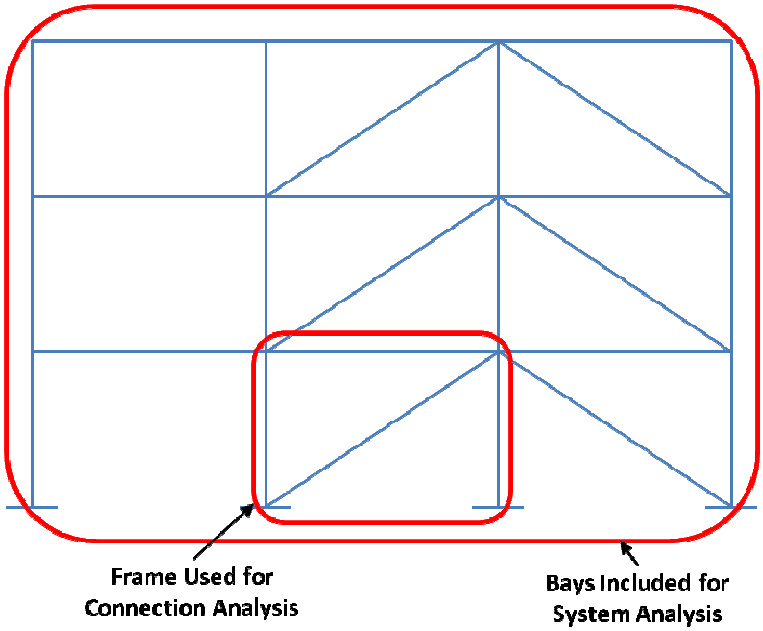

Figure 2.28 System Analysis Illustration

Table 2.6 Frame Load Cases

Load Case	Load Direction (In plane of frame)	Compressive Brace Strength
1	Left to Right	P_{cr}
2	Left to Right	$0.3P_{cr}$
3	Right to Left	P_{cr}
4	Right to Left	$0.3P_{cr}$

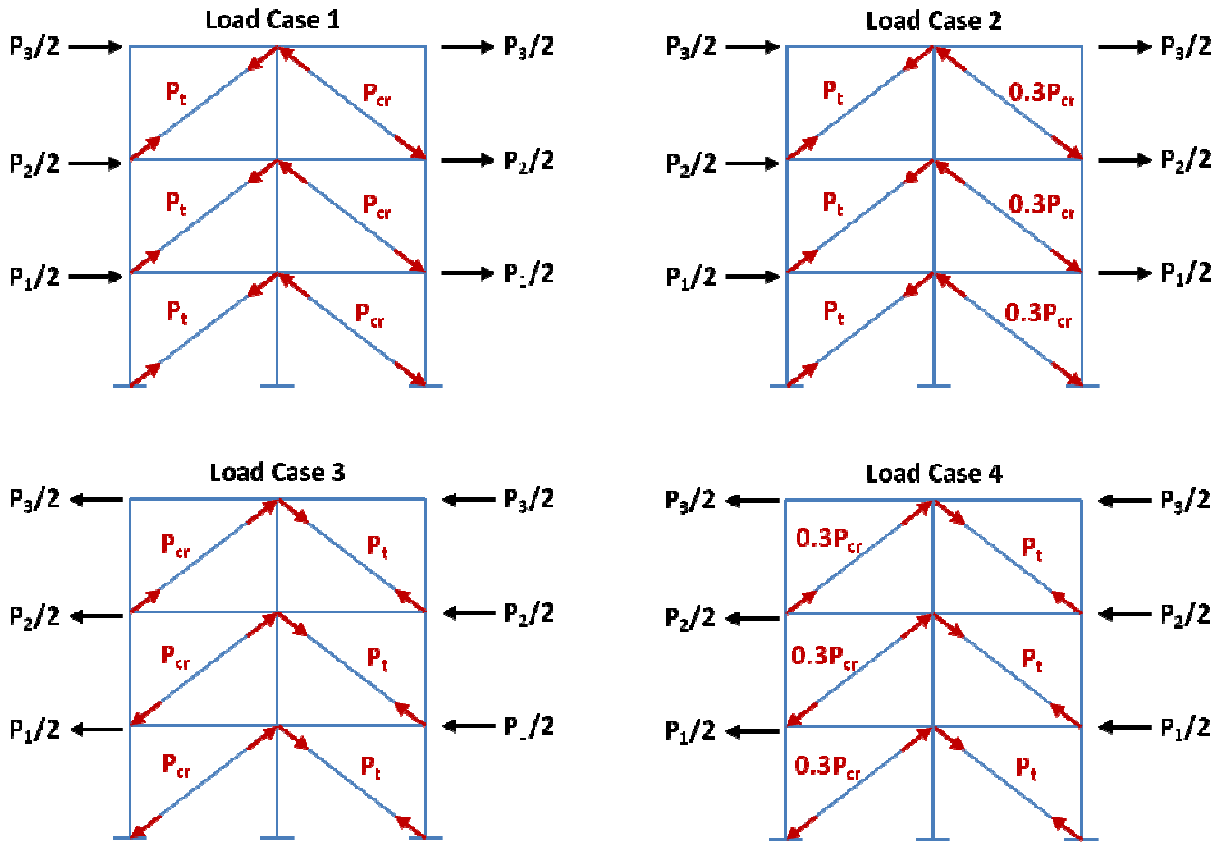

Figure 2.29 Load Case Illustration

A uniform factored gravity load of 100psf was applied throughout the structure. This factor is reasonably close to common floor loads in most structures, and was deemed sufficiently accurate for this analysis.

2.6.1 Column Analysis

Column compressive capacity was calculated using Equation (2.3-4), Equation (2.3-11), and Equation (2.3-12).None of the columns investigated had slender elements, so local buckling criteria were not necessary. The effective length factor for all columns was 1. Column tensile capacity was evaluated using Equation (2.4-1).

(2.4-1)

2.6.2 Beam Analysis

Beams were evaluated for compression, tension, bending, and combined compression and bending. For beams supporting a floor deck or slab, the member was assumed to be continuously laterally braced. Most beams supported a steel deck with concrete topping slab. These beams were analyzed assuming both full composite action and no composite action to bound the flexural strength. The nature of the stud details in the obtained drawings made determining the likely extent of composite action impossible in many cases, so a bounding analysis was done instead. For beams with composite slab over deck and full composite action, the axial compressive strength was computed from Equation (2.4-2). F'_c is the concrete compressive strength, b is the effective width of the concrete, and t_{slab} is the slab thickness. A_{steel} is the cross-sectional area of the beam, and F_y is the beam yield strength, which was used because the beam is braced along its length by the slab. For beams without composite action, the concrete strength in Equation (2.4-2) was set to 0.

$$R_{cr} = F_y A_{steel} + 0.85 F'_c b t_{slab} \tag{2.4-2}$$

The beam bending strength with composite action was computed from Equation (2.4-3). C_c, the concrete compressive force, was computed fro Equation (2.4-4). C_s, the steel compressive force, was computed from Equation (2.4-5), and T_s, the steel tensile force was computed from Equation (2.4-6). y_{cc}, y_{cs}, and y_{ts} are the distances to the section neutral axis from the center of the concrete compressive force, steel compressive force, and steel tension force, respectively. Similarly, C_c, C_s, and T_s are the compressive force, steel compressive force, and steel tension force, respectively. t_{slab} is the concrete slab thickness. A_{sc} and A_{st} are the steel areas in tension and compression, respectively.

$$M_n = C_c y_{cc} + C_s y_{cs} + T_s y_{ts} \tag{2.4-3}$$

$$C_c = 0.8 F'_c b h \quad h = \min(t_{slab}, 2y_{cc}) \tag{2.4-4}$$

$$C_s = A_{sc} F_y \tag{2.4-5}$$

$$T_s = A_{st} F_y \tag{2.4-6}$$

For beams without composite slab that were continually laterally braced, the plastic moment capacity governs the design, as given in Equation (2.4-7).

$$M_n = Z_x F_y \tag{2.4-7}$$

The combined compression and bending action was evaluated using the interaction equation from AISC Specifications Section H1.1, given here as Equation (2.4-8). The axial load was always greater than 20% of the axial capacity, so the low axial load equation from AISC was not used.

$$\frac{P_u}{R_{cr}} + \frac{8}{9}\frac{M_u}{M_n} \leq 1 \qquad (2.4\text{-}8)$$

2.6.3 Other System Components

Column splices were an expected area of deficiency in frames analyzed, but the drawings obtained indicated that the braced frames had column splices that utilized CJP welds per modern design requirements. Because no deficiencies were found, a more detailed description was not included.

Column base plate and foundation analysis was attempted for the frames analyzed, but sufficient information was not available on the drawings that were collected. As a result, no analysis of column base plates or foundations is presented here.

2.7 Analysis Results

Figure 2.30 summarizes the observed deficiencies in the connections analyzed. It shows the percentages of analyzed connections with a DCR greater than 1 for each failure mode. The results are shaded to indicate the severity of the deficiency in each case. Figure 2.31 summarizes the same information as Figure 2.30, in that it shows the number of frames failing each design check. However, the shading in Figure 2.31 indicates where the limit state falls within the failure hierarchy for each connection. If a limit state is indicated as "primary", then it had the highest DCR of all limit states for that connection, and is thus likely to control the strength of the system. In some cases, a limit state that is often deficient may typically be only slightly deficient, meaning that it is unlikely to be the cause of a connection failure. Figure 2.32 shows limit states for the framing members using the same convention as Figure 2.30. The complete list of DCRs for the connections can be found in Appendix A.

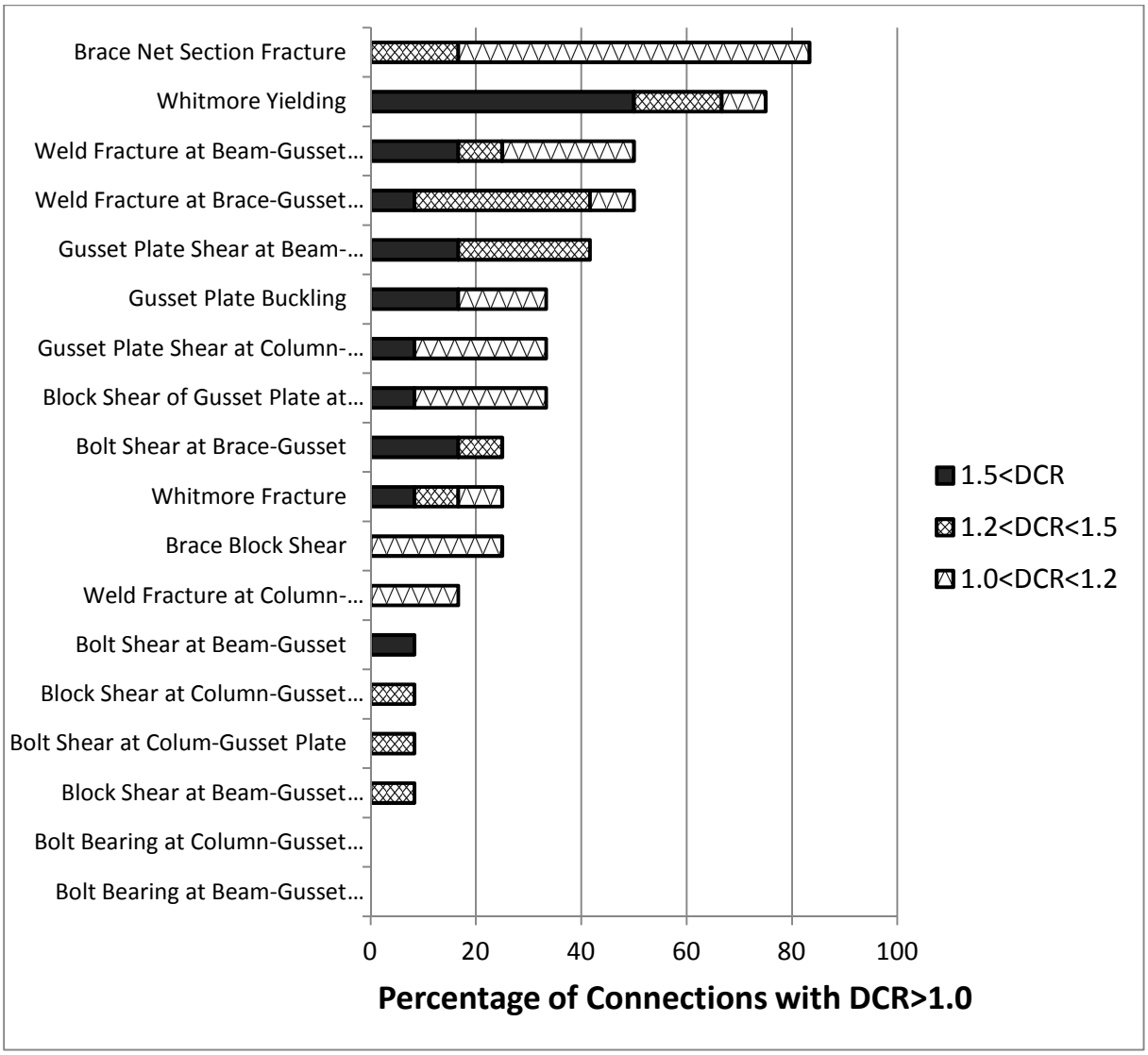

Figure 2.30 Connection Limit States - by DCR

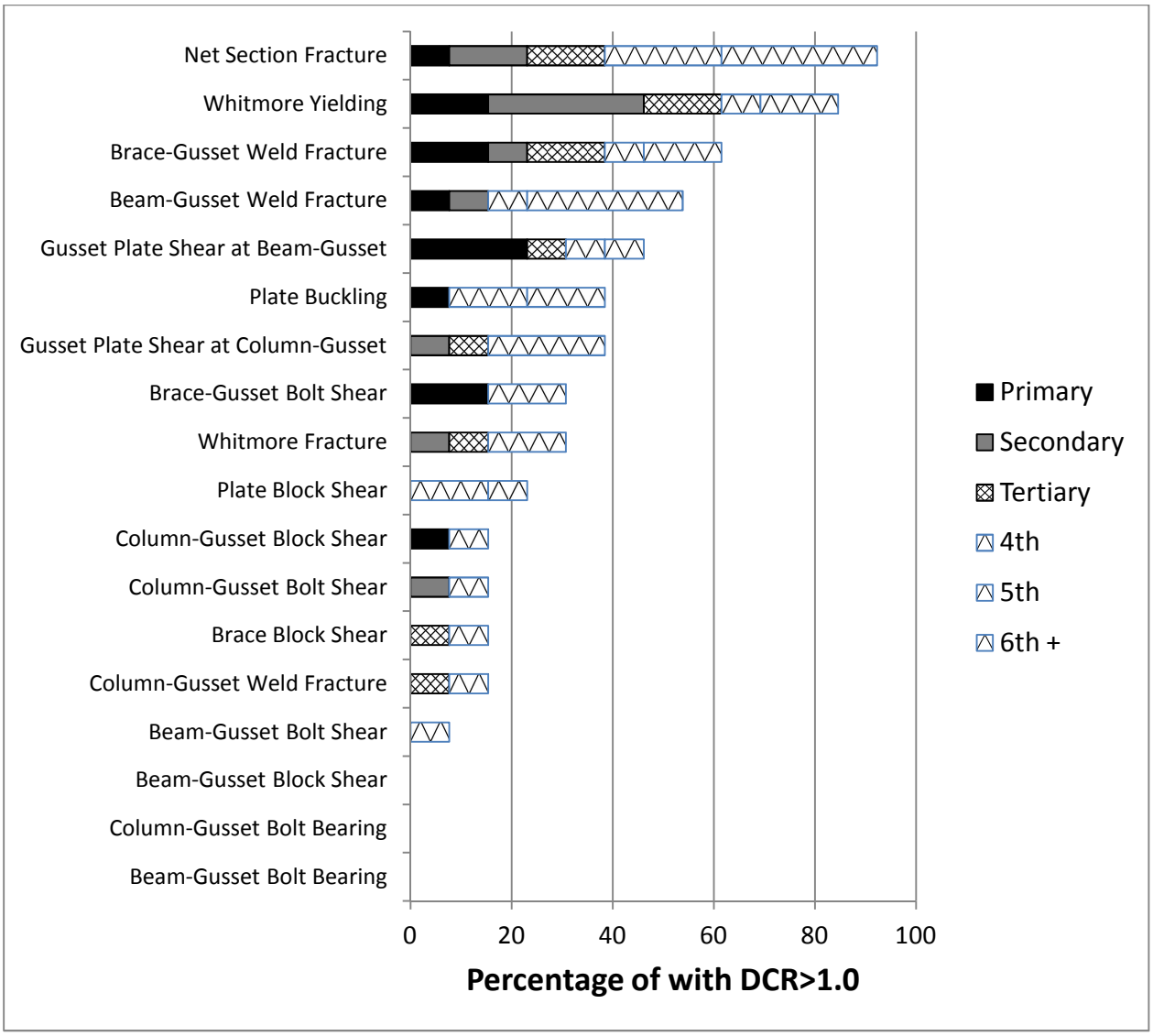

Figure 2.31 Connection Limit States - by Failure Hierarchy

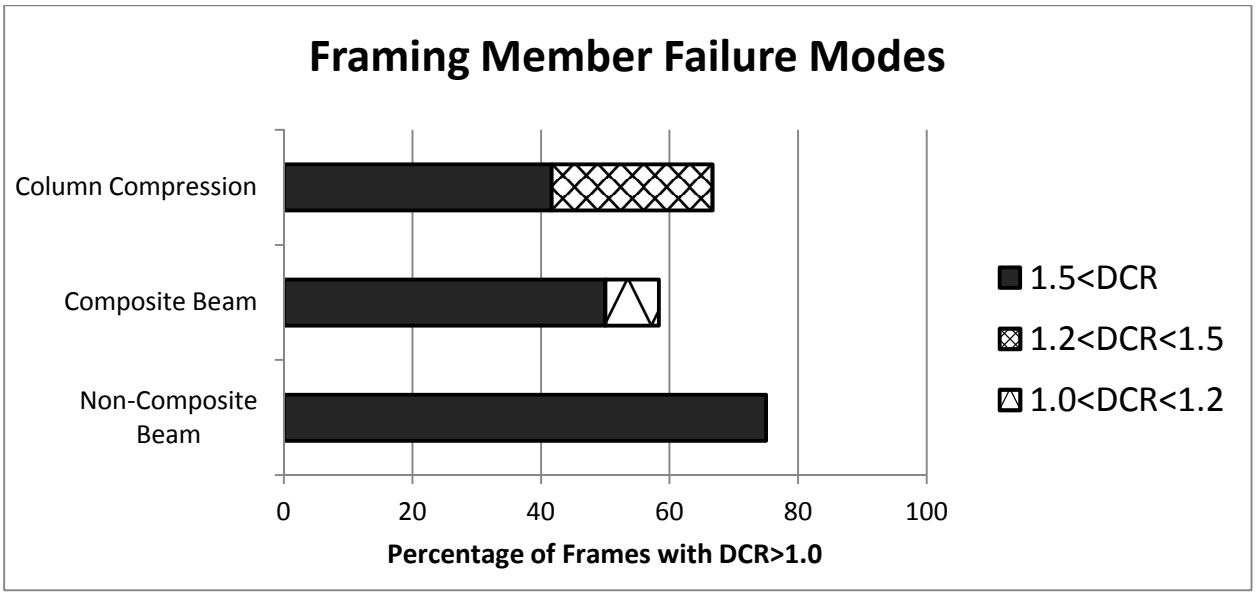

Figure 2.32 Framing Member Limit States

2.7.1 Whitmore Yielding

Nearly all of the analyzed frames have insufficient capacity for Whitmore yielding. In many cases, the DCR was greater than 1.5, and it was very frequently the primary or secondary failure mode. Two factors contributed to the high incidence of Whitmore yielding. First, gusset plates were frequently much thinner than current design would require. Gusset plate buckling, which is a major concern for modern SCBF design and typically forces the use of thicker gussets, was not an issue in these connections because clearance for brace end rotation was not provided. The second contributing factor is the brace to gusset weld (or bolts). These connections were generally too short to develop the brace tensile strength, and shorter connections lead to a smaller Whitmore width.

It is also important to note that 8 of 13 beam-column-brace connections and 5 of 7 mid-span connections had some portion of the Whitmore width falling within the beam. This is significant, because the effects of the beam flange on the Whitmore section are typically ignored in analysis. It is likely, however, that some portion of the beam flange would likely resist yielding along the Whitmore width, particularly once strains in the gusset plate and beam web grew large.

Whitmore yielding is a reasonably ductile limit state, making its prevalence less concerning. Whitmore fracture is a more brittle failure, but for welded connections, it occurs at a much higher load and thus had lower DCR values.

2.7.2 Gusset Plate Buckling

Gusset plate buckling appears to be problematic in approximately 40% of connections. However, the behavior observed is more accurately categorized as compressive yielding of the Whitmore section. In all of the connections analyzed, the critical buckling stress for the plate was greater than 95% of the yield stress. Most of the gusset plates had very small values of KL/r, for which the buckling equation is bounded by compressive yielding. These plates would likely yield in compression without significant buckling, so these predicted failures can be used as further evidence of pressing issues with Whitmore yielding.

2.7.3 Brace Net Section Fracture

Net section fracture was also prevalent, though typically at much lower DCRs than Whitmore yielding. Net section reinforcing was not provided in any of the connections analyzed. Net section fracture is a brittle failure mechanism and is very undesirable in SCBF systems. It appears to be a common concern in evaluating older CBF systems.

2.7.4 Gusset Plate Shear Yielding

Gusset plate shear yielding had a DCR greater than 1 in approximately 50% of connections. It was frequently the limit state with the highest DCR in connections. Yielding was more commonly predictedt the beam connection than at the column. This is in part because most braces make an angle of less than 45˚ with the beam, meaning that the horizontal force, which much be transmitted to the beam, is larger than the vertical force transmitted to the column. Additionally, the prevalence of thin gusset plates makes this limit state more prevalent. Like Whitmore yielding, gusset plate shear yielding is a ductile limit state and thus of less concern.

2.7.5 Weld Fracture

Over half of the connections analyzed had deficient welds. Brace-to-gusset welds and gusset-to-beam welds were each deficient in half of the connections analyzed. Weld fracture is a very brittle failure mechanism and is of great concern in evaluation and retrofit of these systems.

2.7.6 Bolt Bearing

Bolt bearing was not deficient for any of the connections analyzed. Bolted connections that had deficiencies were controlled by bolt shear.

2.7.7 Bolt Shear

Bolted connections were less common than welded ones in the connections analyzed. The majority of systems utilizing bolted components had bolt shear limit state deficiencies. Almost all of the DCRs were greater than 1.5, meaning the bolts were far over capacity. Bolt shear is also a relatively brittle failure mode, so its prevalence as an issue in bolted systems is concerning.

2.7.8 Block Shear

Block shear was identified as problematic in some connections, though it was typically not one of the controlling limit states for those connections. Block shear of either the brace or gusset plate at the brace-gusset connection was the most common. In most of those instances, weld fracture had a higher DCR than block shear for both the brace and gusset plate, so it is unlikely that block shear would actually occur prior to weld fracture. Block shear is an undesirable failure mode, so the DCRs greater than 1 are still concerning, even if they are not predicted to control the connection strength.

2.7.9 Beams

Over half of the systems analyzed had beams with insufficient capacity to develop the brace strength, despite the use of composite floor slab action to improve beam strength. Almost all of these deficiencies occurred in chevron brace configurations, where beams are subjected to substantial bending and shear forces from the unbalanced brace load ($0.3F_{cr}A_g$ compressive capacity and F_yA_g tensile capacity) in addition to the axial forces. DCRs for these systems were generally very high – typically in the range of 2-4, but as high as 8.However, it is likely that brace buckling would never occur in these systems, because few of the connections have sufficient capacity to buckle the brace. Despite this, many of these beams have DCRs greater than 1.0 even without the unbalanced brace force. This is due to high axial compressive loads, and bending from gravity loads. Beam yielding at the midspan due to these combined loads would result in beam damage, as well as floor damage due to deflections. This would likely require extensive building repairs. The beams in these systems were clearly not designed to develop the full brace

capacity or unbalanced loads, and thus are undersized. The implications of such a deficient component in the system are not entirely clear, but chevron beams are clearly an issue of concern for older systems.

2.7.10 Columns

Column compressive capacities were exceeded at the lower levels of approximately 50% of systems. DCRs were often higher than 1.5, but were never nearly as high as the DCRs observed for beams. In reality, it is unlikely that the full brace capacity would be developed at every level in the same direction simultaneously, so the demands estimated for the columns are very high. Column DCRs were largest in taller structures, where it is even less likely that all braces would simultaneously reach capacity. Nonetheless, it is possible that column buckling would be observed in some of these systems, particularly shorter structures. Column buckling is a concern for system collapse prevention, and the cost of column replacement is substantial, so prevention of this failure mode is of high importance.

2.7.11 Slenderness and Compactness

The cross-sectional width-to-thickness ratios of beams, columns, and braces were evaluated to determine their compactness classifications. Figure 2.33 shows the statistics for these systems. It records the compactness classification of the least compact member of its type in the analyzed frame. For example if a building is recorded as having non-compact columns, it means at least one column in the frame analyzed is non-compact, but none are slender. In the buildings analyzed, compactness was a large problem in beams. Most of the beams in these systems were very deep with thin webs – over half of the systems to had slender webs. The majority of columns met the seismically compact criteria, and none were slender. Brace compactness was more evenly distributed. In most systems, the braces at the bottom floors were seismically compact, but many of the braces near the top of the structure were of similar outer dimensions with thinner walls. As a result, less than half of the frames had braces that were all seismically compact.

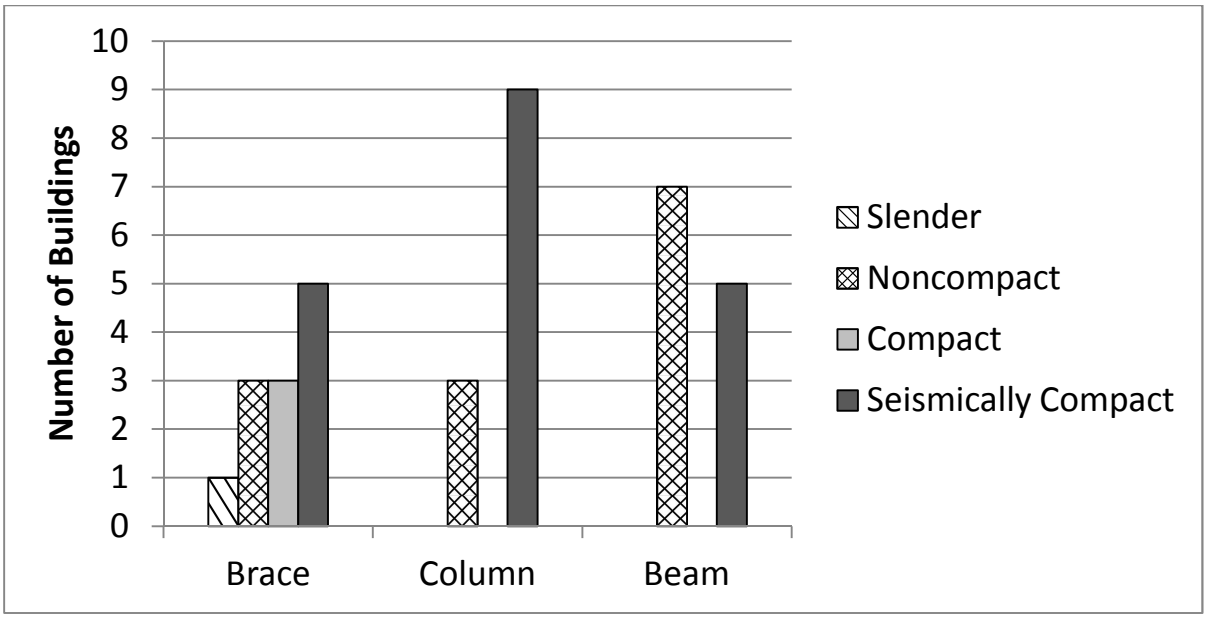

Figure 2.33 Local Compactness of Braced Frame Members

A more specific investigation of HSS braces was conducted because it was the most common brace type and thus most likely to be used for testing. For each frame that was analyzed that used HSS braces, the width-to-thickness ratios of all braces in bays above and below were recorded. Typically, these structures were 2-4 stories in height. Figure 2.34 shows the brace width-to-thickness ratio for the surveyed HSS braces. The 0-13.5 bin contains braces that meet the highly ductile seismic compactness requirement. The 13.5-15.4 bin contains braces that meet the moderately ductile seismic compactness requirement. All other braces are classified as non-compact. No braces were classified as slender, the 33.7+ bin, but many were very close to that limit. The large number of braces with width-to-thickness ratios at or above twice the modern limit is a source of concern for the performance, and particularly the ductility, of these systems.

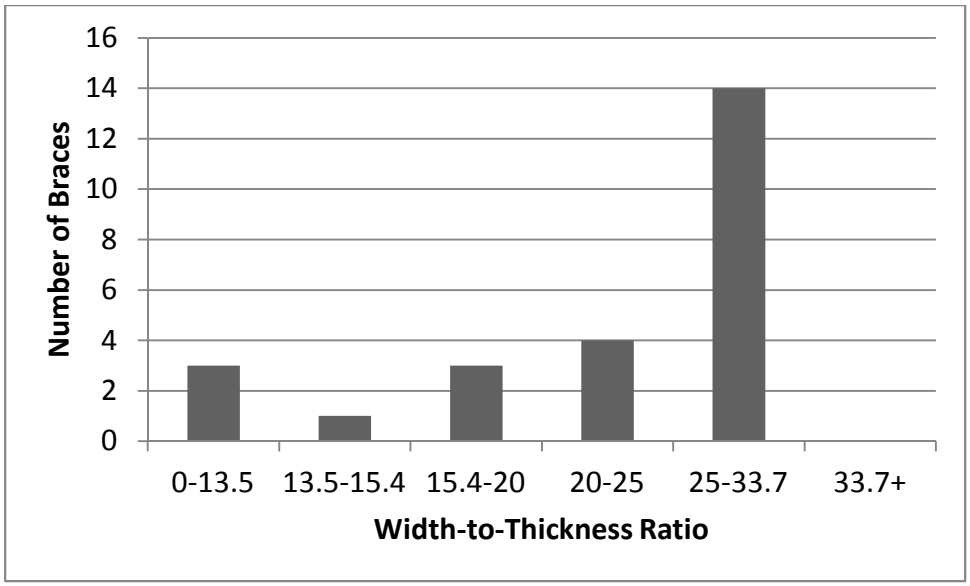

Figure 2.34 HSS Width-to-Thickness Ratios

Braces were also checked against the recommended slenderness ration (KL/r) of 200 for SCBF systems. None of the braces investigated had KL/r values greater than 200, so global slenderness was not a concern.

2.8 Conclusions of Survey

None of the connections analyzed were capable of resisting the brace expected yield capacity by modern design standards. In particular, gusset plates were typically undersized, and brace-gusset splice lengths were often too short. Although many of the connection deficiencies relate to ductile limit states, the majority of the connections had one or more deficient welds, and others had deficient bolts. Both of these deficiencies could lead to poor system performance, making them good candidates for future study.

Additionally, none of the connections analyzed had sufficient clearance to allow for brace end rotation, thus increasing the likelihood of damage to the connection and reducing the brace's ability to buckle. In most cases, the only way to retrofit the connection to ensure proper brace clearance would be to replace the existing gusset plate. It might also be possible to install braces designed to buckle in the plane of the frame, thus reducing the demand for clearance and potentially allowing the use of the existing connection.

Even with extensive connection retrofits, most frames would still not have sufficient beam and column capacity to develop the braces. This issue is more difficult to resolve, as retrofitting beams and columns

requires substantially more effort than retrofitting connections. Also, vertical discontinuities in the building load path raise additional concerns about the ability of the structure to transfer lateral loads from the braces to the foundation.

Based on these observations: the following characteristics were targeted for future study in this thesis, as well as Johnson (2014) and Sen (2014).

- Shared welded shear tab connections
- Shared bolted shear tab connections
- Bolted end plate connections
- Chevron frame configurations with weak beams
- Connections without adequate brace end rotation clearance
- Connections with thin gusset plates
- Connections with undersized bolts and welds

Specifically, the specimens in this thesis focus on shared welded shear tab connections, such as shown in Figure 2.23. Connections of this type in the infrastructure review were found to have deficient welds and gusset plates in all cases, and the configuration was common in the buildings surveyed. Further information is provided in Chapter 3.

Chapter 3: Specimen Design

3.1 Summary of Design Parameters

This chapter details the motivation and methodology for the design of the test specimens. This section gives a description of how demands and capacities were calculated for specimen components and provides a summary of the parameters of each specimen. Sections 3.2-3.7 describe the motivation for each test specimen and the specifics of its design.

In order to be consistent with the protocols of the infrastructure review and to make the results more directly comparable, the same methodology was used to calculate capacities and demands for the test specimens as for the infrastructure review. The demands placed on the connection were the expected brace buckling capacity in compression and the expected brace yield capacity in tension. The equations and formulations for the brace and connection limit states are given in Chapter 2, so they are not repeated here. Specimens NCBF1-R3 and NCBF1-R4 utilized a knife plate retrofit which was designed to different requirements than other connection components. Its design is detailed in Section 3.5. Specimen NCBF1-R5 utilized a bolted retrofit, and the bolt design is addressed in Section 3.7.

Table 3.1.1 gives a brief summary of the characteristics and objectives of each test. The complete experimental setup is described in Chapter 4. Specimen NCBF1 is an NCBF connection designed to be similar to a common connection configuration found in the infrastructure review in Chapter 2. Specimens NCBF1-R1 through NCBF1-R5 are retrofits of specimen NCBF1, so their descriptions explain how they modify NCBF1. Table 3.1.2 gives the demand-capacity ratios for each of the limit states pertaining to each test. These DCRs were calculated without the use of resistance factors, as was the procedure for the infrastructure review. Highlighted cells indicate demand-capacity ratios greater than 1. In many cases, retrofits did not affect the DCRs associated with some of the limit states, so many values are consistent across the table. This table is discussed in more detail throughout the chapter.

For the brace width-to-thickness ratio DCRs, the brace width-to-thickness ratio is divided by the value required for seismic compactness in the AISC provisions. None of the specimens met gusset plate clearance requirements for allowing the brace end to rotate while buckling per AISC.

Table 3.1 Specimen Summaries

Test	Description	Goal
NCBF1	Existing NCBF. Single welded shear tab connection. Thin gusset plate, short splice length, and non-compact brace.	Evaluate a typical existing connection and brace with major deficiencies.
NCBF1-R1	Replace NCBF1 brace with compact section. Reuse gusset plates and frame from NCBF1 - Repair.	Improve brace performance to increase system drift range.
NCBF1-R2	Replace NCBF1 brace with compact section (same as NCBF1-R1). Use new gusset plates and all non-tough welds.	Improve brace performance to increase system drift range.
NCBF1-R3	In-plane buckling brace retrofit with square HSS brace. Knife plate extended into shear tab.	In-plane buckling to reduce demands on gusset plates and welds.
NCBF1-R4	In-plane buckling brace retrofit with rectangular HSS brace. Knife plate not extended into shear tab.	In-plane buckling to reduce demands on gusset plates and welds, shorter knife plate to reduce local strains.
NCBF1-R5	Noncompact NCBF1 brace filled with concrete and bolts added to shear tab.	Prolong brace life and protect vulnerable shear tab weld.

Table 3.2 Specimen DCRs

Limit State	NCBF1	NCBF1-R1	NCBF1-R2	NCBF1-R3	NCBF1-R4	NCBF1-R5
Brace Net Section Fracture	1.26	1.15	1.15	1.21	1.16	1.26
Brace-Gusset Plate Weld Fracture	0.92	0.92	0.92	0.92	0.92	0.92
Brace Block Shear	1.14	0.76	0.76	0.76	0.76	1.14
Gusset Plate Block Shear	1.16	1.33	1.33	1.22	1.78	1.16
Gusset Plate Whitmore Yielding	1.33	1.50	1.50	1.28	1.89	1.33
Gusset Plate Buckling	0.74	0.84	0.84	0.70	1.03	0.74
Gusset Plate Shear Yielding at Beam	1.16	1.16	1.16	1.16	1.16	1.16
Beam-Gusset Weld Fracture	1.55	1.55	1.55	1.55	1.55	1.55
Shear Tab to Gusset/Beam Weld Fracture	1.08	1.08	1.08	1.08	1.08	1.08
Shear Tab to Column Weld Fracture	0.65	0.65	0.65	0.65	0.65	0.65
Brace Width-to-Thickness Ratio	2.00	0.84	0.84	0.84	1.00	2.00

3.2 NCBF1

NCBF1 was designed with the following objectives:

- Geometrically similar to a common connection from the infrastructure review;
- DCRs for targeted limit states that are similar to reference connections; and
- Fit within the constraints of the experimental setup.

NCBF1 was designed to represent a common connection configuration and the associated deficiencies from the infrastructure review. This connection configuration is referred to herein as a shared shear plate

connection. In this configuration, a single shear tab is welded to the column flange. The shear tab is welded to both the gusset plate and the beam web. One side of one flange of the beam web is coped to allow the shear tab to rest flat on the beam web and gusset plate. The gusset plate is then welded to the beam flange. Figure 3.1, Figure 3.2 and Figure 3.3 demonstrate the shared shear plate connection.

The design of NCBF1 was based upon two connections found in the survey of existing buildings (Chapter 2). The first connection is from building 86WA3A and is shown in Figure 3.1. The second is from building 92WA2A and is shown in Figure 3.2. These two connections are representative of the shared welded shear tab connection, which was one of the most common connection configurations found in the infrastructure review. Finally, Figure 3.3 shows the connection detail for NCBF1.

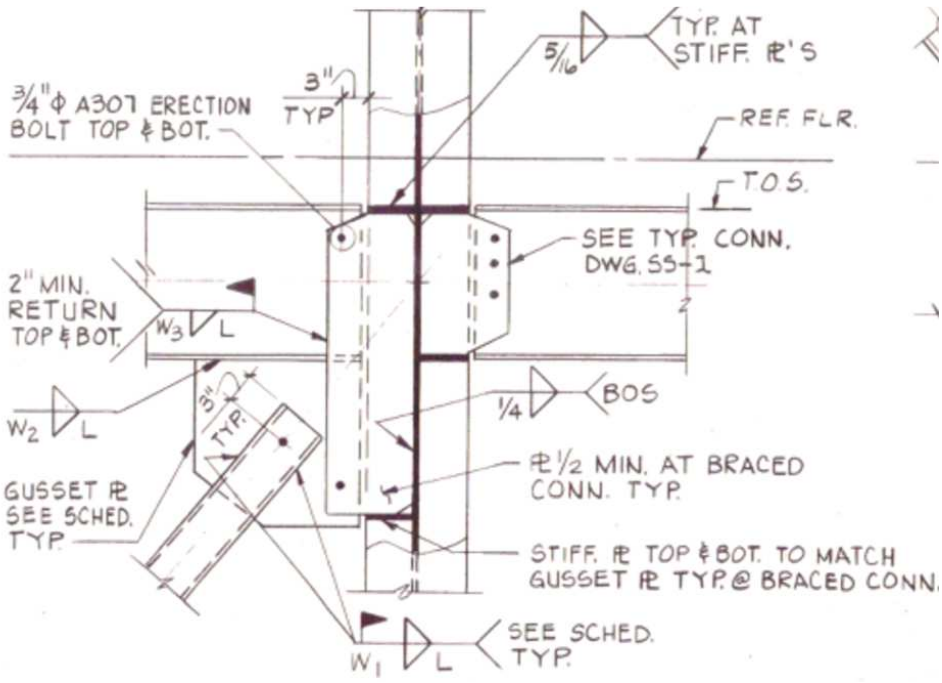

Figure 3.1 Connection from 86WA3A

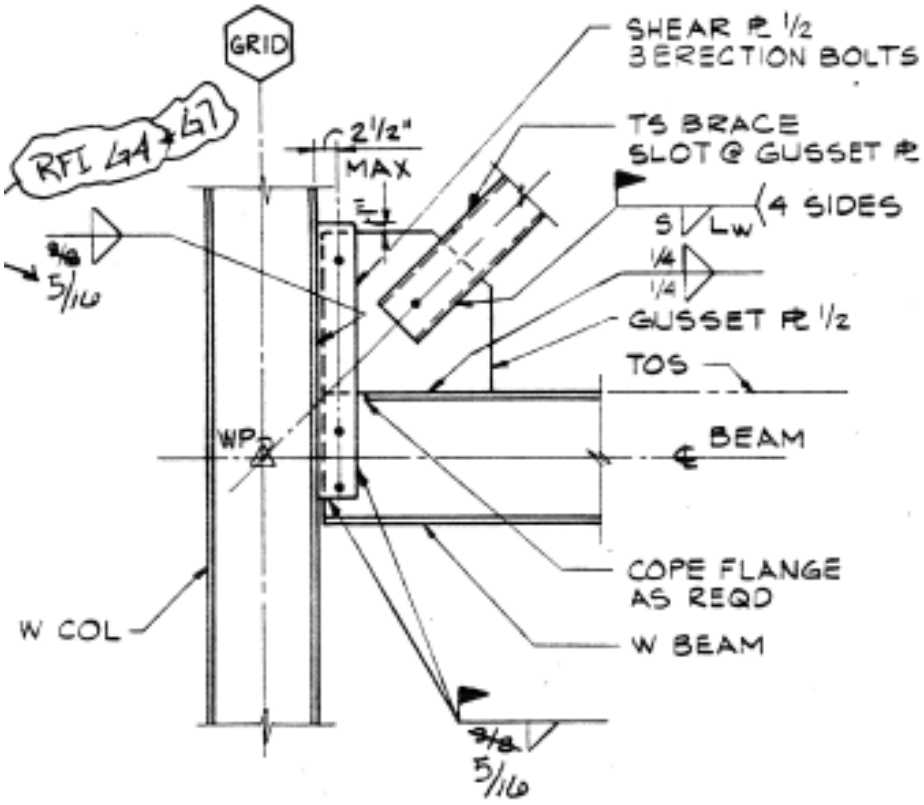

Figure 3.2 Connection from 92WA2A

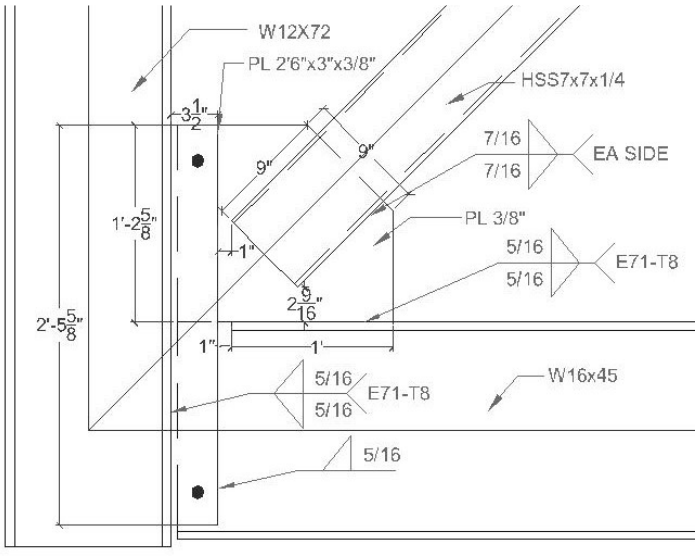

Figure 3.3 Connection Detail for NCBF1

Some notable characteristics of the connections are given in Table 3.3. NCBF1 was designed to match the characteristics of the two reference systems. Some characteristics, such as the brace angle, were not achievable due to the constraints of the experimental setup.

Table 3.3 Characteristics of Shared Shear Tab Connections

Properties	**NCBF1**	**86WA3A**	**92WA2A**
Brace	HSS7x7x1/4	HSS8x8x3/8	HSS6x6x1/4
Brace Angle	45˚	31˚	37˚
Brace Width-to-Thickness Ratio	27	19.9	22.8
Brace Length (ft)	14.0	14.7	21.7
Splice Length (in)	9	18	8
Gusset Plate Thickness (in)	0.375	0.625	0.5
Gusset Plate Yield Strength (ksi)	50	36	36
Beam-Gusset Connection Length (in)	14	24	21
Beam-Gusset Weld Size (in)	0.313	0.250	0.250
Shear Tab Thickness (in)	0.375	0.625	0.5
Shear Tab Length (in)	29.6	42.0	31.0
Shear Tab Weld Size (in)	0.313	0.375	0.313

The brace end was given the minimum clearance allowable for construction, as was the case in both of the reference drawings. A 1 inch gap was provided between the brace end and the gusset plate to shear tab interface weld. The HSS7x7x1/4 brace used for NCBF1 had a width-to-thickness ratio of 27. This is about twice the modern limit of 13.5 for highly ductile seismic compactness. Braces in modern SCBF systems are required to meet the highly ductile compactness criteria. The calculated compactness requirements from the Specifications and the Provisions for 50 ksi steel are given in

Table 3.4. The two reference frames had brace width-to-thickness ratios that were slightly lower than NCBF1, but that were still significantly higher than required by modern design. A higher width-to-thickness ratio was used for NCBF1 because it was more representative of the distribution of HSS braces used across all of the frames surveyed. The distribution of surveyed HSS width-to-thickness ratios is give in Figure 2.34.

Table 3.4 Width-to-Thickness Limits for 50ksi HSS

Criteria	Width-to-Thickness Limit
Seismically Compact -Highly Ductile	13.5
Seismically Compact -Moderately Ductile	15.4
Non-compact	33.7

Both reference connections had a range of deficiencies, with some notable similarities. The DCRs for the reference connection and NCBF1 limit states are given in Table 3.5. Limit states with DCRs greater than 1 are highlighted by shading. Each limit state is also assigned a priority that indicates the level of importance ascribed to matching NCBF1s DCR to that of the reference frames.

The first high priority limit state was Whitmore yielding. For the reference connections, as well as many other connections in the infrastructure review, the DCR for Whitmore yielding was significantly larger than 1. Typically, this was a result of both short splice lengths and thin gusset plates. A thin gusset plate and short splice length were chosen for NCBF1 to a DCR for Whitmore yielding in between the values for the two reference connections. Both reference structures used A36 steel for gusset plates. Modern A36 steel differs significantly in its properties when compared to A36 steel from the 1980s. Because modern A36 steel has very unpredictable material properties (R_y = 1.6) and is difficult to acquire, A572 grade 50 steel was used for plates instead. Using steel with a higher yield stress requires thinner plates to achieve the same DCRs. As a result, the NCBF1 plate is proportionally thinner than the plates in the reference structures.

Gusset-to-beam weld fracture had very high DCRs for both of the reference connections, so it was assigned high priority as well. In order to maintain the square gusset plate shape, the length of the weld could not be adjusted substantially. Instead, the size of the throat was selected to give a DCR comparable to the reference connections.

The shear tab weld, which connects both the gusset plate and the beam to the shear tab, was only deficient in one of the two reference connections. However, it was deemed worthwhile to investigate. The length of

the weld was dictated by the connection geometry, so the DCR was achieved by modifying the throat of the weld.

Moderate priority was ascribed to limit states that were of interest, but were not primary objectives of the test. Brace block shear and gusset plate block shear at the brace-gusset connection were both moderate priority. These limit states are typically ductile, and are less likely than Whitmore yielding to substantially impact the system performance. DCRs for these limit states were largely dictated by the geometry developed to target the high priority modes,.

As mentioned in Chapter 2, no HSS connections from the infrastructure review included net section reinforcement. Correspondingly, NCBF1 was designed without them. The DCR for net section fracture was a function of the brace size and the gusset-beam weld length, both of which were selected to achieve higher priority design objectives.

The shear tab to column weld was also moderate priority, insomuch as it was not deficient for either of the reference connections, so it was designed not to be deficient in NCBF1.

Although the reference connections had deficient brace-gusset splice welds, NCBF1 was designed with stronger brace-gusset splice welds A pilot NCBF test at UW demonstrated that deficient brace-gusset welds led to fracture at the splice at very low drifts (Hsiao et al 2010). In order to more effectively evaluate the other connection deficiencies, NCBF1 used large splice welds to keep the DCR for weld fracture below 1, since this parameter had been evaluated in past research.

Gusset plate buckling was not an issue in any of the reference connections due to the lack of brace end clearance. Therefore, it was not investigated in NCBF1.

Shear yielding of the gusset plate at the gusset-to-beam weld could impact the system performance to some extent, but its DCR was dictated by the plate thickness and connection length, both of which were designed for more critical connection limit states.

Table 3.5 DCRs for Shared Shear Tab Connections

Limit State	NCBF1	86WA3A	92WA2A	Priority
Brace Net Section Fracture	1.26	1.07	1.25	Moderate
Brace-Gusset Plate Weld Fracture	0.92	1.25	1.42	Low
Brace Block Shear	1.14	0.64	1.09	Moderate
Gusset Plate Block Shear	1.16	0.86	0.97	Moderate
Gusset Plate Whitmore Yielding	1.33	1.14	1.62	High
Gusset Plate Buckling	0.74	0.45	0.64	Low
Gusset Plate Shear Yielding at Beam	1.16	0.54	0.57	Low
Beam-Gusset Weld Fracture	1.55	1.65	2.03	High
Shear Tab to Gusset/Beam Weld Fracture	1.08	0.64	1.42	High
Shear Tab to Column Weld Fracture	0.65	0.83	0.90	Moderate

As mentioned in Chapter 2, notch toughness requirements were not imposed on welds in brace frames prior to 1988. To emulate this, a weld electrode that did not meet demand-critical weld requirements was used for the NCBF specimens. The wire used met AWS specification E70-T7. However, due to a fabrication error, the gusset plate to beam and shear tab to column welds used E71-T8 electrodes, which did meet demand critical weld requirements. The errors are called out in Figure 3.2.3.

3.3 NCBF1-R1

NCBF1-R1 was designed as a repair of NCBF1. Despite connection deficiencies, NCBF1 failed at a low drift level due to the lack of brace compactness, as described in Chapter 5. To improve the seismic performance, NCBF1-R1 replaced the non-compact HSS7x7x1/4 brace with a HSS5x5x3/8 brace, which has similar cross sectional area and meets modern seismic compactness requirements. The brace replacement targeted two objectives:

- Determine if replacing a non-compact brace with a compact one can increase system ductility
- Evaluate the performance of the deficient connection under the larger deformation demands imposed by a more ductile brace.

NCBF1-R1 was identical to NCBF1 except for the brace replacement, and the detail is shown in Figure 3.4. This represents a possible repair to an existing system. By replacing the non-compact brace with a compact one, rate of brace degradation can be reduced, improving system ductility. The same splice length was used as in NCBF1 in order to avoid elevated concern with Whitmore yielding, brace-gusset weld fracture, and block shear. Ideally, a repair would increase the brace end clearance to meet modern requirements, but this was not possible given the dimensions of the existing gusset plate. Changing the brace type modified the DCRs for the connection slightly, as shown in Table 3.6. Most notably, changing to a seismically compact brace reduced net section and brace block shear deficiencies. A slight increase in the DCR for Whitmore yielding and gusset plate block shear occurred due to the narrower brace section.

Table 3.6 NCBF1-R1 DCR Changes

Limit State	**NCBF1**	**NCBF1-R1**
Brace Net Section Fracture	1.26	1.15
Brace-Gusset Plate Weld Fracture	0.92	0.92
Brace Block Shear	1.14	0.76
Gusset Plate Block Shear	1.16	1.33
Gusset Plate Whitmore Yielding	1.33	1.50
Gusset Plate Buckling	0.74	0.84
Gusset Plate Shear Yielding at Beam	1.16	1.16
Beam-Gusset Weld Fracture	1.55	1.55
Shear Tab to Gusset/Beam Weld Fracture	1.08	1.08
Shear Tab to Column Weld Fracture	0.65	0.65

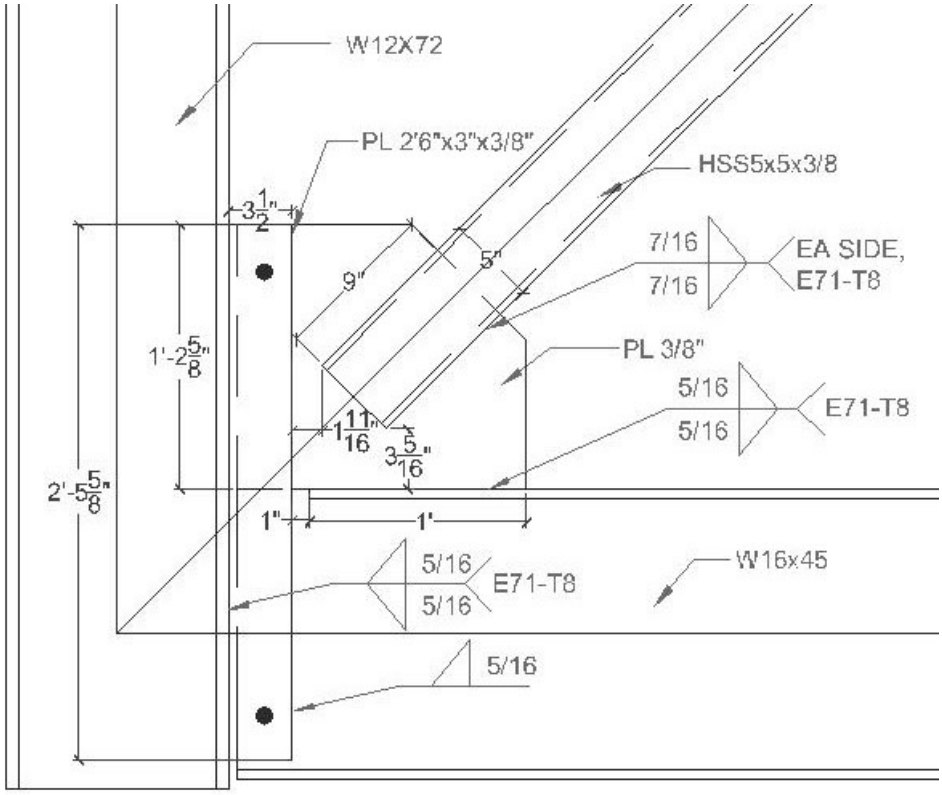

Figure 3.4 Connection Detail for NCBF1-R1

Because damage to the connections and frame was minimal for NCBF1, they were reused for NCBF1-R1. The gusset plates were heat-straightened, and minor weld damage was back-gouged and repaired. The fractured brace was removed and replaced with a seismically compact HSS5x5x3/8. This brace has almost the same cross-sectional area as the HSS7x7x1/4 (differ by only 1%), making it an ideal replacement because it maintains the lateral force capacity of the frame when the brace is in tension. The welds connecting the brace to the gusset plate used E71-T8 weld wire, since the brace attachment is a repair, which would use modern weld material.

3.4 NCBF1-R2

The design objectives and resulting design for NCBF1-R2 were very similar to NCBF1-R1 for three reasons: first, it was unclear if the performance of NCBF1-R1 was affected by existing connection damage from its use in NCBF1, as discussed in Chapter 5. Second, the tearing of the gusset-beam weld in NCBF1-R1 progressed slowly due to the use of a notch-tough weld, whereas a non-notch-tough weld

might have failed more rapidly. Finally, a data acquisition failure during the testing of NCBF1-R1 limited the usefulness of the test. One key difference, however, was that NCBF1-R2 represented a retrofit rather than a repair.

In considering these factors, NCBF1-R2 was fabricated with the same details as NCBF1-R1, but using new plates and welds in the connections, as shown in Figure 3.5. The columns were re-used because they sustained minimal damage. Additionally, the weld material used on the specimen was changed to E71-T11, which also does not meet demand-critical weld requirements. E70-T7 was found to be less viable for fabrication, since it can only be welded in the flat and downhand positions, whereas E71-T11 is an all position weld. The connection detail for NCBF1-R2 is shown in Figure 3.4.1, and the DCRs are identical to those for NCBF1-R1 which are shown in Table 3.6.

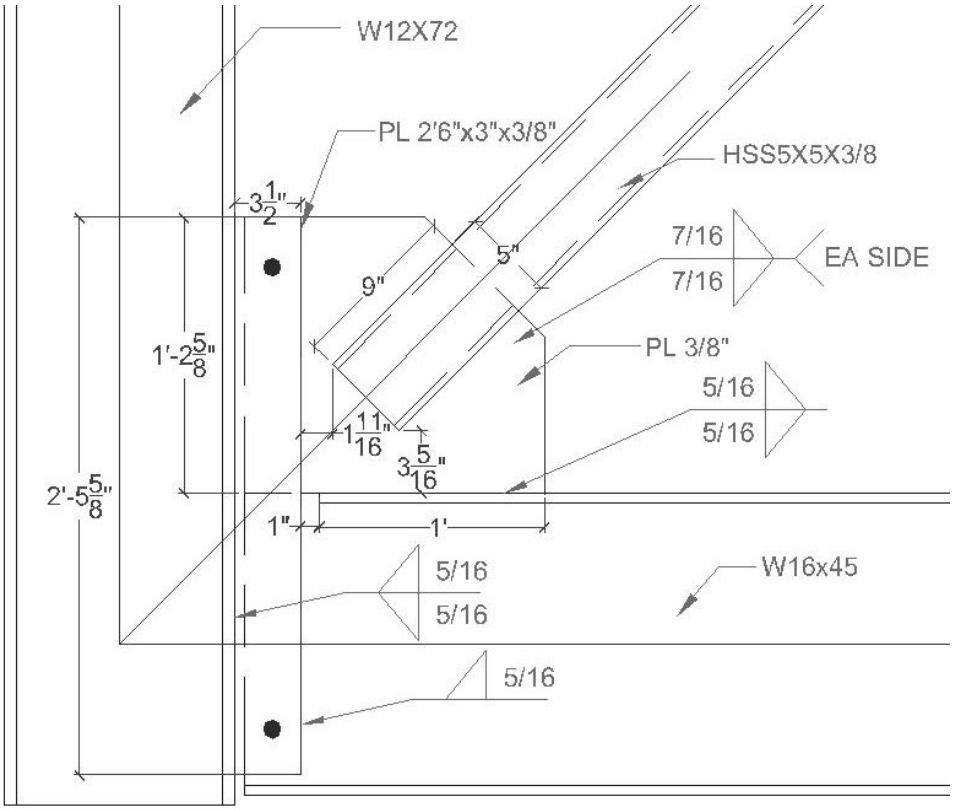

Figure 3.5 Connection Detail for NCBF1-R2

3.5 NCBF1-R3

NCBF1-R3 was designed to address shortcomings of NCBF1-R1 and NCBF1-R2. Both NCBF1-R1 and NCBF1-R2 suffered weld failures in the connection, as described in Chapter 5. These failures appeared to be at least partially related to the lack of brace end clearance and the large rotational demands on the gusset plate by out-of-plane brace buckling. NCBF1-R3 was designed to be a retrofit solution for connections like NCBF1 that reduces the rotational demands on the gusset plate while preserving the majority of the connection components, thereby minimizing the retrofit cost. To achieve this retrofit objective, NCBF1-R3 featured in plane brace buckling with a knife plate that was slotted and welded to the gusset plate, as shown in Figure 3.6. A gap between the gusset plate and the brace end provides a region for the knife plate to bend. This decreases the brace stiffness for in-plane buckling while increasing its stiffness for out of plane bucking. By using a brace that buckles in-plane, the rotational demands on the connection would be reduced and may prevent premature connection fracture.

Table 3.7 gives the DCRs for NCBF1-R3. The knife plate was designed from existing knife plate guidelines (Roeder et al 2012). These guidelines recommend that the expected yield capacity of the knife plate exceed the expected yield capacity of the brace, as described in Equation 3.5-1. The factor β is a balance factor, which for yielding is given a value of 1.0 (Roeder et al 2011).

$$\beta\left(R_y F_y A_g\right)_{kp} > \left(R_y F_y A_g\right)_{br} \tag{3.5-1}$$

The knife plate was also checked for block shear along the connection to the brace and the connection to the gusset plate using the equations from Chapter 2. In both cases, the area in shear in the knife plate was larger than the area in shear in the attached component, so the strength of the knife plate did not govern the strength of the connection. The knife plate was chosen to have a width less than that of the column flange, as a wider knife plate might interfere with non-structural elements in an existing building.

Table 3.7 DCRs for NCBF1-R3

Limit State	**NCBF1**	**NCBF1-R3**
Brace Net Section Fracture	1.26	1.21
Brace-Gusset Plate Weld Fracture	0.92	0.92
Brace Block Shear	1.14	0.76
Gusset Plate Block Shear	1.16	1.22
Gusset Plate Whitmore Yielding	1.33	1.28
Gusset Plate Buckling	0.74	0.70
Gusset Plate Shear Yielding at Beam	1.16	1.16
Beam-Gusset Weld Fracture	1.55	1.55
Shear Tab to Gusset/Beam Weld Fracture	1.08	1.08
Shear Tab to Column Weld Fracture	0.65	0.65
Knife Plate Yielding	///	1.04

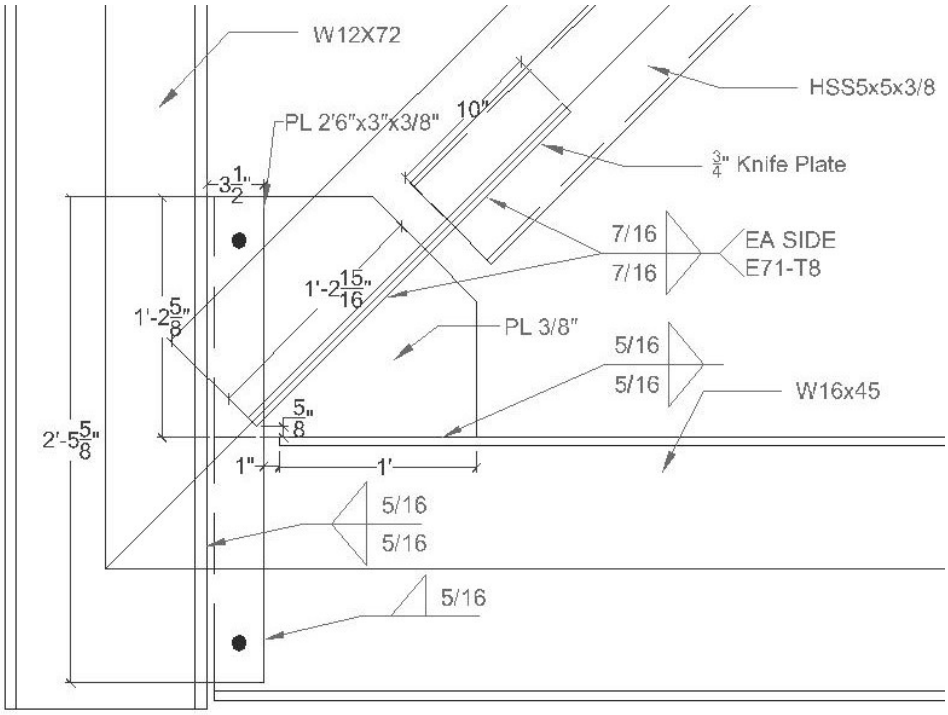

Figure 3.6 Connection Detail of NCBF1-R3

To check if in-plane buckling would occur, the buckling strength for both in-plane and out-of-plane buckling was calculated. For in-plane buckling, the length between the ends of the knife plates was used with an effective length factor, K, of 1.0. Because the knife plate extended so far into the connection and likely increased the fixity of the brace ends, an effective length factor of 0.75 was used for computing the out of plate buckling length. For in-plane buckling, the true brace length was used. Based on these values, in-plane buckling was predicted to occur at a lower axial load than out-of-plane buckling. A summary of the calculated values is given in Table 3.8.

Table 3.8 Buckling Calculations for NCBF1-R3

	Out-of-Plane	In-Plane
L (ft)	14.86	12.00
K	0.75	1.00
Fy (ksi)	50.00	50.00
Ry	1.40	1.40
KL/r	71.54	77.01
Fe (ksi)	55.92	48.27
Fcr (ksi)	34.39	32.41
Pc (kip)	-212.54	-200.29

3.6 NCBF1-R4

NCBF1-R4 was a second in-plane buckling retrofit designed to address the shortcomings of NCBF1-R3, discussed in Chapter 5, since NCBF1-R3 did not achieve its objective of investigating the effectiveness of in-plane buckling at protecting the connection. Thus, that objective was again addressed in NCBF1-R4. NCBF1-R4 used an HSS6x4x3/8 brace, which has the same cross-sectional area as the HSS5x5x3/8. By using a brace with a weak axis, the likelihood of in-plane buckling was increased significantly. Table 3.9 gives the buckling calculations for NCBF1-R4. The effective length factor for out-of-plane buckling was increased from 0.75 to 1 to give a more conservative estimate based on the outcome of NCBF1-R3.

Table 3.9 Buckling Calculations for NCBF1-R4

	Out-of-Plane	In-Plane
L (ft)	14.46	12.00
K	1.00	1.00
Fy (ksi)	50.00	50.00
Ry	1.40	1.40
KL/r	81.07	93.08
Fe (ksi)	43.54	33.04
Fcr (ksi)	30.92	26.54
Pc (kip)	-191.09	-164.00

The knife plate for NCBF1-R4 was also shortened relative to NCBF1-R3, as shown in Figure 3.7. In NCBF1-R3, weld tearing in the shear tab initiated near the end of the knife plate, which was lapped over the gusset plate to shear tab weld, shown in Figure 3.8 as a dashed line. In an effort to reduce strain concentrations around the welds and thus avoid premature weld tearing, the knife plate was shortened, removing the portion of the knife plate bordered by the dashed line in Figure 3.8. As a result of this shortening, the DCRs for gusset plate limit states increased. Notably, Whitmore yielding and gusset plate block shear both had DCRs greater than 1.75. The DCRs for NCBF1-R4 are given in Table 3.10.

Table 3.10 DCRs for NCBF1-R4

Limit State	**NCBF1**	**NCBF1-R4**
Brace Net Section Fracture	1.26	1.16
Brace-Gusset Plate Weld Fracture	0.92	0.92
Brace Block Shear	1.14	0.76
Gusset Plate Block Shear	1.16	1.78
Gusset Plate Whitmore Yielding	1.33	1.89
Gusset Plate Buckling	0.74	1.03
Gusset Plate Shear Yielding at Beam	1.16	1.16
Beam-Gusset Weld Fracture	1.55	1.55
Shear Tab to Gusset/Beam Weld Fracture	1.08	1.08
Shear Tab to Column Weld Fracture	0.65	0.65
Knife Plate Yielding	///	1.04

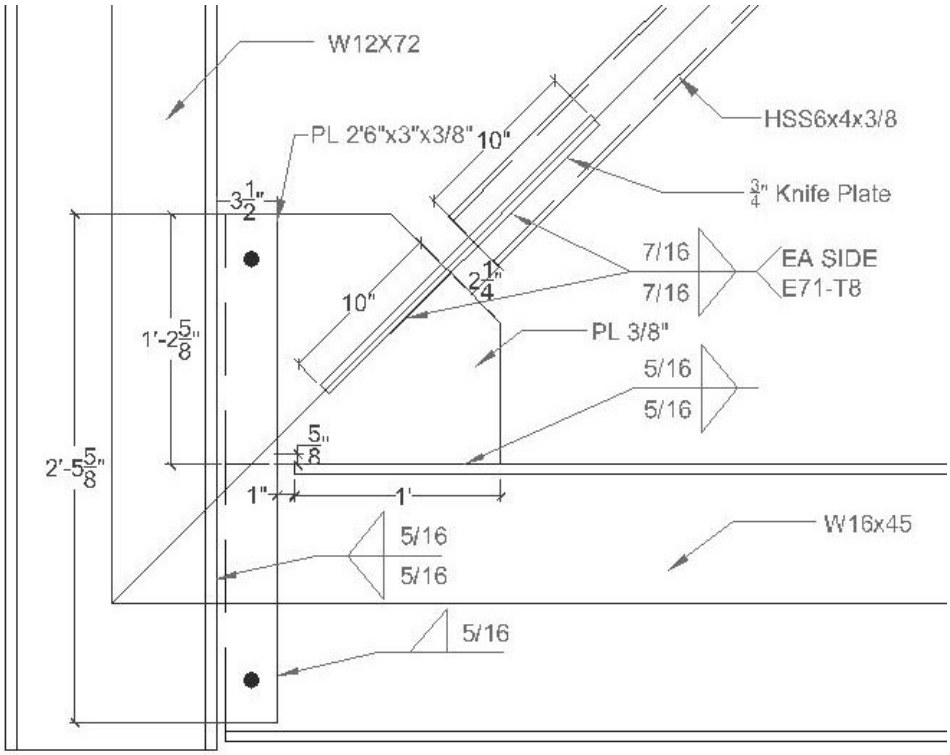

Figure 3.7 Connection Detail for NCBF1-R4

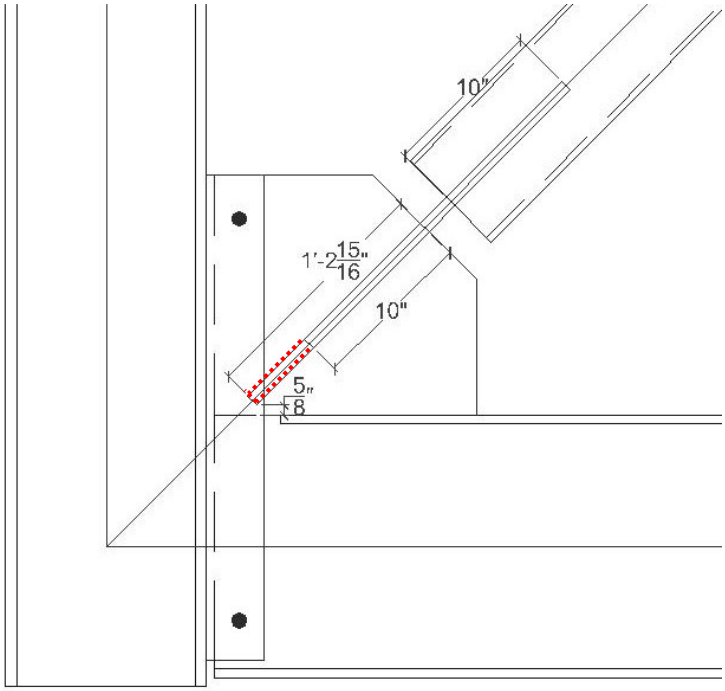

Figure 3.8 Shortened Knife Plate Length for NCBF1-R4

3.7 NCBF1-R5

NCBF1-R5 sought to address two of the largest shortcomings of NCBF1, the brace that did not meet modern compactness requirements and the vulnerability of the shear tab weld, using straightforward and inexpensive retrofits. The non-compact brace, which led to premature brace fracture, was filled with concrete to delay local buckling. The shear tab weld, which failed in all other retrofit specimens, was reinforced with high-strength bolts. The retrofitted connection is shown in Figure 3.9.

Filling the brace with concrete can delay the onset of local buckling and reduce its severity (Liu et al 1988). To fill the brace, the frame was placed in the vertical position, as it would be in an existing structure. A plywood block-out was placed in the end of the brace to prevent concrete from flowing out of the brace at the bottom. The plywood also ensured a 3 inch gap between the concrete fill and the edge of the gusset plate. This was done to ensure that the concrete did not contact the gusset plate during the test. By preventing this contact, the amount of axial load taken by the concrete was reduced, because any axial load would instead have to be transferred by bond strength between the tube and the concrete. Increased compressive brace capacity was not the objective of this test because it would increase demands on the connection, so avoiding a sharp increase in buckling capacity was desirable. High-slump concrete was poured into the opening at the top of the brace and flowed down the length of the brace. The brace was vibrated with rubber mallets to ensure proper consolidation. A 3 inch gap between the concrete and the gusset plate was also created at the top corner.

Since reducing rotational demands was not sufficient, as demonstrated by weld failure in NCBF1-R4, bolts were added to the shear tab as a backup load resisting mechanism. The bolts were sized to carry the vertical component of the brace force (assuming no eccentricity) in the absence of the weld. The bolts are inherently more flexible than the welds, so it was not expected that they would act together. The bolts were intended as a backup system, which also clamped the shear tab to the gusset plate and the beam and provided some rotational restraint to the weak gusset plate. Prior to weld tearing in previous tests, the shear tab was sometimes observed to rotate relative to the beam and gusset plate, which could have contributed to fracture.

Table 3.11 shows the DCRs for NCBF1 and NCBF1-R5. Note that the capacities listed for bolt shear, bearing, and slip were computed assuming no load was taken by the weld. The bolts were not designed to be slip critical, but the slip strength value gives a concept of how much strength the bolts might contribute before weld fracture. The block shear strength of the shear tab was calculated because of the reduction in

area resulting from the loss of bolts. The reduced area was still capable of resisting the expected demand. The other DCRs are unchanged, as no modification was made to the brace-to-gusset connection.

Table 3.11 Bolt Limit States for NCBF1-R5

Limit State	**NCBF1**	**NCBF1-R5**
Brace Net Section Fracture	1.26	1.26
Brace-Gusset Plate Weld Fracture	0.92	0.92
Brace Block Shear	1.14	1.14
Gusset Plate Block Shear	1.16	1.16
Gusset Plate Whitmore Yielding	1.33	1.33
Gusset Plate Buckling	0.74	0.74
Gusset Plate Shear Yielding at Beam	1.16	1.16
Beam-Gusset Weld Fracture	1.55	1.55
Shear Tab to Gusset/Beam Weld Fracture	1.08	1.08
Shear Tab to Column Weld Fracture	0.65	0.65
Bolt Shear	NA	0.98
Bolt Bearing	NA	0.66
Block Shear	NA	0.86
Bolt Slip	NA	3.07

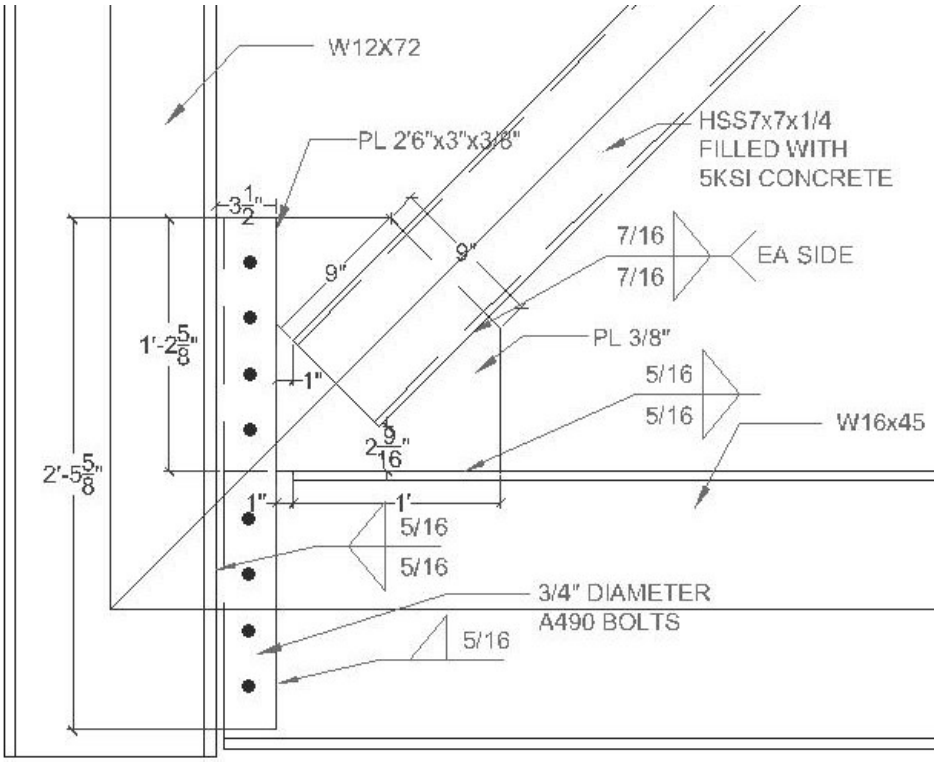

Figure 3.9 Connection Detail for NCBF1-R5

Chapter 4: Test Setup

4.1 Introduction

This chapter provides a summary of the experimental setup utilized for experiments at the University of Washington structural engineering laboratory. The test setup was originally constructed in 2005 for a series of single story, single bay braced frame tests (Johnson 2005), but was partially dismantled in 2010. This setup was reassembled with minor modifications to the out-of-plane restraint system in 2013 for this test program. This chapter describes the experimental configuration in general (Section 4.2) and the instrumentation used for monitoring and recording system behavior (Section 4.3).

4.2 Overview of Experimental Configuration

This section provides on overview of the experimental setup used for the tests. Details on the components of this setup can be found in Appendix C.

The experimental configuration at the University of Washington recreates as accurately as possible the loading and boundary conditions experienced by a single bay braced frame in a multistory structure. The focuses of study for the frames are the gusset plates and brace, as well as the post-fracture residual system stiffness. As such, the focus of the experimental setup is to provide the most realistic conditions for those components.

Figure 4.1 provides an annotated photograph of the experimental setup and Figure 4.2 provides an annotated schematic of the setup. The dimensions of components of a typical frame and the experimental setup are provided in Figure 4.3.

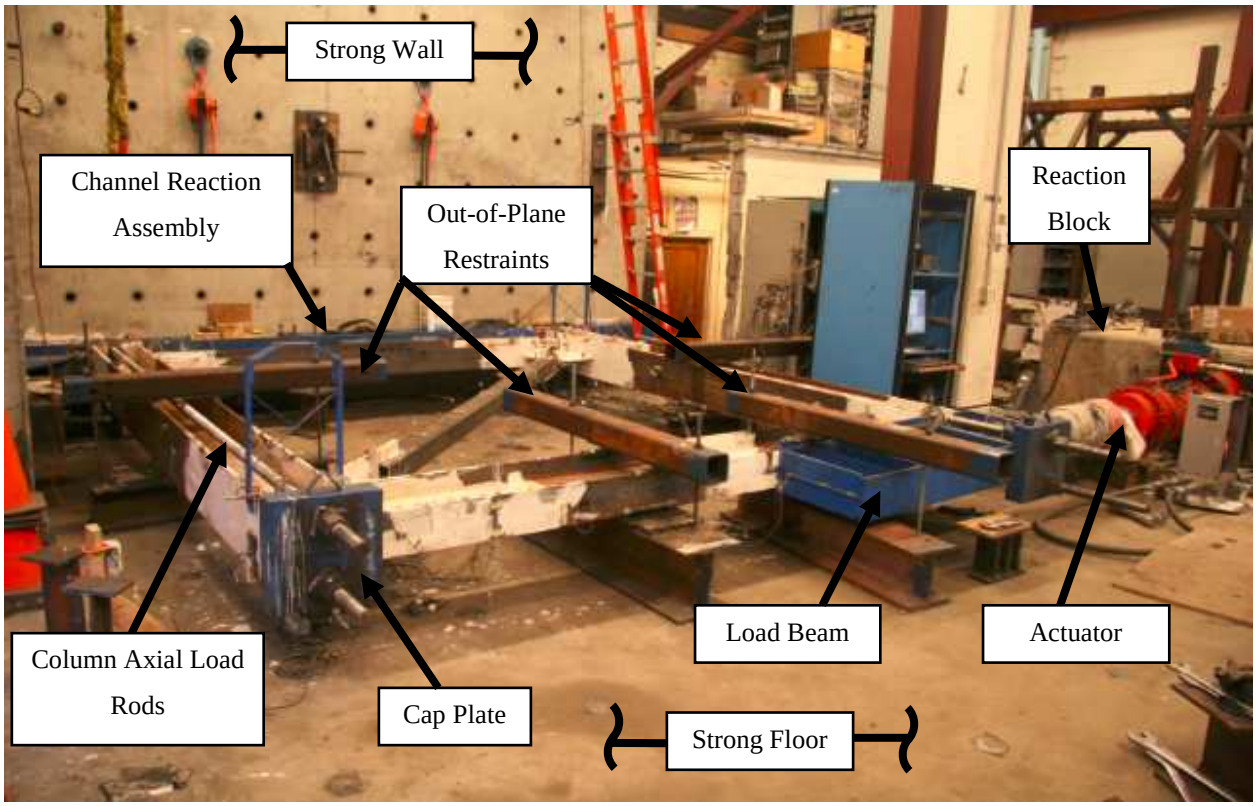

Figure 4.1 Overview of Test Setup

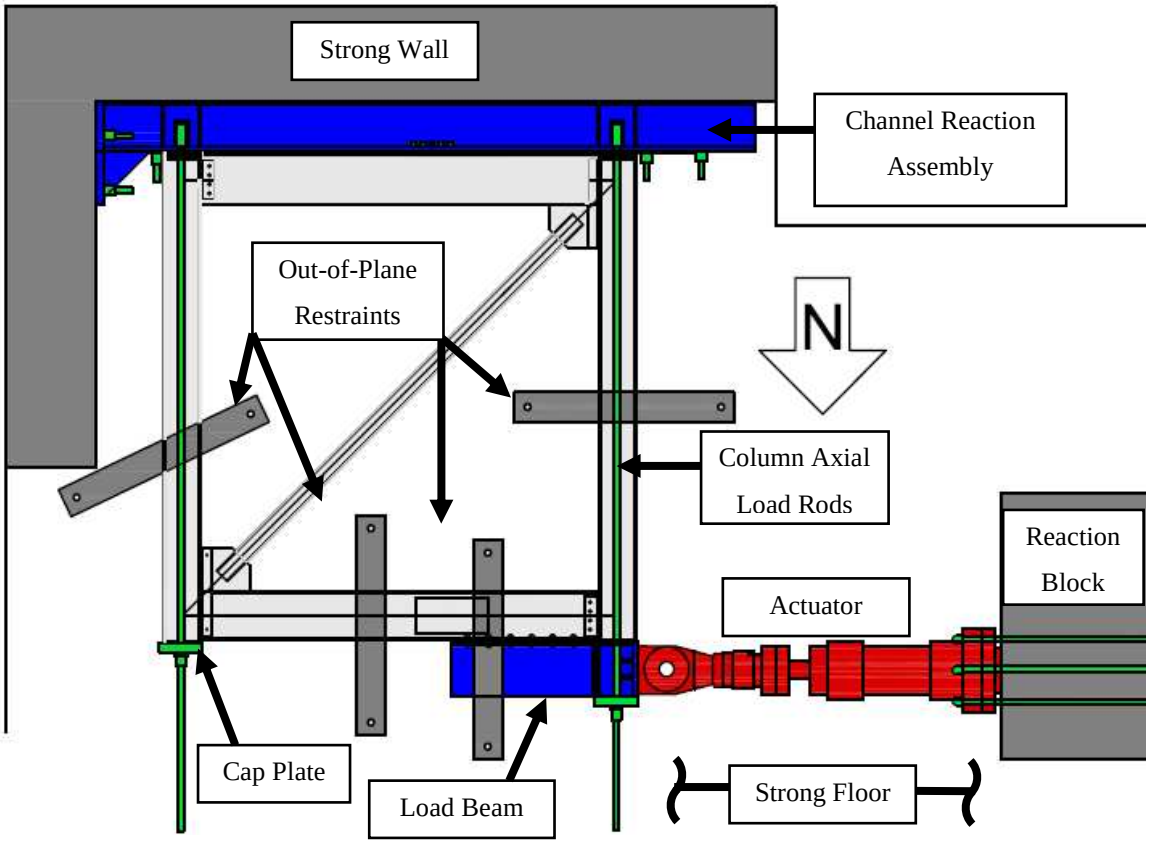

Figure 4.2 Test Setup Schematic

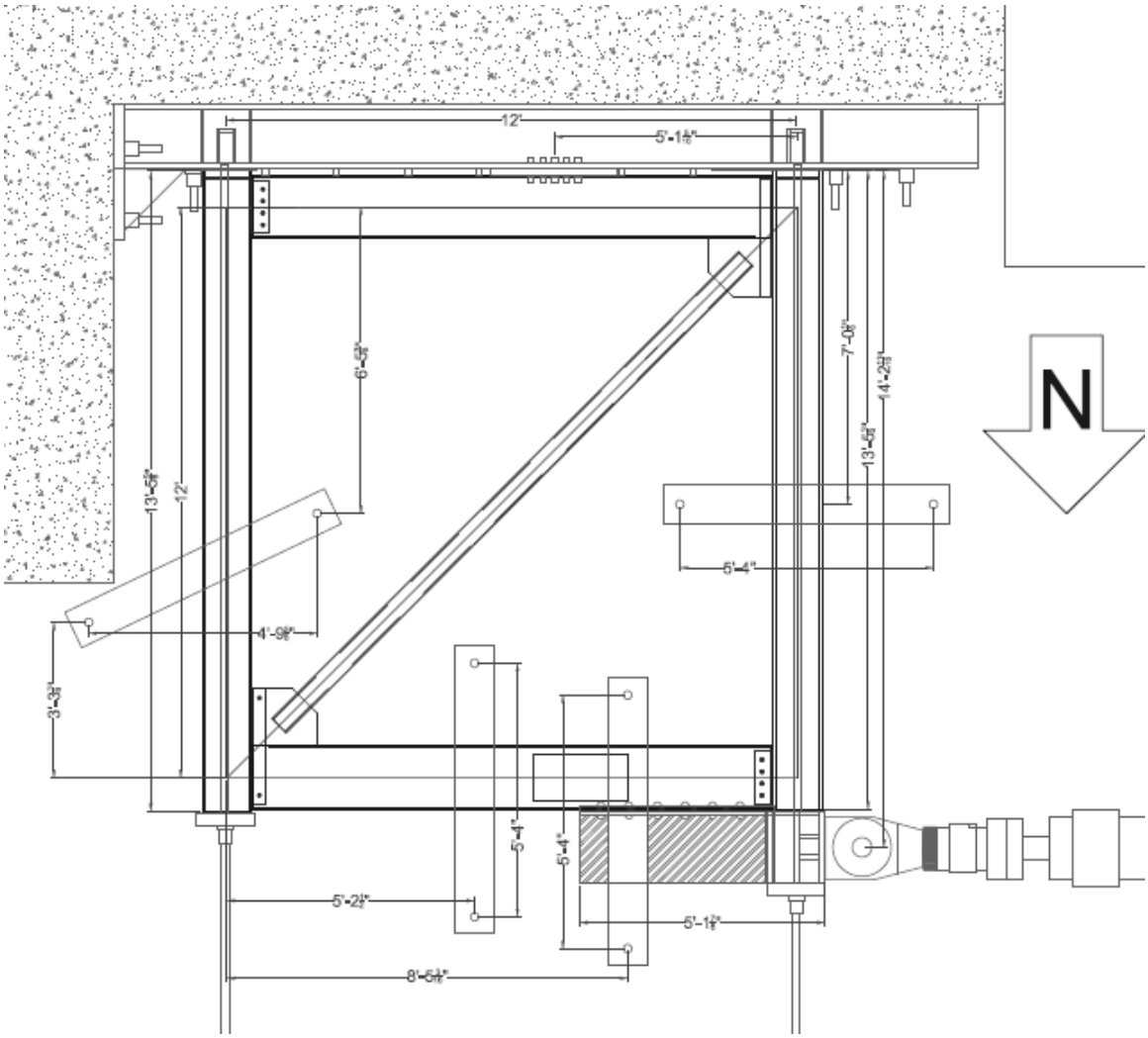

Figure 4.3 Typical Frame Dimensions

The load path through the experimental system is intended to recreate the load path typical of a braced frame in a structure. Displacement controlled load is applied using an MTS actuator with a capacity of 470 kips when pushing and 330 kips when pulling. Displacements were gradually applied, cyclic, and monotonically increasing. The load protocol for each specimen can be found in Chapter 5.

Pretensioned rods attach the actuator base to the reaction block, which provides reaction force for the actuator. The reinforced concrete reaction block is pretensioned to the strong floor with high strength threaded rods. A hydrostone layer between the reaction block and the strong floor provides a continuous contact surface to prevent sliding.

The actuator head is attached to a swivel, which prevents bending moments from transferring between the frame and the actuator. This swivel is bolted to the load beam. Which rests on the top of the West column as well as the North flange of the North beam over part of its length. The load beam is attached to the North flange of the North beam via 10 high-strength bolts, which transfer the actuator load via shear.

The reaction for the shear force and overturning moments on the frame is provided at the South end. The channel assembly provides a bearing surface for the South end of both columns. Additionally. it is fastened to the South flange of the South beam with 10 high-strength bolts, which transfer shear load from the frame to the reaction assembly. The channel assembly is attached to the strong wall with pretensioned rods, providing rigid support for the base of the frame.

In order to prevent uplift of the columns and to simulate gravity load from the structure, axial load was applied to the specimen using high-strength pretensioned rods. Two rods for each column applied a total of 450 kips of compressive axial load.

In order to prevent out-of-plane moment of the beams and columns, sliding out-of-plane restraints were placed at four locations on the specimen, as seen in Figure 4.3. The configuration of these restraints was changed slightly from the original experimental setup. A schematic of a typical restraint is shown in Figure 4.4, and an image of one is shown in Figure 4.5. The locations of the restraints remained the same, but all top restraints were changed to HSS5x5x3/8 sections, and some of the rod spacings were adjusted to improve accessibility.

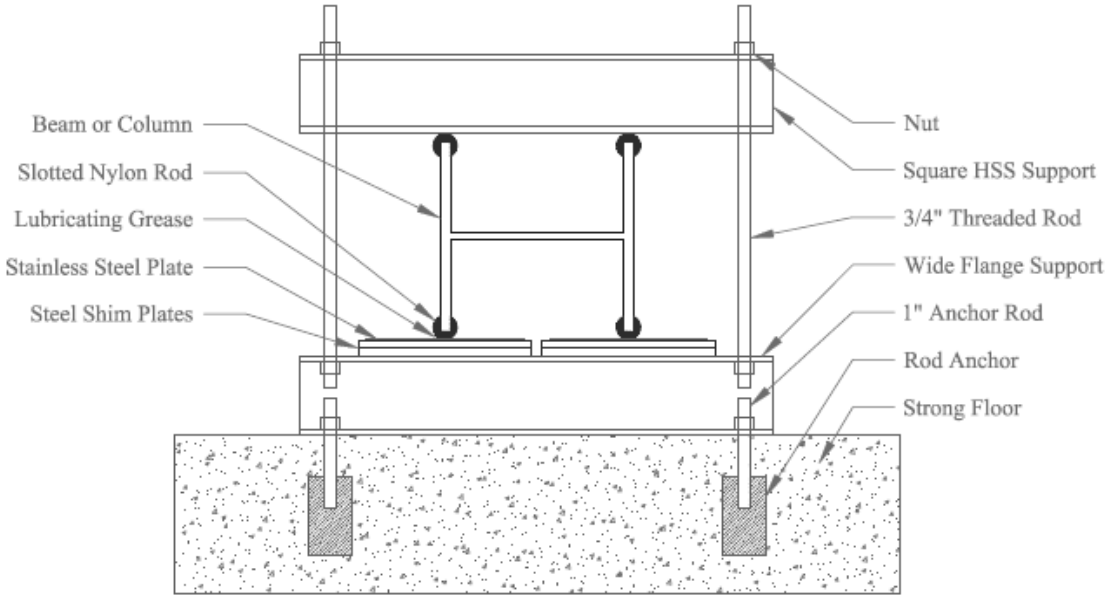

Figure 4.4 Out-of-Plane Restraint Schematic

Figure 4.5 East Column Out-of-Plane Restraint

4.3 Instrumentation

4.3.1 Data Acquisition Systems

The potentiometers and strain gauges were controlled using LabVIEW version 7.1 on a PC designated for data acquisition. Instrument gain factors were computed and input into the LabVIEW interface to convert

measured voltages to strains or displacements. Values from instruments were recorded twice per second and stored in delimited output files. The National Instruments hardware used for this data acquisition system included SCXI 1001 Chassis, SCXI 1100 and SCXI 1300 modules for potentiometers, and SCXI 1121 and SCXI 1321 modules for strain gauges. A Hewlett Packard E3611A DC Power supply provided constant voltage power for data acquisition.

The Optotrak position sensors and markers were attached to the Optotrak System Control Unit, which fed information to a personal computer designated for use with the system. NDI First Principles software was used to control the data acquisition. Data was recorded twice per second and stored in delimited output files.

4.3.2 Strain Gauges

All strain gauges used for these tests were Tokyo Sokki Kenkyuho Co. Ltd. FLA-6-11-5L model. These strain gauges are uniaxial with a 6mm gauge length and a nominal gauge factor of 2.12. Their accuracy is reported as reliable for the strain range$\pm$0.05. In conjunction with stress-strain material data obtained from coupon tests, the strain gauge measurements were used to calculate axial loads, shears forces, and bending moments in the system components.

To ensure adhesion between the strain gauge and steel surface, the following procedure was used. The steel surface was belt sanded with fine grit sandpaper to remove rust and mill scale, exposing the clean steel beneath. Three rotations of acid and base were each applied to the steel surface, which was then sanded fine grit sandpaper, followed by a washing and drying with distilled water. The strain gauge was then attached to transparent adhesive tape aligned with the steel member axes in the prepared area. Tokyo Sokki Kenkyuho Co. Ltd. strain gauge glue was applied to the underside of the strain gauge, and the gauge was placed on the surface under sustained pressure for 3 minutes. Protective epoxy was painted over each gauge and then covered in electrical tape. The ends of the gauges wires were attached to the appropriate strain modules. Strain gauge resistances were recorded and input into the LabView data acquisition interface.

The typical strain gauge layout is shown in Figure 4.6, and the strain gauge purposes are shown in Table 4.1. Strain gauge layouts for each specimen are given in Appendix B. The column gauges were placed in pairs at two locations along the column length. These locations were chosen to be sufficiently far apart to allow for accurate calculation of column shear force, but also sufficiently far from connection regions

where yielding might occur, as large strains can make readings inaccurate. The beam gauges were also placed sufficiently far from the connection and load beam to ensure no yielding occurred at the gauge locations. The brace gauges were placed at the quarter point on the brace. The brace may yield along most of its length, but local deformations are most likely at the center and the ends, so the gauges were placed sufficiently far from these locationss. With this set of strain gauges, it is possible to compute the complete load path through the frame, making them a valuable tool for evaluating system performance.

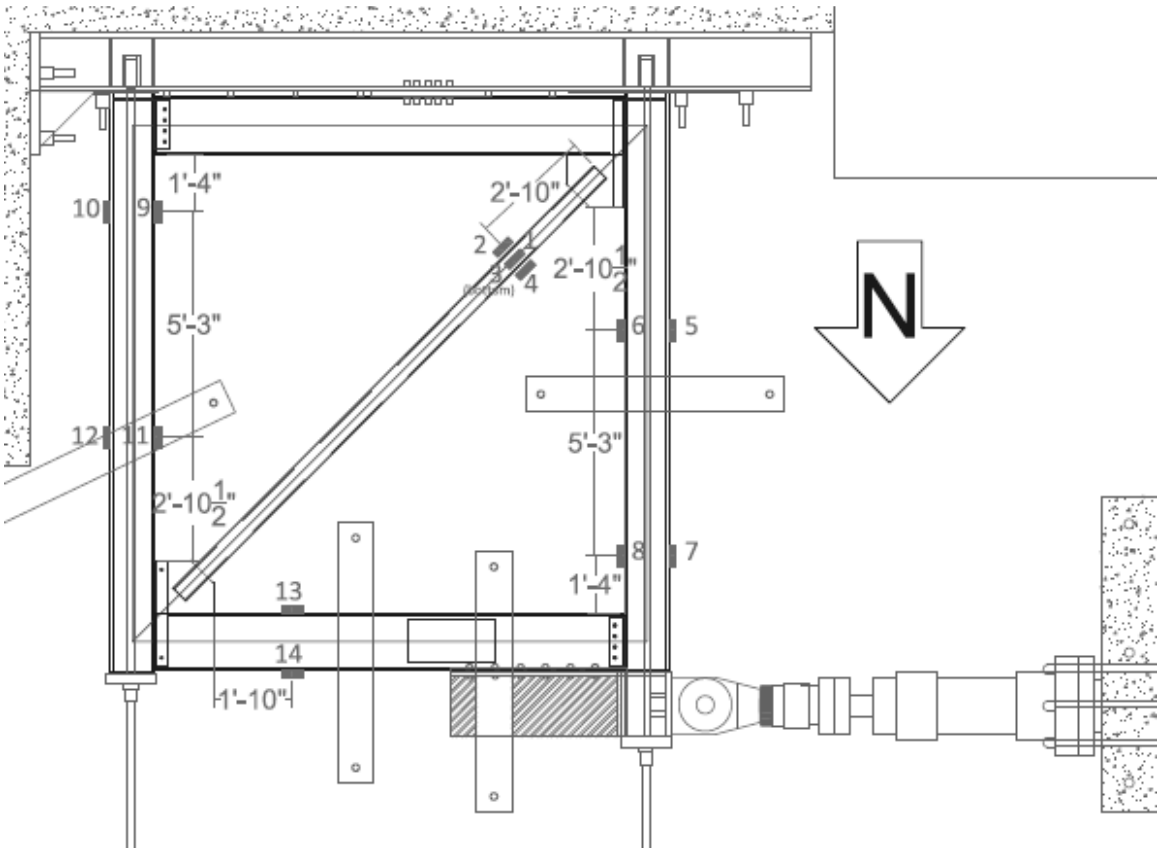

Figure 4.6 Typical Strain Gauge Layout

Table 4.1 Strain Gauge Assignments

Channel Group	Number	Purpose
Brace	1-4	Brace Axial Force
Columns	5-8	West Column Axial Load, Shear, and Moment
	9-12	East Column Axial Load, Shear, and Moment
Beams	13-14	North Beam Axial Load and Moment

4.3.3 Potentiometers

Three types of potentiometers were used to measure specimen absolute and relative displacements. For displacements larger than 3 inches, UniMeasure model P510 string potentiometers were used. These were necessary for measuring absolute displacements of the North half of the frame, because lateral displacements of the frame typically reach ±5 inches during testing. BEI Duncan linear conductive potentiometers were used for displacements smaller than 3 inches, with the 9600 Series models used for displacements between 1 and 3 inches, and the 600 Series models used for displacements smaller than 1 inch. Examples of the three potentiometer types are shown in Figure 4.7.

Figure 4.7 Potentiometers (a) Unimeasure P510 (b) BEI Duncan 9600 (c) BEI Duncan 600

Figure 4.8 shows the typical potentiometer layout for the frame, and Figure 4.9 shows the typical potentiometer layout for the reaction block. A description of the instrument purposes is given in Table 4.2. Complete potentiometer layouts for each specimen are given in Appendix B. The global specimen measurements were designed to capture the load-drift behavior of the system. Three different measures of the lateral drift were taken, although the frame diagonal is considered to be most accurate, as described in Chapter 6.

Brace axial elongation was measured to determine its contribution to the total diagonal elongation of the frame. The out-of-plane mid-span deflection of the brace was also measured, as it correlates strongly with brace and connection damage.

Measurements of the rotations of the beams and columns at the edges of the gusset plates were taken, as plastic hinges most often form at these locations, and the magnitude of these rotations is important for quantifying beam and column performance.

Numerous potentiometers were also placed to monitor slip, out-of-plane movement, and uplift of test setup components. These instruments were intended to capture possible movements that could substantially affect the system performance. The majority of these instruments measure lateral slip along the system load path, which causes the drift experienced by the frame the be smaller than the drift applied by the actuator. Instruments at the column bases monitor column uplift, which can occur if the actuator load overcomes the column compressive load. Finally, potentiometers at the work points monitor the out-of-plane displacement, which should be small due to out-of-plane restraints, but can be affected by connection damage and brace out-of-plane buckling.

Table 4.2 Potentiometer Assignments

Channel Group	Number	Purpose
Global	1	Actuator Load
	2	Actuator Displacement
	4,5	Elongation of Frame Diagonal
	7	Lateral Frame Displacement
Brace	6	Elongation of Brace
	8	Brace Midspan Deflection
Framing Members	9,10	Beam Plastic Hinge Rotation
	11,12	Column Plastic Hinge Rotation
	13-16	Shear Tab Connection Rotation
	17-20	Work Point Out-of-Plane Displacement
Slip Monitors	21-22	West Column Uplift
	23	West Column Slip
	24-25	East Column Uplift
	26	East Column Slip
	27-28	Channel Assembly Uplift
	29	Channel Assembly Slip
	30	South Beam Slip
	31	North Beam Slip
	32-33	Actuator Base Slip
	34-36	Reaction Block Slip

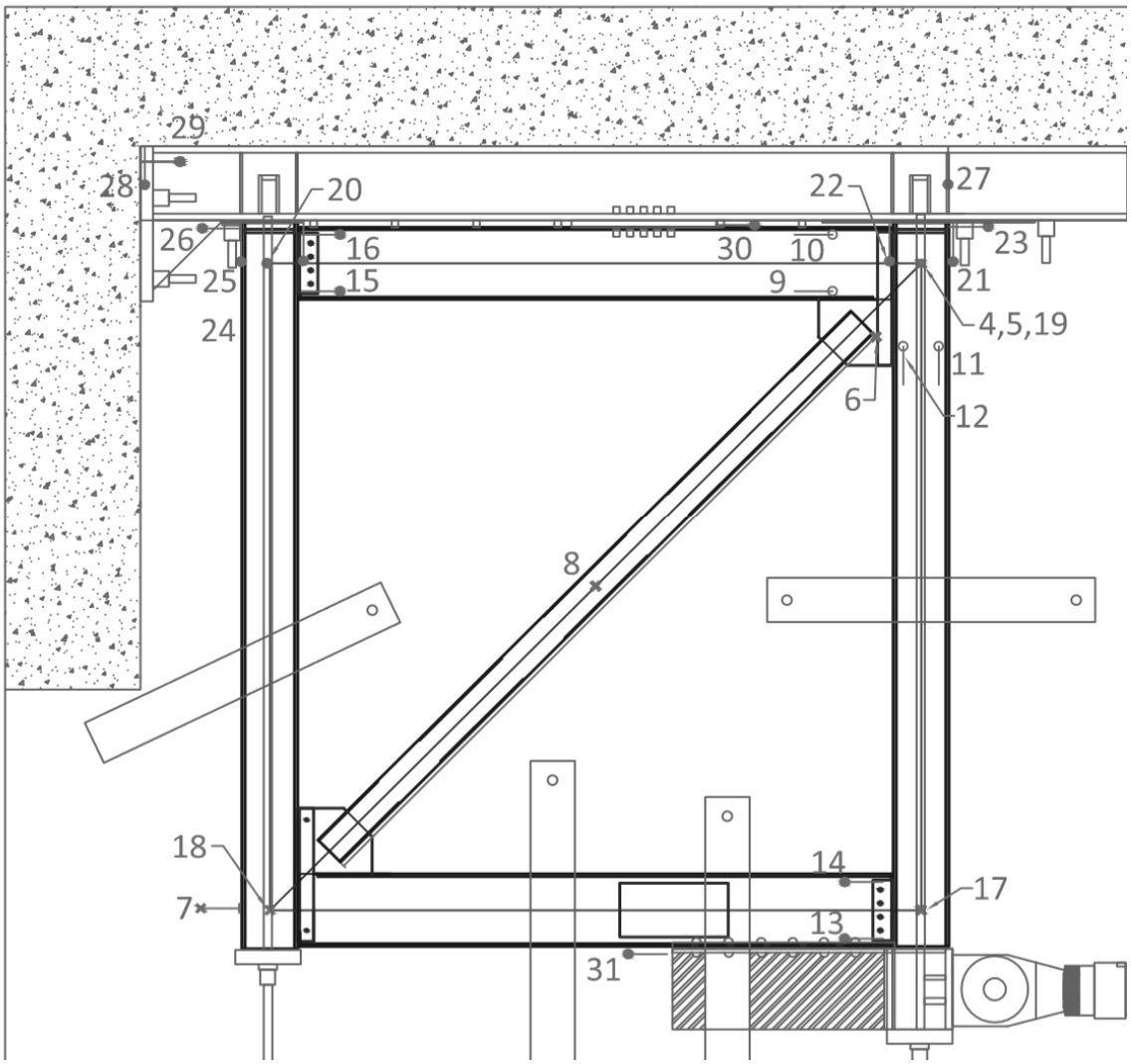

Figure 4.8 Typical Potentiometer Layout - Frame

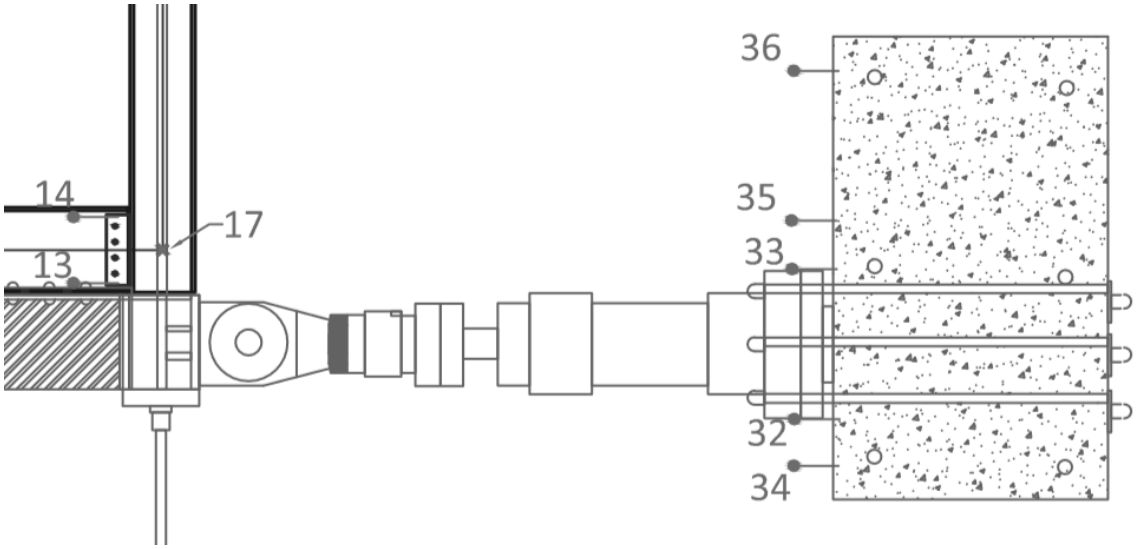

Figure 4.9 Typical Potentiometer Layout - Reaction Block

4.3.4 Optotrak LEDs

To record the precise three-dimensional position of frame components, the NDI Optotrak Certus System was employed. The system uses position sensors, which are arrays of three infrared cameras. These sensors detect light from infrared LEDs, called markers, which are placed on the specimen. The Optotrak system records x,y,z coordinates with 0.001mm of precision. The accuracy of these measurements is dependent on a number of factors. In particular, the further the position sensor is from a marker, the less reliable the measurements are. However, accuracy can be improved substantially by using multiple position sensors with a shared coordinate systems, as was done for this test series. These measurements are generally reliable to a precision of 0.1mm or better.

The two position sensors used in this test were mounted on the strong wall order to provide the largest shared viewing area of the frame, as shown in Figure 4.10. Due to space limitations, it was not possible to view the entire frame with the position sensors. The configuration used was able to capture the majority of the brace length, the Northeast connection, and portions of the adjacent beam and column. Figure 4.11 shows the viewable area of each position sensor on the specimen, and Figure 4.12 shows the viewable volume schematic for the position sensors.

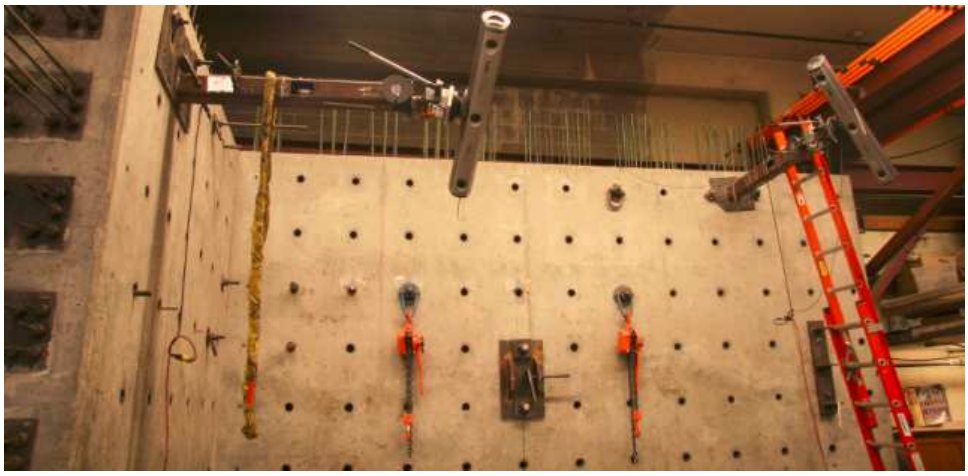

Figure 4.10 Optotrak Position Sensors Mounted on Strong Wall

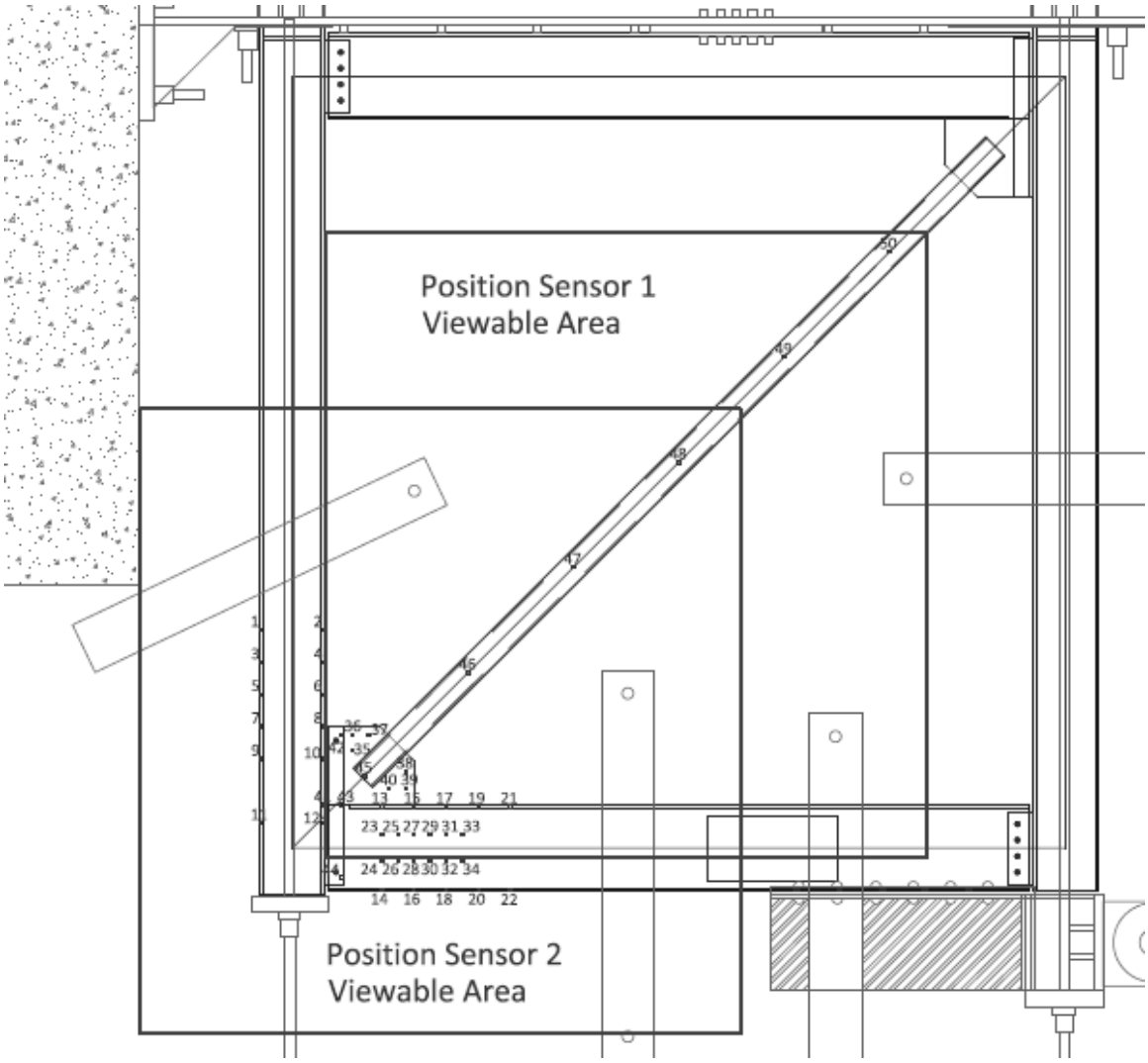

Figure 4.11 Optotrak Position Sensor Viewable Area

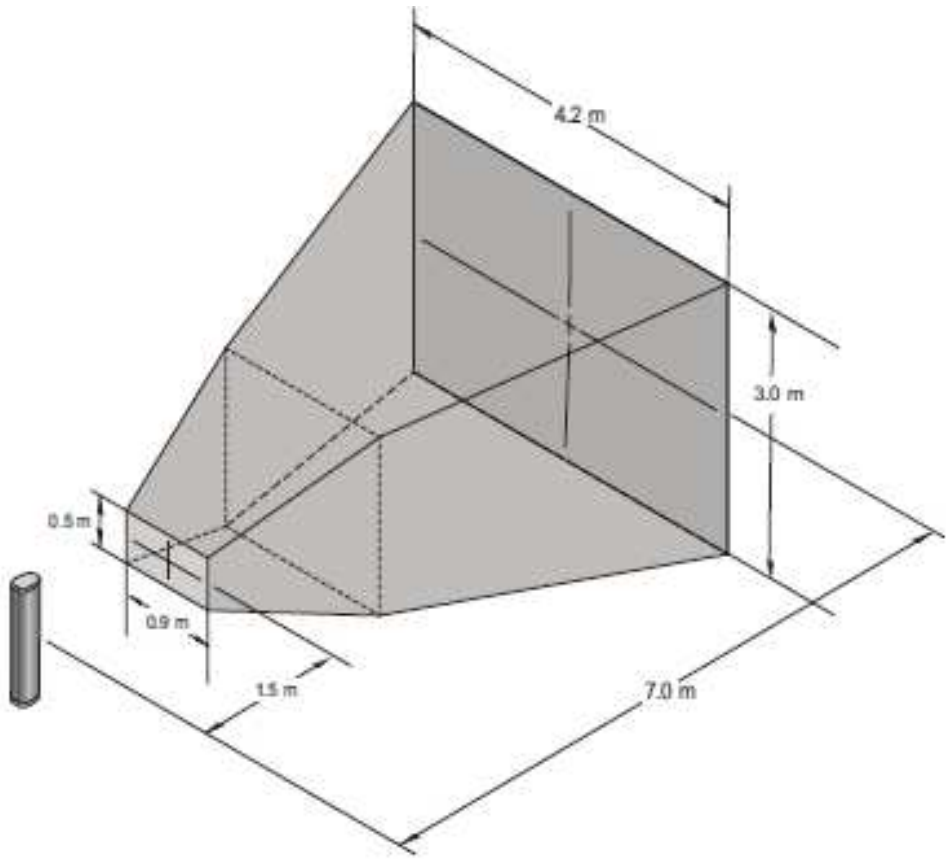

Figure 4.12 Position Sensor Viewable Area (NDI Manual)

Markers were placed to capture both absolute and relative movement of the specimen. In many cases, markers were placed to duplicate the measurements of physical sensors in order to provide a basis for comparison and verification of results from the two systems. Figure 4.13 and Figure 4.14 show a photo and a schematic, respectively, of the typical marker layout on the specimen. Table 4.3 gives the location and purpose of each of the sensors shown in Figure 4.13.

Markers on the beam and column flanges were intended to provide data on the in-plane and out-of-plane movement and rotation of the beams and columns, as well as to identify locations of local buckling. Markers on the gusset plate and shear tab were used to compute the out-of-plane movement and rotation. The brace markers captured the out-of-plane and in-plane bucked shape of the brace

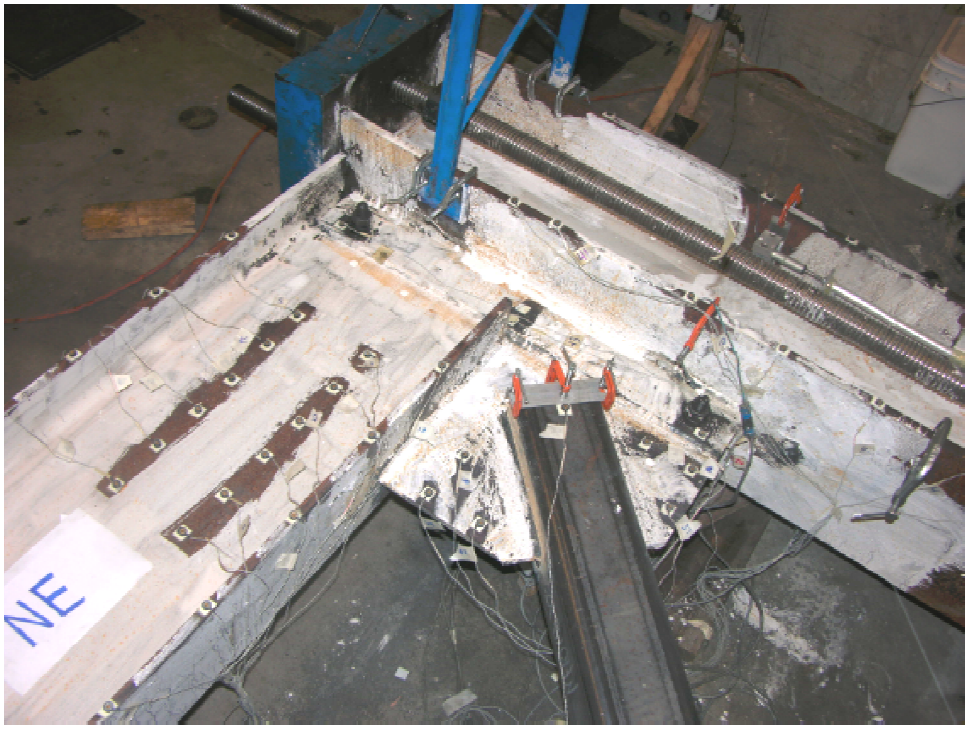

Figure 4.13 Optotrak Markers on Northeast Connection

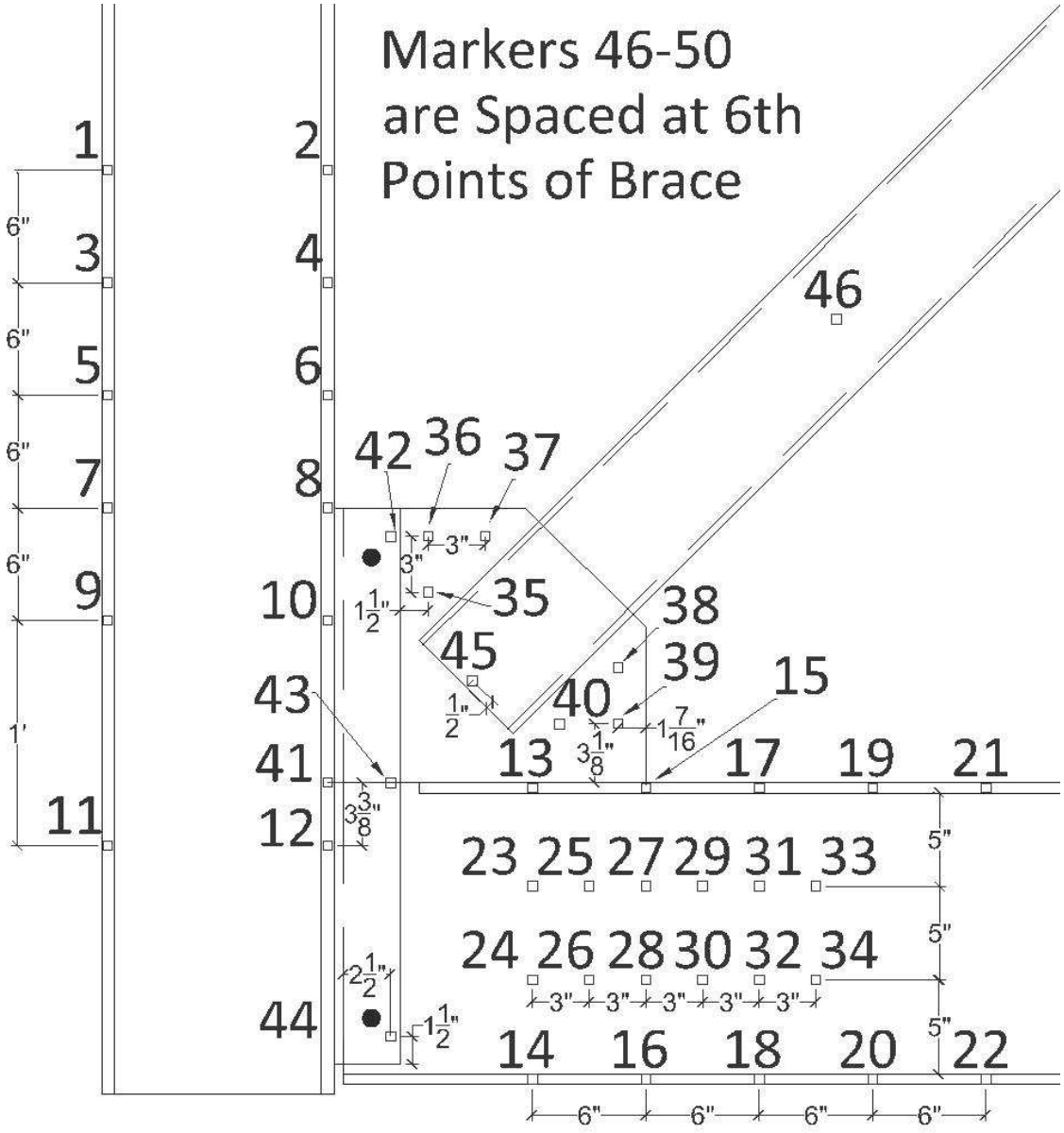

Figure 4.14 Optotrak Marker Layout Schematic

Table 4.3 Optotrak Marker Locations

Sensors	Location	Purpose
1,3,5,6,9,11	East Column, East Flange	Column Movement and Rotation
2,4,6,8,12,41	East Column, West Flange	Column Movement and Rotation
13,15,17,19,2	North Beam, South Flange	Beam Movement and Rotation
14,16,18,20,2	North Beam, North Flange	Beam Movement and Rotation
23-34	North Beam Web	Local Deformation of Beam Web
35-40	North Gusset Plate	Gusset Plate Out-of-Plane Movemnt
42,43,44	North Shear Tab	Shear Tab Out-of-Plane Movement
45-60	Brace	Brace Movement and Rotation

4.3.5 Visual Observations

To supplement information acquired from the data acquisition systems, visual observations and photographs were used. To aid visual observations, areas of each specimen where damage was expected were coated in a whitewash mixture consisting of a 4:1 ratio of water and Hydrostone. This mixture coated the mill scale on the steel and dried into a white paint-like coating. When yielding occurs in the steel members, the mill scale and whitewash flake off, providing a sharp visual contrast that helps to identify yield patterns.

At each peak actuator displacement, a photograph was taken of a whiteboard which identified the test, current cycle number, and displacement. This allowed for accurate filing of photographs so they could be attributed properly. Visual observations were recorded on a laptop computer along with cycle information and key values read from the data acquisition system.

4.4 Load Protocol

A monotonically increasing, cyclic displacement history was applied using the actuator LDVT. The actuator displacements were controlled from a personal computer using FlexTest software. At each peak displacement, the FlexTest software was used to pause the loading protocol, allowing time to record observations and take photographs. The loading protocol was then resumed and continued to the next peak displacement. The load history completes 2 cycles at each displacement level. The displacement increases in 1/8 inch increments until a peak displacement of 1 inch. It is then incremented by 1/4 inch until 1 1/2 inches of displacement, and at 1/2 inch increments thereafter until failure. For typical specimens, the expected displacement at yield is 5/8 inches (Kotulka 2007), which corresponds to the

fifth imposed displacement level in this load history. The displacement history is shown in Figure 4.15, ad a table of displacements is given in Table 4.4.

In order to ensure pseudo-static conditions, the peak to peak time for each cycle was specified so that the maximum loading rate never exceeded 0.02 inches per second. This is based on the ATC recommendations, shown below. The yield rotation, θ_y, occurs at an estimate lateral displacement of 5/8 inches.

- For $0 \leq \theta < 1.0\theta_y \rightarrow$ 60 seconds to peak.
- For $1.0\theta_y \leq \theta < 2.0\theta_y \rightarrow$ 80 second to peak
- For $2.0\theta_y \leq \theta < 4.0\theta_y \rightarrow$ 120 seconds to peak
- For $\theta \geq 4.0\theta_y \rightarrow$ 160 seconds to peak

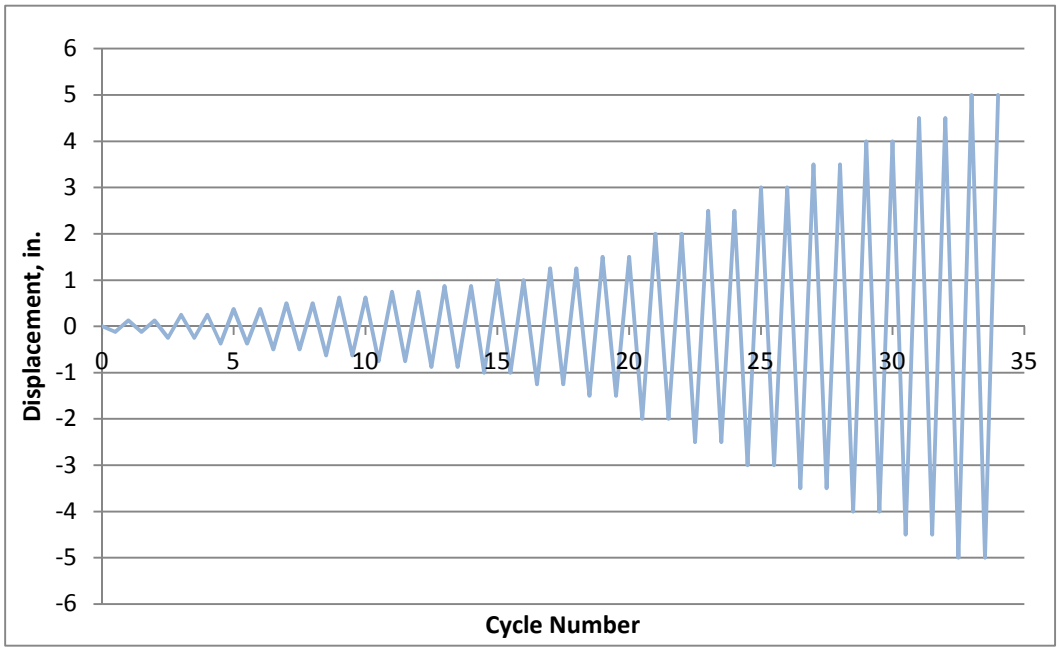

Figure 4.15 Actuator Input Load Protocol

Table 4.4 Actuator Displacement Table

Cycle #	Displacement (in)
1	0.125
1	-0.125
2	0.125
2	-0.125
3	0.25
3	-0.25
4	0.25
4	-0.25
5	0.375
5	-0.375
6	0.375
6	-0.375
7	0.5
7	-0.5
8	0.5
8	-0.5
9	0.625
9	-0.625
10	0.625
10	-0.625
11	0.75
11	-0.75
12	0.75
12	-0.75
13	0.875
13	-0.875
14	0.875
14	-0.875
15	1
15	-1
16	1
16	-1
17	1.25
17	-1.25

Cycle #	Displacement (in)
18	1.25
18	-1.25
19	1.5
19	-1.5
20	1.5
20	-1.5
21	2
21	-2
22	2
22	-2
23	2.5
23	-2.5
24	2.5
24	-2.5
25	3
25	-3
26	3
26	-3
27	3.5
27	-3.5
28	3.5
28	-3.5
29	4
29	-4
30	4
30	-4
31	4.5
31	-4.5
32	4.5
32	-4.5
33	5
33	-5
34	5
34	-5

It should be noted that the different measurements used to record lateral displacement – the actuator LDVT and several string potentiometers – typically differ by a significant margin, because of two primary factors. First, the numerous connections between the point of displacement application in the actuator and

the point of reaction in the strong wall are susceptible to slip. These slip values are monitored using potentiometers in order to quantify the contribution of flexibility in various connections. A second source of error is frame overturning. When the frame deforms under lateral load, some of the deformation is pure shear, from which story drifts are typically computed. The remainder is a result of overturning of the frame due to the eccentricity between the point of load application and reaction. This overturning manifests in axial compression and elongation of the columns, as well as uplift of the columns from their bases, which are friction contact only with the channel assembly. The measurement of the diagonal elongation of the frame between work points is considered to give the most reliable measurement, because it receives minimal contributions from each of the two primary sources of error.

Chapter 5: Experimental Observations

5.1 Introduction

This chapter describes the experimental performance of specimens NCBF1, NCBF1-R1, NCBF1-R2, NCBF1-R3, NCBF1-R4, and NCBF1-R5. Braced frame systems are statically indeterminate systems that are subject to complicated demands of varying severity during seismic events. The observable damage to components of the system at various levels of inter-story drift are described herein by performance states, which are defined in Section 5.2. Nomenclature was developed to assist in identifying the location of components within the specimen, which is presented in Section 5.3. The actuator displacement history for each specimen is given in Section 5.4.

Sections 5.5-5.10 describe the motivation for design and the experimental performance of each test. Photographs, written observations, and tables of damage progression are included in these descriptions. Observations were taken at each peak displacement for a cycle, as well as at intermediate points if a sudden slip or fracture was observed. As described in Chapter 3, specimen NCBF1 is representative of a typical NCBF and is intended to evaluate expected NCBF performance. The NCBF-RX specimens investigate various retrofit options for NCBF1 with the goal of improving drift capacity, system ductility, and limit state hierarchy.

5.2 Performance State Overview

In order to facilitate discussion of the performance of each of the NCBF specimens, nomenclature was created to describe the performance states of system components. The nomenclature for these performance states and basic descriptions are given in Table 5.1. Detailed descriptions and examples of these performance states are detailed in subsequent sections.

Table 5.1Performance State Overview

Symbol	Performance State	Description
Y1	Initial Yielding	Yield Lines First Visible to Whitewash Flaking Over <20% of Area
Y2	Moderate Yielding	Whitewash Flaking Over 20-50% of Area
Y3	Severe Yielding	Whitewash Flaking Over >50 of Area
B1	Initial Buckling	Brace Mid-Span Deflection Visible, but Less than Brace Depth
B2	Moderate Buckling	Brace Mid-Span Deflection Less than 2 Times Brace Depth
B3	Severe Buckling	Brace Mid-Span Deflection Greater than 2 Times Brace Depth
BC	Brace Cupping	Local Buckling of the Brace
BF	Brace Fracture	Complete Fracture of the Brace
BNS	Brace Net Section	Cracking in the Net Section of the Brace
LB	Initial Local Buckling	Out-of-Plane Deformation Less than Member Depth
W1	Initial Weld Tearing	Weld Tears Less than 10% of the Weld Length
W2	Moderate Weld Tearing	Weld Tears Less than 30% of the Weld Length
W3	Severe Weld Tearing	Weld Tears Greater than 30% of the Weld Length
WF	Weld Fracture	Complete Fracture of Weld
MT	Metal Tearing	Tearing of Metal Components (Plates, Beam Web)
BTF	Bolt Fracture	Shear Fracture of Bolt
BTE	Bolt Hole Elongation	Local Yielding of Plate Around Bolt Hole Causing Hole Elongation

5.2.1 Yielding (Y1, Y2, Y3)

Yielding is identified on members by the flaking of whitewash. When components yield, the mill scale coating them begins to flake off, taking the whitewash coating with it. As a result, locations of yielding become visible in the cracks in the whitewash. Yielding in these tests was typically observed in the gusset plates, shear tabs, and in the beams and columns near connecting elements. All braces were cold-form HSS, and thus did not have mill scale. As a result, whitewash could not be used to detect yielding in the brace.

Typically, Y1, initial yielding, is first visible as thin cracks in the whitewash. This performance state continues until more than 20% of the area contains yield lines. As yielding progresses, larger, contiguous areas of whitewash may flake off, and additional yielding lines may appear. Y2 - moderate yielding, describes components with between 20% and 50% of the component contains yield lines. If more than

50% of the area contains yield lines, then the element enters performance state Y3 - severe yielding. This performance state is often also characterized by large, contiguous areas of flaked whitewash. Figures 5.1-5.3 show the yielding performance states for the gusset plate. Figures 5.4-5.6 show the yielding performance states for the shear tab. Finally, Figures 5.7-5.8 show the yielding performance states in the column flange.

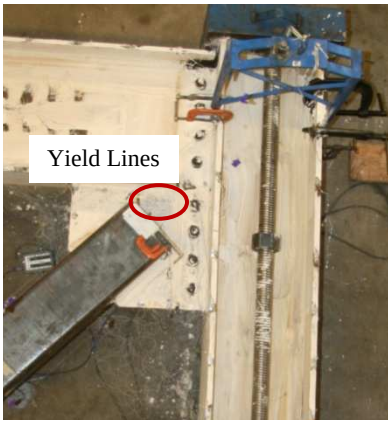

Figure 5.1 Gusset Plate Y1
NCBF1-R5

Figure 5.2 Gusset Plate Y2
NCBF1-R5

Figure 5.3 Gusset Plate Y3
NCBF1-R5

Figure 5.4 Shear Tab Y1
NCBF1-R5

Figure 5.5 Shear Tab Y2
NCBF1-R5

Figure 5.6 Shear Tab Y3
NCBF1-R5

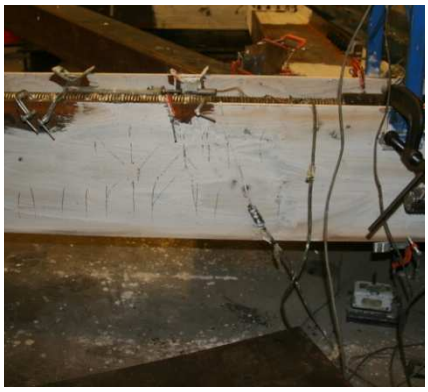

Figure 5.7 Column Flange Y1
NCBF1-R5

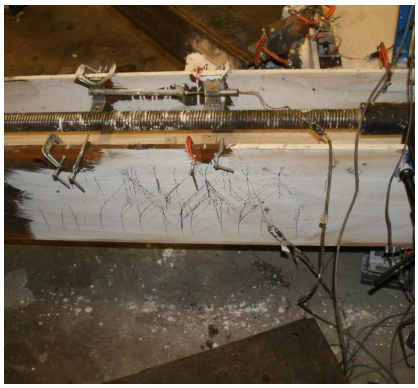

Figure 5.8 Column Flange Y2
NCBF1-R5

5.2.2 Brace Performance (B1, B2, B3, BC, BF, BNS)

Global buckling of the brace is divided into 3 categories. Initial brace buckling, B1, includes behavior from when the brace begins to lose axial load resistance in compression until the mid-span deflection reaches the depth of the brace, as shown in Figure 5.9. Moderate brace buckling, B2, describes brace mid-span deflections between one and two times the brace depth, as shown in Figure 5.10. Severe brace buckling, B3, describes all brace deflections greater than two times the brace depth, as shown in Figure 5.11.

If the out-of-plane displacement of the brace becomes large enough, a plastic hinge will form. Ultimately, the brace will sustain localized damage to the brace flanges with increased local buckling. This is described as brace cupping, BC, as shown in Figure 5.12. In some cases, if the width-to-thickness ratio for the brace is large, brace cupping may occur before severe brace buckling.

Performance state BF is reached if the tears in the brace result in complete fracture of the brace cross section. This is the desired ultimate limit state for braced frames. Figure 5.13 shows a brace that has reached the brace fracture performance state.

In some cases, braces may crack at the net section, where the brace is slotted at the edge of the gusset plate. This damage does not fit predictably into the damage progression of B1-B3, so it is given a separate designation - BNS. Figure 5.14 shows a brace whose net section has reached this performance state, and Figure 5.15 shows an illustration of the brace net section.

Figure 5.9 Initial Brace Global Buckling - B1 NCBF1-R2

Figure 5.10 Moderate Brace Global Buckling - B2 NCBF1-R2

Figure 5.11 Severe Brace Global Buckling - B3 NCBF1-R2

Figure 5.12 Brace Cupping - BC NCBF1

Figure 5.13 Brace Fracture - BF NCBF1

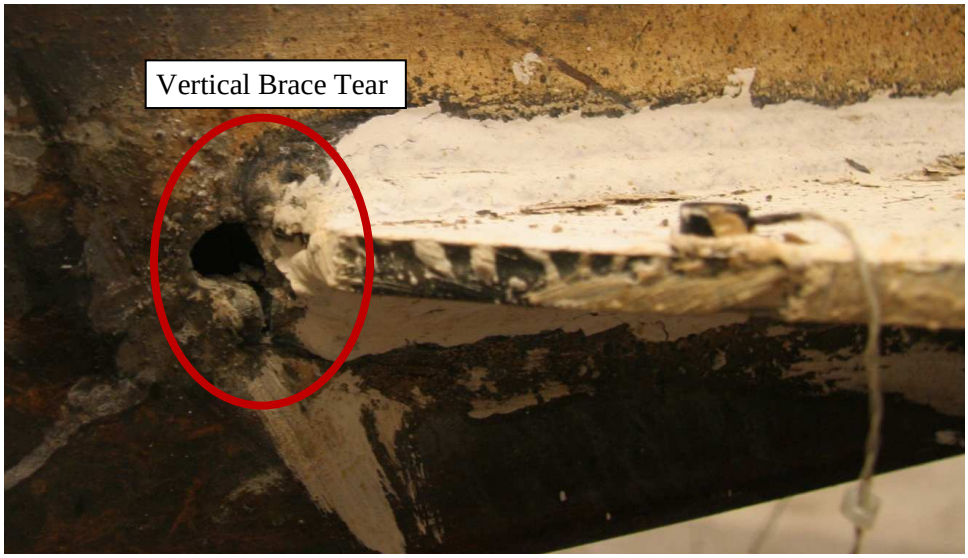

Figure 5.14 Brace Net Section Tearing - BNS NCBF1-R5

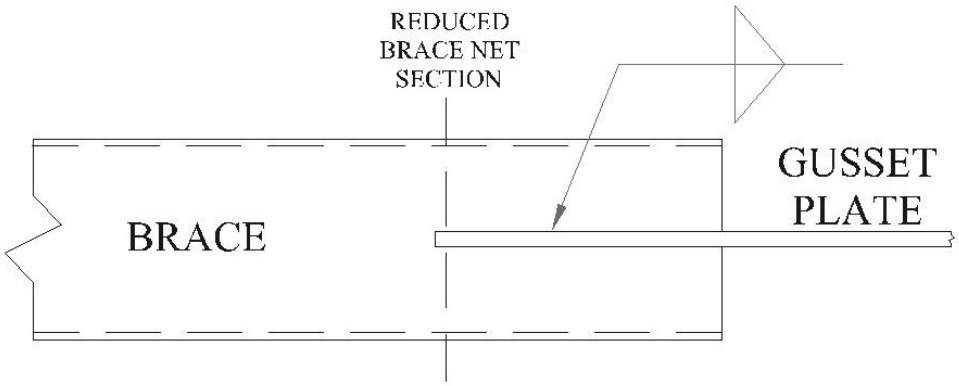

Figure 5.15 Brace Net Section Illustration

5.2.3 Local Buckling (LB)

When a component, such as a web or flange deforms locally out of its plane, it is designated as local buckling, LB, as shown in Figure 5.16 for a column flange. Local buckling pertains only to the performance of the beams and columns in these specimens.

Figure 5.16 Column Flange Buckling - LB NCBF1-R3

5.2.4 Metal Tearing (MT)

The metal tearing performance state pertains to all frame components except the brace. It includes damage up to, but not including complete fracture of the component. Figure 5.17 shows tearing of a shear tab, and Figure 5.18 shows tearing of a beam web.

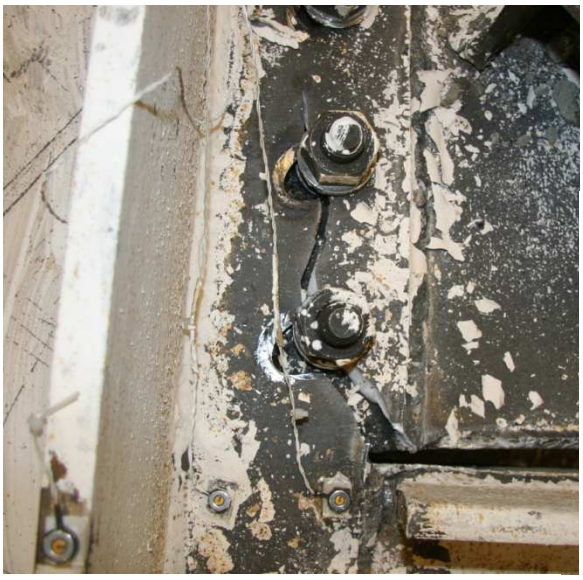

Figure 5.17 Shear Tab MT NCBF1-R5

Figure 5.18 Beam Web MT NCBF1-R5

5.2.5 Weld Tearing and Fracture (W1,W2,W3,WF)

Weld damage is described by four performance states, which indicate progressively larger degrees of weld tearing. Initial weld tearing, W1, describes welds that are torn along less than 10% of their length. Figure 5.19 shows a weld exhibiting this performance state. Moderate weld tearing, W2, includes welds that are torn along 10-30% of their length. Figure 5.20 demonstrates this performance state. Severe weld tearing, W3, describes welds torn over greater than 30% of their length, as shown in Figure 5.21. In some cases, a single weld has multiple separate tears along its length. The weld performance state is determined by the total length of weld cracking, not the length of a single crack. Weld fracture occurs when a weld has torn through its thickness along its entire length and is referred to by the performance state WF. Figure 5.22 shows a typical weld fracture.

Figure 5.19 Initial Weld Tearing - W1 NCBF1-R5

Figure 5.20 Moderate Weld Tearing - W2 NCBF1-R5

Figure 5.21 Severe Weld Tearing - W3 NCBF1-R5

Figure 5.22 Weld Fracture - WF NCBF1-R5

5.2.6 Bolt Damage (BTE BTF)

Bolt hole elongation, BTE, refers to visibly discernible deformation of the base metal around the bolt, which results in an elongated, oblong hole. Figure 5.23 shows a typical elongated bolt hole.

Bolt fracture, BTF, refers to the complete shear fracture of the bolt. Figure 5.24 shows a typical fractured bolt.

Figure 5.23 Bolt Hole Elongation - BTE NCBF1-R5

Figure 5.24 Bolt Fracture - BTF NCBF1-R5

5.3 Location Nomenclature

This section describes the nomenclature used to locate damage on each specimen. Figure 5.25 shows a typical framing member cross section and the terminology used. Figure 5.26 shows terminology used to describe global locations on the framing members. The nomenclature for the North and South gusset plate connections, respectively, are listed in Table 5.2 and Table 5.3, respectively. The corresponding locations for Table 5.2 are shown in Figure 5.27, and the locations for Table 5.3 are shown in Figure 5.28. Note that the weld connecting the shear tab to the gusset plate and the beam is given a different name in each region: gusset plate and beam. While it is a continuous weld, each region serves a fundamentally different purpose from a performance standpoint, so they are named separately.

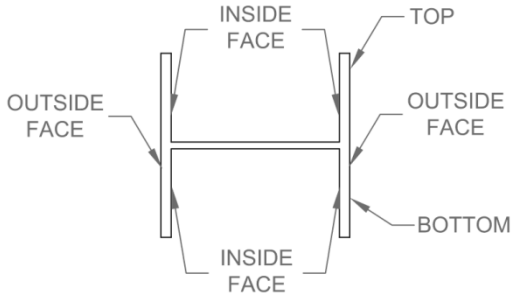

Figure 5.25 Wide Flange Cross Section Notation

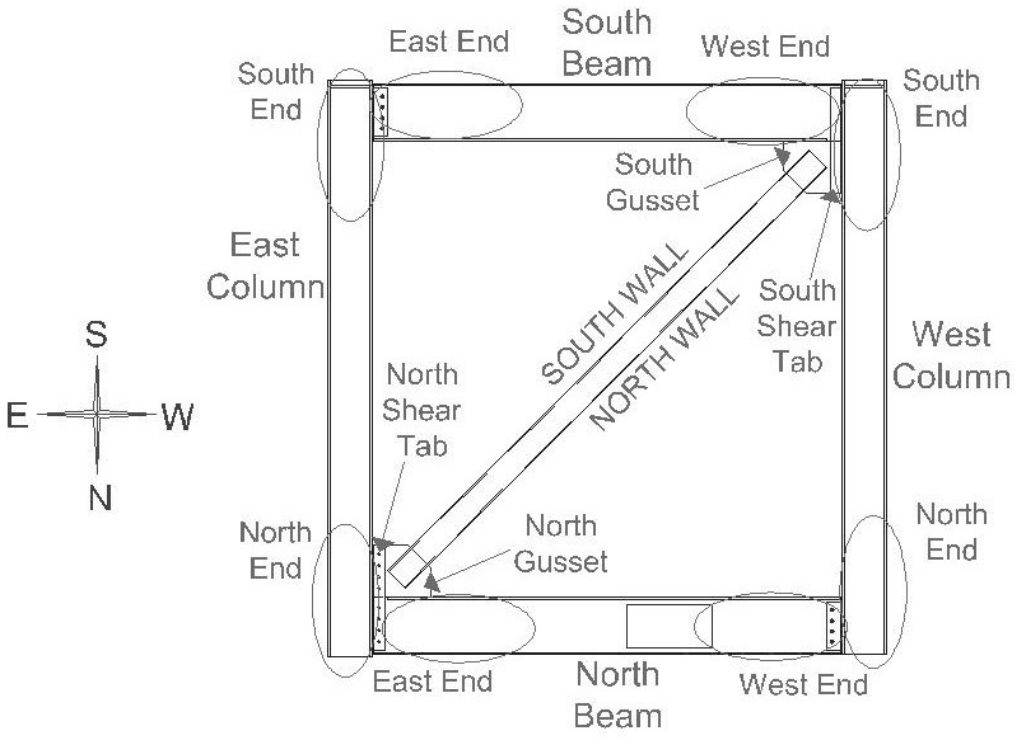

Figure 5.26 Frame Identifiers

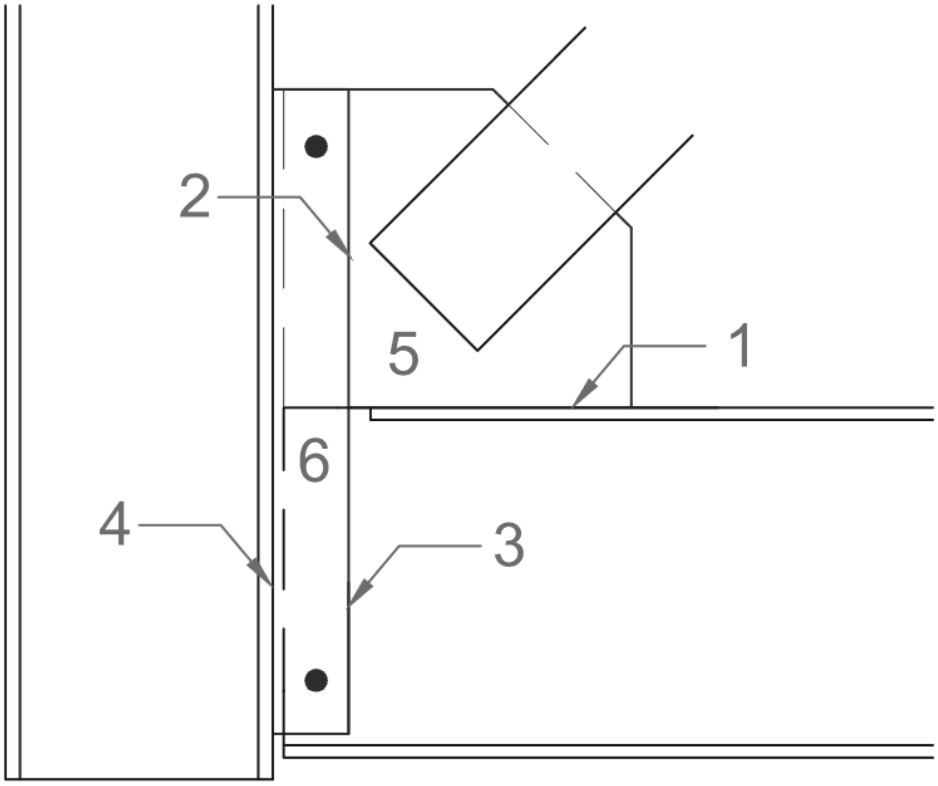

Figure 5.27 South Connection Location Identifiers

Table 5.2 South Connection Nomenclature

#	**Description**
1	Weld - South Gusset Plate to Beam
2	Weld - South Gusset Plate to Shear Tab
3	Weld - South Beam to Shear Tab
4	Weld - South Shear Tab to Column
5	South Gusset Plate
6	South Shear Tab

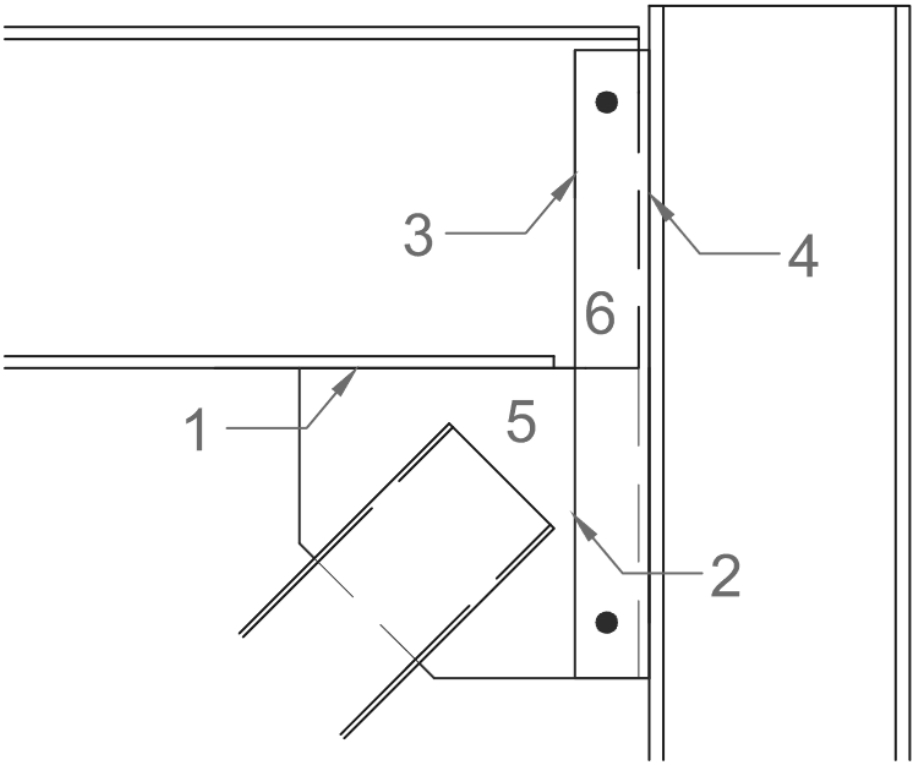

Figure 5.28 North Connection Location Identifiers

Table 5.3 North Connection Nomenclature

#	**Description**
1	Weld - North Gusset Plate to Beam
2	Weld - North Gusset Plate to Shear Tab
3	Weld - North Beam to Shear Tab Weld
4	Weld - North Shear Tab to Column
5	North Gusset Plate
6	North Shear Tab

5.4 Actuator Displacement History

Slowly applied cyclic displacements of increasing amplitude were applied to each of the specimens. The actuator displacement history for specimens NCBF1 and NCBF1-R1 is shown in Figure 5.29. The displacement history was modified slightly for specimens NCBF1-R2, NCBF1-R3, NCBF1-R4, and NCBF1-R5, as shown in Figure 5.30.

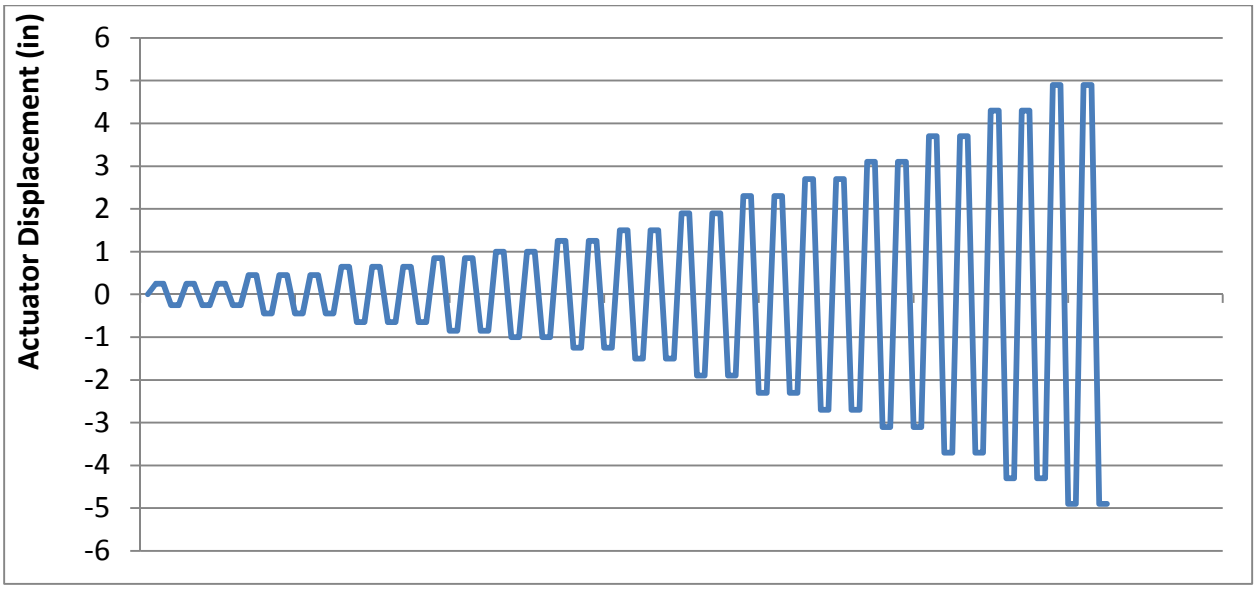

Figure 5.29 NCBF1 and NCBF1-R1 Actuator Displacement History

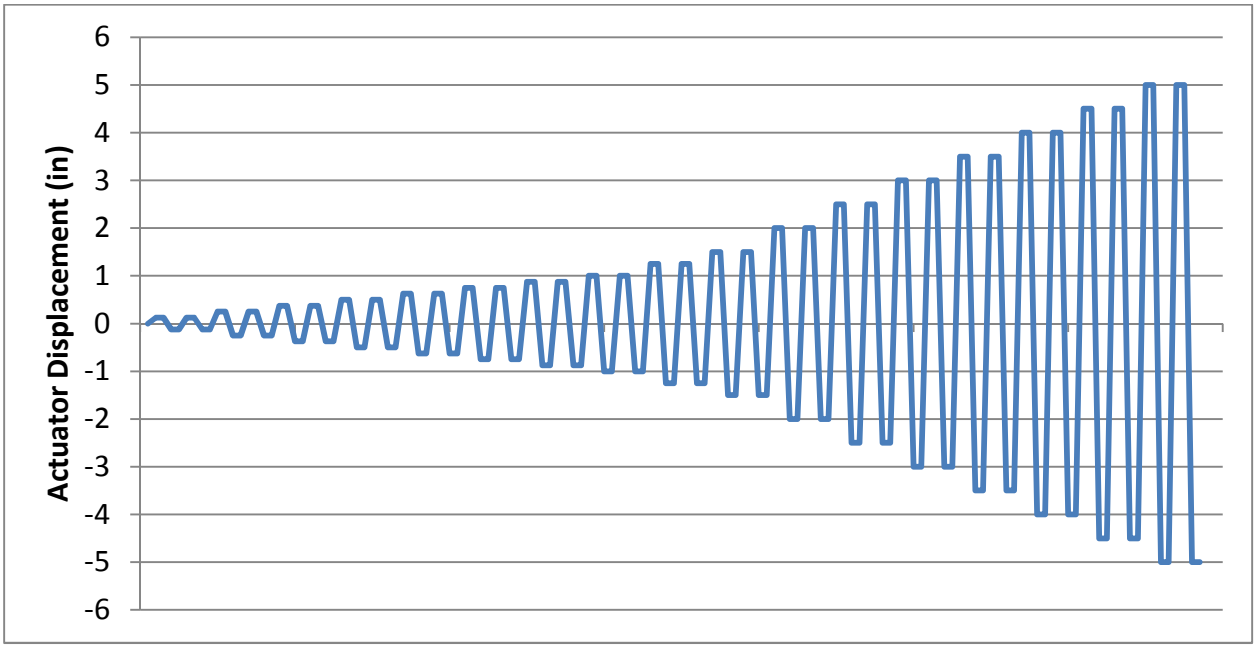

Figure 5.30 NCBF1-R2 through NCBF1-R5 Actuator Displacement History

5.5 NCBF1

5.5.1 Specimen Overview

Specimen NCBF1 was designed to represent a common connection configuration and the typical deficiencies it exhibited in the infrastructure review, as described in Chapter 3. The connection is a shared shear tab, which is welded to both the gusset plate and the beam, as shown in Figure 5.31. Figure 5.32 shows the undamaged connection and Figure 5.33 shows the frame configuration. Welds for NCBF1 used an E70-T7 electrode, which does not meet notch-toughness requirements for demand-critical welds. This practice was common during the period of construction of the reference structures. Two of the welds on the specimen unintentionally used an E71-T8 electrode, which does meet the requirements for demand critical welds.

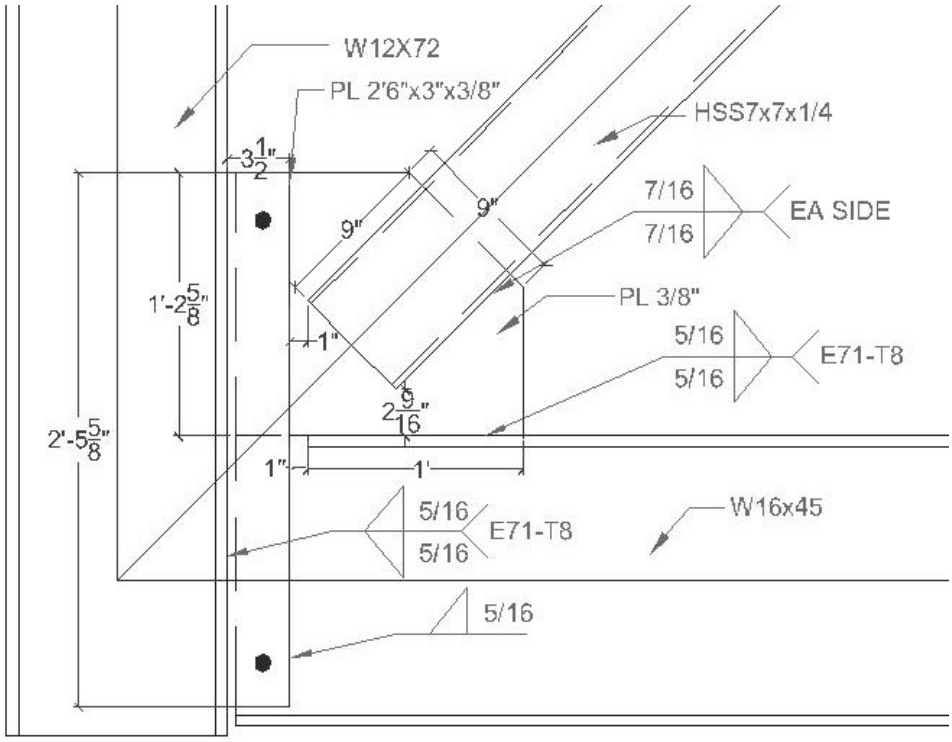

Figure 5.31 NCBF1-R1 Connection Schematic

Figure 5.32 NCBF Undamaged North Connection

Figure 5.33 NCBF1 Frame Overview

The connection for NCBF1 was designed with a range of deficiencies, listed in Table 5.4. The most severe deficiency was the local compactness, or local slenderness, of the brace. Thus, it was expected that the brace compactness would be most detrimental to the system performance. Both the gusset plate-to-beam weld and the shear tab weld were deficient, so some degree of tearing was expected in one or both of these welds. Brace net section fracture also had a high DCR due to the lack of cover plates. Finally, yielding of the gusset plate Whitmore section had a high DCR, so extensive yielding of the gusset plate was expected.

Table 5.4 NCBF1 DCRs

Limit State	**NCBF1**
Brace Net Section Fracture	1.26
Brace-Gusset Plate Weld Fracture	0.92
Brace Block Shear	1.14
Gusset Plate Block Shear	1.16
Gusset Plate Whitmore Yielding	1.33
Gusset Plate Buckling	0.74
Gusset Plate Shear Yielding at Beam	1.16
Beam-Gusset Weld Fracture	1.55
Shear Tab to Gusset/Beam Weld Fracture	1.08
Shear Tab to Column Weld Fracture	0.65
Local Slenderness	2.04

The load-drift history for NCBF1 is shown in Figure 5.34. Drift values given here and in the remainder of this section are computed from the frame diagonal, as described in Chapter 5. NCBF1 suffered brace cupping and fracture at a relatively low drift level due to the high local slenderness of the brace. Damage to other frame components was limited, despite the expected deficiencies.

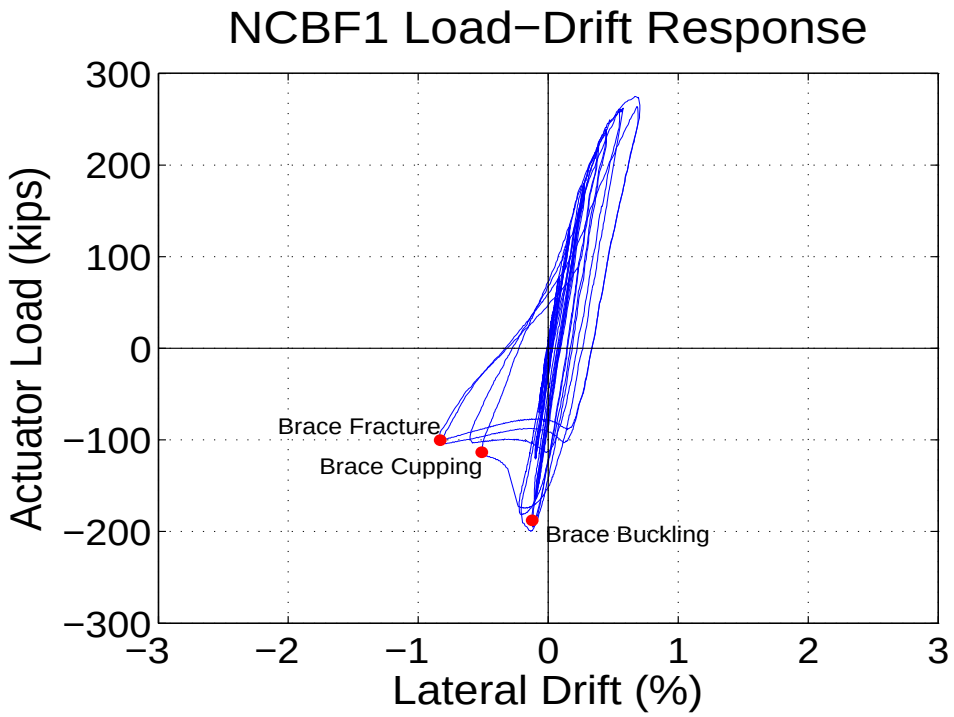

Figure 5.34 NCBF1 Load-Drift Response History

5.5.2 Performance State Summary

Table 5.5 shows the progression of performance states during the test for the welds and brace for NCBF1. The positive drift, negative drift, drift range, and cycle number are given. Performance states for other components are not included due to the lack of whitewashing on the specimen.

Table 5.5 NCBF1 Performance States

	Drift %			North Welds				South Welds				
Cycle #	Total	Neg.	Pos.	Gusset to Beam	Gusset to Shear Tab	Beam to Shear Tab	Shear Tab to Column	Gusset to Beam	Gusset to Shear Tab	Beam to Shear Tab	Shear Tab to Column	Brace
1	0.07	-0.04	0.04									
2	0.07	-0.04	0.04									
3	0.15	-0.07	0.08									
4	0.15	-0.07	0.08									
5	0.15	-0.07	0.08									
6	0.26	-0.10	0.16									
7	0.26	-0.10	0.16									
8	0.26	-0.09	0.17									
9	0.37	-0.11	0.26									
10	0.37	-0.10	0.27									
11	0.37	-0.09	0.04									
12	0.49	-0.12	0.37									B1
13	0.50	-0.11	0.39									
14	0.65	-0.20	0.45									
15	0.66	-0.22	0.44									
16	1.07	-0.50	0.58									BH
17	1.13	-0.58	0.55									
18	1.49	-0.79	0.69									
19	1.52	-0.83	0.69				W1					
20	1.52	///	0.69									BF

5.5.3 Test Narrative

No damage was observed during the first 11 cycles of the test, up to a total drift range of 0.37%.

At the compressive peak of cycle 12 (-0.12% drift), initial global buckling of the brace, performance state B1, was observed, as shown in Figure 5.35. This corresponded to the point of maximum compressive resistance for the frame, as shown in Figure 5.34. As a result of the brace buckling, the gusset plates began to bend upward at both connections. Both gusset plates were bending away slightly from the shear tab, creating a small gap, as shown in Figure 5.36. This gap continued to open for subsequent cycles.

Figure 5.35 Initial Visible Brace Buckling - B1

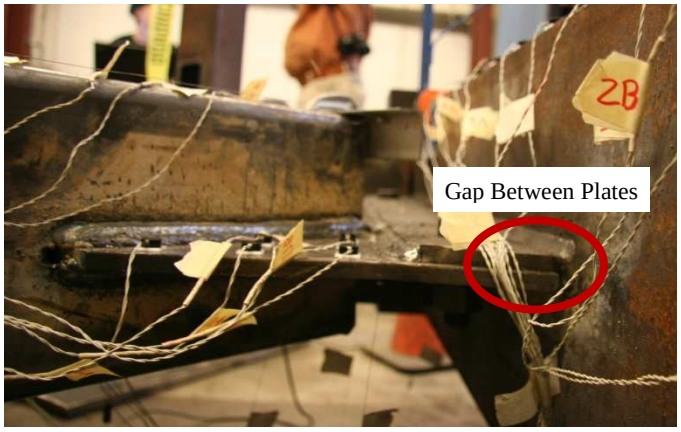

Figure 5.36 Bending of North Gusset Plate

At the compressive peak of cycle 16 (-0.50% drift), local deformations of the brace walls appeared 1 foot North of the brace mid-span. The brace behavior was classified as performance state BC, as shown in Figure 5.37 and Figure 5.38.The cupping of the brace corresponded with a substantial drop in compressive resistance for the frame, as shown in Figure 5.34 The bending of the gusset plates away from the shear tabs increased at the occurrence of brace cupping, as shown in Figure 5.39. As expected, the severe local slenderness of the brace resulted in rapid degradation of compressive strength and severe local buckling.

Figure 5.37 Brace Buckled Shape at Cupping

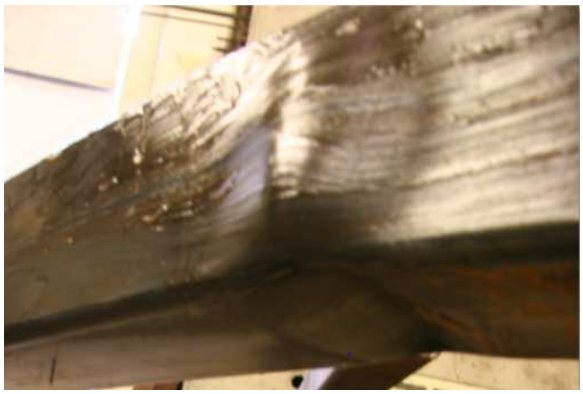

Figure 5.38 Brace Cupping - BC

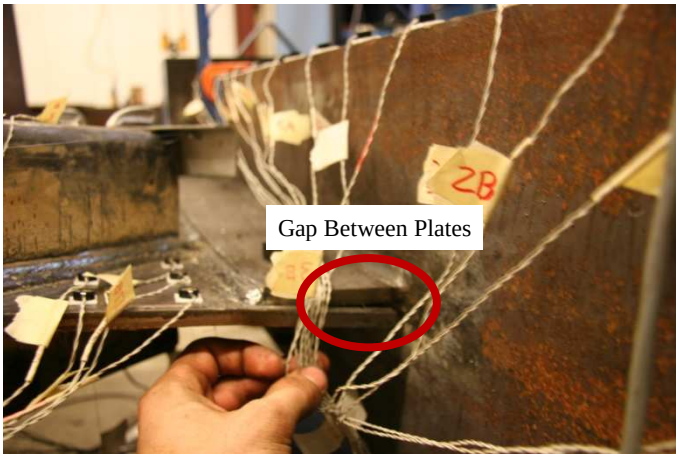

Figure 5.39 Increased Bending of North Gusset Plate

At the compressive peak of cycle 19, the second cycle at this drift level (-0.83% drift), a 1 inch weld tear developed at the South end of the North shear tab-to-column weld. This tear was classified as performance state W1, as shown in Figure 5.40. Tearing in this weld is surprising, as its DCR was substantially lower than 1, while the DCR for the gusset and beam to shear tab weld had a DCR greater than 1.

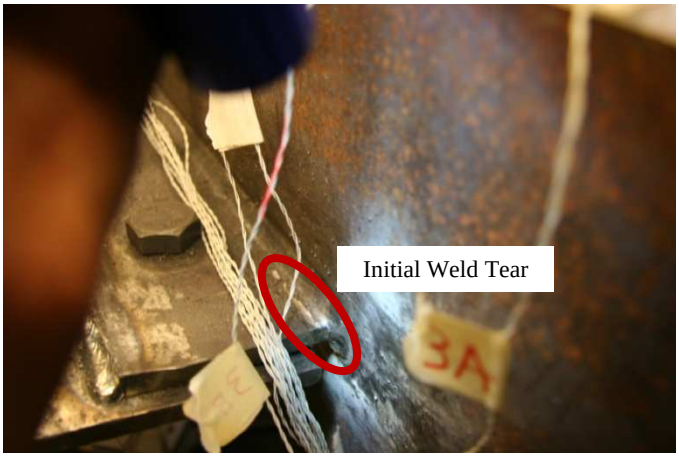

Figure 5.40 Initial Tearing in North Shear Tab-to-Column Weld - W1

Prior to reaching the tensile peak of cycle 20, brace tearing initiated at the bottom corners of the brace and propagated up the side walls of the brace, as shown in Figure 5.41. This tearing caused the brace to deflect downward to attain equilibrium. This caused downward bending of the connections, shown for the

South connection in Figure 5.42. Brace fracture occurred prior to reaching the tension peak, as shown in Figure 5.43.

Figure 5.41 Mid-Cycle Brace Tearing

Figure 5.42 Downward Bending of South Gusset Plate

Figure 5.43 Brace Fracture

5.5.4 Test Summary

NCBF1 suffered brace cupping and fracture at a very low drift range compared to SCBFs. The slenderness of the brace walls clearly contributed to rapid degradation of brace compression strength and low fracture life. Despite a DCR greater than 1.5 for the gusset-to-beam weld, no damage to this weld was observed. Deficiencies in the brace net section and the shear tab weld, as well as other minor deficiencies, appeared to have very little impact on the system performance. This demonstrates that a brace with high local slenderness may be a more concerning deficiency than many of the connection deficiencies.

Additional tests presented in the subsequent sections describe various retrofit attempts aimed at improving the ductility of this system.

5.6 NCBF1-R1

5.6.1 Specimen Overview

Specimen NCBF1-R1 investigates a simple repair for NCBF1. NCBF1 suffered rapid brace deterioration in compression due to the high local slenderness. NCBF1-R1 used an HSS5x5x3/8 brace, which has the same cross-sectional area as the HSS7x7x1/4 used in NCBF1, but meets modern compactness limits for braces. As described in Chapter 2, more compact braces have less rapid loss of compressive strength after buckling and longer fracture life. Since the non-compact brace in NCBF1 was the limiting factor for its performance, replacing it is a straightforward method to improve performance.

Because the connections and frame for NCBF1 sustained minimal damage, NCBF1-R1 reused these components, with only the brace being replaced. The gusset plate required minor heat-straightening, and two small weld tears were gouged and repaired. As was the case with NCBF1, whitewash was not applied to the specimen, so a description of component yielding is not included in this chapter. Figure 5.44 shows the schematic for the retrofit, Figure 5.45 shows the undamaged North connection.

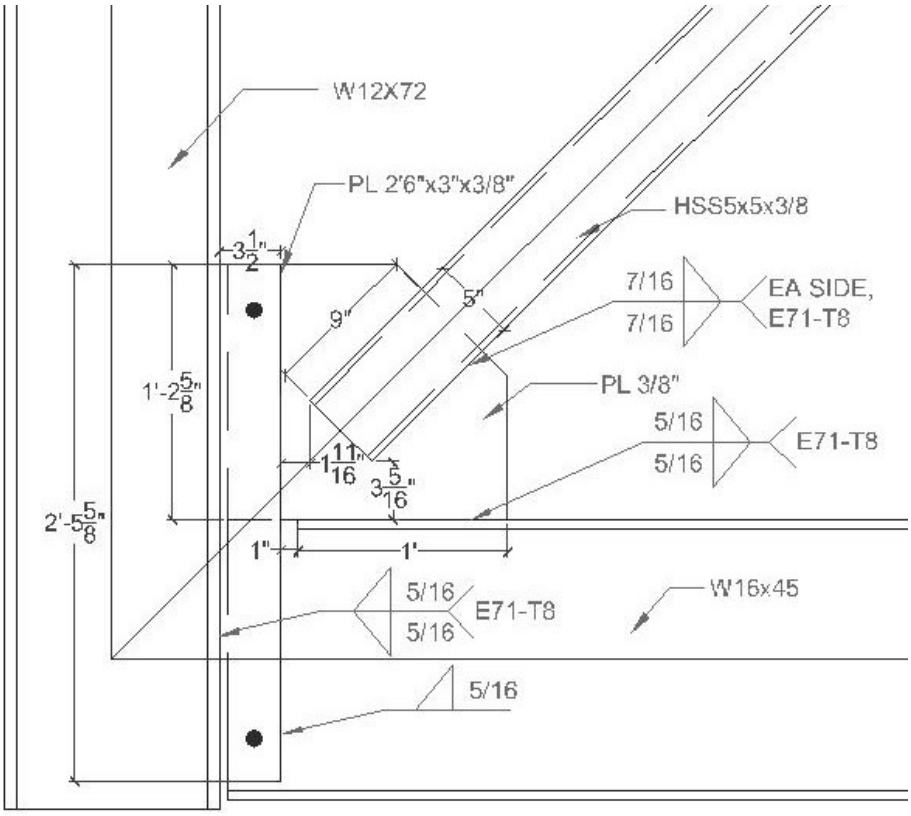

Figure 5.44 NCBF1-R1 Connection Schematic

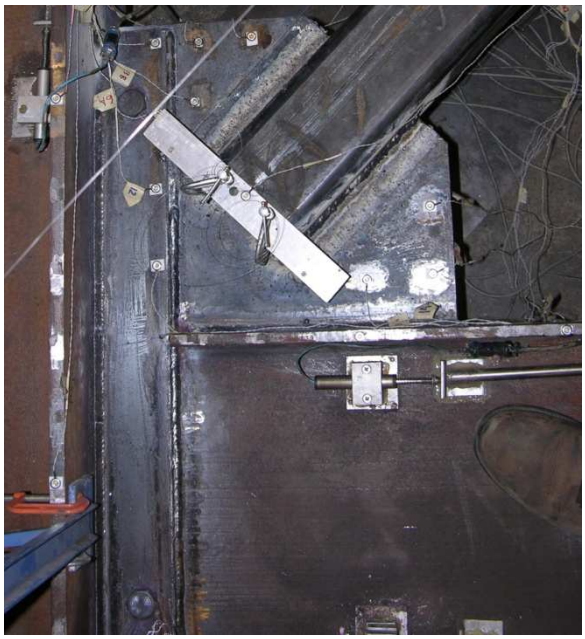

Figure 5.45 NCBF1-R1 Undamaged North Connection

Table 5.6 shows the changes in DCRs for NCBF1-R1 relative to the original NCBF1. The only changes, aside from the brace local slenderness, are to the limit states associated with the brace-to-gusset plate connection. The DCR change of greatest interest is for Whitmore yielding of the gusset plate. Due to the smaller brace width, the Whitmore section for NCBF1-R1 was slightly smaller, increasing the DCR to 1.5. As a result, greater damage to the gusset plate was expected in NCBF1-R1 than in NCBF1.This narrower brace also increased the DCR for block shear of the gusset plate slightly, while it reduced the DCR for brace block shear due to thicker brace walls. Finally, the net section DCR decreased due the narrower brace, which has a higher shear lag factor. None of these changes were large enough to dramatically affect the system performance.

Table 5.6 NCBF1-R1 DCR Changes

Limit State	NCBF1	NCBF1-R1
Brace Net Section Fracture	1.26	1.15
Brace-Gusset Plate Weld Fracture	0.92	0.92

Brace Block Shear	1.14	0.76
Gusset Plate Block Shear	1.16	1.33
Gusset Plate Whitmore Yielding	1.33	1.50
Gusset Plate Buckling	0.74	0.84
Gusset Plate Shear Yielding at Beam	1.16	1.16
Beam-Gusset Weld Fracture	1.55	1.55
Shear Tab to Gusset/Beam Weld Fracture	1.08	1.08
Shear Tab to Column Weld Fracture	0.65	0.65
Brace Local Slenderness	2.04	0.85

A load-drift envelope for NCBF1-R1 is given in Figure 5.46. Due to a data acquisition failure, only select peak data points were available. For this test, lateral drift was calculated from the Optotrak system, rather than the frame diagonal. The brace for NCBF1 buckled substantially out-of-plane, but did not cup or fracture. NCF1-R1 failed when the North gusset-beam weld and the North gusset-shear tab weld failed, disconnecting the brace from the framing members.

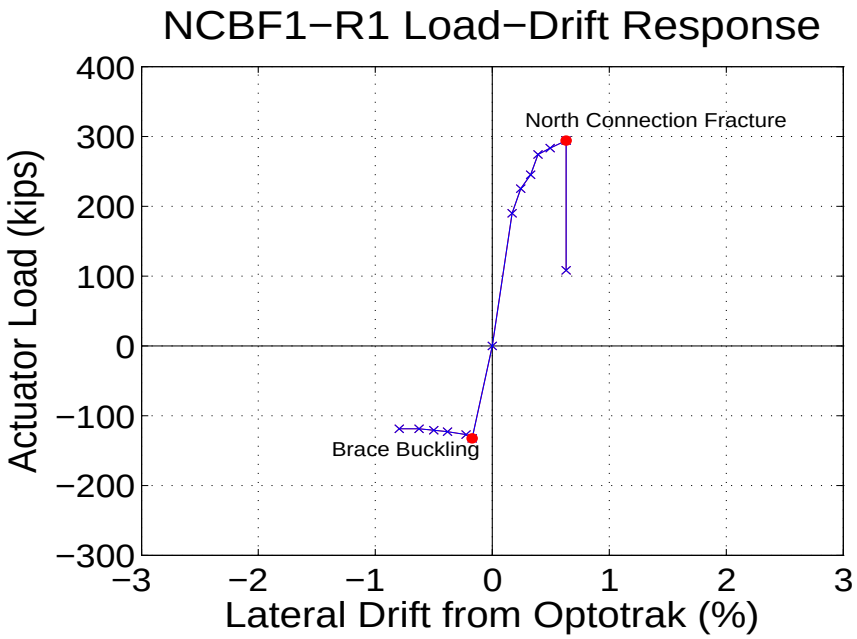

Figure 5.46 NCBF1-R1 Load-Drift Envelope

5.6.2 Performance State Summary

Table 5.7 shows the progression of performance states during the test for the welds and brace for NCBF1. The positive drift, negative drift, drift range, and cycle number are given. Performance states for other components are not included due to the lack of whitewashing on the specimen. All drift values for this specimen come from lateral movement of Optotrak sensors, rather than the frame diagonal elongation, making these values only approximately comparable with other tests.

Table 5.7 NCBF1-R1 Performance States

	Drift %			North Welds				South Welds				
Cycle #	Total	Neg.	Pos.	Gusset to Beam	Gusset to Shear Tab	Beam to Shear Tab	Shear Tab to Column	Gusset to Beam	Gusset to Shear Tab	Beam to Shear Tab	Shear Tab to Column	Brace
1	0.09	-0.04	0.04									
2	0.09	-0.04	0.05									
3	0.17	-0.08	0.09									
4	0.17	-0.08	0.09									
5	0.17	-0.08	0.09									
6	0.30	-0.13	0.16									
7	0.30	-0.12	0.17									
8	0.30	-0.13	0.17									B1
9	0.41	-0.17	0.24									
10	0.42	-0.17	0.25									
11	0.42	-0.17	0.25									
12	0.55	-0.23	0.33									
13	0.55	-0.23	0.33									
14	0.69	-0.38	0.31									
15	0.69	-0.38	0.29									
16	0.86	-0.46	0.39	W1				W1				B2
17	0.90	-0.50	0.40									
18	1.12	-0.63	0.49									
19	1.12	-0.62	0.45									
20	1.43	-0.80	0.63	W2		W1	W1					
21	1.43	-0.75	0.64									
22	1.43	///	0.64	WF	WF	W2						

5.6.3 Test Narrative

During the first 7 cycles, no damage to the specimen was observed, and the specimen reached a total drift range of 0.30%.

At the compressive peak of cycle 8, the third cycle at this drift level (-0.13% drift), initial brace buckling was visible, putting the brace in performance state B1, as shown in Figure 5.47. This buckling corresponded to the peak compressive lateral load resisted by the specimen, as shown in Figure 5.46.

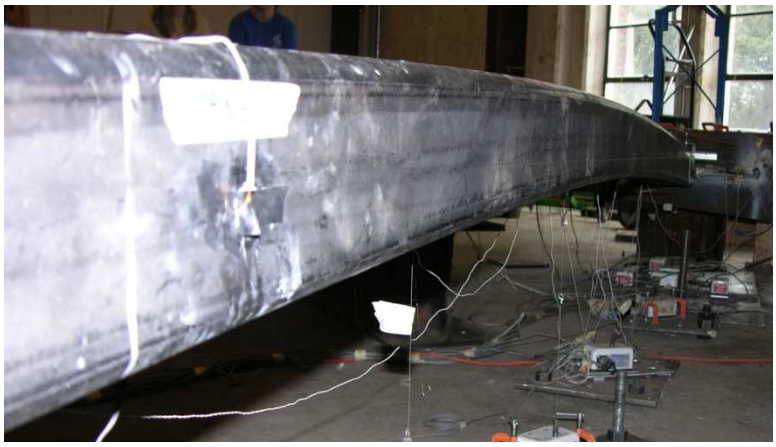

Figure 5.47 Brace Buckling - B1

At the compressive peak of cycle 16 (-0.46% drift), hairline weld cracks appeared at the ends of both the North and South gusset-to-beam welds. Both welds entered performance state W1. Initial tearing for the North gusset-to-beam weld and the South gusset-to-beam weld is shown in Figure 5.48 and Figure 5.49, respectively. Tearing of these welds was expected, as there was little brace end clearance, and the DCRs for the gusset-to-beam welds were high. At this point, NCBF1-R1 had exceeded the maximum compressive drift achieved in NCBF1, so higher demands were being placed on these welds than the welds in NCBF1, which suffered no damage.

Upward bending of the gusset plates was significant, and bending of the gusset plates away from the shear tabs was observed in both connections. This bending is shown for the North gusset plate in Figure 5.50. The mid-span deflection of the brace also increased sufficiently to categorize it as performance state B2, as shown in Figure 5.51. Unlike NCBF, NCBF1-R1 did not suffer a substantial loss of lateral load resistance as brace buckling progressed, as shown in Figure 5.46.

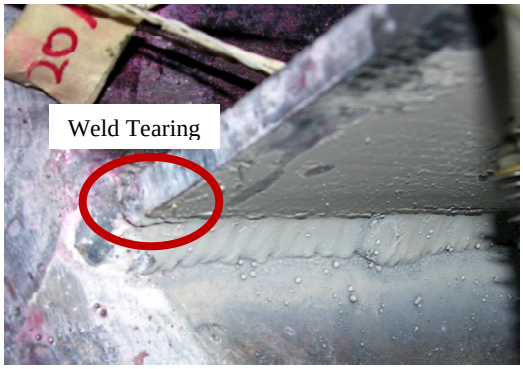

Figure 5.48 W1 in North Gusset-to-Beam

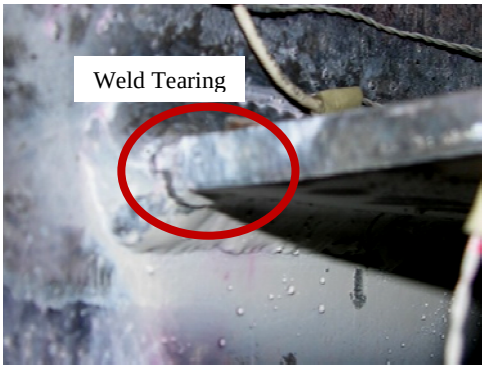

Figure 5.49 W1 in South Gusset-to-Beam Weld

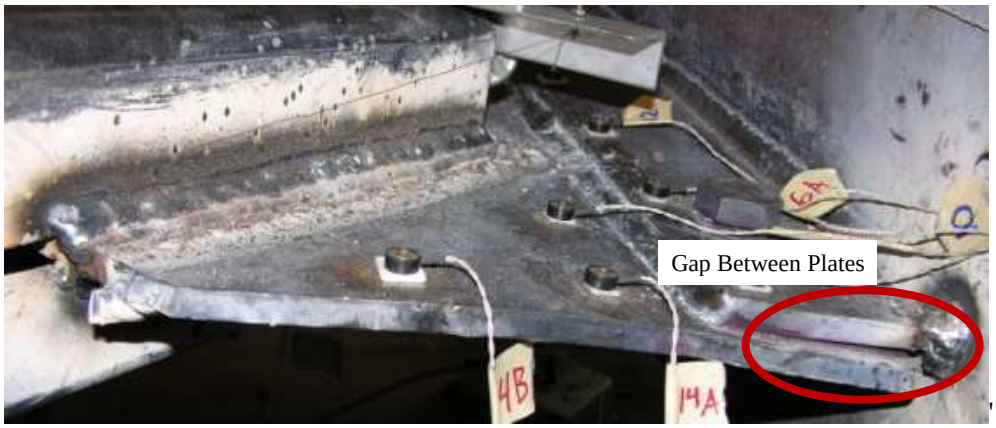

Figure 5.50 Upward bending and Prying of North Gusset Plate

Figure 5.51 Brace Buckling - B2

At the tensile peak of cycle 17, the second cycle at this drift level (0.40% drift), the shear tabs retained some of their upward bending from the compressive cycle, forcing the gusset plate to hinge downward at the edge of the shear tab. This bending is shown for the South gusset plate in Figure 5.52. Also a this drift level, the slope of the load-drift envelope in tension began to decrease, as shown in Figure 5.46. This was likely a result of yielding it the brace or connections, which was not directly observable.

Figure 5.52 Downward Hinging of South Gusset Plate

At the compressive peak of cycle 20 (-0.80% drift), weld tearing increased significantly. The North gusset-to-beam weld had a 4 inch tear, classified as performance state to W2, as shown in Figure 5.53. A 1 inch weld tear developed at the North end of the North beam-to-shear tab weld, classified as performance state W1. Another 1 inch weld tear developed at the North end of the North shear tab-to-column weld, also indicating performance state W1. These cracks are shown in Figure 5.54.

Figure 5.53 W2 in North Gusset-to-Beam Weld

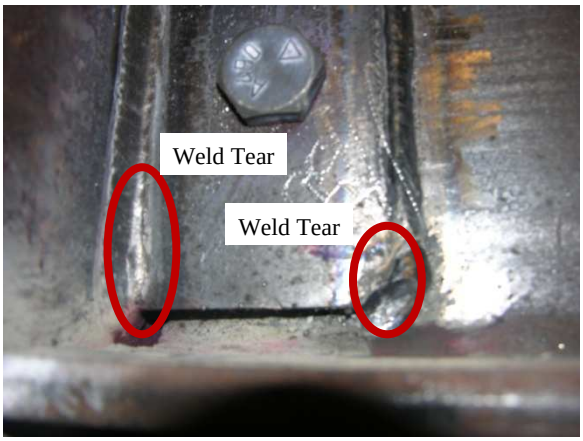

Figure 5.54 W1 in North Beam-to-Shear Tab and Shear Tab to Column Welds

Prior to reaching the tensile peak of cycle 22, the North gusset-to-beam and North gusset-to-shear tab welds both fractured completely. This fracture disconnected the brace and gusset plate from the frame, effectively ending the test, as shown in Figure 5.55. These fractures corresponded to a 60% loss of lateral load capacity, as shown in Figure 5.46.

Figure 5.55 Fracture of North Gusset-to-Beam and Gusset-to-Shear Tab Welds

5.6.4 Test Summary

NCBF1-R1 suffered a rapid connection failure that disconnected the brace from the framing members. This failure was undesirable, but may not cause collapse of a structure, as the beam-column connection remained largely intact. The North gusset-to-beam weld, which used a notch-tough electrode, had a slow-propagating tear, but once the tear reached the non-tough gusset-to-shear tab weld, the connection failed

instantaneously. This demonstrates the vulnerability of non-tough welds. It is likely that if W-NGB had not been notch tough that the specimen would have failed more rapidly.

NCBF1-R1 also demonstrated the improved performance of a compact brace over a non-compact brace. NCBF1 had a high buckling capacity, but quickly lost compressive resistance after buckling and progressed rapidly to fracture. By contrast, NCBF1-R1 reached a lower buckling load due to the smaller radius of gyration, but it maintained a much more consistent compressive capacity after buckling. NCBF1-R1 demonstrated that brace replacement addresses some, but not all of the issues with NCBF1, and it highlights the vulnerability of the deficient welds that was not evident from the results of NCBF1.Damage from the other deficient limit states was not observed, indicating that these deficiencies have less severe implications for performance.

5.7 NCBF1-R2

5.7.1 Specimen Overview

Specimen NCBF1-R2 investigates a simple retrofit for NCBF1. NCBF1 suffered rapid brace deterioration in compression due to the high width-to-thickness ratio of its walls. NCBF1-R2 uses an HSS5x5x3/8 brace, which has the same cross-sectional area as the HSS7x7x1/4 used in NCBF1, but meets modern compactness limits for braces. This specimen was similar to NCBF1-R1, but it used new gusset plates and a different weld electrode, as described in detail in Chapter 3. All welds on this specimen used an E71-T11 electrode, which does not meet demand-critical weld requirements. The only exception was the brace-gusset plate weld. This weld would be replaced in a retrofit scheme, because the brace was replaced, so it uses E71-T8 with notch toughness requirements.

Figure 5.56 shows the schematic for the retrofit, and Figure 5.57 shows an image of the undamaged connection. NCBF1-R2 reused the columns from NCBF1-R1. No significant damage occurred in the columns during NCBF1-R1, so they were deemed acceptable for reuse. The existing plates were removed, and the columns were rotated so the new plates could be attached to a clean face of the column. New beams were used for NCBF1-R2.

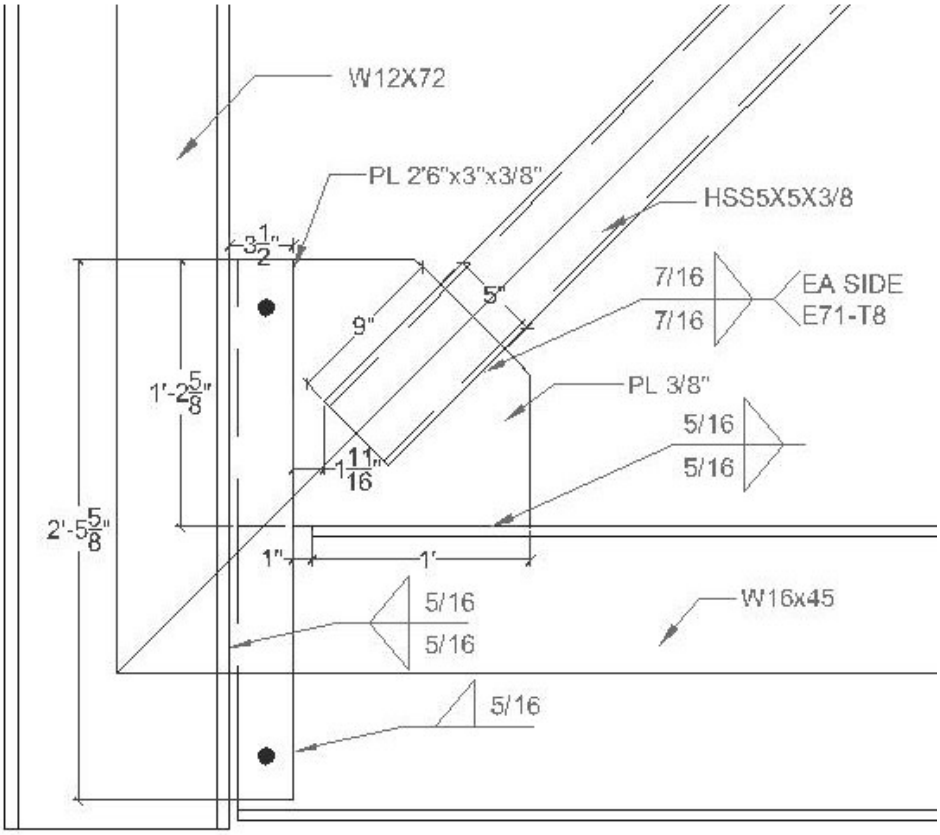

Figure 5.56 NCBF1-R2 Connection Schematic

Figure 5.57 North NCBF1-R2 Undamaged Connection

Table 5.8 shows the changes in DCRs from NCBF1 to NCBF1-R2, which are the same as those for NCBF1. The only changes, aside from the brace local slenderness, which was shown in NCBF1-R1 to have a substantial impact on the performance, are to the limit states associated with the brace-to-gusset plate connection. The DCR change of greatest interest is for Whitmore yielding of the gusset plate. Due to the smaller brace width, the Whitmore section for NCBF1-R1 was slightly smaller, increasing the DCR to 1.5. As a result, greater damage to the gusset plate was expected in NCBF1-R2 than in NCBF1.This narrower brace also increased the DCR for block shear of the gusset plate slightly, while it reduced the DCR for brace block shear due to thicker brace walls. Finally, the net section DCR decreased due the narrower brace, which has a higher shear lag factor. None of these changes were large enough to dramatically affect the system performance. Because NCBF1-R1 suffered weld fractures and was nominally the same as NCBF1-R2, it was expected that a similar weld failure would occur in NCBF1-R2.

Table 5.8 DCRs for NCBF1-R2

Limit State	NCBF1	NCBF1-R2
Brace Net Section Fracture	1.26	1.15
Brace-Gusset Plate Weld Fracture	0.92	0.92
Brace Block Shear	1.14	0.76
Gusset Plate Block Shear	1.16	1.33
Gusset Plate Whitmore Yielding	1.33	1.50
Gusset Plate Buckling	0.74	0.84
Gusset Plate Shear Yielding at Beam	1.16	1.16
Beam-Gusset Weld Fracture	1.55	1.55
Shear Tab to Gusset/Beam Weld Fracture	1.08	1.08
Shear Tab to Column Weld Fracture	0.65	0.65
Brace Local Slenderness	2.04	0.85

Figure 5.58 shows the load-drift history for NCBF1-R2..NCBF1-R2 suffered tearing and eventual fracture of the North beam-to-shear tab and gusset-to-shear tab welds, disconnecting the brace and beam from the column. The frame attained higher drift levels than NCBF1, and the brace performance was significantly more ductile. However, the ultimate connection failure was highly undesirable.

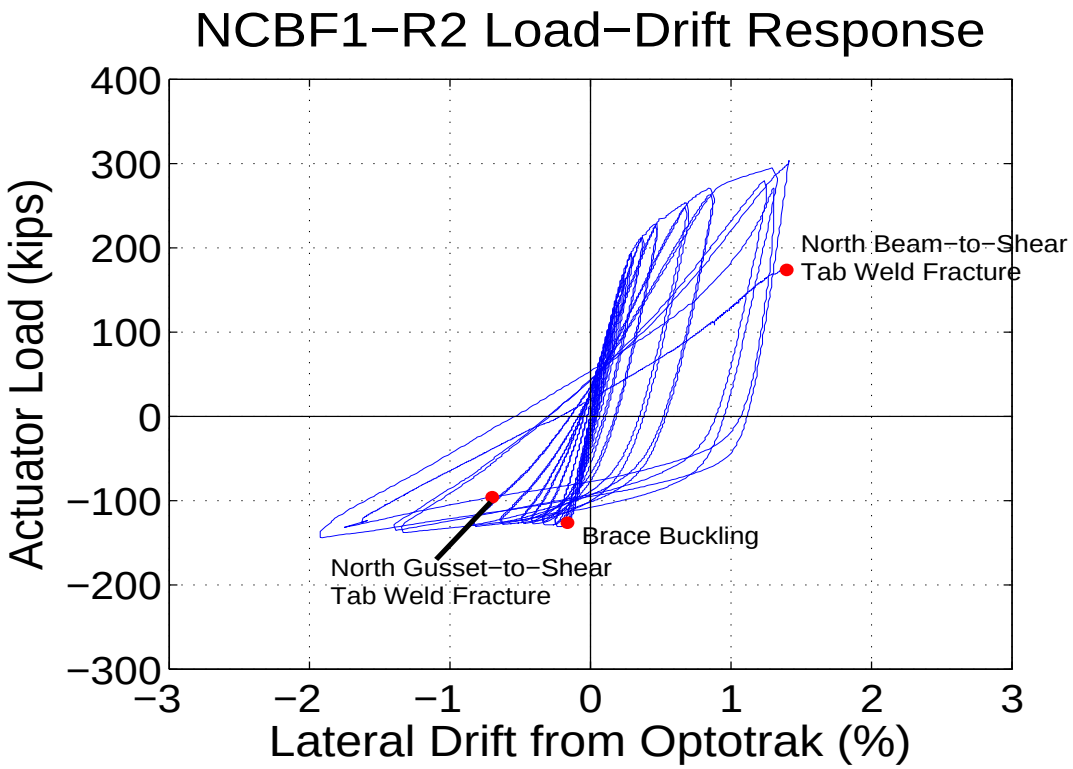

Figure 5.58 NCBF1-R2 Load-Drift Response History

5.7.2 Performance State Summary

Table 5.9 and Table 5.10 show the progression of performance states during the test for the North and South gusset plate connections, respectively. Table 5.11 shows the progression of performance states during the test for the brace, beams, and columns. The positive drift, negative drift, drift range, and cycle number are given in each table. Unlike the previous two specimens, whitewash was applied to NCBF1-R2, so observations of yielding are included in the performance state tables.

Table 5.9 North Connection Performance States

	Drift %			North Plates		North Welds			
Cycle #	Total	Neg.	Pos.	Gusset Plate	Shear Tab	Gusset to Beam	Gusset to Shear Tab	Beam to Shear Tab	Shear Tab to Column
1	0.08	-0.04	0.04						
2	0.08	-0.04	0.04						
3	0.17	-0.08	0.09						
4	0.17	-0.08	0.09						
5	0.24	-0.11	0.13						
6	0.25	-0.11	0.14						
7	0.36	-0.16	0.20						
8	0.36	-0.17	0.18						
9	0.47	-0.24	0.24	Y1	Y1				
10	0.49	-0.25	0.24						
11	0.62	-0.33	0.29						
12	0.62	-0.33	0.29						
13	0.78	-0.41	0.37						
14	0.78	-0.41	0.36						
15	0.95	-0.48	0.47						
16	0.95	-0.49	0.46						
17	1.31	-0.63	0.68	Y2	Y2				
18	1.31	-0.63	0.67						
19	1.67	-0.82	0.86						
20	1.69	-0.83	0.86						
21	2.62	-1.33	1.29						
22	2.62	-1.39	1.24						
23	3.34	-1.92	1.41		Y3	W1		W1	
24	3.34	-1.63	1.31				WF	W3	
25	3.34	///	1.40	Y3	BF	W2		WF	

Table 5.10 South Connection Performance States

	Drift %			South Plates		South Welds			
Cycle #	Total	Neg.	Pos.	Gusset Plate	Shear Tab	Gusset to Beam	Gusset to Shear Tab	Beam to Shear Tab	Shear Tab to Column
1	0.08	-0.04	0.04						
2	0.08	-0.04	0.04						
3	0.17	-0.08	0.09						
4	0.17	-0.08	0.09						
5	0.24	-0.11	0.13						
6	0.25	-0.11	0.14						
7	0.36	-0.16	0.20						
8	0.36	-0.17	0.18						
9	0.47	-0.24	0.24						
10	0.49	-0.25	0.24	Y1					
11	0.62	-0.33	0.29		Y1				
12	0.62	-0.33	0.29						
13	0.78	-0.41	0.37						
14	0.78	-0.41	0.36						
15	0.95	-0.48	0.47						
16	0.95	-0.49	0.46						
17	1.31	-0.63	0.68	Y2					
18	1.31	-0.63	0.67						
19	1.67	-0.82	0.86						
20	1.69	-0.83	0.86						
21	2.62	-1.33	1.29						
22	2.62	-1.39	1.24		Y2				
23	3.34	-1.92	1.41						
24	3.34	-1.63	1.31					W1	
25	3.34	///	1.40	Y3					

Table 5.11 Frame Performance States

	Drift %			Frame				
Cycle #	Total	Neg.	Pos.	Brace	West Column	East Column	North Beam	South Beam
1	0.08	-0.04	0.04					
2	0.08	-0.04	0.04					
3	0.17	-0.08	0.09					
4	0.17	-0.08	0.09					
5	0.24	-0.11	0.13					
6	0.25	-0.11	0.14					
7	0.36	-0.16	0.20	B1				
8	0.36	-0.17	0.18					
9	0.47	-0.24	0.24					
10	0.49	-0.25	0.24					
11	0.62	-0.33	0.29					
12	0.62	-0.33	0.29					
13	0.78	-0.41	0.37					
14	0.78	-0.41	0.36					
15	0.95	-0.48	0.47	B2				
16	0.95	-0.49	0.46					
17	1.31	-0.63	0.68					
18	1.31	-0.63	0.67					
19	1.67	-0.82	0.86					
20	1.69	-0.83	0.86					
21	2.62	-1.33	1.29	B3				
22	2.62	-1.39	1.24					
23	3.34	-1.92	1.41		Y1		Y1	
24	3.34	-1.63	1.31					
25	3.34	///	1.40					

5.7.3 Test Narrative

During the first 6 cycles of the test, up to 0.25% total drift range, the specimen remained elastic and no damage was observed.

At the compressive peak of cycle 7 (-0.16% drift), upward out-of-plane buckling of the brace was visible, classified as performance state B1. This initial buckling is shown in Figure 5.59. At the initiation of brace buckling, the compressive behavior of the system changed substantially, as shown in Figure 5.58. Although the lateral load capacity of the system did not begin to decrease, it became relatively stable as the displacement increased in subsequent cycles.

Figure 5.59 Initial Brace Buckling - B1

At the tensile peak of cycle 9 (+0.24% drift), initial yielding was observed in the North gusset plate and North shear tab. This yielding, classified as performance state Y1, is shown in Figure 5.60 and Figure 5.61. Additionally, both gusset plates bent upward to accommodate the out-of-plane buckling of the brace. The bending of the North and South gusset plates can be seen in Figure 5.62 and Figure 5.63, respectively.

Figure 5.60 North Gusset Plate - Y1

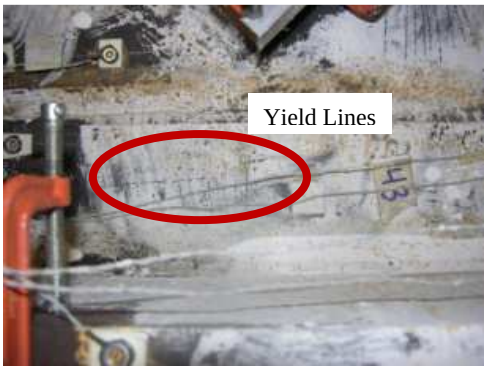

Figure 5.61 North Shear Tab - Y1

Figure 5.62 North Gusset Plate Bending

Figure 5.63 South Gusset Plate Bending

At the compressive peak of cycle 9 (-0.24% drift), the South gusset plate formed initial yield lines at the end of the brace, entering performance state Y1. This is shown in Figure 5.64.

Figure 5.64 South Gusset Plate - Y1

At the tensile peak of cycle 11 (+0.29% drift), initial yielding was observed in the South shear tab, indicating performance state Y1. This yielding is shown in Figure 5.65. Also, the straightening of the brace caused retained some upward rotation, and the gusset plate bent at the edge of the shear tab, as shown for the North connection in Figure 5.66.downward bending of the gusset plates relative to the shear tabs. The shear tabs

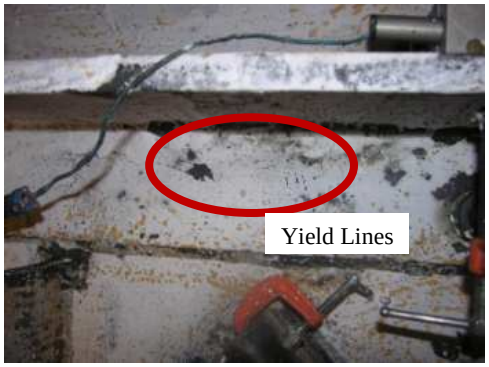

Figure 5.65 South Shear Tab - Y1

Figure 5.66 North Gusset Plate Downward Bending

At the compressive peak of cycle 15 (-0.48% drift) the brace transitioned to performance state B2, as shown in Figure 5.67. The compressive resistance of the frame at this drift was comparable to the resistance at performance state B1, as shown in Figure 5.58. This is demonstrative of the post-buckling strength retention of compact sections.

Figure 5.67 Brace Buckling - B2

At the tensile peak of cycle 17 (+0.68% drift), the North gusset plate, North shear tab, and South gusset plate all transitioned to performance state Y2. The North and South connections are shown in Figure 5.68 and Figure 5.69, respectively. The slope of the load-drift behavior of the frame in tension decreased substantially at this point, as shown in Figure 5.58. This is indicative of yielding, which was extensive in the South gusset plate. Yielding may also have occurred in the brace at this point, but it was not directly observable.

Figure 5.68 North Gusset Plate and North Shear Tab - Y2

Figure 5.69 South Gusset Plate - Y2

At the compressive peak of cycle 19 (-0.82% drift), the gusset plates began bending away from the shear tabs as a result of the upward buckling of the brace. The small gap between the two plates in the South connection is shown in Figure 5.70.

Figure 5.70 Bending of South Gusset Plate from Shear Tab

At the compressive peak of cycle 21 (-1.33% drift), the brace transitioned to performance state B3, as shown in Figure 5.71. The frame continued to maintain lateral load resistance in compression, as shown in Figure 5.58.

Figure 5.71 Brace Buckling - B3

At the tensile peak of cycle 22, the second cycle at this displacement level (+1.24% drift), the South shear tab yielding increased, transitioning to performance state Y2, as shown in Figure 5.72.

Figure 5.72 South Shear Tab - Y2

At the tensile peak of cycle 23 (+1.41% drift), initial yielding was observed in the North flange of the North beam, 12 inches East of the end of the load beam. This was classified as performance state Y1, as shown in Figure 5.73.

Figure 5.73 North Flange of North Beam - Y1

Also at the tensile peak of cycle 23, a substantial increase in the downward bending of the North gusset plate at the shear tab was observed. Residual upward bending of the shear tab increased from previous cycles, forcing a hinge to form in the gusset plate at the edge of the shear tab, as shown in Figure 5.74. Yielding also increased in the North shear tab, which moved to performance state Y3, as shown in Figure 5.75.

Figure 5.74 Bending of North Gusset Plate

Figure 5.75 North Shear Tab - Y3

At the compressive peak of cycle 23 (-1.92% drift), initial weld damage was observed. A 1 inch weld tear initiated at the North end of the North beam-to shear tab weld. This tear was classified as performance state W1 and is shown in Figure 5.76. A 1/4 inch long hairline crack developed at the West end of the North gusset-to-bea weld. This was also categorized as performance state W1, and it is shown in Figure 5.77. It is surprising that tearing initiated first in this weld, as the DCR for the beam-to-gusset weld was significantly higher than for the shear tab weld.

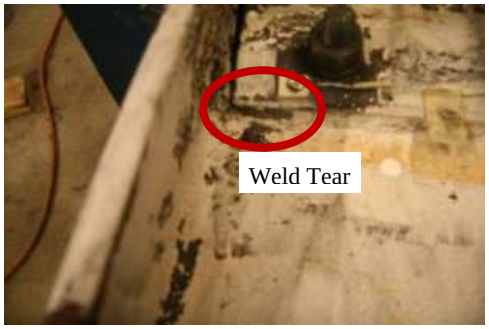

Figure 5.76 W1 in North Beam-to-Shear Tab Weld

Figure 5.77 W1 in North Gusset-to-Beam Weld

Also at the compressive peak of cycle 23, yielding was observed in the West flange of the West Column at the South connection. This yielding, classified as performace state Y1, is shown in Figure 5.78.

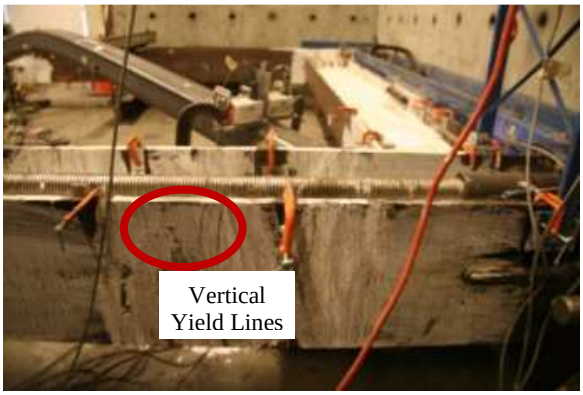

Figure 5.78 West Flange, West Column - Y1

At the tensile peak of cycle 24, the second cycle at this displacement level (1.31% drift), a large crack appeared in the middle of the North gusset-to-shear tab weld. This crack was 4 inches in length, immediately putting the North gusset-to-shear tab weld in performance state W3. This crack is pictured in Figure 5.79. A second weld crack developed at the South end of the North beam-to-shear tab weld. This crack was 1.5 inches in length, bringing the North beam-to-shear tab weld into performance state W2, as shown in Figure 5.80. Also, new weld tear was also observed in the South connection. A 1 inch tear developed at the South end of the South beam-to-shear tab weld, classified as W1 and shown in Figure 5.81.

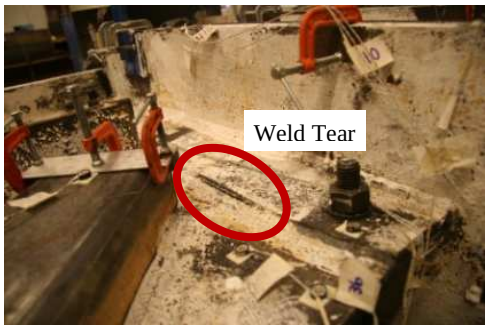

Figure 5.79 W3 in North Gusset-to-Shear Tab Weld

Figure 5.80 New Tear in North Beam-to-Shear Tab Weld

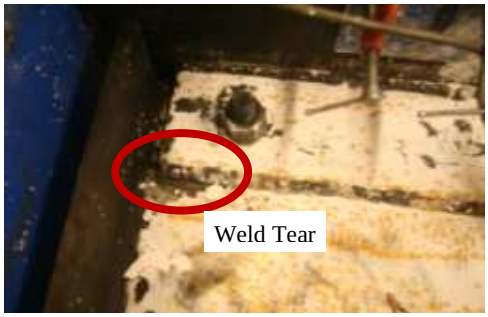

Figure 5.81 W1 in South Beam-to-Shear Tab Weld

At the compressive peak of cycle 24 (-1.63% drift), complete fracture of the North gusset-to-shear tab weld occurred, as shown in Figure 5.82. As a result of this fracture, the North shear tab curled downward significantly along the length of the North beam-to-shear tab weld, shown in Figure 5.83. This fracture did not substantially affect the lateral load capacity of the system in compression, as shown in Figure 5.58.

Figure 5.82 Fracture of North Gusset-to-Shear Tab Weld

Figure 5.83 Downward Bending of N Shear Tab

Prior to reaching the tensile peak of cycle 25, the North beam-to-shear tab weld fractured completely, ending the test. The fracture of the North beam-to-shear tab weld is shown in Figure 5.84. The weld fracture also caused the fracture of both erection bolts in the NE shear tab. The North beam was pulled downward by the brace, causing the North flange of the beam to bear against the North shear tab, as shown in Figure 5.85. The point of fracture on the load-drift history is shown in Figure 5.58.

Figure 5.84 Complete Fracture of the North Shear Tab Weld

Figure 5.85 North Beam Bearing on North Shear Tab

A 2 inch weld crack also formed at the East end of the North gusset-to-beam weld, classified as performance state W1. The crack is shown after frame disassembly in Figure 5.86. Both the north and South gusset plate had slightly increased yielding, moving both plates to performance state Y3. The gusset plates are shown in Figure 5.87 and Figure 5.88.

Figure 5.86 W1 in North Gusset-to-Beam Weld (After Disassembly)

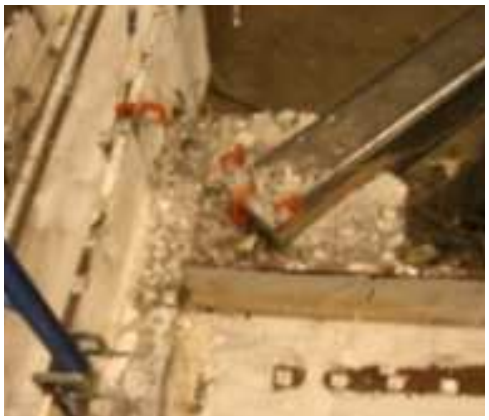

Figure 5.87 North Gusset Plate - Y3

Figure 5.88 South Gusset Plate - Y3

5.7.4 Test Summary

NCBF1-R2 achieved a total drift range of 3.34%, which constitutes a substantial improvement over the performance of NCBF1. The brace did not buckle locally or tear, and survived to much higher drift levels than the non-compact brace used in NCBF1. However, NCBF1-R2 suffered a rapid connection failure, which resulted in complete fracture of the connection between the brace/beam and the column in just two cycles after crack initiation. The nature of this failure, which disconnects the beam from the column, is disconcerting because of its implications for structural performance.

This connection failed by a different, and less desirable series of weld fractures than NCBF1-R1. These connections were almost identical to one another, which highlights the level of uncertainty associated with the performance of deficient and non-notch tough welds. Brace end rotation appeared to put substantial demands on the connection, as was the case with NCBF1-R1. Improving the brace performance and drift range came at the cost of a less desirable failure mode.

It is somewhat surprising that the shear tab weld failed first in NCBF1-R2, as the DCR for the gusset plate-to-beam weld was significantly larger. Other limit states with DCRs greater than 1, including net section fracture and gusset plate and brace block shear, did not occur, indicating that high DCRs for these limit states may not be as large of a concern. The gusset plates yielded extensively, as expected given the high DCR for Whitmore yielding. However, this yielding does not appear to have adversely affected the system performance, although it is possible that high strain concentrations caused initiation of weld tearing.

5.8 NCBF1-R3

5.8.1 Specimen Overview

Specimen NCBF1-R3 investigates an in-plane buckling retrofit to potentially reduce the out-of-plane deformation demands on the NCBF1 connection. Specimens NCBF1-R1 and NCBF1-R2 demonstrated that replacing the non-compact brace with a compact one significantly increased the drift capacity of the system. However, these retrofits caused higher damage concentration in the connections, resulting in sudden and undesirable failures. Weld tearing in the gusset-beam weld and the gusset-shear tab weld propagated and led to failure in both tests. It appeared likely that the end rotation of the brace during buckling was contributing to the demands that caused weld tearing. An in-plane buckling retrofit could reduce these rotational demands, potentially protecting the connection welds without requiring replacement of the gusset plate.

NCBF1-R3 used the same brace, HSS5x5x3/8 as specimens NCBF1-R1 and NCBF1-R2. Two knife plates were installed perpendicular to the gusset plate and parallel to the brace axis to increase the brace effective length for in-plane buckling while decreasing the effective length for out-of-plane buckling, as shown in Figure 5.89. A photograph of the connection is shown in Figure 5.90.

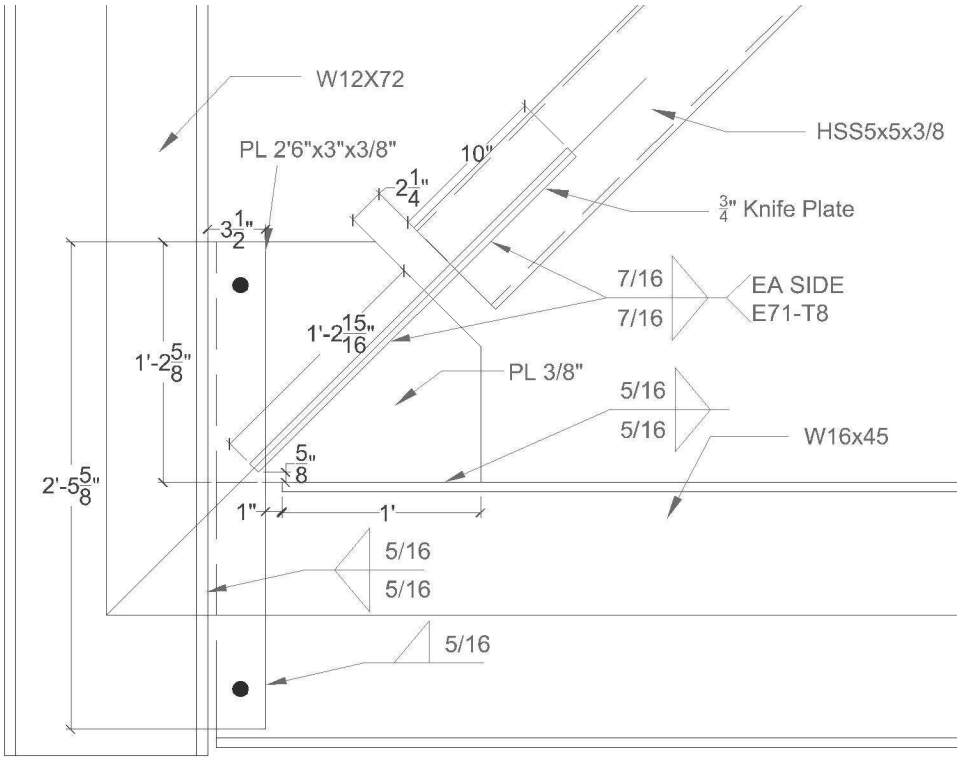

Figure 5.89 NCBF1-R3 Connection Detail

Figure 5.90 NCBF1-R3 Connection

Table 5.8.1.1 shows the changes in DCRs from NCBF1 to NCBF1-R3. As with previous retrofits, brace local slenderness was decreased substantially. The DCR for brace net section decreased modestly, because while a more compact brace was used, a larger slot was required for the thick knife plate, and the effects of these changes essentially offset. By extending the knife plate far into the connection, the gusset plate DCRs were kept essentially the same. The Whitmore width remained essentially the same, as did the area resisting block shear. Limit states not associated with the brace-to-gusset plate connection were unchanged, as with the previous retrofits.

NCBF1-R3 had lower DCRs for gusset plate limit states than NCBF1-R2, so less yielding was expected in the gusset plates. The DCRs for the welds were unchanged, but it was expected that reducing the rotational demands would be sufficient to overcome these deficiencies.

Table 5.12 DCRs for NCBF1-R3

Limit State	NCBF1	NCBF1-R3
Brace Net Section Fracture	1.26	1.21
Brace-Gusset Plate Weld Fracture	0.92	0.92
Brace Block Shear	1.14	0.76
Gusset Plate Block Shear	1.16	1.22
Gusset Plate Whitmore Yielding	1.33	1.28
Gusset Plate Buckling	0.74	0.70
Gusset Plate Shear Yielding at Beam	1.16	1.16
Beam-Gusset Weld Fracture	1.55	1.55
Shear Tab to Gusset/Beam Weld Fracture	1.08	1.08
Shear Tab to Column Weld Fracture	0.65	0.65
Brace Local Slenderness	2.04	0.85
Knife Plate Yielding	///	1.04

During early cycles of the test, it was discovered that the brace was buckling out-of-plane downward. Limited clearance between the frame and the floor would not permit completion of the test, so a support with a friction reducing interface was placed under the mid-span of the brace, as shown in Figure 5.91. The specimen had sustained negligible damage at that point, so the test was restarted with the support in place.

Figure 5.91 NCBF1-R3 Brace Support

The brace for NCBF1-R3 buckled both in-plane and out-of plane. Weld tearing in the North gusset-to-beam weld and the North shear tab weld initiated at the North end of the knife plate. These tears propagated, resulting in fracture of the gusset-to-beam weld and the beam-to-shear tab weld. The latter of these fractures disconnected the beam from the column, ending the test. The load-drift response history for NCBF1-R3 is given in Figure 5.92.

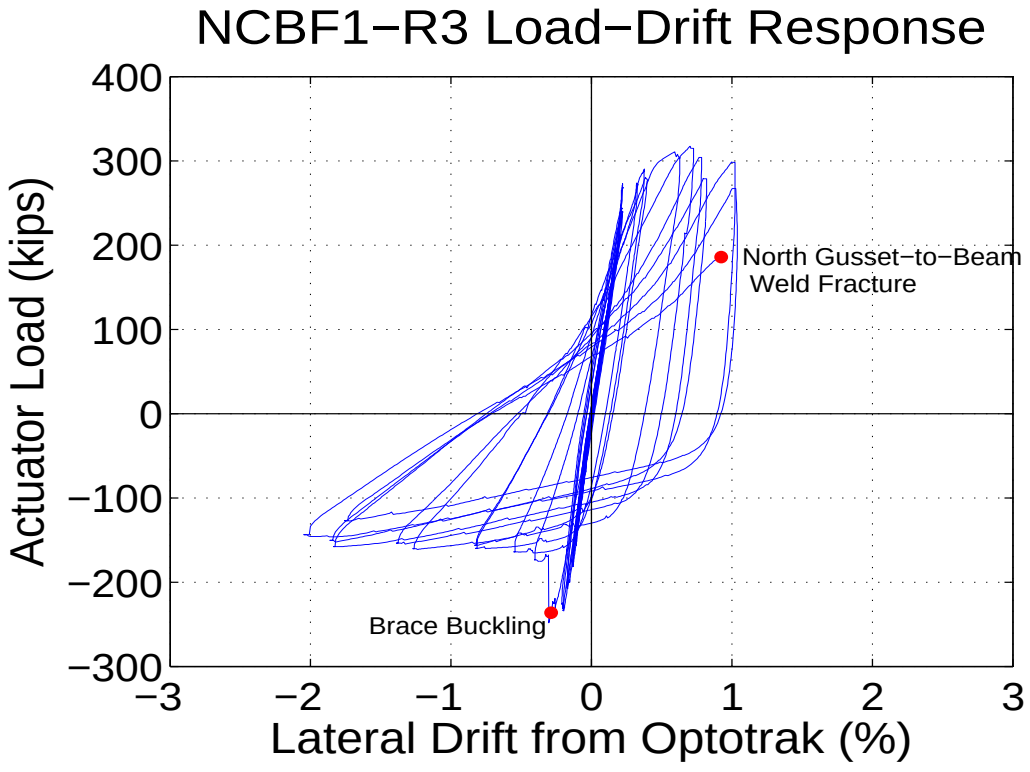

Figure 5.92 NCBF1-R3 Load-Drift Response History

5.8.2 Performance State Summary

Table 5.13 and Table 5.14 show the progression of performance states during the test for the North and South gusset plate connections, respectively. Table 5.15 shows the progression of performance states during the test for the brace, beams, and columns. The positive drift, negative drift, drift range, and cycle number are given in each table. Whitewash was applied to NCBF1-R3, so observations of yielding are included in the performance state tables.

Table 5.13 North Connection Performance States

	Drift %			North Plates			North Welds			
Cycle #	Total	Neg.	Pos.	Gusset Plate	Shear Tab	Knife Plate	Gusset to Beam	Gusset to Shear Tab	Beam to Shear Tab	Shear Tab to Column
1	0.07	-0.03	0.04							
2	0.07	-0.03	0.04							
3	0.10	-0.04	0.06							
4	0.11	-0.04	0.07							
5	0.17	-0.07	0.10							
6	0.17	-0.07	0.10							
7	0.23	-0.09	0.13							
8	0.23	-0.09	0.13							
9	0.28	-0.11	0.17							
10	0.29	-0.12	0.17							
11	0.35	-0.14	0.21	Y1						
12	0.35	-0.13	0.20							
13	0.38	-0.17	0.21							
14	0.39	-0.17	0.21							
15	0.42	-0.20	0.22		Y1					
16	0.43	-0.21	0.22							
17	0.63	-0.40	0.23			Y2				
18	0.88	-0.55	0.33							
19	1.20	-0.82	0.38	Y2		Y3				
20	1.23	-0.83	0.40							
21	1.90	-1.27	0.63	Y3	Y3					
22	2.11	-1.39	0.72							
23	2.61	-1.84	0.78				W2			
24	2.68	-1.86	0.82							
25	3.06	-2.05	1.02		MT		W3		W2	
26	3.06	-1.76	1.02						W3	
27	3.06	///	0.92				WF	W3	WF	

Table 5.14 South Connection Performance States

	Drift %			South Plates			South Welds			
Cycle #	Total	Neg.	Pos.	Gusset Plate	Shear Tab	Knife Plate	Gusset to Beam	Gusset to Shear Tab	Beam to Shear Tab	Shear Tab to Column
1	0.07	-0.03	0.04							
2	0.07	-0.03	0.04							
3	0.10	-0.04	0.06							
4	0.11	-0.04	0.07							
5	0.17	-0.07	0.10							
6	0.17	-0.07	0.10							
7	0.23	-0.09	0.13							
8	0.23	-0.09	0.13							
9	0.28	-0.11	0.17							
10	0.29	-0.12	0.17							
11	0.35	-0.14	0.21	Y1	Y1					
12	0.35	-0.13	0.20							
13	0.38	-0.17	0.21							
14	0.39	-0.17	0.21							
15	0.42	-0.20	0.22		Y2					
16	0.43	-0.21	0.22							
17	0.63	-0.40	0.23			Y2				
18	0.88	-0.55	0.33							
19	1.20	-0.82	0.38	Y2	Y3	Y3				
20	1.23	-0.83	0.40							
21	1.90	-1.27	0.63							
22	2.11	-1.39	0.72							
23	2.61	-1.84	0.78	Y3			W2			
24	2.68	-1.86	0.82							
25	3.06	-2.05	1.02							
26	3.06	-1.76	1.02					W1	W1	
27	3.06	///	0.92							

Table 5.15 Frame Performance States

	Drift %			Frame				
Cycle #	Total	Neg.	Pos.	Brace	West Column	East Column	North Beam	South Beam
1	0.07	-0.03	0.04					
2	0.07	-0.03	0.04					
3	0.10	-0.04	0.06					
4	0.11	-0.04	0.07					
5	0.17	-0.07	0.10					
6	0.17	-0.07	0.10					
7	0.23	-0.09	0.13					
8	0.23	-0.09	0.13					
9	0.28	-0.11	0.17					
10	0.29	-0.12	0.17					
11	0.35	-0.14	0.21					
12	0.35	-0.13	0.20					
13	0.38	-0.17	0.21					
14	0.39	-0.17	0.21					
15	0.42	-0.20	0.22					
16	0.43	-0.21	0.22					
17	0.63	-0.40	0.23	B1				
18	0.88	-0.55	0.33					
19	1.20	-0.82	0.38	B2	Y1			
20	1.23	-0.83	0.40					
21	1.90	-1.27	0.63				Y1	
22	2.11	-1.39	0.72					
23	2.61	-1.84	0.78	B3		Y1		
24	2.68	-1.86	0.82					
25	3.06	-2.05	1.02		Y2			
26	3.06	-1.76	1.02					
27	3.06	///	0.92				BE,MT	

5.8.3 Test Narrative

During the first 10 cycles of the test, up to 0.29% total drift range, the frame behaved elastically, and no damage to components was observed.

At the tensile peak of cycle 11 (+0.21% drift), yield lines were observed in the South shear tab and both gusset plates, classified as performance state Y1. Figure 5.93 and Figure 5.94 show yielding of the North

and South gusset plates. Figure 5.95 shows yielding of the South shear tab, which was concentrated around the end of the knife plate.

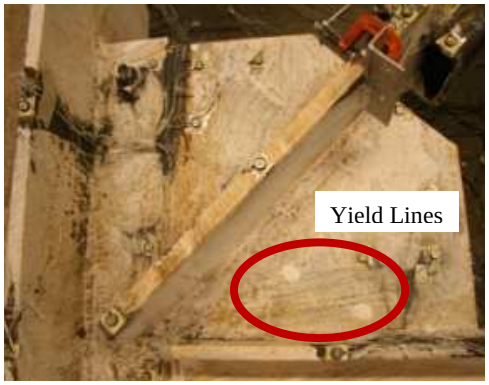

Figure 5.93 North Gusset Plate - Y1

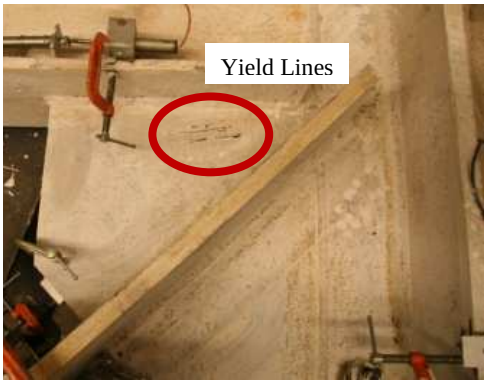

Figure 5.94 South Gusset Plate - Y1

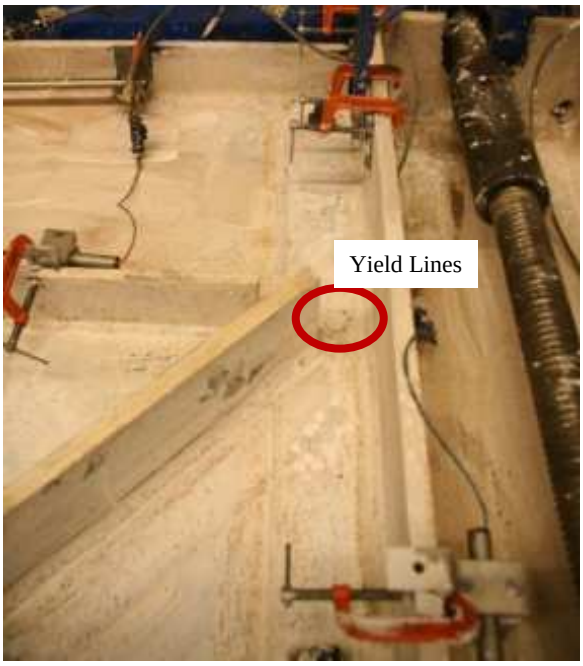

Figure 5.95 South Shear Tab - Y1

At the tensile peak of cycle 15 (+0.22% drift), the North shear tab entered performance state Y1 with emergence of yield lines around the end of the knife plate, shown in Figure 5.96. The south shear tab yielded along most of its length, transitioning to performance state Y2, as shown in Figure 5.97.

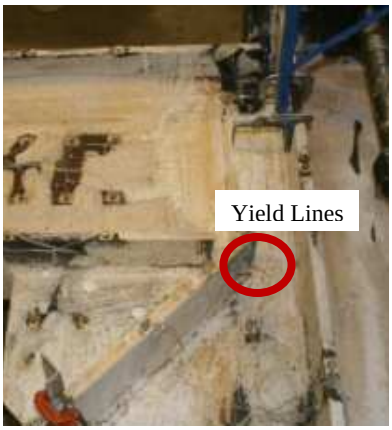

Figure 5.96 North Shear Tab - Y1

Figure 5.97 South Shear Tab - Y2

At the compressive peak of cycle 17 (-0.40% drift), the brace buckled suddenly in-plane to the South, entering performance state B1 and causing a significant drop in compressive resistance, as shown in Figure 5.92. This sudden buckling likely occurred due to the restraint at the brace midspan, which may have restricted in-plane movement via friction until the resistance was suddenly overcome as slip occurred. The brace buckled shape is shown in Figure 5.98. As a result of the buckling, both knife plates yielded substantially in the clear region between the brace and the gusset plate on the South side. Yielding in the North and South plates, shown in Figure 5.99 and Figure 5.100, was characterized as performance state Y2. The brace buckling also resulted in a substantial loss of compressive lateral load resistance, as shown in Figure 5.92.

Figure 5.98 Brace In-Plane Buckling - B1

Figure 5.99 North Knife Plate - Y2

Figure 5.100 South Knife Plate - Y2

At the tensile peak of cycle 19 (+0.38% drift), the South shear tab was yielded over the majority of its area, indicating performance state Y3. The South gusset plate also had increased yielding, transitioning to performance state Y2. Yielding in the South connection is shown in Figure 5.101. The North gusset plate also had increased yielding, categorized as performance state Y2, as shown in Figure 5.102. At this point, the slope of the load-drift behavior of the frame in tension decreased substantially, indicating extensive

yielding. The observed yielding in the shear tabs and gusst plates likely contributed to this, as the expected tensile strength of the gusset plate was lower than that of the brace.

Also, initial yielding was observed in the West flange of the West column at the North connection. This yielding was classified as performance state Y1, and is shown in Figure 5.103.

Figure 5.101 South Shear Tab - Y3 and South Gusset Plate - Y2

Figure 5.102 North Gusset Plate - Y2

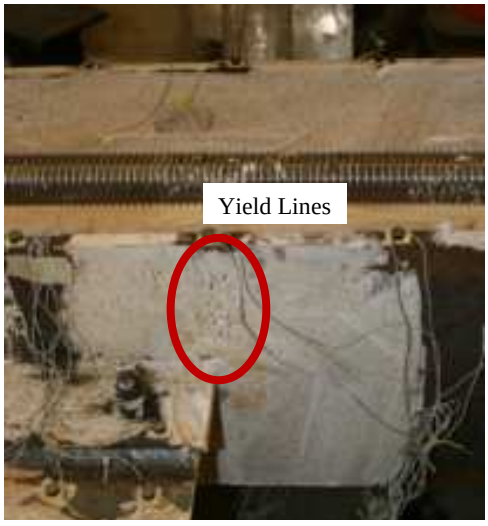

Figure 5.103 West Column West Flange - Y1

At the compressive peak of cycle 19 (-0.82% drift), brace in-plane buckling increased to performance state B2, as shown in Figure 5.104. After the initial sudden buckling, the compressive resistance of the system remained relatively stable as displacement increased, as shown in Figure 5.92. This is consistent with the behavior of the compact brace sections used in NCBF1-R1 and NCBF1-R2. As a result of the increased buckling, both knife plates transitioned to performance state Y3, with yielding over almost the entire region between the gusset plate and the brace. Yielding of the North and South knife plates is shown in Figure 5.105 and Figure 5.106. Although the knife plates were designed to carry the full tensile capacity of the brace without yielding, the rotational demands due to brace buckling still caused extensive yielding.

Figure 5.104 Brace Buckling - B2

Figure 5.105 North Knife Plate - Y3

Figure 5.106 South Knife Plate - Y3

At the tensile peak of cycle 21 (+0.63% drift), yielding in the North connection increased substantially. The gusset plate and shear tab transitioned to performance state Y3, as shown in Figure 5.107. This increased yielding corresponded to the peak tensile load resisted by the frame. After this point, the extensive connection damage caused a gradual weakening of the system in tension.

Additionally, initial yielding was observed in the North beam at the end of the load beam. This yielding, classified as performance state Y1, is shown in Figure 5.108.

Figure 5.107 North Gusset Plate and Shear Tab - Y3

Figure 5.108 North Flange, North Beam - Y1

At the compressive peak of cycle 21 (-1.27% drift), the brace began to buckle upward out-of-plane, in addition to the in-plane buckling. At this cycle, the in-plane deformation was four times as large as the out-of plane deformation at the midspan. The upward buckling of the brace is shown in Figure 5.109. As a result of this upward buckling, upward bending was observed in both gusset plates. Bending of the North and South gusset plates is shown in Figure 5.110 and Figure 5.111.

Figure 5.109 Brace Upward Out-of-Plane Buckling

Figure 5.110 Upward Bending of N Gusset Plate

Figure 5.111 Upward Bending of S Gusset Plate

At the tensile peak of cycle 22, the second cycle at this displacement level (+0.72% drift), both gusset plates hinged downward slightly at the edge of the shear tab. The shear tabs retained some upward out-of-plane rotation from the brace out-of-plane buckling, and the gusset plate folded downward to accommodate the straightening of the brace. The bending of the North gusset plate is shown in Figure 5.112.

Figure 5.112 North Gusset Plate Downward Bending at Shear Tab

At the tensile peak of cycle 23 (+0.78% drift), yielding in the South gusset plate increased to performance state Y3, as shown in Figure 5.113. Additionally, the South shear tab was almost completely yielded at this drift level. Also, two weld cracks were observed. 3 inch long weld cracks formed in both gusset-beam welds on the underside at the face of the column. These cracks, classified as performance state W2, are shown in Figure 5.114 and Figure 5.115 for the North and South connections, respectively.Damage of this type was not observed in the first three specimens, so it may have resulted from the knife plate retrofit.

Figure 5.113 South Gusset Plate - Y3

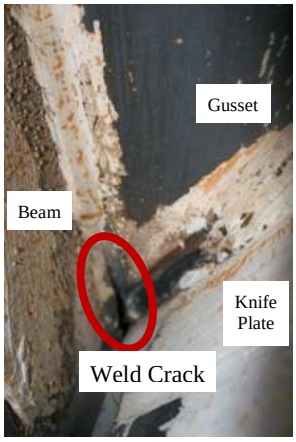

Figure 5.114 W2 in North Gusset-to-Beam Weld (Underside)

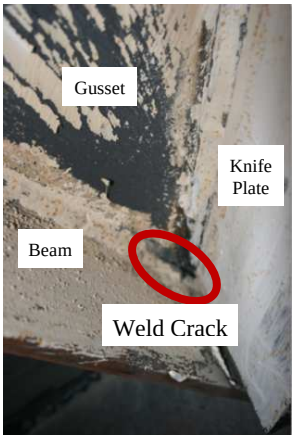

Figure 5.115 W2 in South Gusset-to-Beam Weld (Underside)

At the compressive peak of cycle 23 (-1.84% drift), the combined in-plane and out-of-plane deformations classified the brace in performance state B3. The in-plane and out-of-plane deformations were roughly equal at this cycle. Figure 5.116 shows the in-plane buckling, and Figure 5.117 shows the out-of-plane buckling.

Figure 5.116 Brace In-Plane Buckling - B3

Figure 5.117 Brace Out-of-Plane Buckling - B3

Also at the compressive peak of cycle 23, additional frame damage was observed at several locations. The East flange of the East column at the North connection entered performance state Y1, as shown in Figure 5.118. The West Column, West Flange at the south connection also entered performance state Y1, shown in Figure 5.119. Upward bending of the web of the North beam was observed at the North shear tab, as shown in Figure 5.120. The North erection bolt fastening the beam web to the shear tab effectively clamped the two components, causing the beam web to curl upward in conjunction with the downward bending of the shear tab, which is shown in Figure 5.121.

Figure 5.118 Scattered Yielding in East Column - Y1

Figure 5.119 Initial Yielding in West Column - Y1

Figure 5.120 Upward Bending of N Beam Web

Figure 5.121 Downward Bending of N Shear Tab

At the tensile peak of cycle 25, (+1.02% drift), a crack formed in the North beam-to-shear tab weld at the end of the knife plate. The crack was 4" in length, classified as performance state W2. At the end of the knife plate, the weld crack propagated West 1/8" into the shear tab. This damage is shown in Figure 5.122. This supports the concept that damage may concentrate around the end of the knife plate.

Figure 5.122 North Beam-to-Shear Tab Weld - W2 and North Shear Tab - MT

At the compressive peak of cycle 25 (-2.05% drift), a 6 inch weld crack formed at the West end of the North gusset-to-beam weld. This crack, classified as performance state W3, is shown in Figure 5.123. This crack was unusual in that it covered a large portion of the weld length immediately after initiation, whereas previous specimens initially had more gradual crack growth. Also, yielding increased in the West Flange of the West column at the South connection. The new yielding, classified as W2, is shown in Figure 5.124.

Figure 5.123 W3 in North Gusset-to-Beam Weld

Figure 5.124 Yielding of West Column

At the tensile peak of cycle 26, the second cycle at this displacement level (+1.02% drift), the North gusset plate began to exhibit torsional deformation. The plate was twisting about the axis of the brace. Figure 5.125 and Figure 5.126 show the bending of the South and West edges of the gusset plate, respectively. This deformation was due to the combined in-plane and out of plane buckling of the brace, which caused it to twist slightly as it deformed.

Figure 5.125 Upward Bending of N Beam Web

Figure 5.126 Downward Bending of N Shear Tab

Also at the tensile peak of cycle 26, two weld cracks were observed in the South connection. A 1 inch tear in the North gusset-to-shear tab weld at the North end, classified as performance state W1, is shown in

Figure 5.127. A 1 inch tear in the South beam-to-shear tab weld at the end of the knife plate, classified as performance state W1, is shown in Figure 5.128.

Figure 5.127 W-SGS - W1

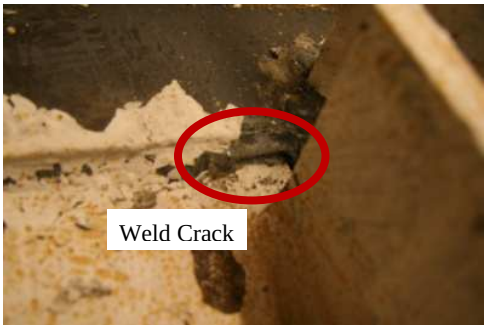

Figure 5.128 W-SBS - W1

At the compressive peak of cycle 26 (-1.76% drift), tearing in the North gusset-to-beam weld increased to the point where only 1/2 an inch of intact weld remained. This is shown in Figure 5.129. A new weld tear also initiated in the South gusset-to-beam weld at the East end. The 1 inch tear, which did not change the performance state of the weld, is shown in Figure 5.130.

Figure 5.129 Increased Tearing in North Gusset-to-Beam Weld

Figure 5.130 New Tear in South Gusset-to-Beam Weld

At the tensile peak of cycle 27 (0.92% drift), the North gusset-to-beam weld fractured completely, as shown in Figure 5.131. As a result of this fracture, tearing in the North beam-to-shear tab weld increased substantially, transitioning to performance state W3, as shown in Figure 5.132. In conjunction with this tear, the North shear tab bent downward more severely in the beam region, shown in Figure 5.133. The weld fracture caused a substantial loss of tensile resistance in the frame, shown in Figure 5.92.

Figure 5.131 Fracture of North Gusset-to-Beam Weld

Figure 5.132 W3 in North Beam-to-Shear Tab Weld

Figure 5.133 Downward Bending of N Shear Tab

A large weld tear also formed in the North gusset-to-shear tab weld, starting at the end of the knife plate and propagating South. This tear was also classified as W3, as shown in Figure 5.134. The metal tearing in the North shear tab at the end of the knife plate also intensified significantly. The tear propagated South 2 inches and was 1/2 an inch wide, as shown in Figure 5.135. No new damage was observed in the South connection.

Figure 5.134 W3 in North Gusset-to-Shear Tab Weld

Figure 5.135 Increased MT of North Shear Tab

Prior to reaching the compressive peak of cycle 27, complete fracture of the North beam-to-shear tab weld occurred, ending the test, as shown in Figure 5.136.

Figure 5.136 Fracture of North Beam-to-Shear Tab Weld

As a result of this fracture, the tearing of the North shear tab propagated and joined with the tear in the North gusset-to-shear tab weld, as shown in Figure 5.137. A small portion of the North gusset-to-shear

tab weld at the South end was intact. The North erection bolt in the North connection had a pullout failure in the beam web as a result of the weld fracture. This is shown in Figure 5.138.

Figure 5.137 North shear tab - MT

Figure 5.138 Erection Bolt Pullout from North Beam Web

The South connection did not sustain a significant increase in damage during this cycle. The final state of the South connection is shown in Figure 5.139.

Figure 5.139 Final Damage to South Connection

5.8.4 Test Summary

NCBF1-R3 was not successful at protecting the connection welds from damage. Although the frame was able to sustain large drifts relative to NCBF1, the ultimate failure mode for the frame was the fracture of the beam to column weld, which is a highly undesirable failure in a structure. The brace did not buckle purely in-plane, and the out of plane deformations may have contributed to the deterioration of the North connection. As this specimen and previous specimens demonstrated, welds without notch toughness requirements are vulnerable to unstable crack growth over a relatively small number of cycles. Additionally, yielding in the connections was extensive despite the reduction in DCR for Whitmore yielding achieved with a longer knife plate. Extensive yielding in the connection may reduce the lateral load that can be carried by the frame. The longer knife plate may also have caused concentration of damage, as weld tears in the gusset-to-beam and shear tab welds initiated at the North end of the knife plate. As the lengthening of the knife plate did not prevent out-of-plane buckling or reduce damage to the connection, it appears that it was not an effective design.

This test also demonstrated that a higher effective length factor for out-of-plane buckling is necessary for this connection, which is very flexible to out-of-plane deformations. The gusset plate and shear tab are thin (3/8 inch), which makes the connection more flexible and thus reduces the brace end fixity.

5.9 NCBF1-R4

5.9.1 Specimen Overview

NCBF1-R4 was a retrofit of NCBF1 that used an in-plane buckling brace with the goal of protecting the welds by reducing the rotational demands on the connection. In plane buckling was achieved using a knife plate connection, pictured in Figure 5.141. NCBF1-R3 also utilized a knife plate retrofit, but its brace buckled significantly out-of-plane in addition to in plane. In order to reduce the extent of out-of-plane buckling for NCBF1-R4, an HSS6x4x3/8 brace was used in place of the HSS5x5x3/8 brace used for NCBF1-R3. Additionally, concentration of weld damage around the end of the knife plates in NCBF1-R3 raised concerns that the knife plate might be concentrating strains at its end. To address this issue, a shorter knife plate was used in NCBF1-R3. Rather than extending the knife plate back to the shear tab, a considerably shorter 10 inch gusset to knife plate splice length was used. Figure 5.140 shows a detail of the connection for NCBF1-R4.

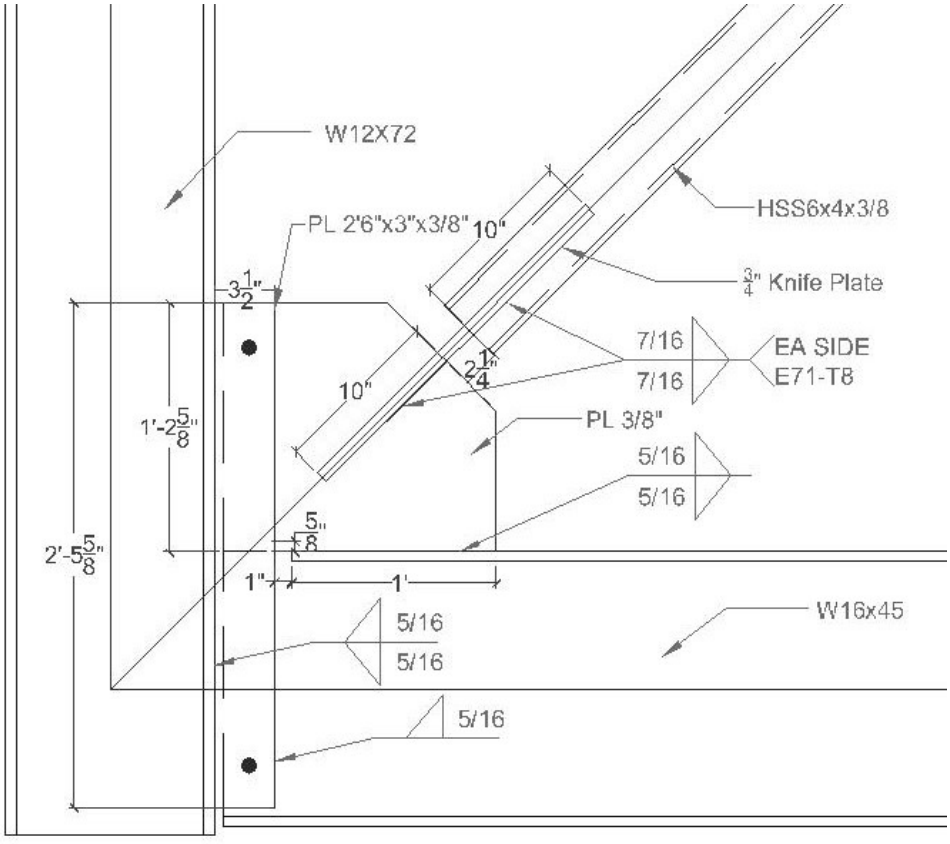

Figure 5.140 NCBF1-R4 Connection Detail

Figure 5.141 NCBF1-R4 Undamaged North Connection

Table 5.16 shows the DCRs for NCBF1-R4. Shortening the knife plate caused very high DCRs for gusset plate Whitmore yielding and gusset plate block shear. These values were sufficiently large to raise concerns over a possible gusset plate failure. However, this was seen as a viable option to attempt to protect the deficienct welds in the connection. The rectangular HSS had a slightly higher local slenderness than the square HSS used for other the othe retrofits, but it was still much lower than for NCBF1. The other DCRs for the connection either remained the same or changed marginally.

Table 5.16 NCBF1-R4 Connection DCRs

Limit State	**NCBF1**	**NCBF1-R4**
Brace Net Section Fracture	1.26	1.16
Brace-Gusset Plate Weld Fracture	0.92	0.92
Brace Block Shear	1.14	0.76
Gusset Plate Block Shear	1.16	1.78
Gusset Plate Whitmore Yielding	1.33	1.89
Gusset Plate Buckling	0.74	1.03
Gusset Plate Shear Yielding at Beam	1.16	1.16
Beam-Gusset Weld Fracture	1.55	1.55
Shear Tab to Gusset/Beam Weld Fracture	1.08	1.08
Shear Tab to Column Weld Fracture	0.65	0.65
Brace Local Slenderness	2.04	1.07
Knife Plate Yielding	///	1.04

Figure 5.142 shows the load-drift history for NCBF1-R4.The brace for NCBF1-R4 buckled almost purely in plane. At 1.26% drift in tension, the North beam-to-shear tab and North gusset-to-shear tab welds fractured suddenly, resulting in complete disconnection of the North beam and the brace from the East column. This event forced the conclusion of the test.

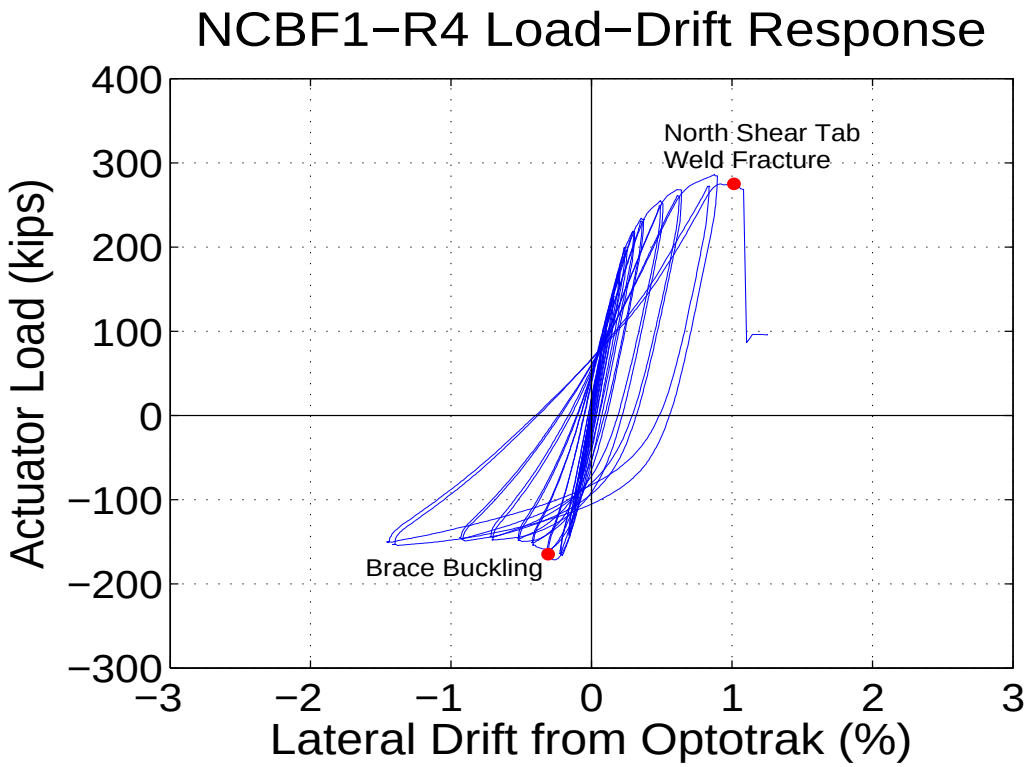

Figure 5.142 NCBF1-R4 Load-Drift Response History

5.9.2 Performance State Summary

Table 5.17 and Table 5.18 show the progression of performance states during the test for the North and South gusset plate connections, respectively. Table 5.19 shows the progression of performance states during the test for the brace, beams, and columns. The positive drift, negative drift, drift range, and cycle number are given in each table. Whitewash was applied to NCBF1-R4, so observations of yielding are included in the performance state tables.

Table 5.17 North Connection Performance States

	Drift %			North Plates			North Welds			
Cycle #	Total	Neg.	Pos.	Gusset Plate	Shear Tab	Knife Plate	Gusset to Beam	Gusset to Shear Tab	Beam to Shear Tab	Shear Tab to Column
1	0.07	-0.04	0.03							
2	0.07	-0.04	0.03							
3	0.15	-0.08	0.07							
4	0.15	-0.08	0.07							
5	0.23	-0.12	0.11							
6	0.23	-0.12	0.11							
7	0.33	-0.16	0.17	Y1						
8	0.33	-0.16	0.17							
9	0.44	-0.23	0.21		Y1					
10	0.44	-0.23	0.20							
11	0.57	-0.32	0.25			Y1				
12	0.57	-0.32	0.24							
13	0.74	-0.43	0.31			Y3				
14	0.74	-0.43	0.31							
15	0.91	-0.52	0.39							
16	0.91	-0.52	0.37							
17	1.23	-0.71	0.52	Y2						
18	1.23	-0.72	0.49							
19	1.57	-0.92	0.65	Y3	Y2					
20	1.58	-0.95	0.63							
21	2.33	-1.42	0.91				W1			
22	2.33	-1.46	0.84							
23	2.72	//////	1.26		Y3		W2	WF	WF	

Table 5.18 South Connection Performance States

	Drift %			South Plates			South Welds			
Cycle #	Total	Neg.	Pos.	Gusset Plate	Shear Tab	Knife Plate	Gusset to Beam	Gusset to Shear Tab	Beam to Shear Tab	Shear Tab to Column
1	0.07	-0.04	0.03							
2	0.07	-0.04	0.03							
3	0.15	-0.08	0.07							
4	0.15	-0.08	0.07							
5	0.23	-0.12	0.11							
6	0.23	-0.12	0.11							
7	0.33	-0.16	0.17							
8	0.33	-0.16	0.17							
9	0.44	-0.23	0.21	Y1						
10	0.44	-0.23	0.20							
11	0.57	-0.32	0.25			Y1				
12	0.57	-0.32	0.24							
13	0.74	-0.43	0.31							
14	0.74	-0.43	0.31							
15	0.91	-0.52	0.39			Y2				
16	0.91	-0.52	0.37							
17	1.23	-0.71	0.52	Y2						
18	1.23	-0.72	0.49							
19	1.57	-0.92	0.65							
20	1.58	-0.95	0.63		Y1					
21	2.33	-1.42	0.91			Y3				
22	2.33	-1.46	0.84							
23	2.72	//////	1.26							

Table 5.19 Frame Performance States

	Drift %			Frame				
Cycle #	Total	Neg.	Pos.	Brace	West Column	East Column	North Beam	South Beam
1	0.07	-0.04	0.03					
2	0.07	-0.04	0.03					
3	0.15	-0.08	0.07					
4	0.15	-0.08	0.07					
5	0.23	-0.12	0.11					
6	0.23	-0.12	0.11					
7	0.33	-0.16	0.17					
8	0.33	-0.16	0.17					
9	0.44	-0.23	0.21					
10	0.44	-0.23	0.20					
11	0.57	-0.32	0.25	B1				
12	0.57	-0.32	0.24					
13	0.74	-0.43	0.31					
14	0.74	-0.43	0.31					
15	0.91	-0.52	0.39	B2	Y1			
16	0.91	-0.52	0.37					
17	1.23	-0.71	0.52					
18	1.23	-0.72	0.49					
19	1.57	-0.92	0.65					
20	1.58	-0.95	0.63					
21	2.33	-1.42	0.91	B3				
22	2.33	-1.46	0.84					
23	2.72	//////	1.26					

5.9.3 Pre-Test Observations

NCBF1-R4 reused the columns from NCBF1-R3 because they had sustained minimal damage in the previous test. The columns were flipped so that the welds from the previous test were on the outside faces of the columns. The West column had moderate yielding at the South connection in the West flange and the web, shown in Figure 5.143 and Figure 5.144, respectively. The East column had initial yielding at the North connection on the East flange, shown in Figure 5.145.

Figure 5.143 Existing Damage to West Column Flange

Figure 5.144 Existing Damage to West Column Web

Figure 5.145 Existing Damage to East Column East Flange

5.9.4 Test Narrative

No damage was observed in the first 6 test cycles, up to a total drift range of 0.23%.

At the tensile peak of cycle 7 (+0.17% drift), initial yield lines appeared in the North gusset plate parallel to the knife plate, resulting in performance state Y1 for the gusset plate. These lines are shown in Figure 5.146.

Figure 5.146 Y1- Initial Yielding in North Gusset Plate

At the tensile peak of cycle 9 (+0.21% drift). Performance state Y1 was observed in the North shear tab and the South gusset plate, shown in Figure 5.147 and Figure 5.148, respectively.

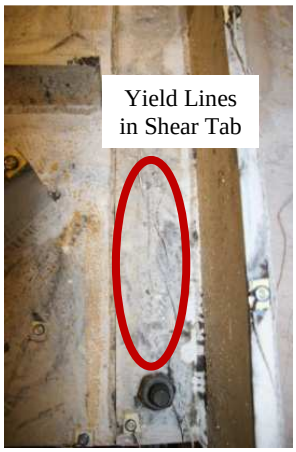

Figure 5.147 North Shear Tab - Y1

Figure 5.148 South Gusset Plate - Y1 (Underside)

At the compressive peak of cycle 11 (-0.32% drift), the brace behavior progressed to performance state B1 with the first visible in-plane buckling toward the South, shown in Figure 5.149. The brace buckling corresponded to a peak in compressive frame resistance, as shown in Figure 5.142. Concurrent with this buckling, performance state Y1 was observed on the South side of both the North and South knife plates, as shown in Figure 5.150 and Figure 5.151, respectively. No yielding was observed on the opposite faces of the plates.

Figure 5.149 In-Plane Buckling of Brace - B1

Figure 5.150 North Knife Plate, South Side - Y1

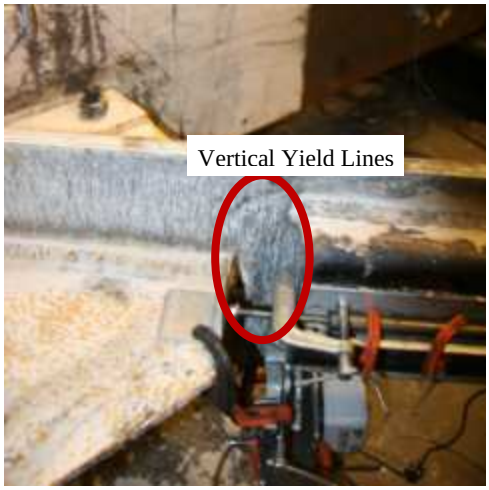

Figure 5.151 South Knife Plate, South Side - Y1

At the compressive peak of cycle 13 (-0.43% drift), the North knife plate transitioned from performance state Y1 to Y3 due to a substantial increase in yielding, shown in Figure 5.152. The South knife plate remained in performance state Y1. Also, downward bending of both gusset plates was observed. This

bending resulted from mild downward out-of-plane deflection of the brace. The bending of the South gusset is shown in Figure 5.153, and the bending of the North gusset is shown in Figure 5.154.

Figure 5.152 North Knife Plate, South Side - Y3

Figure 5.153 Downward Bending of S Gusset Plate

Figure 5.154 Downward Bending of N Gusset Plate

At the tensile peak of cycle 15 (+0.39% drift), new yielding was observed in the West flange of the West Column at the South connection, shown in Figure 5.155. At this point, slope of the load-drift behavior in tension decreased substantially, indicating that yielding was occurring, as shown in Figure 5.142. Some of this was likely due to yielding in the connections, which increased substantially in subsequent cycles. The brace yielding may also have contributed, but it was not directly observable.

Figure 5.155 West Column, West Flange - Y1

At the compressive peak of cycle 15 (-0.52% drift), the brace entered performance state B2. Buckling continued to be primarily in-plane to the South, as shown in Figure 5.156.As a result of the increased buckling, the South knife plate entered performance state Y2, shown in Figure 5.157. The increase in buckling corresponded with a slight decrease in compressive lateral load capacity, though much less than NCBF1, as shown in Figure 5.142. As with previous specimens, the compact brace maintained a large portion of its compressive strength as buckling progressed.

Figure 5.156 Brace In-Plane Buckling - B2

Figure 5.157 South Knife Plate, South Side - Y2

At the tensile peak of cycle 17 (+0.52% drift), both gusset plates transitioned into performance state Y2. Yielding was more widespread in the North gusset, shown in Figure 5.158, than in the South gusset plate, shown in Figure 5.159.

Figure 5.158 North Gusset Plate - Y2

Figure 5.159 South Gusset Plate - Y2

At the tensile peak of cycle 19 (+0.65 drift), there was a significant increase in damage in the North connection. The North gusset plate entered performance state Y3, with a large portion of the plate completely clear of whitewash. The North shear tab entered performance Y2 at the same time. This yielding is shown in Figure 5.160. The extensive yielding in the connections was indicative of the high DCRs for gusset plate Whitmore yielding and block shear.

Figure 5.160 North Gusset Plate Y3 and North Shear Tab Y2

At the compressive peak of cycle 19 (-0.92%), drift increased downward bending of both gusset plates was observed. This bending resulted from a slight increase in downward out-of-plane buckling of the brace, which was at this point 2 inches at the brace mid-span. The North and South gusset plates are shown in Figure 5.161 and Figure 5.162, respectively.

Figure 5.161 North Gusset Plate Bending

Figure 5.162 South Gusset Plate Bending

At the tensile leak of cycle 20, the second cycle at this displacement level (+0.63% drift), the South shear tab entered performance state Y1, as shown in Figure 5.163.

Figure 5.163 South Shear Tab - Y1

At the tensile peak of cycle 21 (+0.91% drift), a weld crack was observed in the underside of the North gusset-to-beam weld at the east end. The tear was 1 inch in length, categorized as performance state W1, as shown in Figure 5.164. This tear was similar to tears observed in NCBF1-R3, indicating that tearing at this location may result from the knife plate retrofit geometry.

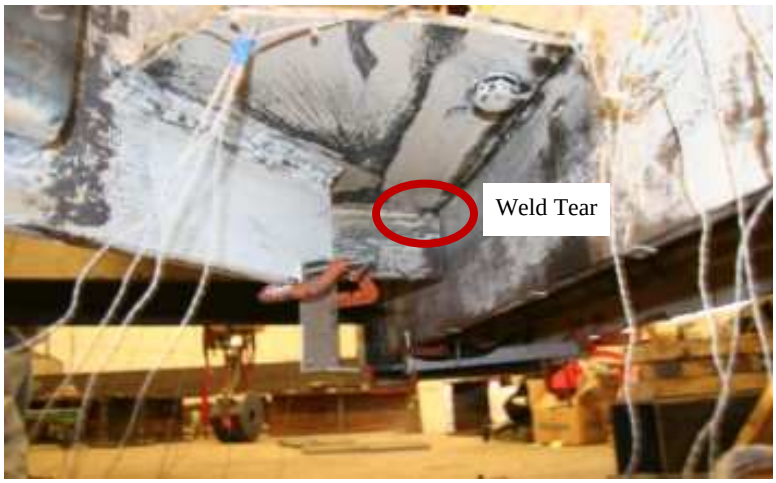

Figure 5.164 W1 in North Gusset-to-Beam Weld

At the compressive peak of cycle 21 (-1.42% drift), the in-plane buckling of the brace transitioned to performance state B3, as shown in Figure 5.165. As a result of this buckling, yielding increased in both

knife plates. Yielding in the North knife plate is shown in Figure 5.166. Yielding in the south knife plate, which progressed to performance state Y3, is shown in Figure 5.167. Additionally, the in-plane rotations of the North and South knife plates are shown in Figure 5.168 and Figure 5.169, respectively. As mentioned for NCBF1-R3, the knife plates yielded extensively due to the rotational demands from in-plane buckling, despite being designed to resist the full tensile capacity of the brace.

Figure 5.165 Brace In-Plane Buckling - B3

Figure 5.166 North Knife Plate - Y3

Figure 5.167 South Knife Plate - Y3

Figure 5.168 North Knife Plate Bending

Figure 5.169 South Knife Plate Bending

At the tensile peak of cycle 23 (+1.26% drift), the North beam-to-shear tab weld and the North gusset-to-beam weld fractured completely, described as performance state WF. This fracture disconnected the gusset plate and the beam from the East column, effectively ending the test. The weld fracture is shown in Figure 5.170. As a result of the weld fracture, the North beam pulled South at the North connection, causing the North flange to bear against the North shear tab, as shown in Figure 5.171. Finally, tearing of the North gusset-to-beam weld increased to 2 inches in length, progressing to performance state W2, shown in Figure 5.172. No additional damage was observed in the South connection.

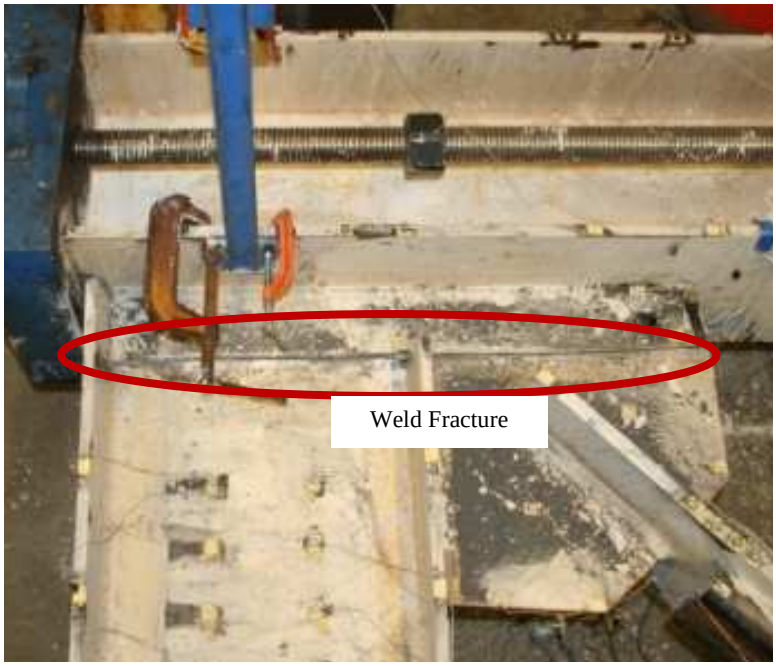

Figure 5.170 Fracture of North Shear Tab Weld

Figure 5.171 North Beam Flange Bearing on North Shear Tab

Figure 5.172 W2 in North Gusset-to-Beam Weld

Test Summary

Specimen NCBF1-R4 achieved a larger drift range than NCBF1, but it suffered an undesirable failure. NCBF1-R4 achieved a total drift range of 2.72%, which is significantly higher than the 1.5% drift range achieved in NCBF1. The use of a seismically compact brace section for NCBF1-R4 prevented the rapid brace degradation seen in NCBF1.

The use of a rectangular brace cross section was also successful at promoting in-plane buckling over out-of-plane buckling. While NCBF1-R3 buckled equally in and out of plane, NCBF1-R4 buckled almost exclusively in-plane. This indicates that the use of rectangular HSS rather than square HSS may be necessary in retrofit schemes to ensure in-plane buckling.

In-plane buckling was effective at preventing tearing of the gusset-beam welds at the outer ends, which were not observed in this test as it had been in previous specimens. This supports the concept that the rotational demands of the brace buckling out-of-plane, in addition to the lack of brace end clearance in the connection, leads to early tearing of these welds. However, the in-plane buckling retrofit and the shortened knife plate were not effective at protecting the shear tab weld, which fractured suddenly. This indicates that the rotational demands from the out-of-plane buckling of the brace are not the primary contributing factor to the premature fracture of this weld. Instead, it appears that lateral drift is a better indicator of damage. This rapid fracture also highlighted, as previous specimens have, the risk of rapid weld failure when electrodes without notch-toughness requirements are used, as is likely the case in older buildings. The rapid loss of lateral resistance observed in this system was a result of a high rate of tear propagation in the weld, which led to almost immediate failure.

Yielding in the gusset plates and shear tabs was severe, as was the case in NCBF1-R3. The substantial increase in DCRs associated with shortening the knife plate did not appear to increase damage to the gusset plates, as no tearing was observed. This indicates that even very high DCRs for Whitmore yielding may be tolerable. However, it is worth noting that high strains in the gusset plate may have contributed to the initiation of tearing in the shear tab weld.

5.10 NCBF1-R5

5.10.1 Specimen Overview

Specimen NCBF1-R5 was designed to address two observed deficiencies of previous tests using retrofit strategies that are fast and inexpensive to construct. The first issue addressed was the brace compactness. Specimen NCBF1 failed at low drift levels due to brace cupping and fracture. Previous retrofits focused on replacement of the brace with a seismically compact brace, which was effective at improving brace performance. For this specimen, the HSS7x7x1/4 brace was instead filled with regular strength, self-consolidating concrete. The concrete was intended to provide restraint of the brace cross-section against local buckling, thereby increasing the brace durability. The second retrofit measure addressed the repeated fracture of the shear tab to gusset plate and beam weld. Attempts to protect this weld using in-

plane buckling braces were unsuccessful in NCBF1-R3 and NCBF1-R4. In this test, the weld was reinforced using high strength bolts. These bolts supplement the capacity of the weld, which is over capacity by design standards. They also prevent the bending of the shear tab away from gusset plate and beam, which may have been a contributing factor to the weld fractures in previously described specimens. These two retrofits are simple and do not require extensive construction operations. They also address the two most critical performance issues of the previous specimens. Figure 5.173 shows a detail of the connection.

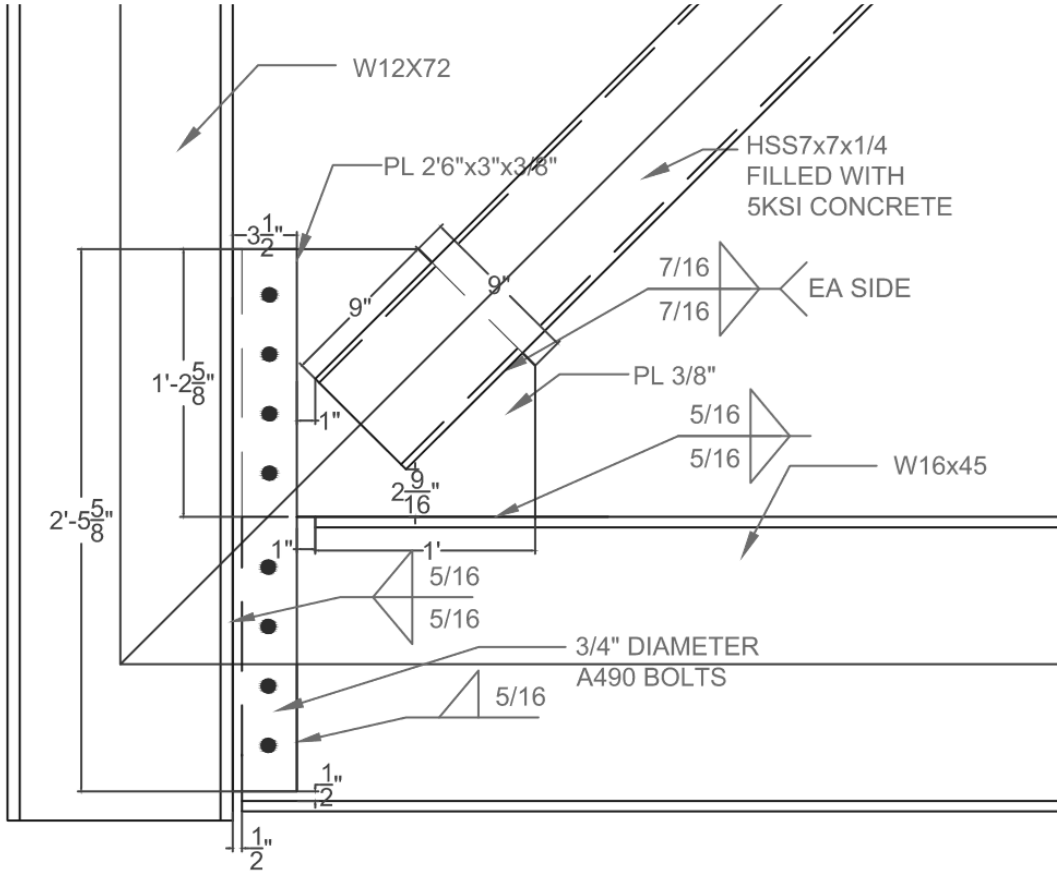

Figure 5.173 NCBF1-R5 Connection Detail

Table 5.20 shows the DCRs for NCBF1-R5, which are essentially the same as for NCBF1 with the addition of several limit states associated with the shear tab bolts. Given the high DCRs for the gusset plate limit states, as was the case in previous tests, substantial yielding in the gusset plates was expected. Brace net section fracture was not problematic in previous specimens despite DCRs greater than 1, so it

was not expected to be a factor here. The bolt DCRs shown are assuming no contribution to strength from the weld, while the DCR for the shear tab weld assumes no contribution to strength from the bolts. Brace slenderness did not decrease, as the same brace was used, but the addition of concrete fill was expected to address this issue.

Table 5.20 NCBF1-R5 DCRs

Limit State	NCBF1	NCBF1-R5
Brace Net Section Fracture	1.26	1.26
Brace-Gusset Plate Weld Fracture	0.92	0.92
Brace Block Shear	1.14	1.14
Gusset Plate Block Shear	1.16	1.16
Gusset Plate Whitmore Yielding	1.33	1.33
Gusset Plate Buckling	0.74	0.74
Gusset Plate Shear Yielding at Beam	1.16	1.16
Beam-Gusset Weld Fracture	1.55	1.55
Shear Tab to Gusset/Beam Weld Fracture	1.08	1.08
Shear Tab to Column Weld Fracture	0.65	0.65
Bolt Shear	///	0.98
Bolt Bearing	///	0.66
Shear Tab Block Shear	///	0.86
Bolt Slip	///	3.07
Brace Local Slenderness	2.04	2.04

The actuator displacement history was modified slightly during the test. The unmodified displacement history can be found in Section 5.4. The actuator was stopped prior to the compressive peak of cycle 29, which was the final test cycle, because the brace buckled down in compression and was about to contact

the testing floor. The frame was then loaded to the tension peak of cycle 30, at which point brace fracture occurred.

NCBF1-R5 had a partial failure that led to a loss in lateral load resistance when the NE gusset to beam weld fractured at 1.8% drift in compression. The specimen had a complete failure with the fracture of the brace at the center at 2.1% drift in tension. Figure 5.174 shows the load-drift response history of the frame.

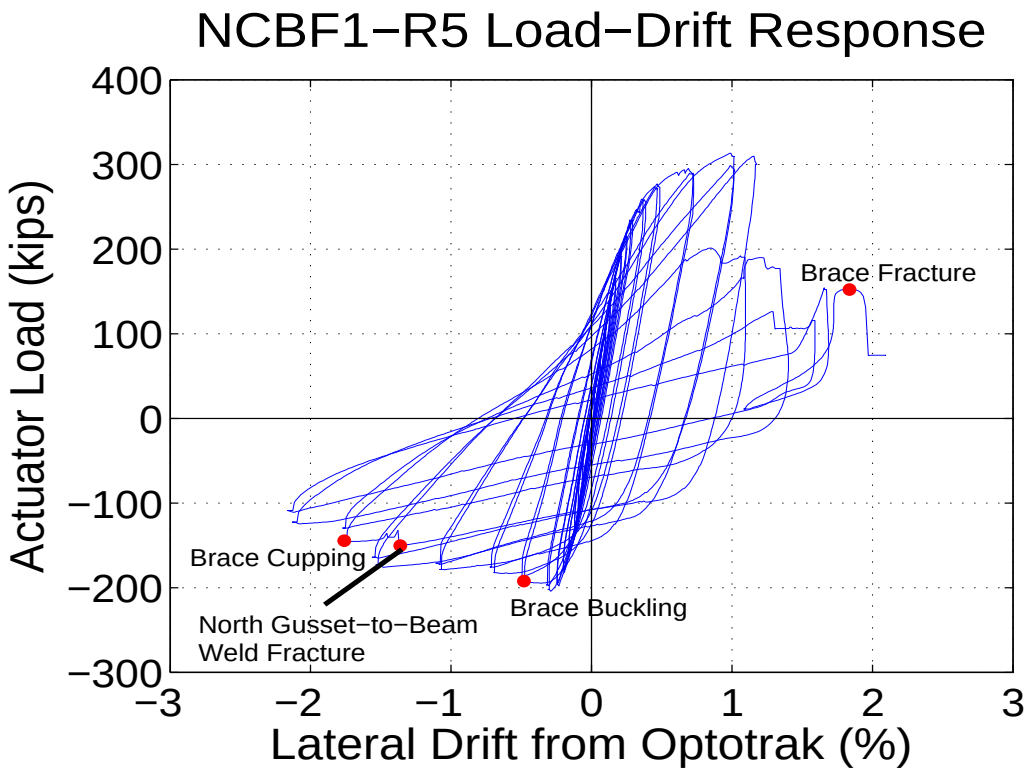

Figure 5.174 NCBF1-R5 Load-Drift Response History

5.10.2 Performance State Summary

Table 5.21 and Table 5.22 show the progression of performance states during the test for the North and South gusset plate connections, respectively. Table 5.23 shows the progression of performance states during the test for the brace, beams, and columns. The positive drift, negative drift, drift range, and cycle number are given in each table. Whitewash was applied to NCBF1-R4, so observations of yielding are included in the performance state tables.

Table 5.21 North Connection Performance States

	Drift %			North Plates		North Welds			
Cycle #	Total	Neg.	Pos.	Gusset Plate	Shear Tab	Gusset to Beam	Gusset to Shear Tab	Beam to Shear Tab	Shear Tab to Column
1	0.06	-0.03	0.03						
2	0.06	-0.03	0.03						
3	0.14	-0.07	0.07						
4	0.14	-0.07	0.07						
5	0.20	-0.09	0.11						
6	0.20	-0.09	0.11						
7	0.26	-0.12	0.14	Y1					
8	0.26	-0.12	0.13						
9	0.33	-0.16	0.17						
10	0.33	-0.16	0.17						
11	0.41	-0.20	0.21						
12	0.41	-0.20	0.21						
13	0.50	-0.25	0.25		Y1				
14	0.50	-0.25	0.25						
15	0.60	-0.31	0.29	Y2					
16	0.60	-0.32	0.28						
17	0.87	-0.48	0.39						
18	0.89	-0.51	0.38						
19	1.20	-0.69	0.51						
20	1.20	-0.72	0.47						
21	1.84	-1.09	0.75	Y3	Y2	W1			
22	1.84	-1.12	0.72						
23	2.58	-1.55	1.03		Y3	W2			
24	2.59	-1.57	1.02			W3			
25	2.95	-1.77	1.18			WF		W2	
26	2.95	-1.80	1.10		BE,MT				
27	3.48	-2.13	1.35					W3	
28	3.77	-2.18	1.59						
29	4.27	//////	2.09						

Table 5.22 South Connection Performance States

	Drift %			South Plates		South Welds			
Cycle #	Total	Neg.	Pos.	Gusset Plate	Shear Tab	Gusset to Beam	Gusset to Shear Tab	Beam to Shear Tab	Shear Tab to Column
1	0.06	-0.03	0.03						
2	0.06	-0.03	0.03						
3	0.14	-0.07	0.07						
4	0.14	-0.07	0.07						
5	0.20	-0.09	0.11						
6	0.20	-0.09	0.11						
7	0.26	-0.12	0.14	Y1					
8	0.26	-0.12	0.13						
9	0.33	-0.16	0.17						
10	0.33	-0.16	0.17						
11	0.41	-0.20	0.21						
12	0.41	-0.20	0.21		Y1				
13	0.50	-0.25	0.25						
14	0.50	-0.25	0.25						
15	0.60	-0.31	0.29	Y2					
16	0.60	-0.32	0.28						
17	0.87	-0.48	0.39		Y2				
18	0.89	-0.51	0.38						
19	1.20	-0.69	0.51						
20	1.20	-0.72	0.47						
21	1.84	-1.09	0.75		Y3				
22	1.84	-1.12	0.72						
23	2.58	-1.55	1.03	Y3					
24	2.59	-1.57	1.02			W1			
25	2.95	-1.77	1.18						
26	2.95	-1.80	1.10						
27	3.48	-2.13	1.35			W2			
28	3.77	-2.18	1.59						
29	4.27	//////	2.09						

Table 5.23 Frame Performance States

	Drift %			Frame				
Cycle #	Total	Neg.	Pos.	Brace	West Column	East Column	North Beam	South Beam
1	0.06	-0.03	0.03					
2	0.06	-0.03	0.03					
3	0.14	-0.07	0.07					
4	0.14	-0.07	0.07					
5	0.20	-0.09	0.11					
6	0.20	-0.09	0.11					
7	0.26	-0.12	0.14					
8	0.26	-0.12	0.13					
9	0.33	-0.16	0.17					
10	0.33	-0.16	0.17					
11	0.41	-0.20	0.21					
12	0.41	-0.20	0.21			N-WF Y1		
13	0.50	-0.25	0.25					
14	0.50	-0.25	0.25					
15	0.60	-0.31	0.29					
16	0.60	-0.32	0.28					
17	0.87	-0.48	0.39	B1				
18	0.89	-0.51	0.38					
19	1.20	-0.69	0.51			S-WF Y1	E-W Y1	
20	1.20	-0.72	0.47					
21	1.84	-1.09	0.75	BNS,B2				
22	1.84	-1.12	0.72					
23	2.58	-1.55	1.03		S-WF Y1	N-WF Y2		
24	2.59	-1.57	1.02					
25	2.95	-1.77	1.18	BH	S-WF-Y2			W-W Y1
26	2.95	-1.80	1.10				E-W-Y2	
27	3.48	-2.13	1.35		S-EF Y1	N-W-Y1		
28	3.77	-2.18	1.59					
29	4.27	//////	2.09	BF				

5.10.3 Test Narrative

For the first 6 cycles, up to 0.2% total drift range, there was no observable damage to the frame.

The first observed yielding occurred at the tensile peak of cycle 7 (+0.14% drift). Initial V-shaped yield lines formed in both the North and South Gusset plates at the brace ends, putting both gusset plates in performance state Y1. The yielding at the South gusset is shown in Figure 5.175.

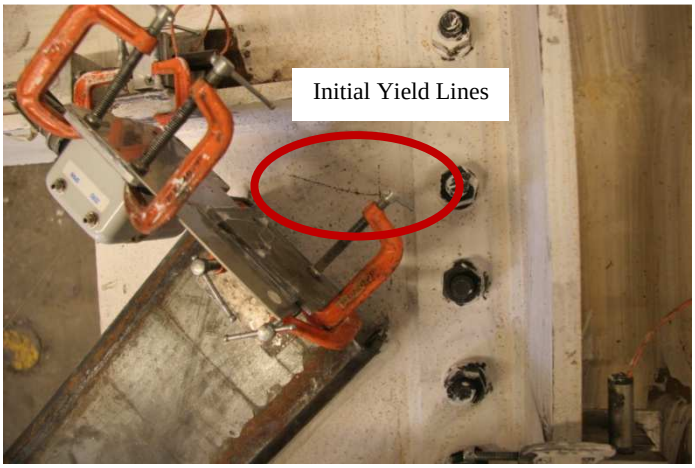

Figure 5.175 Initial Yielding of South Gusset -Y1

At the compressive peak of cycle 11 (-0.20% drift), initial upward bending of both gusset plates was observed. This upward bending resulted from the out-of-plane bending of the brace, which had a mid-span deflection of 0.5" in this cycle. The deflection of the brace was not yet visible. Figure 5.176 shows the upward bending of the South edge of the North Gusset Plate. Additionally, initial yield lines were observed parallel to the beam flange in both gusset plates, shown for the North plate in Figure 5.177.

Figure 5.176 Upward Bending of N Gusset

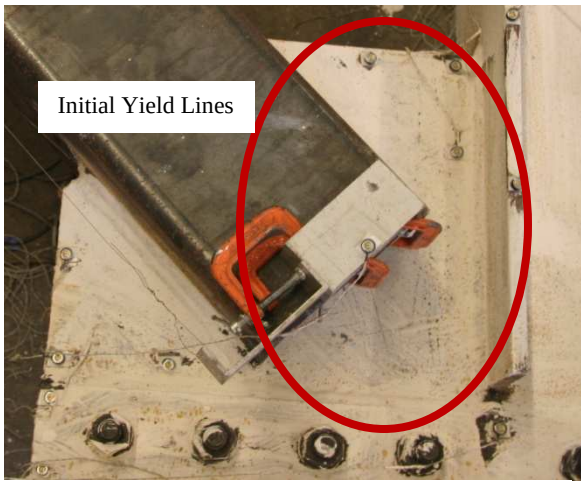

Figure 5.177 Yielding in North Gusset - Y1

At the compressive peak of cycle 12, the second cycle at this displacement level (-0.20% drift), an initial yield line was observed in the North shear tab between the two southernmost bolts. Figure 5.178 shows this yielding. Initial frame yielding was also observed in the West column, West flange, at the North gusset plate. This yielding is shown in Figure 5.179.

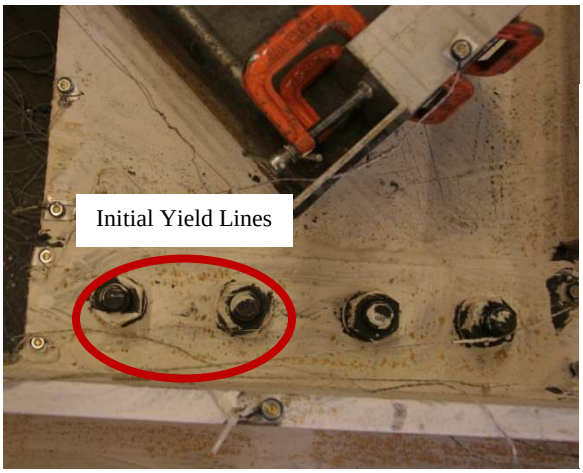

Figure 5.178 Y1 in North Shear Tab

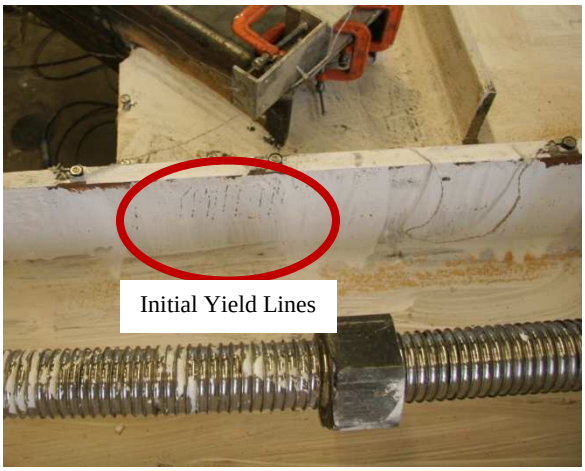

Figure 5.179 Initial Yielding in West Column

At the tensile peak of cycle 13 (+0.25% drift), Y1 was observed in the South shear tab near the north flange of the beam. This yielding is shown in Figure 5.180. Yielding increased in the North shear tab, with yield lines between the four Southernmost bolts. This yielding is shown in Figure 5.181.

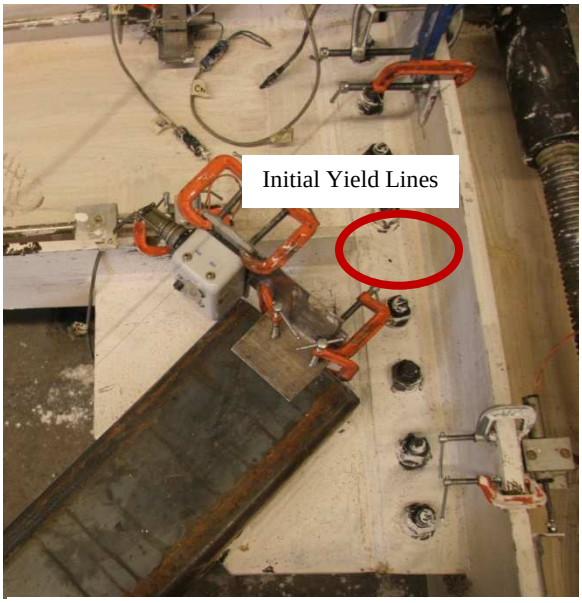

Figure 5.180 Y1 in South Shear Tab

Figure 5.181 Yielding in North Shear Tab

At the tensile peak of cycle 15 (+0.29% drift), both gusset plates progressed to performance state Y2, as shown in Figure 5.182 and Figure 5.183. At this point, the slope of the load-drift frame behavior in tension decreased substantially, indicating yielding in the frame, as shown in Figure 5.174. This is consistent with the observation of substantial yielding in the gusset plates, which were expected to have a lower tensile capacity than the brace.

Figure 5.182 Yielding in North Gusset - Y2

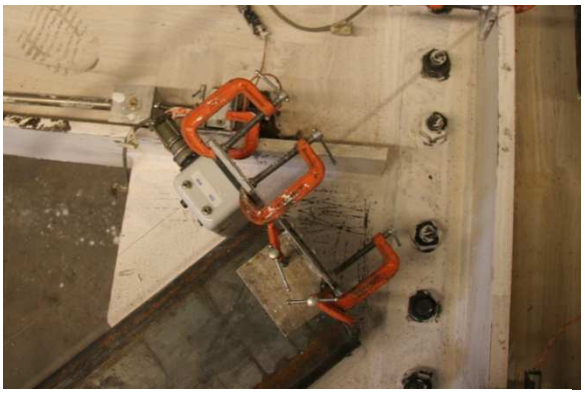

Figure 5.183 Yielding in South Gusset - Y2

At the compressive peak of cycle 15 (-0.31% drift), out-of-plane buckling of the brace became visible. The brace mid-span deflection was 1.7 inches, as shown in Figure 5.184. This point also corresponded to the peak compressive lateral load resistance of the frame, as shown in Figure 5.174. The compressive resistance reached was almost identical to that for NCBF1.

Figure 5.184 Initial Visible Brace Buckling - B1

Yielding in both shear tabs increased at the tensile peak of cycle 17 (+0.39% drift). Figure 5.185 shows yielding in the North shear tab, and Figure 5.186 shows yielding in the South shear tab, which progressed to performance state Y2.

Figure 5.185 North Shear Tab - Y2

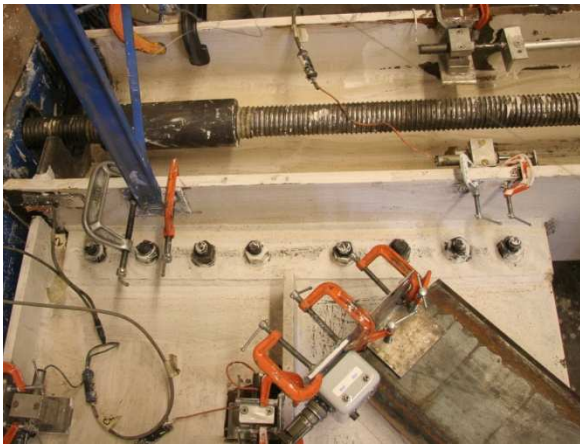

Figure 5.186 South Shear Tab - Y2

At the compressive peak of cycle 17 (-0.48% drift), increased upward bending of the gusset plates and shear tabs was observed. The South edge of the North shear tab was bent upward relative to the column, and the South edge of the North gusset was hinged upward slightly at the edge of the shear tab. Similar behavior was observed at the South connection, shown in Figure 5.187. Slight upward bending of the beam side of the gusset plates was also observed. At the tensile peak of cycle 18, the second cycle at this displacement level (+0.39% drift), downward hinging of the gusset plates was observed at the shear tabs. The shear tabs retained some residual upward bending, causing the gusset plates to hinge downward as the brace straightened. The hinging of the South gusset is shown in Figure 5.188.

Figure 5.187 Upward Bending of South Gusset Plate

Figure 5.188 Downward Bending of South Gusset Plate

At the tensile peak of cycle 19 (+0.51% drift), increased yielding was observed in both connections, but none of the components progressed to more severe performances states. Yielding in the North and South connections is shown in Figure 5.189 and Figure 5.190, respectively.

Figure 5.189 Yielding in North Connection

Figure 5.190 Yielding in South Connection

At the compressive peak of cycle 19 (-0.69% drift), outward bulging of the bottom flange of the brace was observed at 3 locations: 3.5 inches SW, 5 inches NE, and 13 inches NE of the brace mid-point. Figure 5.191 shows the largest bulge, 3.5 inches SW of center. This outward bulging is typical of concrete filled braces, as described in Chapter 2.

Figure 5.191 Bulge 3.5" SW of Brace Center

At the tensile peak of cycle 21 (+0.73% drift), yielding increased significantly in both connections. The North shear tab transitioned to performance state Y2, and the South shear tab and North gusset plate transitioned to performance state Y3. The shear tab yielding at both connections was concentrated in the region along the line of bolts. Figure 5.192 and Figure 5.193 show the yielding in the North and South connections, respectively. Brace net section cracking appeared in all four brace slots. The most severe cracking was on the brace South wall at the North connection, where a 1/8 inch wide, 1/4 inch long crack appeared. Figure 5.194 and Figure 5.195 show net section cracking on the brace South wall at the South and North connections, respectively.

Figure 5.192 North Gusset Plate - Y3 and North Shear Tab - Y2

Figure 5.193 South Gusset Plate Y2 and South Shear Tab - Y3

Figure 5.194 BNS at NE Gusset, South Wall

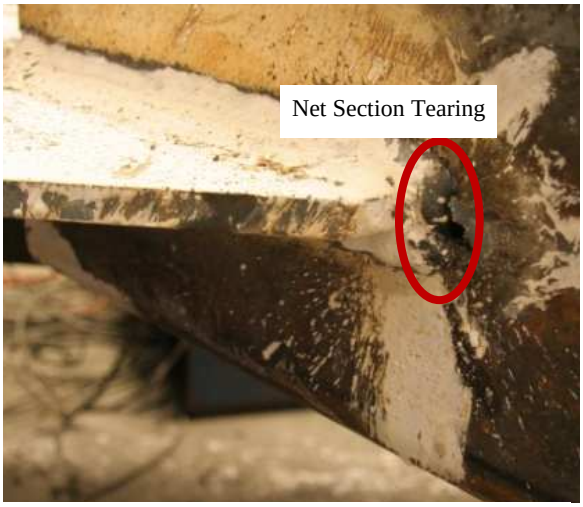

Figure 5.195 BNS at SW Gusset, South Wall

Two new bulges emerged on the bottom flange of the brace at the compressive peak of cycle 21 (-1.07% drift). They were located 12 inches SW and 21 inches NE of the brace center. Additionally, the side walls

of the brace were cupped inward slightly at the locations of each of the bottom flange bulges. The side wall deformations were less than 25% of the bottom flange deformations. The brace mid-span deflection reached 7.9 inches moving the brace into moderate buckling, B2. Figure 5.196 shows the bottom flange bulges, Figure 5.197 shows the side wall cupping, and Figure 5.198 shows global brace buckling. As the buckling of the brace progressed, the compressive resistance of the frame decreased slowly, as shown in Figure 5.174. This indicates higher post-buckling strength than NCBF1, as expected for the concrete fill. The brace did retain less compressive capacity than the compact braces on a percentage basis, but it achieved higher maximum load.

Figure 5.196 Bulging of Brace Bottom Flange

Figure 5.197 Inward Cupping of Brace North Wall

Figure 5.198 Moderate Brace Buckling - B2

Also at the compressive peak of cycle 21, a weld crack initiated at the West end of the North gusset-to-beam weld that was 3/8 of an inch in length, categorized as W1. Figure 5.199 shows the weld crack, which grew to 1 inch in length at the compressive peak of cycle 22, the second cycle at this displacement level (-1.12% drift). The crack was caused by rotational demands from the gusset plate, shown for the South Gusset plate in Figure 5.200. Yielding throughout both gusset plates and shear tabs increased at the tensile peak of cycle 21 (+1.03% drift). The North shear tab and South gusset plate progressed to performance state Y3. Figure 5.201 and Figure 5.202 show the yielding in the North and South connections, respectively.

Figure 5.199 W1 in North Gusset-to-Beam Weld

Figure 5.200 Bending of South Gusset Plate

Figure 5.201 North Shear Tab - Y3

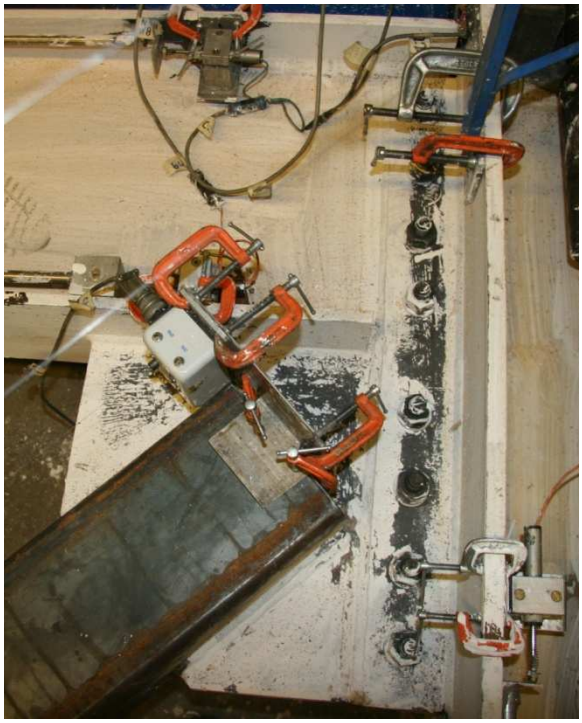

Figure 5.202 South Gusset Plate - Y3

At the compressive peak of cycle 23 (-1.55% drift), a sixth bulge appeared in the bottom flange of the brace, 19 inches Southwest of the brace center. At this point, the heights of the six bulges, from Northernmost to Southernmost were: 3/8 in, 7/16 in, 9/16 in, 7/8 in, 5/8 in, 3/16 in, shown in Figure 5.203. Figure 5.204 shows the corresponding inward cupping of the North wall of the brace.

Figure 5.203 Bulges in Brace Bottom Flange

Figure 5.204 Bulges in Brace North Wall

Also at the compressive peak of cycle 23, the weld crack in the North gusset-to-beam weld grew to 2.75 inches in length and became classified as a moderate weld crack, performance state W2, shown in Figure

5.205. At the location of the weld crack, the gusset plate was curled downward substantially, as shown in Figure 5.206. New frame damage was observed in the West column, South end, West flange, where vertical yield lines were scattered along the depth of the South connection. This is shown in Figure 5.207.

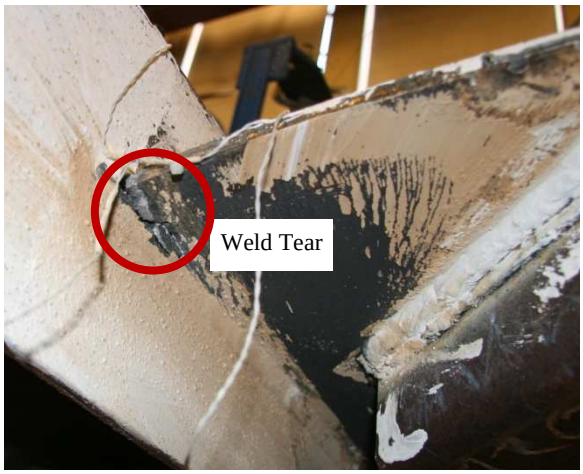

Figure 5.205 W2 in North Gusset-to-Beam Weld

Figure 5.206 North Gusset Plate Bending

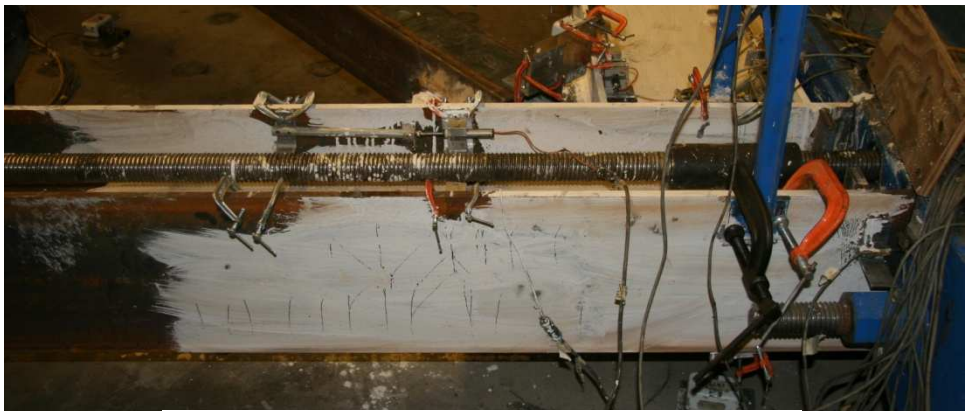

Figure 5.207 West Column South End - Y1

At the compressive peak of cycle 24, the second cycle at this displacement level (-1.57% drift), the weld crack in the North gusset-to-beam weld increased to 6.5 inches in length, entering performance state W3. The end of the North gusset-to-beam weld was dislocated vertically out of the weld seat at the west end. This is shown in Figure 5.208. A new hairline weld crack appeared in the South gusset-to-beam weld at the East end. It was less than 1/2 an inch in length. This is shown in Figure 5.209.

Figure 5.208 North Gusset-to-Beam Weld - W3

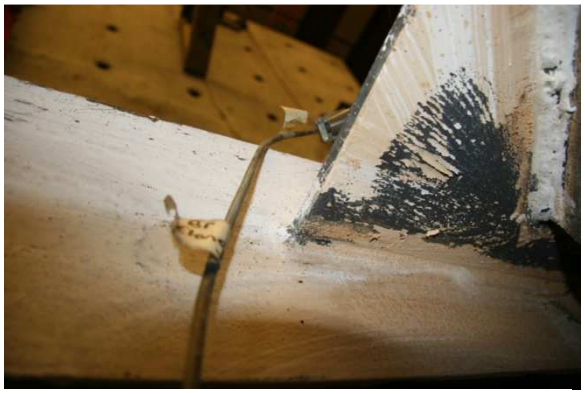

Figure 5.209 South Gusset-to-Beam Weld - W1

At the tensile peak of cycle 25 (+1.18% drift), diagonal yield lines appeared near the South shear tab in the South beam web, shown in Figure 5.210. Yielding in the connections increased slightly.

Figure 5.210 North Beam Web at South Connection - Y1

While loading to the compressive peak of cycle 25 (-1.77% drift), the North gusset-to-beam weld fractured completely. The test was paused momentarily, before loading continued to the peak displacement. The weld fracture is shown in Figure 5.211. This fracture corresponded to a substantial loss of tensile lateral load resistance in subsequent cycles, as shown in Figure 5.174. The fracture of this weld

is unsurprising, as it had a high DCR and fractured in previous tests with substantial out-of-plane brace buckling.

A new weld crack formed, propagating out of the termination of the North gusset-to-beam fracture. The crack, in W-NBT, was 2 inches in length, putting the weld immediately into performance state W2. This crack is shown in Figure 5.212. Both gusset plates were bent in a slight S-shape along their edge due to the hinging of the gusset at the edge of the shear tab. Figure 5.213 shows the deflected shape of the North edge of the South gusset. Yielding in the West flange of the West column at the South end increased, transitioning to performance state Y2. This is shown in Figure 5.214. Brace cupping also formed at the largest of the bulges in the brace, 3 inches SW of the brace midpoint. Figure 5.215 and Figure 5.216 show the brace cupping and brace deflected shape, respectively. The local deformations of the brace center are not characteristic of the typical cupped shape for an HSS, in which the bottom flange of the brace deforms inward. However, the implications of the large local deformations are the same here as they are for the typical case, so the same terminology is used.

Figure 5.211 WF in North Gusset-to-Beam Weld

Figure 5.212 Weld Crack W-NBS - W2

Figure 5.213 Bending of South Gusset Plate

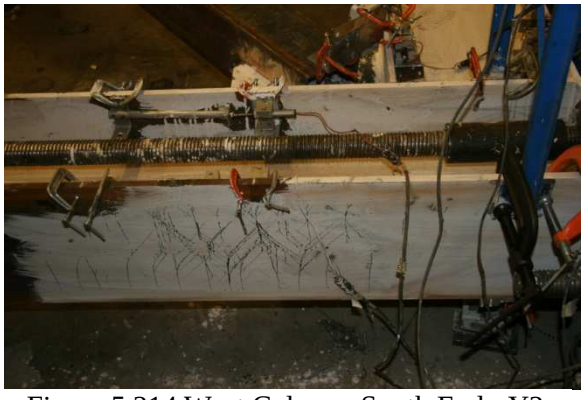

Figure 5.214 West Column, South End - Y2

Figure 5.215 Brace Buckling

Figure 5.216 Brace Cupping - BC

At the tensile peak of cycle 26, the second cycle at this displacement level (+1.18% drift), a tear developed in North shear tab, propagating from the fractured North gusset-to-beam weld diagonally into the Northernmost bolt hole in the gusset plate. Additionally, bolt hole elongation was visible in the two Northern bolts of connecting the gusset plate to the shear tab. The bolt hole elongation and metal tearing, performance states BTE and MT, are shown in Figure 5.217.

The portion of the North shear tab connected to the beam was bent downward substantially along the depth of the beam. The North beam web was bent upward significantly at the shear tab due to the clamping effect of the bolts. This local deformation caused yielding in the web, characterized as performance state Y2. Figure 5.218 shows the downward bending of the North shear tab and the yielding of the North beam web. Figure 5.219 shows the upward bending of the beam web on the underside.

Figure 5.217 North Shear Tab - MT,BTE

Figure 5.218 Bending of North Shear Tab

Figure 5.219 Bending of North Beam Web

At the compressive peak of cycle 26 (-1.80% drift), the crack in North beam-to-shear tab weld grew to 4.5 inches in length, becoming a severe weld crack, performance state W3. Figure 5.220 shows the crack. Additionally, the hinge at the brace center intensified slightly, shown in Figure 5.221.

Figure 5.220 W3 in North Beam-to-Shear Tab Weld

Figure 5.221 Increased Brace Cupping

At the tensile peak of cycle 27 (+1.35% drift), tearing was observed on the bottom corners of the brace at the hinge location. Exposed, crushed concrete was visible through the two diagonal tears. Figure 5.222 shows the tearing. The tear in the North shear tab propagated South to the next bolt hole in the gusset plate. Bolt hole elongation was now visible in the second to Southernmost bolt in the shear tab. Figure 5.223 shows the damage to the shear tab. The increased damage in the brace and connection corresponded to a gradual loss of lateral load resistance in both compression and tension, as shown in Figure 5.174.

Figure 5.222 Brace Tearing

Figure 5.223 North Shear Tab - BE,MT

At the compressive peak of cycle 27 (-2.13% drift), the weld tear in the South gusset-to-beam weld increased to 2 inches in length , entering performance state W2. The weld tear is shown in Figure 5.224.

Figure 5.224 W2 in South Gusset-to-Beam Weld

At the tensile peak of cycle 28, the second cycle at this displacement level (+1.35% drift), the bottom flange of the brace tore completely, as did the majority of both the North and South wall of the brace.

Figure 5.225 shows the damage at the hinge location. The tearing of the brace caused the brace to deflect downward, due to the movement of the neutral axis. As a result, the South gusset plate underwent a significant increase in bending on both edges. Figure 5.226 and Figure 5.227 show the bending of the plate. Yielding appeared in the West column, South end, in the East flange and web, as shown in Figure 5.228 and Figure 5.229, respectively.

Figure 5.225 Tearing of Brace

Figure 5.226 Bending of South Gusset - East

Figure 5.227 Bending of South Gusset- North

Figure 5.228 West Column Web - Y1

Figure 5.229 West Column Flange - Y1

At the compressive peak of cycle 28 (-2.18% drift), the brace buckled upward, despite the downward deflection at the tension peak. The weld tears in the North beam-to-shear tab and South gusset-to-beam welds both increased slightly in length, but did not enter new performance states, as shown in Figure 5.230 and Figure 5.231, respectively.

Figure 5.230 Tearing of North Beam-to-Shear Tab Weld

Figure 5.231 Tearing of South Gusset-to-Beam Weld

At the tensile peak of cycle 29 (+1.59% drift), the brace tearing increased, propagating to the top of both side walls. This is shown in Figure 5.232. The brace downward deflection increased slightly, shown in Figure 5.233.

Figure 5.232 Tearing of Brace

Figure 5.233 Downward Deflection of Brace

The test was paused before reaching the compressive peak of cycle 29 because the brace buckled downward toward the floor. Figure 5.234 shows the brace when the cycle was stopped. Because loading in compression was no longer possible, the specimen was loaded in the tensile direction until brace fracture occurred at +2.09% drift. The fractured brace is shown in Figure 5.235. The only other notable damage increase was the propagation of the tear in the North shear tab, which continued to halfway between the two center bolts of the gusset plate, as shown in Figure 5.236.

Figure 5.234 Maximum Downward Brace Deflection

Figure 5.235 Brace Fracture - BF

Figure 5.236 North Shear Tab - MT

5.10.4 Post-Fracture Cycles

Because the beam to column connections at both corners of the frame remained intact, the frame was returned to 0% drift and cycled with the brace removed. Figure 5.237 shows the actuator displacement history.

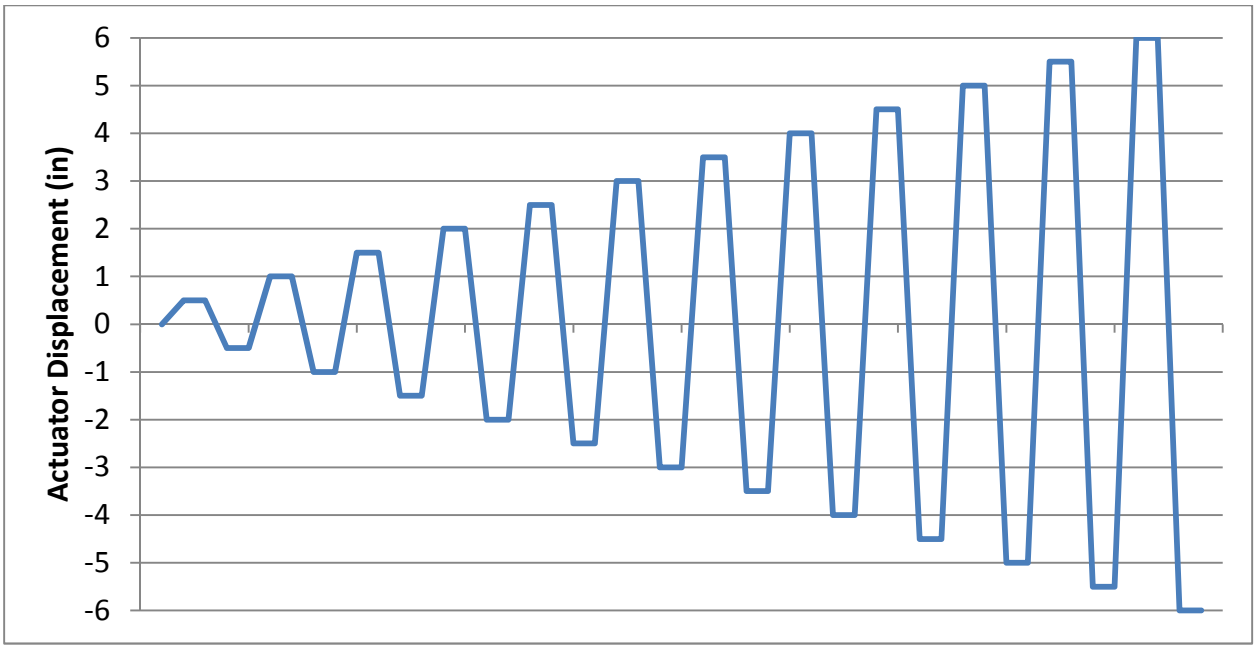

Figure 5.237 Post-Fracture Actuator Displacement History

No notable increases in damage occurred until the maximum displacement levels from the main test cycles were reached. At 5.15% total drift range, new significant new damage became visible. At positive drift, the South gusset plate and North flange of the South beam buckled downward. Figure 5.238 shows the gusset plate, and Figure 5.239 shows the beam. At negative drift, a W1 weld crack formed in the South beam-to-shear tab weld at the North end, shown in Figure 5.240. Additionally, a new weld crack formed at the North end of the North beam-to-shear tab weld, shown in Figure 5.241. The tear in the South gusset-to-beam weld also extended to 4.5 inches in length, moving to performance state W3. This is shown in Figure 5.242.

Figure 5.238 Buckling of South Gusset Plate

Figure 5.239 Bending of South Beam

Figure 5.240 W1 in South Beam-to-Shear Tab Weld

Figure 5.241 W3 in North Beam-to-Shear Tab Weld

Figure 5.242 W3 in South Gusset-to-Beam Weld

At the tensile peak of the 5.64% total drift range cycle, metal tearing was observed in both beams at the shear tabs. The North beam had a 3 inch tear along the Southernmost bolt, shown in Figure 5.243, and the South beam had a 3 inch tear along the Northernmost bolt, shown in Figure 5.244. Weld cracking in the North beam-to-shear tab weld also increased slightly.

At the corresponding compressive peak, a new 2 inch tear formed at the North end of the South beam-to-shear tab weld, shown in Figure 5.245. Additionally, a 1 inch tear formed at the West end of W-SGB, shown in Figure 5.246.

Figure 5.243 Tear in North Beam Web - MT

Figure 5.244 Tear in South Beam Web - MT

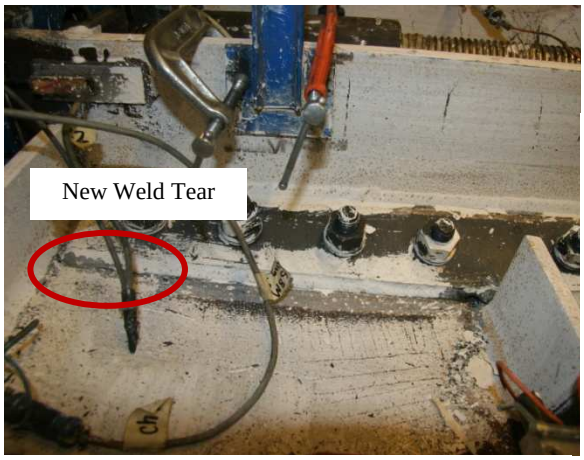

Figure 5.245 New Tear in South Beam-to-Shear Tab Weld

Figure 5.246 New Tear in South Gusset-to-Beam Weld

At the tensile peak of 6.27% total drift range, the North beam-to-shear tab weld completely fractured, leaving only the bolts connecting the beam to the column. This is shown in Figure 5.247. Over subsequent cycles, no major changes in damage occurred. Slight increases in framing member yielding and weld tearing were observed. The test was concluded after a cycle at 6.85% total drift.

Figure 5.247 Fracture of North Beam-to-Shear Tab Weld

5.10.5 Test Summary

NCBF1-R5 achieved a total drift range of 4.27% prior to brace fracture. However, a 35% loss of tensile lateral load capacity occurred at a drift range of 2.95% when the North gusset-to-beam weld fractured. The frame achieved significantly higher drifts than NCBF1, the un-retrofitted connection.

Filling the brace with concrete was successful at delaying local buckling of the non-compact cross section. Global buckling occurred at 0.87% drift range, but brace cupping did not form until 2.95% total drift range, and the brace survived six complete cycles after cupping before fracture occurred.

Adding bolts to the shear tab connections prevented failure of the beam to column connection. Unlike previous retrofits, the addition of bolts was able to preserve the beam to column connection by eliminating the demands bending between the gusset plate and shear tab on the North shear tab weld and by providing additional load-carrying capacity. The North beam-to-shear tab weld fractured during the post-brace fracture cycles, but the bolts were able to carry the demands on the beam to column connection.

Damage to the connections in NCBF1-R5 was substantial, but it achieved a much higher drift range than NCBF1, and had a more desirable failure mode than any of the other NCBF1 retrofits. Yielding in the gusset plates and shear tabs was extensive, as expected given the high DCRs for gusset plate yielding limit states.

Chapter 6: Data Analysis

6.1 Introduction

This chapter describes the analysis of data collected for the specimen with the goal of quantifying aspects of the system performance. Particular emphasis will be placed on the component DCRs, including their effectiveness at predicting component performance and their relative importance to the system behavior. Section 6.2 describes the behavior of the brace, Section 6.3 describes the behavior of the connections, and Section 6.4 describes global behavior of the frame.

6.2 Brace Performance

6.2.1 Brace Deflected Shape

The brace deflections, particularly at the brace mid-span, are an important factor in braced frame performance. The ability of the brace to carry compressive axial load is, to a large extent, a function of the brace deflections. Additionally, rotations from brace buckling are one of the critical demands placed on the connections.

The brace deflection was recorded primarily by Optotrak markers placed along the brace length at the 6th points. Due to constraints of the position sensors (described in Chapter 4), the southern end of the brace was not viewable. As a result, it was necessary to infer the out-of-plane displacement of the South end of the brace. This was accomplished by assuming that the brace deflected profile was symmetric about the brace midpoint. Previous research conducted in this experimental setup (Johnson 2005, Powell 2012) has demonstrated that this assumption is accurate. Points whose displacements were inferred will be identified as such in this section.

All brace displacements presented in this section are relative to the displacements of the brace ends. The brace end typically moves vertically due to deformations of the connection and out-of-plane movement of the framing members. In order to investigate the deflection of the brace as an isolated unit, these deformations are removed. If the brace end displacements at the two ends were different, a linear fit between the points was used to apply the correction to each marker, as shown in Figure 6.1.

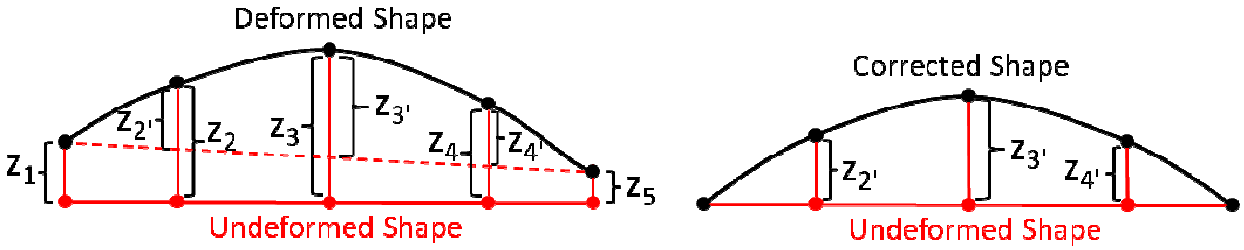

Figure 6.1 Brace Out-of-Plane Deflection Correction

For specimens NCBF1-R3 and NCBF1-R4, brace in-plane displacements were also calculated. The in-plane displacement was corrected to account for the lateral displacement of the frame. The in-plane brace deflection correction is shown in Figure 6.2.The lateral displacement associated with the frame was assumed to vary linearly along the brace length, with the Northernmost marker on the brace used as the reference lateral displacement. The South end of the brace was assumed to have no lateral displacement associated with frame movement. This is a reasonable assumption because the frame is rigidly attached to the channel reaction assembly near the South end of the brace, so the displacements are likely very small.

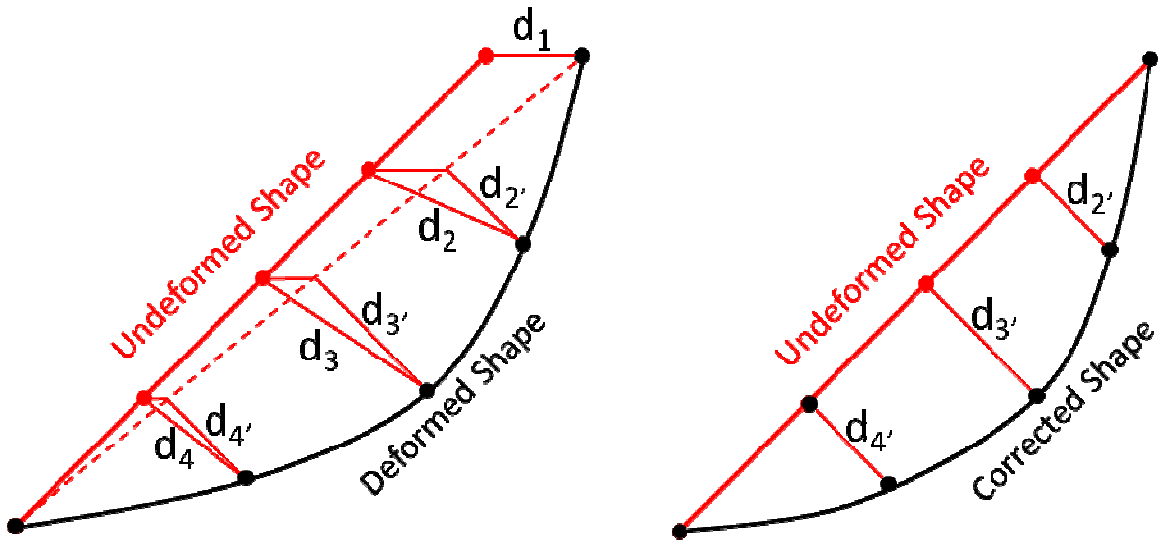

Figure 6.2 Brace In-Plane Deflection Correction

Figure 6.3 shows the brace deflected profile at select drift levels for each specimen. These figures illustrate that the brace deflected shape is typically parabolic at low drift levels, with a reasonably even distribution of curvature along the brace length. However, at higher drift levels, the curvature tends to concentrate near the brace center, and the portions of the brace nearer to the ends become essentially straight. This is particularly clear for NCBF1 and NCBF1-R5. Cupping occurred 1 foot North of the center in NCBF1, so the peak displacement occurred slightly North of the center point. Thus, the actual deflected shape of NCBF1 was likely more triangular than the deflection profile suggests. The NCBF1-R5 deflection profile clearly becomes triangular when the deflections exceeds 10 inches. When the brace curvature becomes sufficiently concentrated at a single location, cupping occurs, which causes large localized strains that typically lead to brace fracture.

The deflected shapes shown here suggest that the brace behaved as a pinned-end compression member. A fixed-end member in compression typically has a bell-shaped deflection profile and develops plastic hinges at the brace center and the ends. By contrast, a pinned-end brace typically has a rounded deflection profile and develops a plastic hinge only at the center. Because the connections tested lacked brace end rotational clearance as required by SCBF design, it initially seemed likely that the braces in these specimens would exhibit a greater degree of rotational restraint at their ends than SCBF braces. However, this does not appear to be the case, as the brace deflection profiles for the NCBF and NCBF retrofit specimens appear to exhibit little or no rotational restraint to the brace. In part, this may result from the weakness of the gusset plates, which had multiple DCRs greater than 1 for all of the connections tested. A weaker gusset plate may provide less rotational restraint, as will be discussed in greater detail in Section 6.3.

NCBF1 Out-of-Plane	NCBF1-R1 Out-of-Plane
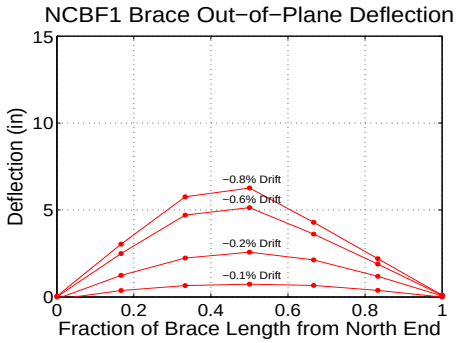	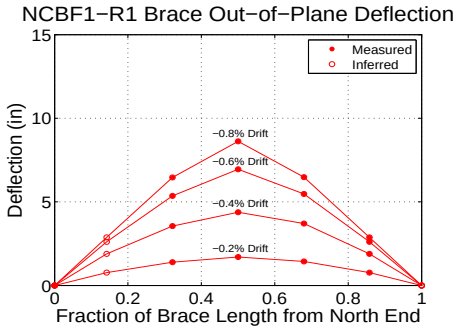
NCBF1-R2 Out-of-Plane	**NCBF1-R3 Out-of-Plane**
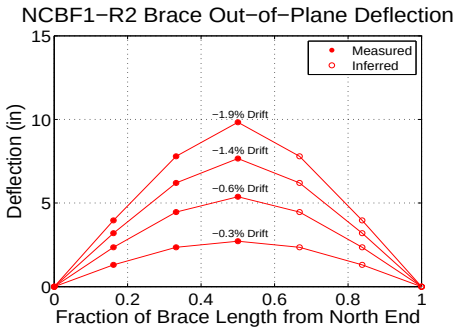	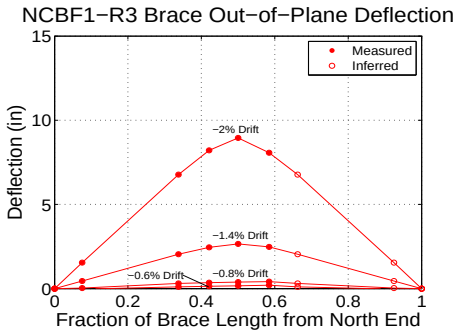
NCBF1-R3 In-Plane	**NCBF1-R4 Out-of-Plane**
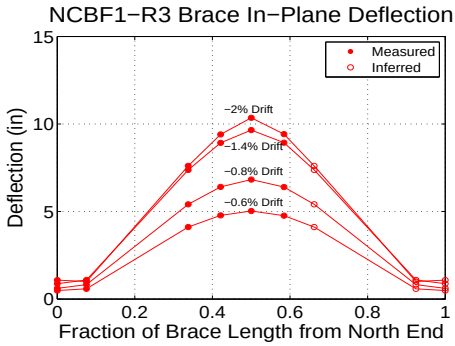	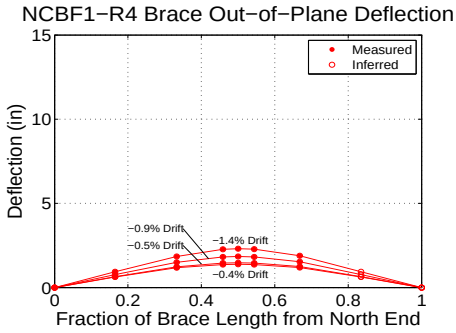
NCBF1-R4 In-Plane	**NCBF1-R5 Out-of-Plane**
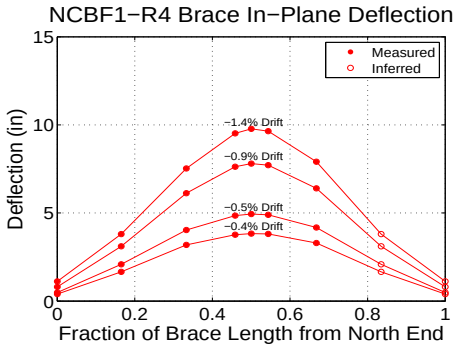	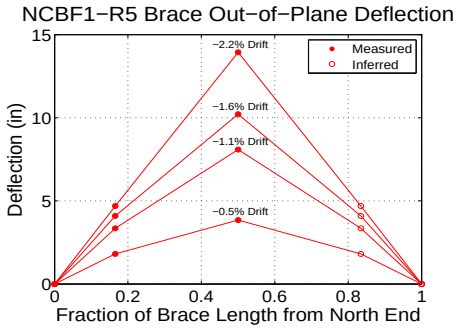

Figure 6.3 Brace Deflected Profiles

Figure 6.4 shows the brace total mid-span deflection for each of the specimens. The total mid-span deflection is the vector sum of the in-plane and out-of-plane deflections. These plots clearly demonstrate the vulnerability of the non-compact brace in NCBF1. All other braces achieved a mid-span deflection of greater than 10 inches, while NCBF1 achieved less than 7 inches prior to fracture. Additionally, the braces for NCBF1-R2, NCBF1-R3, and NCBF1-R4 had not local buckled or fractured at the end of the test, so they likely could have sustained larger deformations. This emphasizes the importance of brace compactness on the ductility of the brace performance.

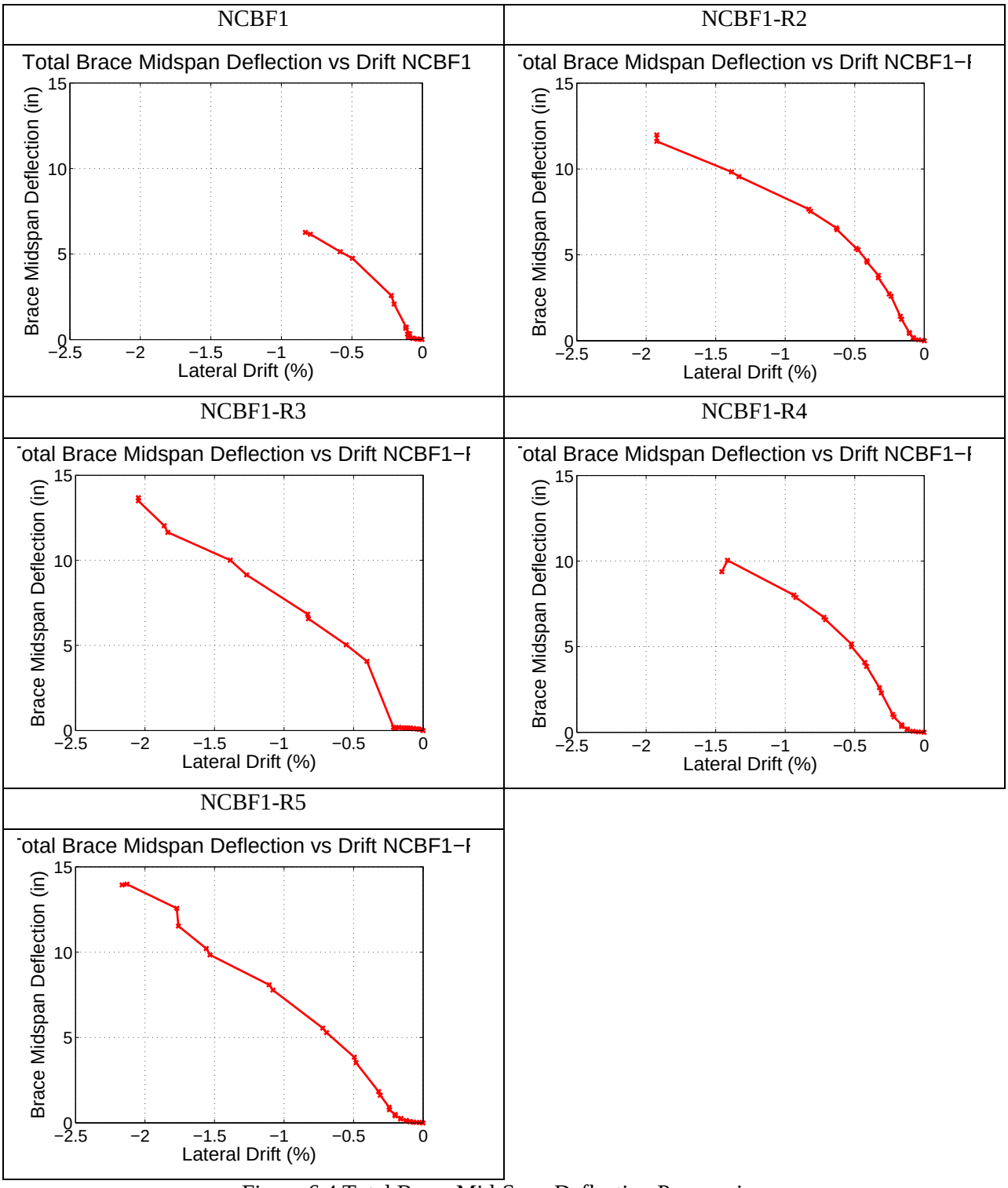

Figure 6.4 Total Brace Mid-Span Deflection Progression

The brace mid-span deflection is related to the brace axial elongation through kinematics. The brace elongation is comprised of axial elongation from brace axial force and elongation due to brace deflection.

If the brace is assumed have a triangular deflection profile, as shown in Figure 6.5, then the brace deflection can be predicted from the brace elongation. Equation (6.3-2) describes this relationship. δ_{ax} axial elongation of the brace, and .δ_b is the elongation due to the brace out-of-plane buckling.

(6.3-2)

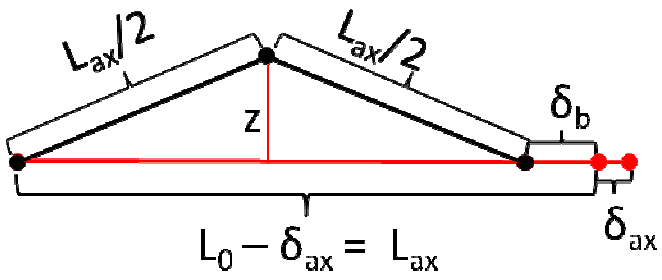

Figure 6.5 Estimation of Brace Midspan Deflection

Both components of the brace axial elongation are difficult to measure in practice, making a direct application of this kinematic theory impractical. However, the principal can be applied using the frame diagonal elongation measurement, which is more reliable. If axial elongation of connections and the brace are ignored, then L_{ax} may be replaced by the frame diagonal measurement to estimate the brace mid-span deflection.

Figure 6.6 shows the brace mid-span deflection as a function of the frame lateral drift in compression for each specimen. This plot demonstrates a strong correlation between compressive drift and brace mid-span deflection. The kinematic model estimate is conservative over almost all drifts for all specimens. The estimate is least accurate for small drifts. Two factors contribute to this. First, the brace has not begun buckling globally at small displacements, so nearly all of the diagonal elongation is by axial elongation of the brace and connections, which was neglected in the approximation. Second, the estimate assumes a triangular brace deflection. However, the brace deflected profile tends to be more rounded, particularly at smaller drifts, as shown in Figure 6.3. A more rounded deflected shape results in a comparatively lower mid-span deflections.

At large drifts, the brace is carrying very little axial load, and thus the elongation due to buckling dominates the behavior. Also, the formation of a plastic hinge causes the brace to transition to a more

triangular deflected shape. These factors contribute to the relatively high accuracy of the estimate at large drifts. This kinematic method serves as a reasonable, conservative estimate of the brace mid-span deflection at larger drift levels.

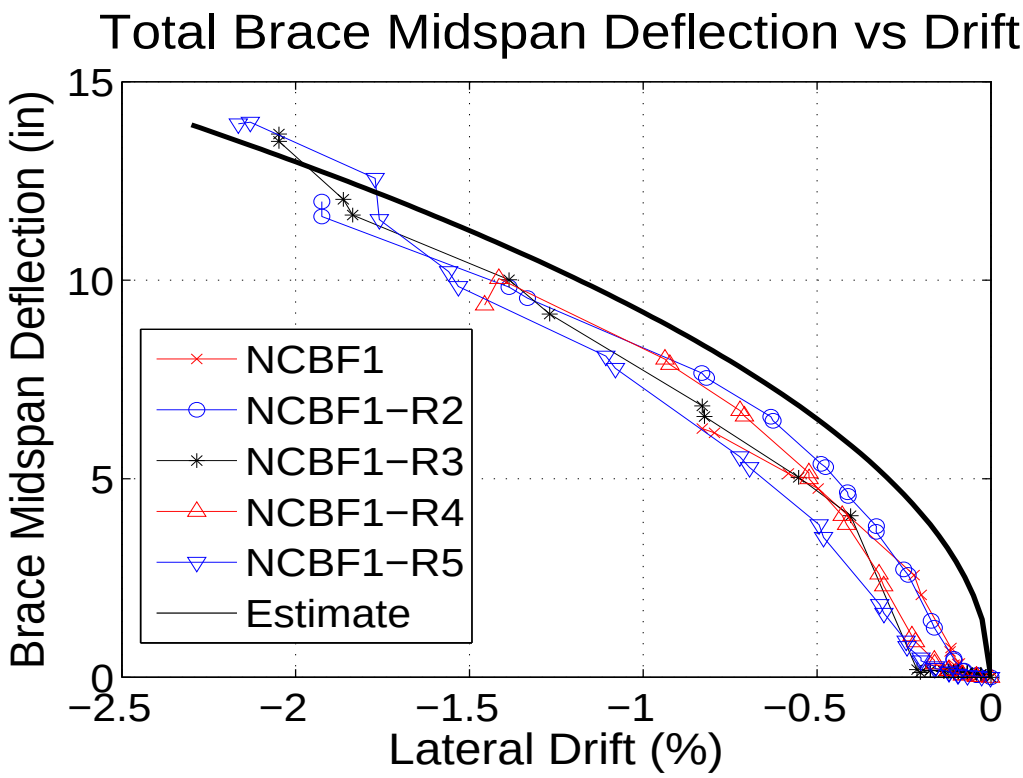

Figure 6.6 Brace Total Mid-Span Deflection

6.2.2 Brace Axial Force

The brace axial force is the primary mechanism by which braced frames resist lateral load, so it is of particular interest when investigating braced frame performance. Typically, braces undergo significant inelastic deformations during seismic loading, due to tensile yielding and compressive buckling. When the yield stress of the brace is exceeded, a linear elastic constitutive model is no longer sufficient to describe the brace performance. Instead, an elastic-perfectly plastic model was used. This model caps the brace stress at the expected yield stress, as shown in Figure 6.7, which depicts the stress strain relationship under monotonically increasing loading. When the material is unloaded, it follows the linear elastic stiffness between until the stress reaches the yield stress in either compression or tension. This is

demonstrated in Figure 6.8 and Figure 6.9, which show a cyclic strain history and the resulting stress response, respectively.

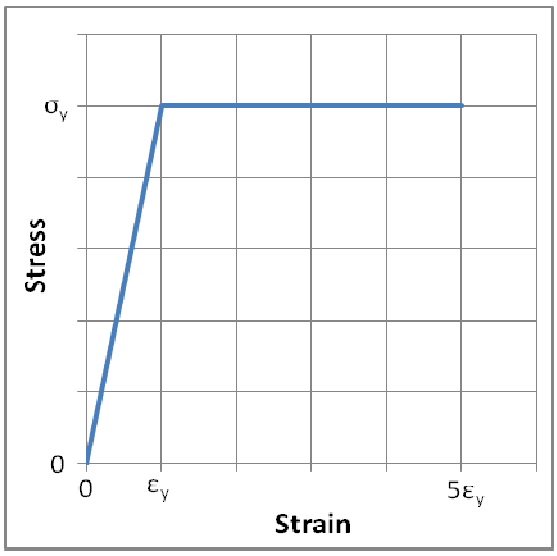

Figure 6.7 Elastic-Perfectly Plastic Material Model

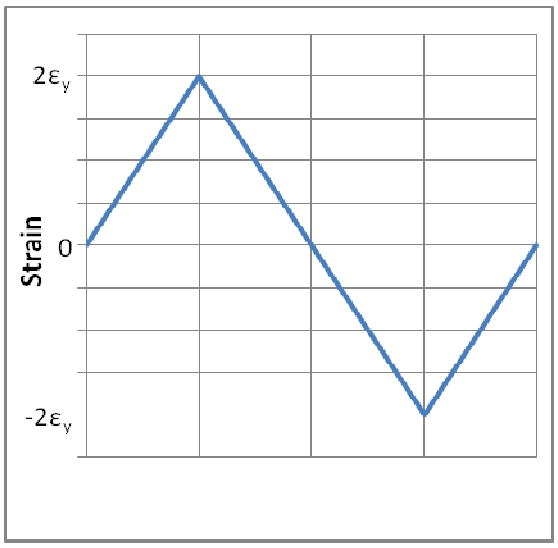

Figure 6.8 Cyclic Strain History

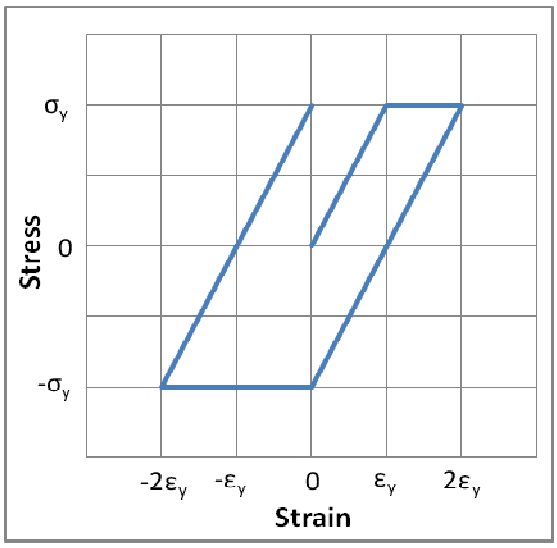

Figure 6.9 Cyclic Response of Material Model

The elastic-perfectly plastic material model was applied to each strain gauge reading, and then the stress readings for the brace strain gauges were averaged to determine the brace axial stress. Axial load was then calculated from Equation (6.3-1), where A is the brace cross-sectional area.

$$F = \sigma_{av} A \tag{6.3-1}$$

Figure 6.10 shows the brace axial force plotted against displacement for each specimen. No usable brace data was acquired from NCBF1-R2, so it is not included here. Figure 6.11, Figure 6.12, and Figure 6.13 compare the brace behavior for each retrofit to that of NCBF1. These plots show the brace axial force in compression against the total brace mid-span deflection.

The compressive brace resistance for NCBF1 dropped substantially after buckling occurred, and brace cupping and fracture occurred soon afterward. The local slenderness of the brace for NCBF1 was twice the maximum allowable in SCBF design. The rapid brace strength degradation and low drift capacity before fracture demonstrate the poor performance of braces with excessive local slenderness.

By comparison, NCBF1-R3 and NCBF1-R4 used compact brace sections. NCBF1-R3 has a substantial drop in strength after buckling, but this is misleading, as the brace was restrained against buckling downward and thus buckled suddenly in-plane. This contrasts with the more gradual progression of buckling observed in the other tests. Figure 6.11 shows that the sudden loss of compressive resistance corresponded to a substantial increase in brace mid-span deflection. After the initial drop in resistance, the compact brace for NCBF1-R3 maintained its compressive capacity much more effectively than NCBF1. This is clearly demonstrated in Figure 6.11 and Figure 6.10.

NCBF1-R4 also demonstrated the more gradual loss of strength characteristic of compact brace sections. The braces for NCBF1-R1, NCBF1-R2, NCBF1-R3, and NCBF1-R4 did not begin cupping prior to connection fracture. All four of these braces were seismically compact, and all reached larger mid-span displacements than NCBF1.

NCBF1-R5 had a concrete filled brace, whose steel section was the same as NCBF1. The brace for NCBF1-R5 lost compressive capacity after buckling much more gradually than NCBF1, as seen in both Figure 6.10 and Figure 6.13. This demonstrates the effectiveness of the concrete fill at improving the brace post-buckling performance. The brace cupped and fractured at significantly larger displacements than NCBF1, verifying that the concrete fill improved the brace durability, as noted in Figure 6.13.

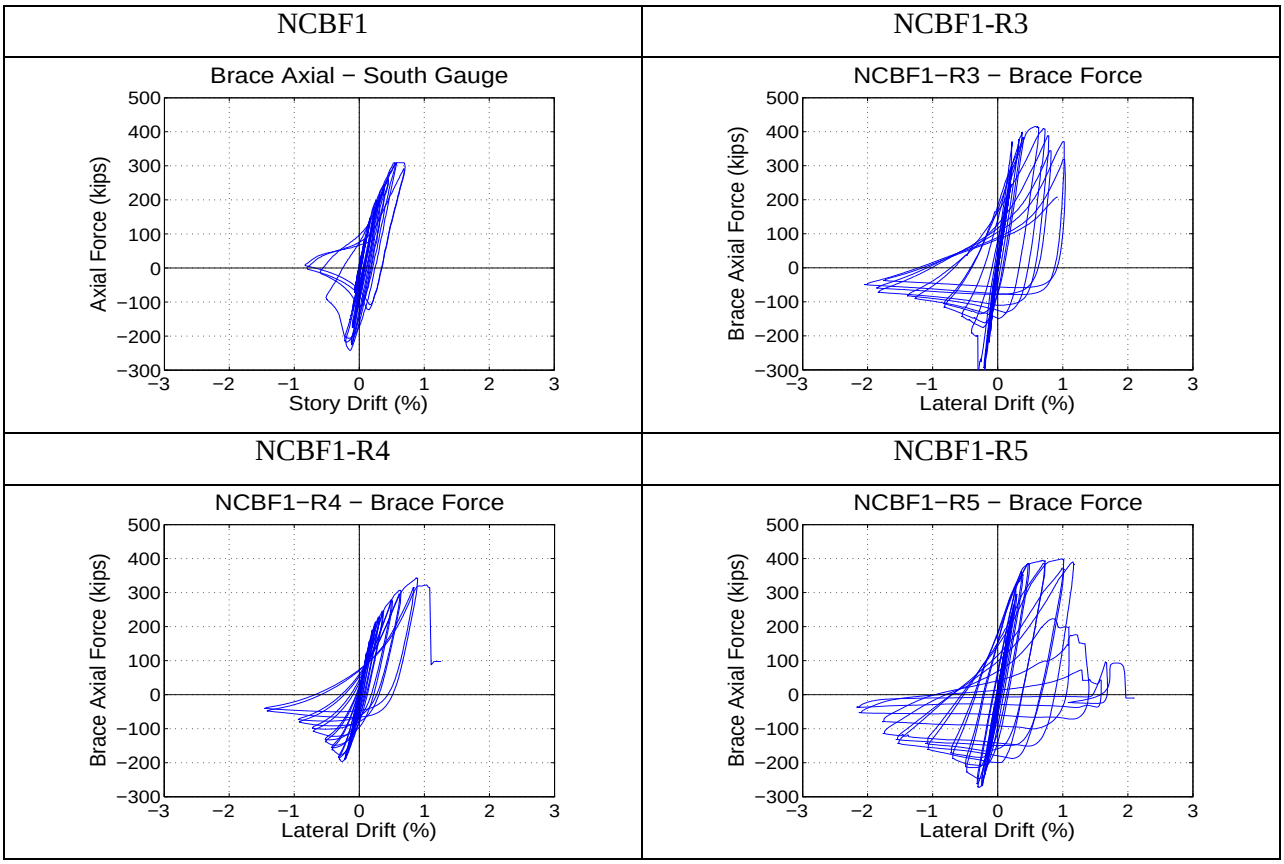

Figure 6.10 Brace Axial Force

The brace compressive axial force and mid-span deflection share an informative relationship, as demonstrated in Figure 6.11, Figure 6.12, and Figure 6.13. When the mid-span deflection exceeds 1 inch, the brace begins to lose compressive axial load capacity, which then continually decreases over subsequent cycles. This is true for compact braces, non-compact braces, and the concrete filled brace. The notable exception is NCBF1-R3. However, as previously mentioned, this specimen's brace behavior is a result of the restraint against out-of-plane buckling that was added.

These figures also clearly demonstrate the vulnerability the non-compact brace for NCBF1, which rapidly lost lateral load capacity after buckling, and fractured at a relatively low mid-span deflection. All three retrofitted braces shown were able to retain compressive resistance out to significantly large mid-span deflections. Also, Figure 6.13 shows the effectiveness of the concrete fill, allowed the brace to retain more of its compressive resistance than NCBF1 and delayed cupping until more than twice the mid-span deflection at which it occurred in NCBF1.

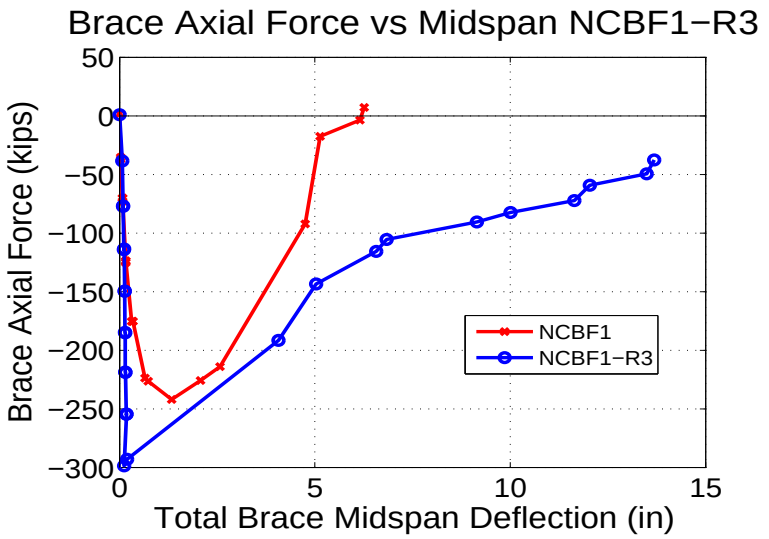

Figure 6.11 Brace Force versus Mid-Span Deflection - NCBF1-R3

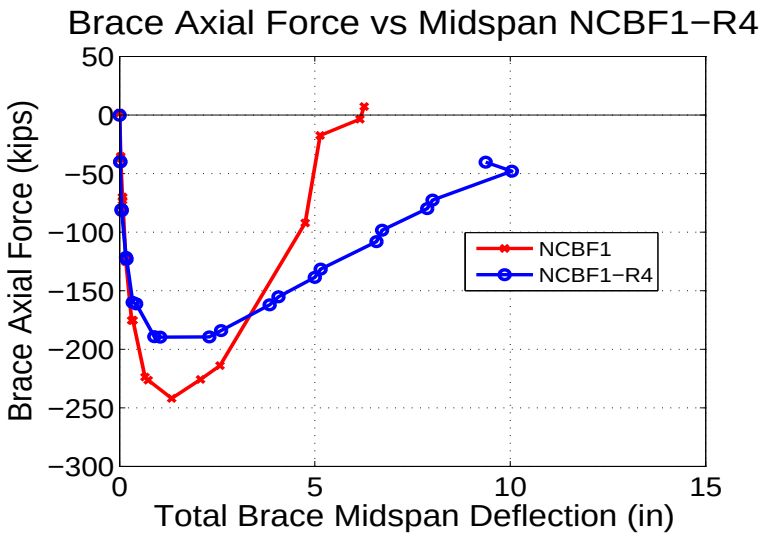

Figure 6.12 Brace Force versus Mid-Span Deflection - NCBF1-R4

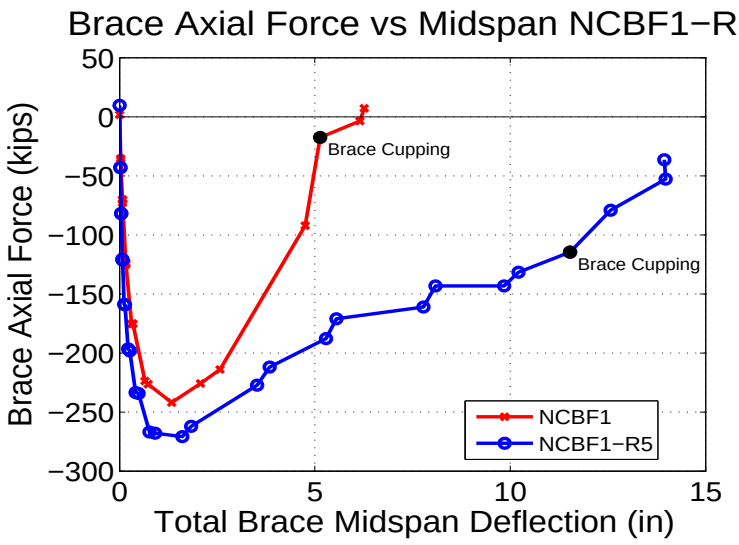

Figure 6.13 Brace Force versus Mid-Span Deflection - NCBF1-R5

6.3 Connection Performance

The NCBF and NCBF retrofit specimens tested all had a wide range of connection deficiencies, which is characteristic of NCBFs, as described in Chapter 2. Many of the specimens tested experienced extensive connection damage or fracture. This makes it clear that the deficiencies of the connections have an adverse impact on the system performance. This section evaluates the contributing factors to the observed connection damage and their relation to the predicted system deficiencies.

6.3.1 Out-of-Plane Rotation

The connection out-of-plane rotation is of particular interest in NCBF systems because of the lack of end clearance for the brace, as illustrated in Figure 6.14. In an SCBF connection, the gusset plate is designed with sufficient brace end clearance to allow for a wide folding region of the plate. This end clearance minimizes the out-of-plane rotations of the gusset plate near the welds, thus protecting the connection. By contrast, NCBF connections lack end clearance requirements, so the bending of the gusset plate is concentrated around the welds, which may lead to weld tearing or fracture. The brace end clearance lines illustrated in Figure 6.14 utilize the elliptical brace end clearance recommendations from Roeder et al (2011), as described in Chapter 2.

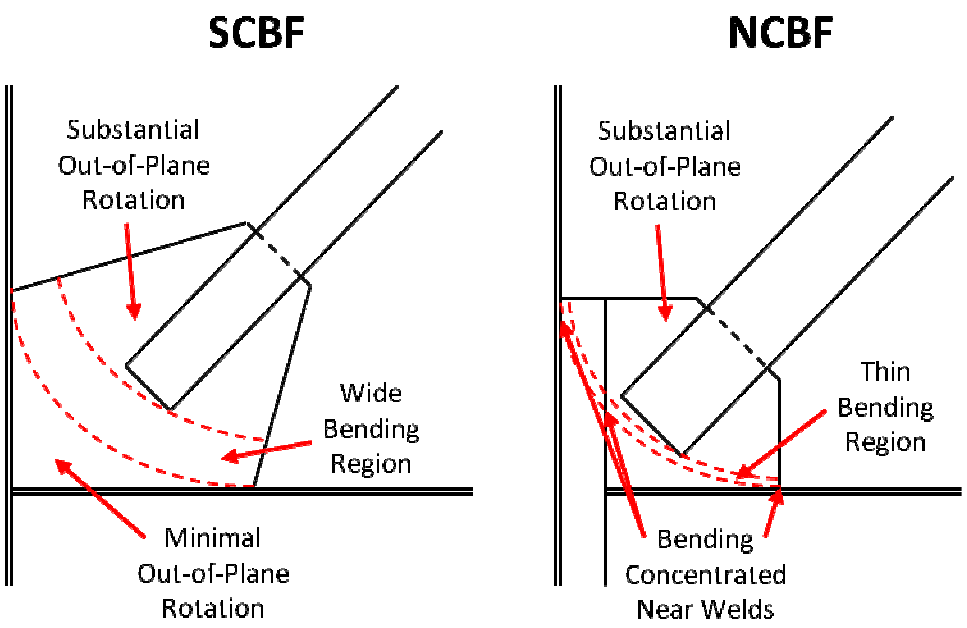

Figure 6.14 Brace End Rotational Clearance

The out-of-plane rotations of the brace end, two edges of the gusset plate, and the end of the shear tab were computed. The Optotrak markers used to compute rotation at each of these locations are shown in Figure 6.15

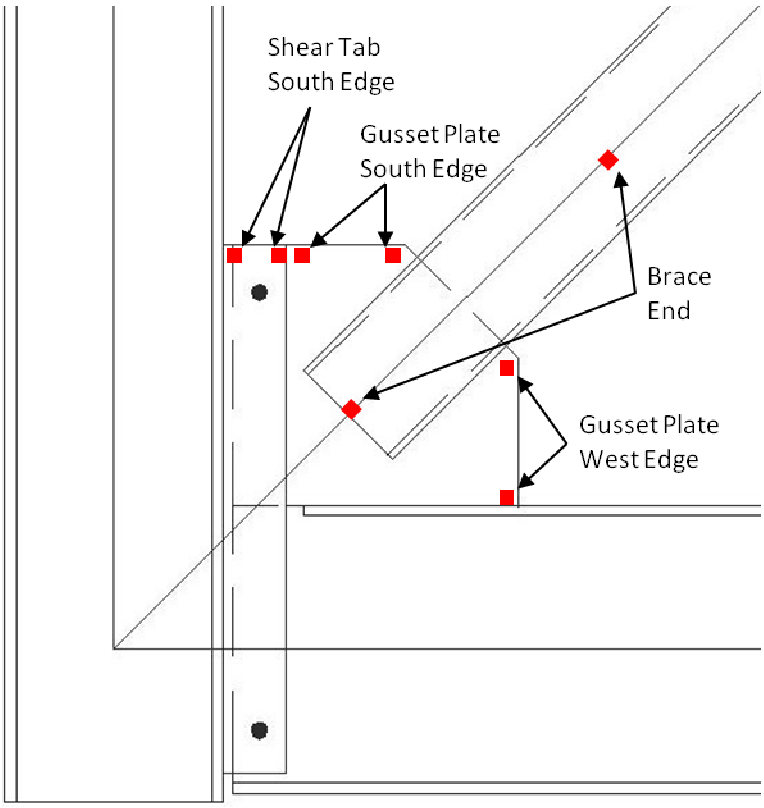

Figure 6.15 North Connection Rotation Sensors

The rotation for each set of Optotrak markers was computed from the difference between the initial position and the deflected position, as shown in Figure 6.16. The rotation was computed using Equation (6.3-3), in which L_{def} is the distance between the two markers in the deformed position and *dz* is the out-of-plane movement of marker B relative to marker A. Figure 6.17 shows a photograph of the out-of-plane rotation of the gusset plate West edge and the markers used to compute that rotation.

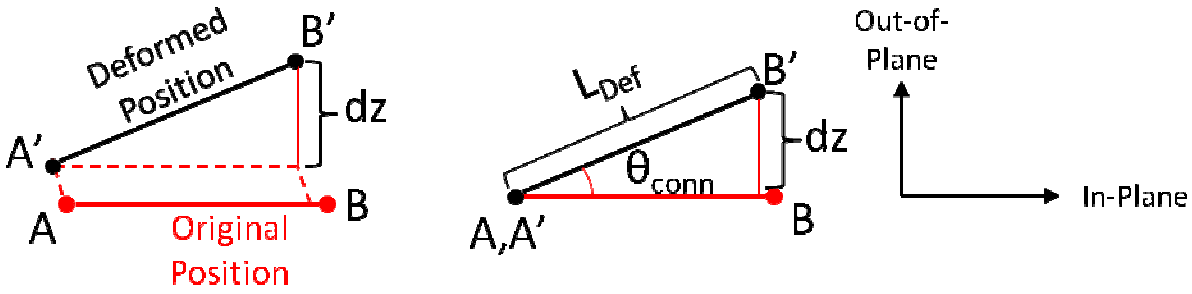

Figure 6.16 Computation of Connection Out-of-Plane Rotations

(6.3-3)

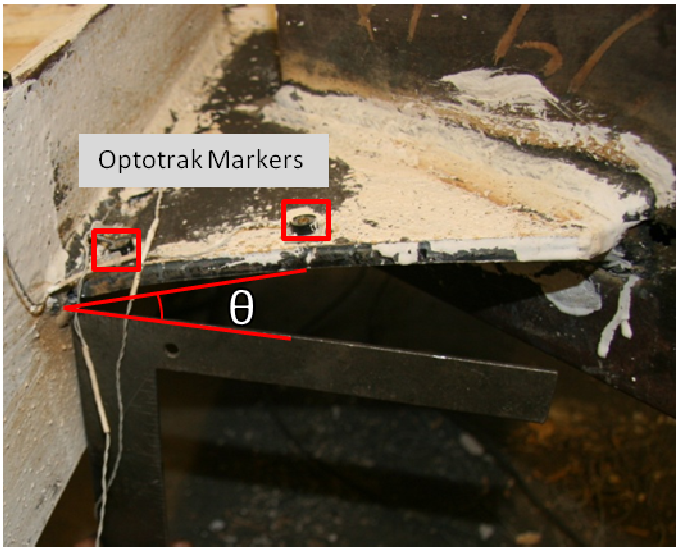

Figure 6.17 Gusset Plate West Edge Rotation Geometry

As Optotrak markers were not typically visible at the South end of the brace, the rotation of each component was calculated only for the North connection.

Figure 6.18 shows each of the connection rotations for all tests plotted against the brace mid-span out-of-plane deflection. It is important to note that the various rotations computed here are not directly comparable, because they are computed about different axes with different gauge lengths. As such, similarities or differences in the magnitudes of values between plots are not necessarily indicative of a direct relationship between them.

Figure 6.18 reveals some interesting trends in the specimen behavior. All four rotations show a strong correlation with the mid-span deflection. This is reasonable because the brace mid-span deflection is the only major out-of-plane movement occurring in the specimen, so it has a strong influence on the connection out-of-plane behavior.

The brace end rotation quantities show particularly remarkable consistency across the specimens. The brace-to-gusset connection geometry varied significantly across the specimens tested, as shown in Figure 6.19. The brace end rotation plot suggests that the variability in the brace-to-gusset connection had almost no influence on the relationship between the brace mid-span deflection and the brace end rotation. The

relationship between these two variables is indicative of the degree of rotational restraint that the connection applies to the brace ends. As such, this plot demonstrates that the brace-to-gusset plate connection geometry has virtually no impact on the rotational restraint of the brace end.

The shear tab and both gusset plate edges exhibited rotations exceeding 0.1 radians for most tests, and approaching 0.2 radians in some cases. These large rotations have the potential to contribute to the initiation of tearing in the welds, which are subjected to these large rotational demands. This is described in more detail later in this section.

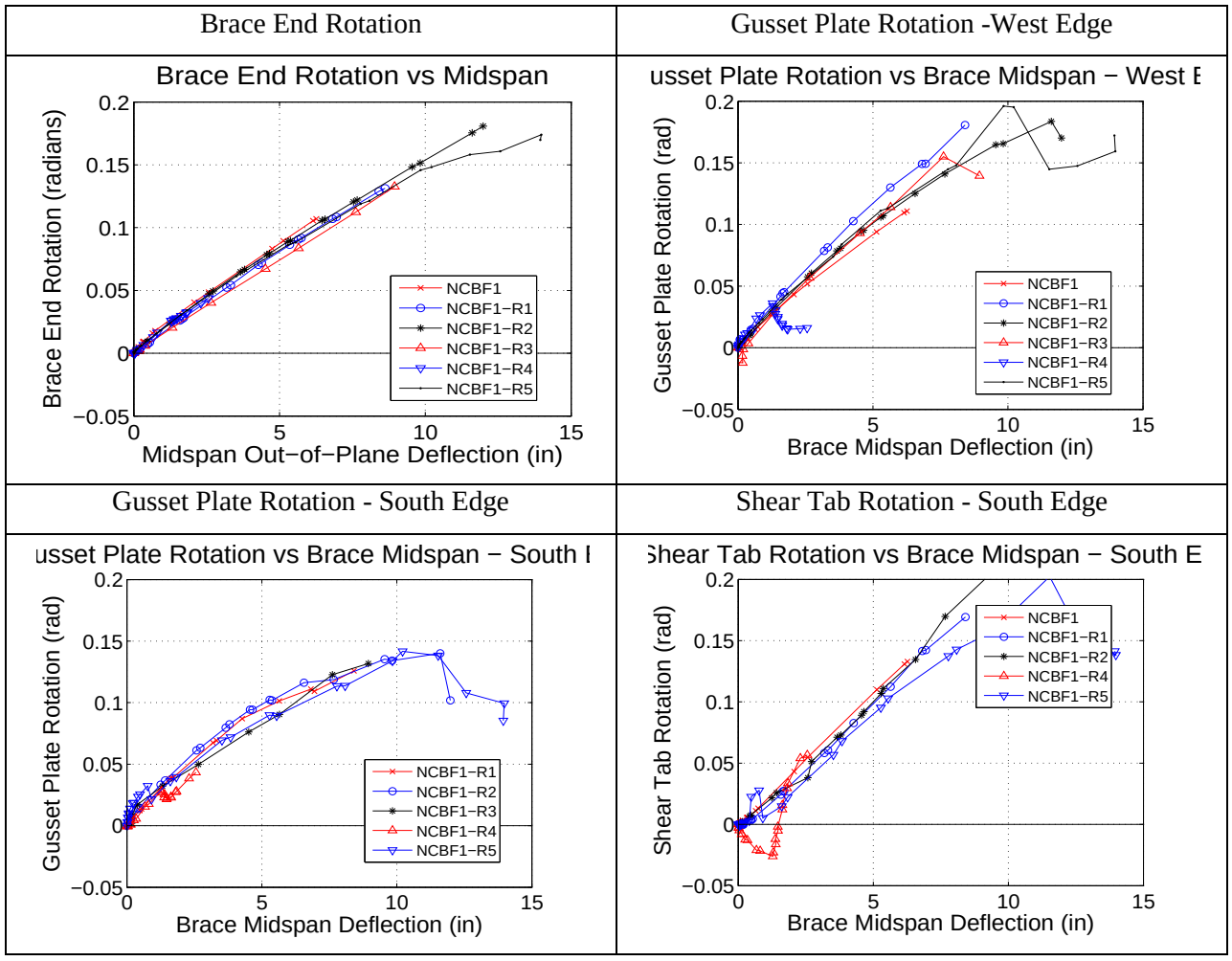

Figure 6.18 Connection Rotations

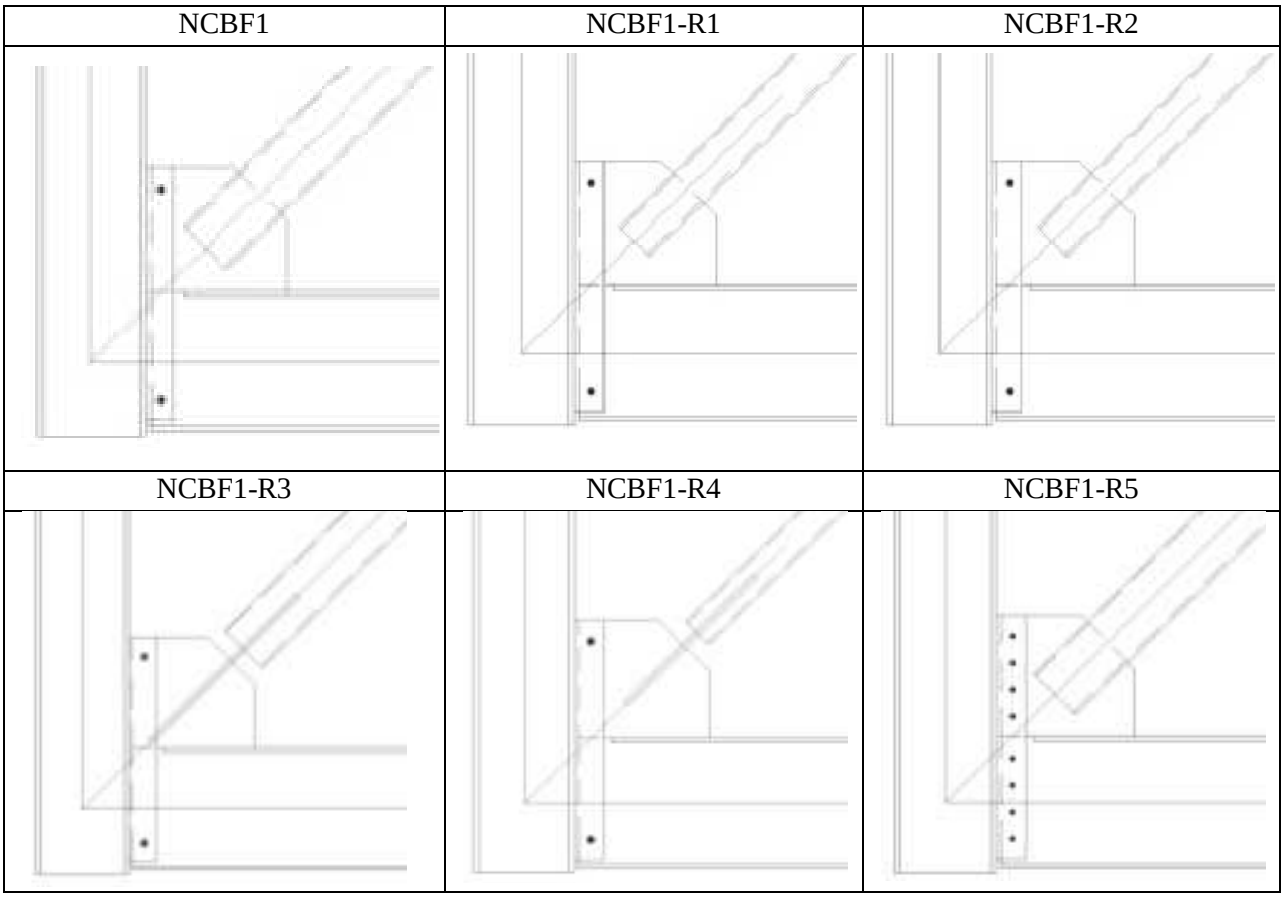

Figure 6.19 Variation in Brace-to-Gusset Connection Geometry

6.3.2 Gusset-to-Beam Weld Damage

Tearing of the gusset-to-beam weld occurred in four of the specimens tested, and contributed to connection failure in three of those specimens. Thus, the characteristics of the tearing of this weld are important to understanding the system vulnerabilities. The DCR for the gusset-to-beam weld was 1.55 for all tests. These tests demonstrated that a DCR this large for gusset-to-beam weld tearing had a significant impact on the system performance and represents a critical connection deficiency. Figure 6.20, Figure 6.21, and Figure 6.22 show the percentage of the gusset-to-beam weld torn as a function of the brace end rotation, the gusset plate edge rotation, and the total drift range, respectively.

Table 6.1 summarizes the key values from these plots.

The North gusset-to-beam weld typically began tearing at the West end while the brace was buckled out-of-plane. Increase in the lengths of tears also typically occurred at compressive peaks, rather than tensile ones. This suggests that the tearing of the gusset-to-beam weld is related to the out-of-plane rotation of the brace end and the connection. The figures below confirm this by demonstrating that the rotation of the

West edge of the gusset plate, which is directly adjacent to the end of the gusset-to-beam weld where tearing typically initiated, had the strongest correlation with the weld tearing. The brace end rotation provides similar results with slightly weaker correlation.

The total drift range is clearly not an effective method of predicting weld tearing, as tearing initiated at a variety of drift ranges. Also, the brace tensile force, which is used to compute the demand on the weld, does not appear to strongly influence the initiation of weld tearing. As mentioned, tearing typically initiated and progressed when the brace was in compression, when the axial loads are smaller.

Because drift range and brace axial load appear to have little relation to tearing of the gusset-to-beam weld, it is apparent that the most critical aspect of the performance for predicting tearing of the gusset-to-beam weld is the out-of-plane rotation of the gusset plate.

Table 6.1 shows that tearing initiated when the gusset plate rotation was between 0.13 and 0.17 radians. NCBF1 and NCBF1-R4, which did not suffer tearing of the gusset-to-beam weld at the gusset plate edge, reached edge rotations of 0.11 and 0.04 radians, respectively. This demonstrates that tearing of the gusset-to-beam weld can be expected when the gusset plate rotation exceeds 0.13 radians.

Additionally, it is notable that the beam-to-gusset weld reached complete fracture within 2 cycles after tearing exceeded 25% of the weld length in all cases. This instability in weld tearing is expected for specimens NCBF1-R3 and NCBF1-R5, where the gusset-beam weld utilized a weld with low notch toughness. However, NCBF1-R1 had a higher toughness gusset-beam weld, but it still progressed relatively quickly to failure. It is possible that existing damage to the gusset plates and welds from NCBF1, which were re-used for NCBF1-R1, affected this behavior. Also, it is possible that the higher notch-toughness of the weld was not sufficient to ensure stability of the weld tear once it reached that length.

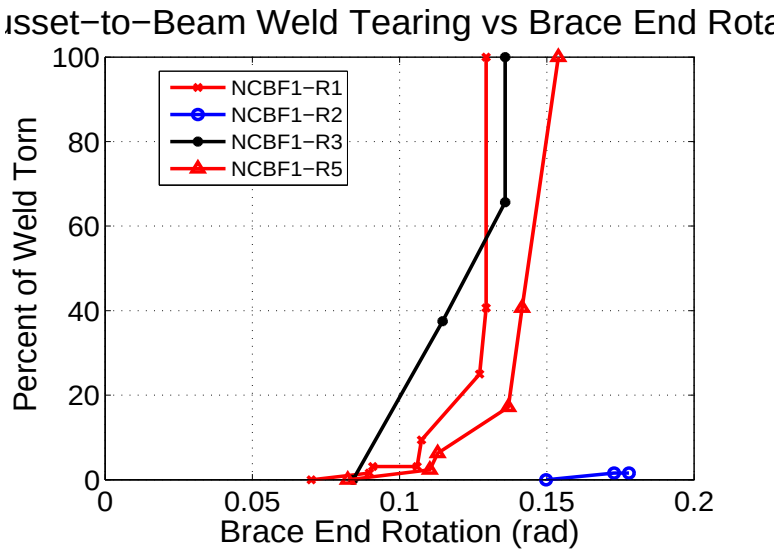

Figure 6.20 Gusset-Beam Weld Tearing versus Brace End Rotation

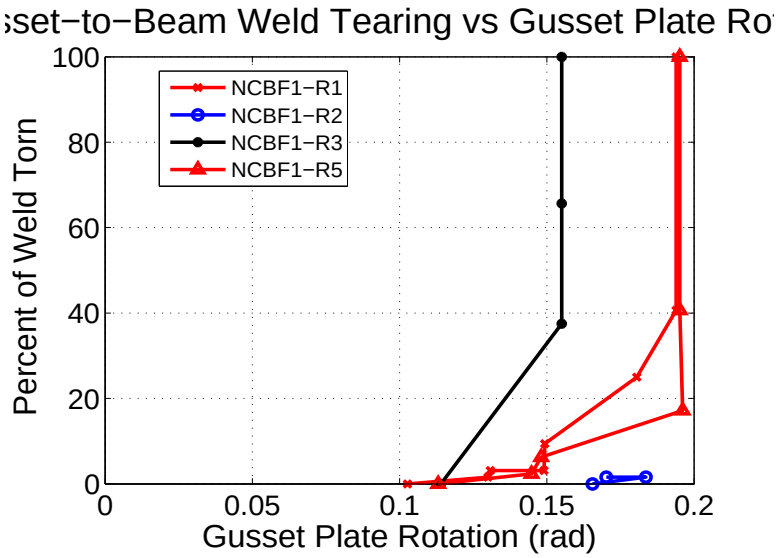

Figure 6.21 Gusset-Beam Weld Tearing versus Gusset Plate Rotation

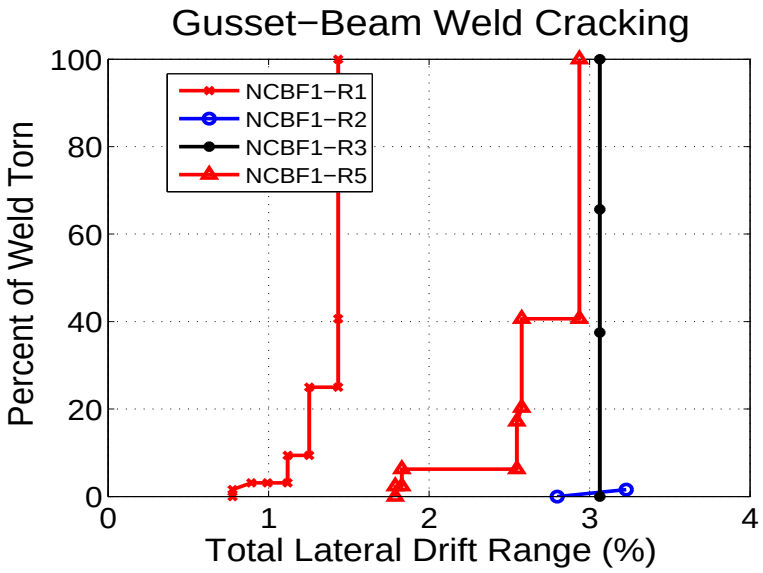

Figure 6.22 Gusset-Beam Weld Tearing versus Drift Range

Table 6.1 Beam-to-Gusset Weld Tearing Comparison

	Values at Weld Tearing Initiation			Maximum Achieved		
Specimen	Brace End θ (rad)	Gusset Plate Edge θ (rad)	Drift Range (%)	Brace End θ (rad)	Gusset Plate Edge θ (rad)	Drift Range (%)
NCBF1	NA	NA	NA	0.091	0.111	1.52
NCBF1-R1	0.898	0.130	NA	0.129	0.194	NA
NCBF1-R2	0.173	0.170	3.23	0.183	0.184	3.34
NCBF1-R3	0.115	0.155	3.06	0.136	0.155	3.06
NCBF1-R4	NA	NA	NA	0.043	0.037	2.72
NCBF1-R5	0.110	0.145	1.79	0.162	0.172	4.27

6.3.3 Gusset Plate Yielding

The gusset plates used in NCBF1 and its retrofits had substantial deficiencies relative to the brace strength, as summarized in Table 6.2. As a result of these deficiencies, yielding and deformation in the gusset plate was typically extensive, as shown in Figure 6.23. Although yielding of the gusset plate was substantial, it did not appear to have a significant adverse impact on the performance of the specimens tested. Yielding of the gusset plate is a ductile limit state, and can actually contribute to the overall ductility of the system by providing an additional yielding mechanism. However, a more severe deficiency in gusset plate strength could lead to a gusset plate failure, so the gusset plate strength is still

important to consider. Additionally, the extensive yielding in the gusset plate may have concentrated strains around the welds, which could have contributed to the initiation of weld tearing.

Table 6.2 NCBF Gusset Plate Deficiencies

Limit State	**NCBF1**	**NCBF1-R1**	**NCBF1-R2**	**NCBF1-R3**	**NCBF1-R4**	**NCBF1-R5**
Gusset Plate Block Shear	1.16	1.33	1.33	1.22	1.78	1.16
Gusset Plate Whitmore Yielding	1.33	1.50	1.50	1.28	1.89	1.33
Gusset Plate Shear Yielding at Beam	1.16	1.16	1.16	1.16	1.16	1.16

NCBF1-R2 NE Connection	NCBF1-R2 SW Connection
	
NCBF1-R3 NE Connection	NCBF1-R3 SW Connection
	
NCBF1-R4 NE Connection	NCBF1-R4 SW Connection
	
NCBF1-R5 NE Connection	NCBF1-R5 SW Connection
	

Figure 6.23 NCBF Connection Yielding

6.3.4 Connection In-Plane Rotation

The in-plane rotation of the frame places demands on the connection, and provides additional insight into the connection performance. As the frame deforms, the beam to column connections must deform in plane to accommodate the rotation between the beam and the column, shown in Figure 6.24. If the connection is flexurally stiff relative to the beam and column, this deformation may be concentrated in the beam and column in the form of plastic hinging at the edges of the gusset plate, as shown in Figure 6.25. If the connection is less stiff than the beans and columns, then deformations of the connecting elements will accommodate the rotation, as shown in Figure 6.26. The true behavior will be combination of these mechanisms.

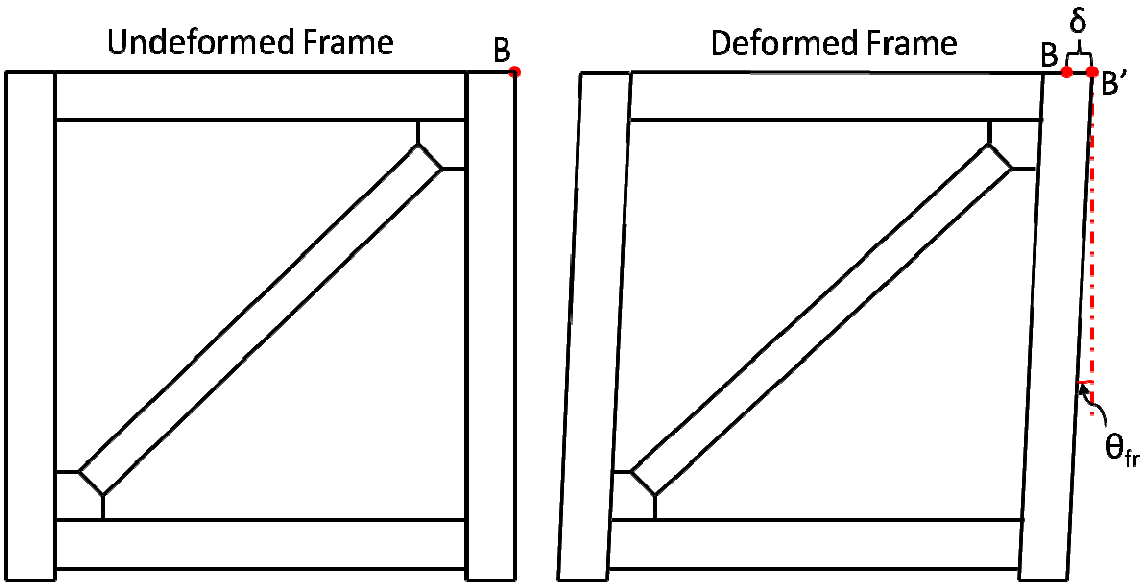

Figure 6.24 Beam-Column Rotation Angle

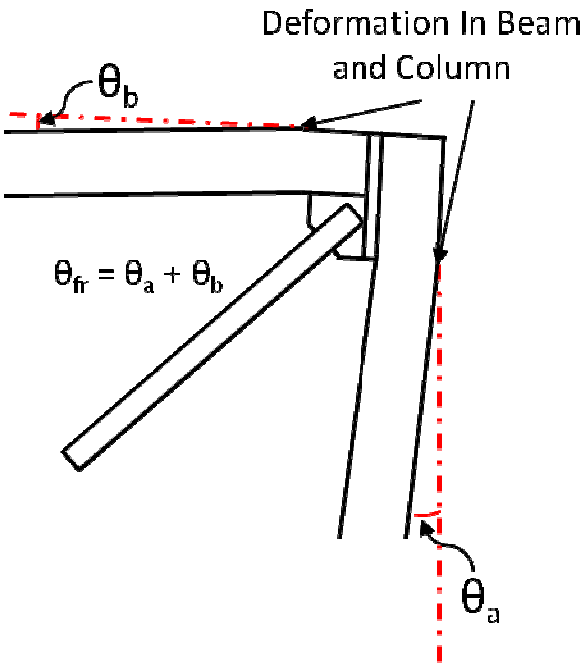

Figure 6.25 In-Plane Rotation - Stiff Connection

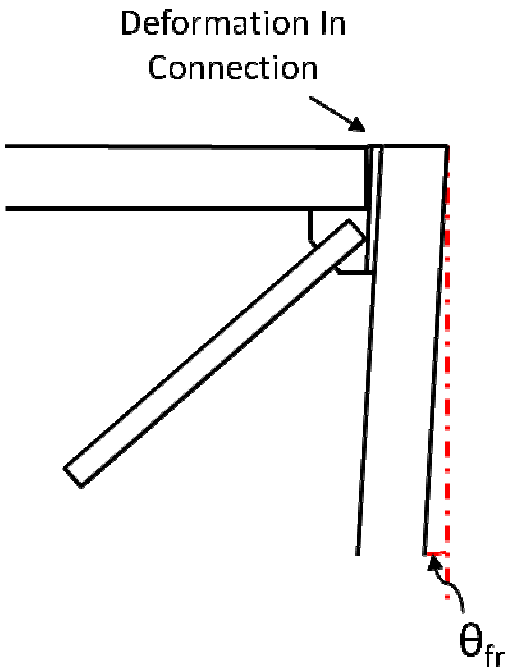

Figure 6.26 In-Plane Rotation - Flexible Connection

The location of large deformations will typically also be the location of the most substantial damage. SCBF tests conducted at the University of Washington have demonstrated that SCBF connections can experience relatively comparable amounts of yielding in the gusset plate and the framing members (Powell 2010). Figure 6.27 and Figure 6.28 show yielding in the column and gusset plate, respectively, in an SCBF connection.

Figure 6.27 Column Flange Yielding (Powell 2010)

Figure 6.28 Gusset Plate Yielding (Powell 2010)

The in-plane rotation of the frames was captured using the Optotrak system. Markers on the flange of the beam and column were used to compute the initial beam-column angle (ideally 90 degrees). The change in angle was then measured from the relative motion of the markers on the beam and column flanges.

The relative motion of the beam and column was recorded in two regions. The first is rotation outside the connection region. This measure includes rotation within the connecting plates, as well at the points of maximum demand in the beam and column at the edges of the gusset plate. Figure 6.29 shows the typical locations of markers used for this measurement. The rotation angle was calculated using the two markers on the beam flange and two markers on the column flange on the interior side of the frame. The angle was also computed using the markers on the exterior flanges. These two values were averaged to calculate the true rotation angle. This procedure helps to remove possible bias from local deformations of the beam or column flanges.

The second measure calculated is rotation within the connection. For this measure, markers on the beam and column flanges that lie within the connection were used. This computes the rotation of the connecting plates, but not the rotation of the beam and column at the edges of the gusset plate. Figure 6.30shows the typical location of these markers. As with the markers outside the connection region, the rotation was calculated for the interior and exterior flanges and then averaged to remove bias.

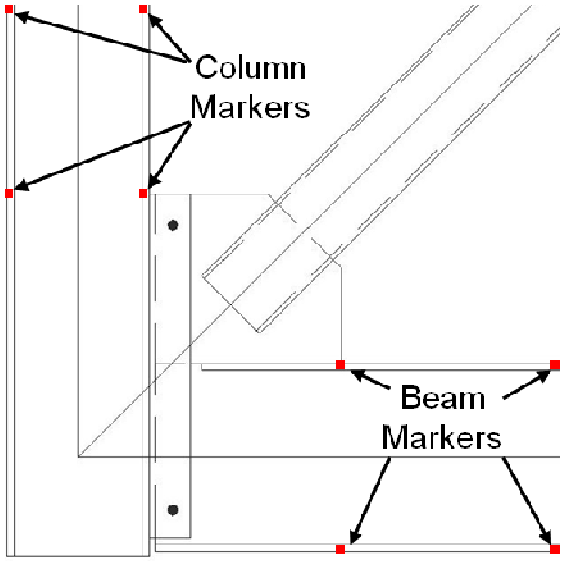

Figure 6.29 Connection Rotation Markers - Outside Connection

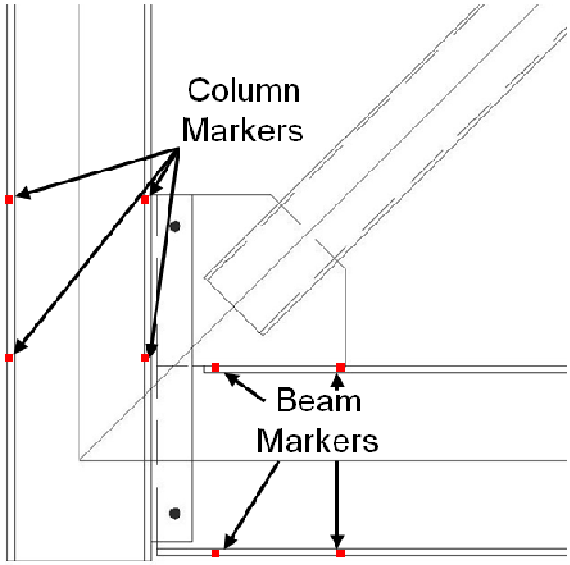

Figure 6.30 Connection Rotation Markers - Within Connection

Rotations outside of the connection region are shown in Figure 6.31. These results show that the rotation of the beam relative to the column varies linearly with drift, which is expected. The consistency in the data demonstrates that the beams and columns of the specimens behaved similarly to one another. This is reasonable, because the gusset plate and the shear tab, which are the primary components of the connection, remained consistent across all tests.

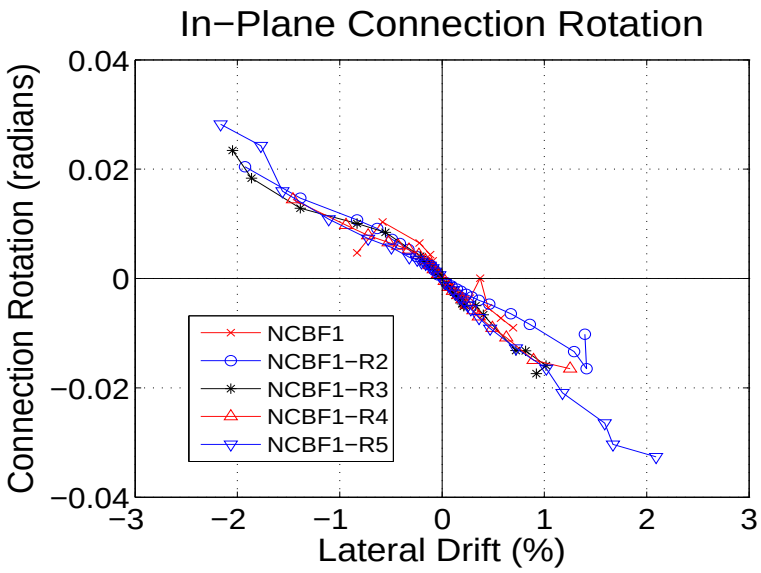

Figure 6.31 Frame In-Plane Rotation Outside Connection

Calculation of rotations in the region within the connection was less reliable, in part due to the smaller distance between the sensors, which results in larger contributions from measurement error. Only two specimens had enough functional sensors to calculate rotation within the connection. These are shown in Figure 6.32 and Figure 6.33. The rotation measured at the two locations is comparable.

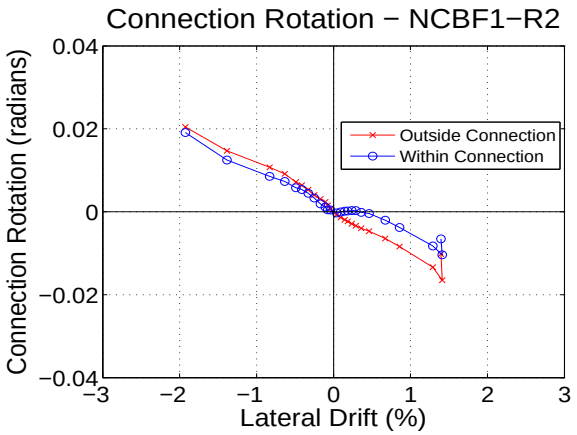

Figure 6.32 NCBF1-R2 In-Plane Connection Rotation

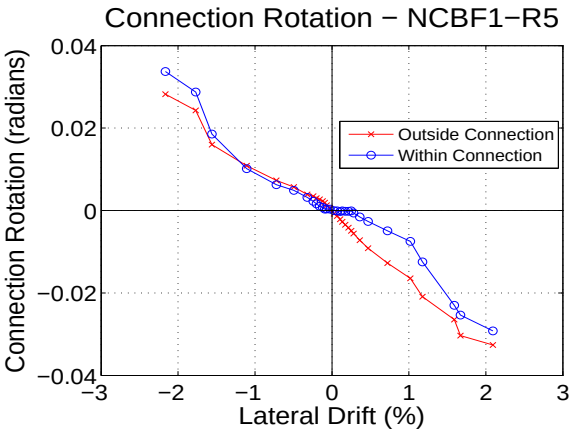

Figure 6.33 NCBF1-R5 In-Plane Connection Rotation

The rotation is presented differently in Figure 6.34 and Figure 6.35. The rotation of the connecting elements is the rotation measured within the connection. The rotation of the beam and column is the difference between the measured rotations inside and outside of the connection. Thus, these plots show the contributions of the framing elements and the connecting elements to the total rotation separately. These plots demonstrate that the rotation is primarily concentrated within the connection. This is particularly true when the brace is in compression and the joint is opening. By contrast, the beam and column rotations are a more significant contributor to rotation for small tensile drifts, but are overtaken by the connection rotation at larger drift levels. These results indicate that while the connection does not behave as a true pin, the majority of the deformation is concentrated in the connecting elements.

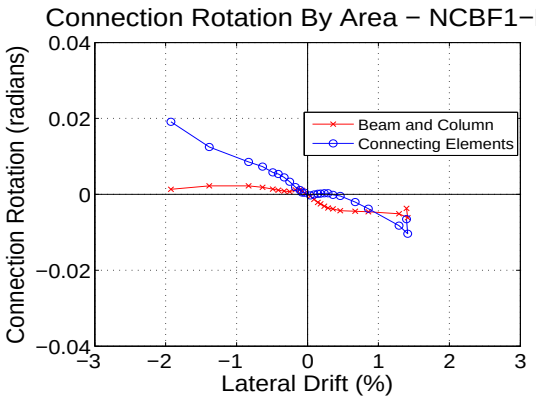

Figure 6.34 NCBF1-R2 In-Plane Connection Rotation by Component

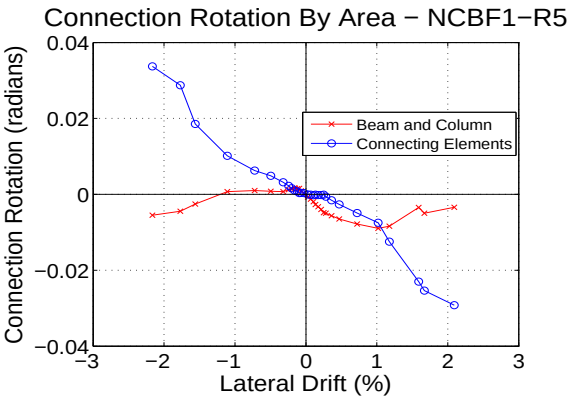

Figure 6.35 NCBF1-R5 In-Plane Connection Rotation By Component

It is possible to quantify the strength of the connection relative to the framing elements in a general sense. The shear tab must transfer flexural, axial, and shear demands between the beam and the column. Table 6.3 shows the geometric properties of the framing elements and the shear tab.

Table 6.3 Geometric Properties of Members

	Column	Beam	Shear Tab
A (in^2)	21.1	13.3	11.1
Sx (in^3)	97.4	72.7	54.9
Zx (in^3)	108	82.3	82.3

The shear tab has a smaller cross-sectional area than both the beam and the column, and it has a section modulus and plastic section modulus that are less than or equal to the beam and column values. This highlights the shear tab as a potential weak point within the system. In addition, the beam and column see their highest demands at the edge of the gusset plate, since the gusset plate contributes to their strength beyond that point. However, in pure frame action, the largest moments are observed at the beam-to-column interface, where the shear tab is located. Thus, the shear tab likely has larger flexural demands from frame action than the beam or column.

As a result of this, the shear tab may sustain larger flexural deformations than either the beam or the column. This confirms the observation from the rotation plots, which indicated that the connection, rather than the beam and column, were contributing most of the rotation. This is also consistent with observations from the tests. Typically, the shear tabs were yielded across most, if not all, of their area by the conclusion of the test, as shown in Figure 6.23. By contrast, beam and column damage at the connections was minimal. This highlights an important difference in behavior between NCBF and SCBF connections. NCBF connections may concentrate deformations in the connecting elements rather than in the framing elements, unlike SCBF systems, where yielding may be more evenly distributed.

6.3.5 Shear Tab Weld Tearing

The lateral drift and the resulting in-plane rotation of the connection had an impact not only on the shear tab yielding, but also on the tearing of the weld connecting the shear tab to the gusset plate and beam, referred to herein as the shear tab weld. Tearing of this weld occurred in all of the retrofit specimens, and it contributed to connection failure in all but one of those tests. The shear tab weld is a critical component of the system, because it provides the only connection between the beam and the column. Failure of this weld could result in a partial system collapse if the beam carries substantial gravity load.

The shear tab weld had a DCR for 1.08 for all of the specimens tested. Based on this value, it is surprising that failure of the shear tab weld was such a consistent issue, as many other components had higher DCRs. However, the DCR for the shear tab weld is based solely on the demands delivered by the brace, but the weld is also subject to demands due to out-of-plane buckling of the brace and the in-plane rotation of the connection due to lateral drift. The effects of these factors are discussed below.

Specimens NCBF1-R3 and NCBF1-R4 aimed to protect the connection welds by utilizing in-plane brace buckling. For NCBF1-R4, which buckled purely in plane, this method was successful for protecting the gusset-beam weld. However, it was not successful at protecting the shear tab weld. Figure 6.36 shows the shear tab weld tearing as a function of brace end rotation. Specimen NCBF1-R4 invalidates what appeared to be some correlation between brace end rotation and shear tab weld tearing for the other specimens, as it complete fracture of the shear tab weld at a very small brace end rotation.

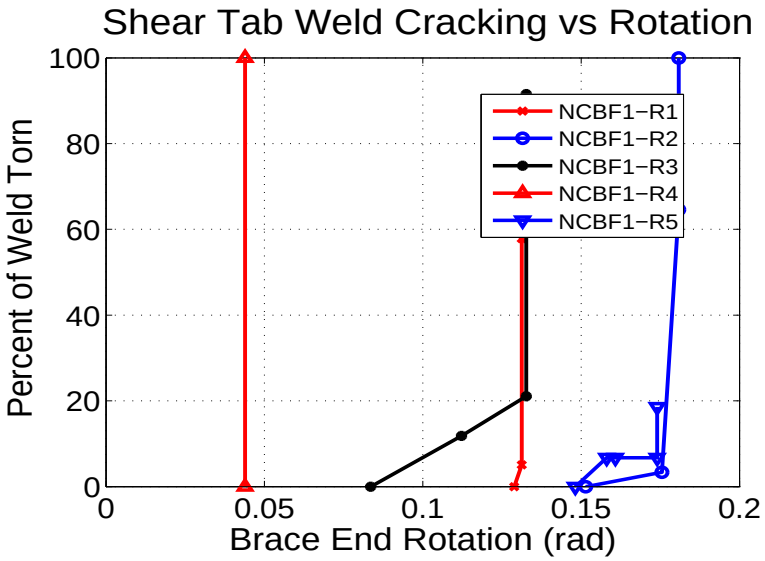

Figure 6.36 Shear Tab Weld Tearing versus Brace End Rotation

Figure 6.37 shows the shear tab weld tearing as a function of total drift range. A clear correlation between drift range and the initiation of tearing is visible. This indicates that the tearing of the shear tab weld is more dependent on the drift range than on the brace end rotation. Table 6.4 gives the drift range at which tearing was first observed in each specimen.

The difference in behavior between NCBF1-R5 and the other specimens is clearly visible in Figure 6.37 and Table 6.4. Specimens NCBF1-R2, NCBF1-R3, and NCBF1-R4 all suffered complete connection failure within two cycles of the initiation of tearing in the shear tab weld. This indicates that the shear tab

weld not only tears at a predictable drift range, but also progresses rapidly to failure after tearing initiates. The rate of tearing propagation is again influenced by the low notch-toughness electrode, which was used for this weld on all specimens. NCBF1-R5 added bolts to the shear tab to reinforce the shear tab weld by preventing bending of the gusset plate away from the shear tab and by providing additional shear capacity. The bolts were clearly effective in that regard. While they did not delay the onset of tearing in the shear tab weld, they substantially delayed the propagation of tearing, allowing NCBF1-R5 to attain higher drift levels.

These results clearly demonstrate that the shear tab weld represents a significant vulnerability in the system, despite being only slightly deficient. Aside from the brace compactness, the defiency of the shear tab weld had the most severe negative impact on the system performance of any of the connection deficiencies.

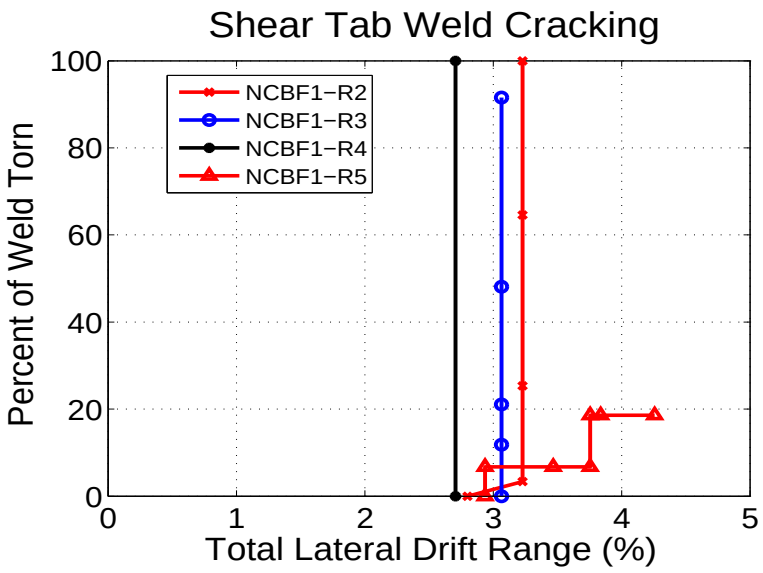

Figure 6.37 Shear Tab Weld Tearing versus Drift Range

Table 6.4 North Shear Tab Weld Tearing

	Drift Range at Weld Tearing (%)	End Rotation at Weld Tearing (radians)	Cycles to Fracture After Weld Tearing
NCBF1	NA	NA	NA
NCBF1-R1	1.43	0.13	1.0
NCBF1-R2	3.23	0.18	1.5
NCBF1-R3	3.06	0.11	2.0
NCBF1-R4	2.71	0.04	0.0
NCBF1-R5	2.94	0.16	>4.0

6.3.6 Knife Plate Rotation

For specimens NCBF1-R3 and NCBF1-R4, the in-plane bending of the knife plates is necessary to accommodate the brace end rotation for in-plane buckling. The performance of this plate is of interest for the performance of these specimens. The rotation of the knife plate was computed using four sensors along the length of the knife plate. The angle between the two sensors in the brace region and the two sensors in the gusset plate region was the knife plate rotation, as demonstrated in Figure 6.38.

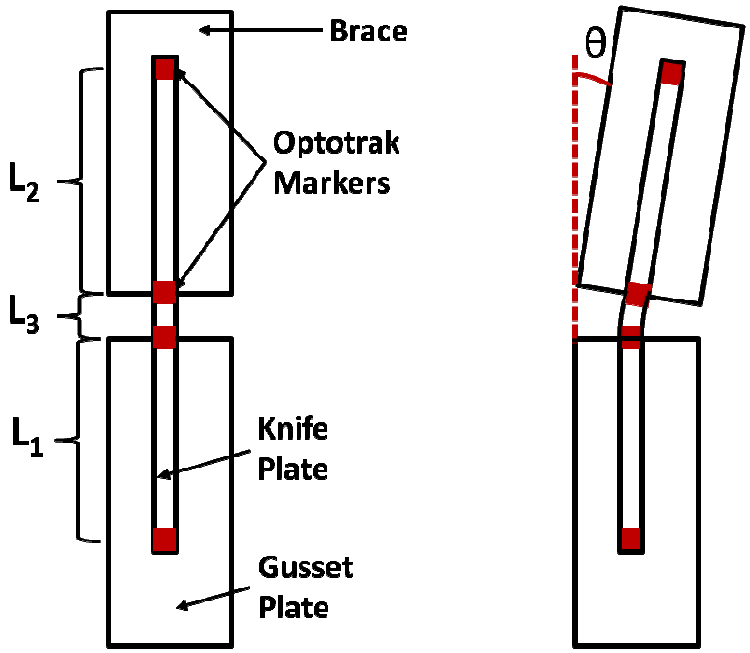

Figure 6.38 Knife Plate Rotation Schematic

The knife plate rotation is plotted in Figure 6.39. The rotation is strongly correlated with the brace mid-span in-plane deflection, which is reasonable. The two specimens exhibited very similar behavior.

Although the knife plates were designed to resist the full brace tensile capacity, yielding developed in the hinge region when the knife plate rotations exceeded 0.04 radians. Given that this is only a small fraction of the rotations achieved in these tests, yielding in the knife plates appears to be inevitable after brace in-plane buckling occurs.

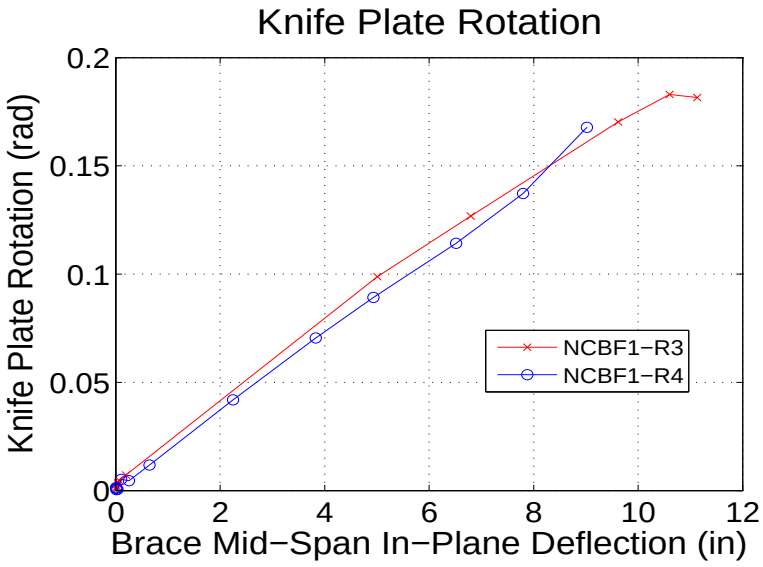

Figure 6.39 Knife Plate Rotation

6.4 System Performance

The system performance combines the effects of the brace and connection components, as well as the framing members, to provide a more complete understanding of how the frame will behave in a structure subjected to seismic loads.

6.4.1 Load-Drift Behavior

The performance of a braced frame is typically characterized by the lateral load resistance and frame lateral drift, from which various system properties can be derived. Table 6.5 provides an overview of the maximum load and drift quantities observed for each of the specimens tested. The lateral loads are presented as both standard and normalized form. The positive lateral load is normalized to the lateral load required to yield the brace in tension, P_y, which is computed using Equation (6.2-1). θ is the brace angle, which is 45˚ for all specimens, R_y is the ratio of expected to nominal yield stress of the brace material for the brace, A_g is the gross area, and F_y is the design yield stress.

.

$$P_y = R_y F_y A_g \cos(\theta) \tag{6.2-1}$$

The negative lateral load is normalized to the lateral load required to buckle the brace in compression, P_{cr}, which is computed using Equation (6.2-2). The critical buckling stress, P_{cr} was computed using the expected yield capacity of the brace, $R_y F_y$, as described in Chapter 2. An effective length factor, K, of 1 was assumed for all cases.

$$P_{cr} = \mathrm{F_{cr}} \mathrm{A_g} \cos(\theta) \tag{6.2-2}$$

The lateral drift measurements for Table 6.5, and for all subsequent sections of this chapter, were computed from the elongation of the frame diagonal between the work points at the Northeast and Southwest corners of the frame. Figure 6.40 illustrates the geometry of this measurement on the frame and how it is converted to lateral drift. Equation (6.2-3) gives the formula for the lateral drift, δ, based on the diagonal elongation, δ_{ax}. The frame diagonal elongation is the most reliable measurement available of the drift experienced by the frame. Losses occur through slip of various components in the load path from the actuator to the strong wall, which makes direct lateral measurements, such as the actuator LDVT, less reliable. Additionally, rocking of the column base causes uniform rotation of the frame, which lateral measurements would read as a component of the drift. The frame diagonal measurement captures only the shear deformations of the frame, which is the most realistic measurement of the frame lateral drift.

$$\delta = \frac{\delta_{ax} \cos(\theta)}{h} \tag{6.2-3}$$

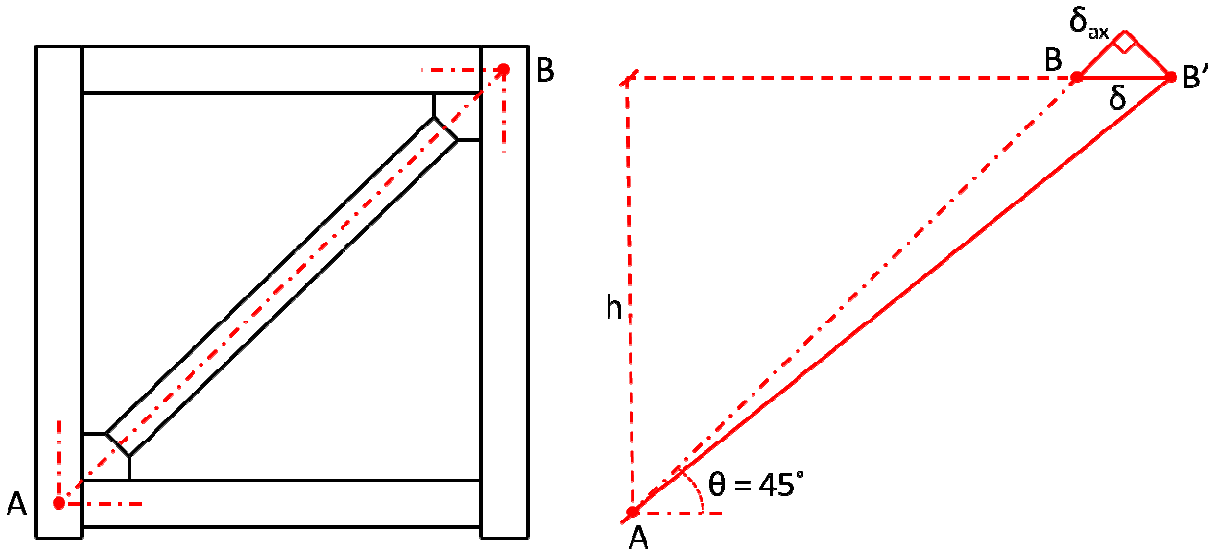

Figure 6.40 Geometry for Frame Diagonal Measurement and Drift Conversion

	Maximum Lateral Resistance				Drift				
Specimen	P+	P-	P+/Py	P-/Pcr	-Drift %	+Drift %	Drift Range %	Description	Failure Mode
NCBF1	274	-200	0.90	0.96	-0.83	0.71	1.54	Existing NCBF	Brace Fracture
NCBF1-R1	293	-133	0.96	0.99	x	x	x	Compact Brace Retrofit	Gusset-Beam and Gusset-Shear Tab Weld Fracture
NCBF1-R2	304	-144	0.99	1.08	-1.93	1.42	3.35	Compact Brace Retrofit	Beam/Gusset-Shear Tab Weld Fracture
NCBF1-R3	317	-248	1.04	1.49	-2.16	1.61	3.77	Knife Plate Retrofit - Square HSS	Gusset-Beam and Beam-Shear Tab Weld Fracture
NCBF1-R4	286	-172	0.93	1.36	-1.48	0.86	2.34	Knife Plate Retrofit - Rectangular HSS	Beam/Gusset-Shear Tab Weld Fracture
NCBF1-R5	313	-204	1.02	0.98	-2.16	1.67	3.83	Concrete Fill and Added Bolts Retrofit	Brace Fracture

Table 6.5 Specimen Performance Overview

All of the specimens tested achieved maximum lateral loads that were roughly equal to the expected lateral capacity based on brace yield strength. This indicates that the brace expected strength is a good predictor of the lateral load capacity for these frames. However, it is important to note that some of the

lateral load resistance is contributed by the columns, as discussed later in this section. Therefore, the lateral load resistance is actually somewhat less than might be expected if the brace reached its expected yield capacity.

Specimens NCBF1, NCBF1-R1, NCBF1-R2, and NCBF1-R5 achieved maximum lateral loads in compression that were roughly equal to the expected lateral load capacity based on brace buckling. Specimens NCBF1-R3 and NCBF1-R4, which were both in-plane buckling braces, achieved lateral loads that were approximately 50% larger than the expected capacities. This indicates that the effective length factor for in-plane buckling in these tests was smaller than the effective length factor for out-of-plane buckling in the other tests, resulting in the larger observed buckling resistance. Again, it is important to also recognize the contribution of the column shear forces to the lateral load resistance of the system.

All of the retrofits of NCBF1 improved the total drift range substantially. However, only NCBF1-R5 achieved the desired failure mechanism of brace fracture. Figure 6.41 through Figure 6.45 show the complete load-drift history for each of the specimens, along with annotations of significant damage to the system. It is notable that only specimens NCBF1 and NCBF1-R5 achieved the desired failure mode of brace fracture. NCBF1 suffered brace fracture at a very low drift level. While it achieved the desired failure hierarchy, it did not achieve the desired ductility. Retrofits NCBF1-R1 through NCBF1-R4 improved the system ductility, but at the cost of a less desirable failure mechanism. Each of these specimens suffered fracture of multiple welds in the North gusset plate connection. NCBF1-R5 was able to both improve system ductility and maintain the desired failure hierarchy, making its performance the most desirable.

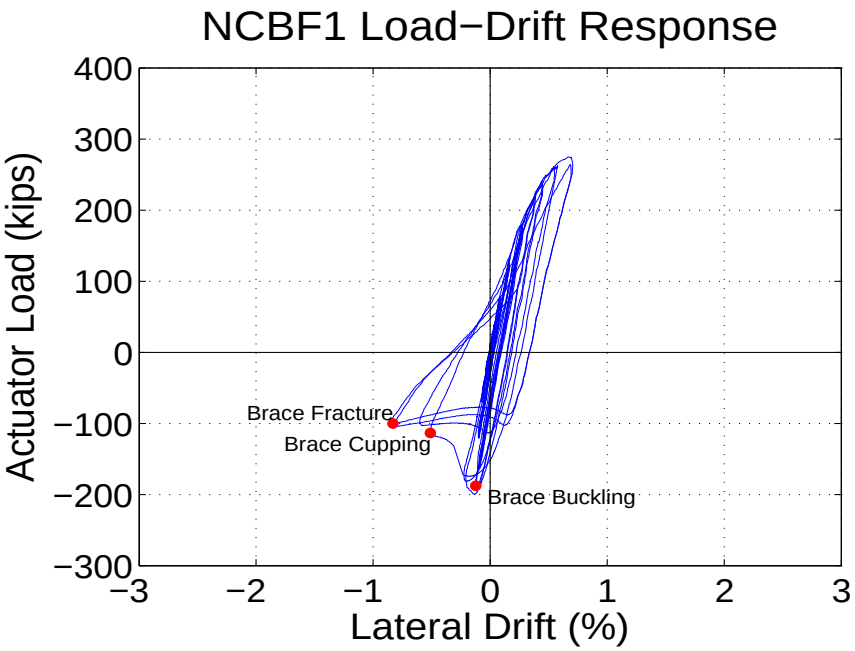

Figure 6.41 NCBF1 Load-Drift History

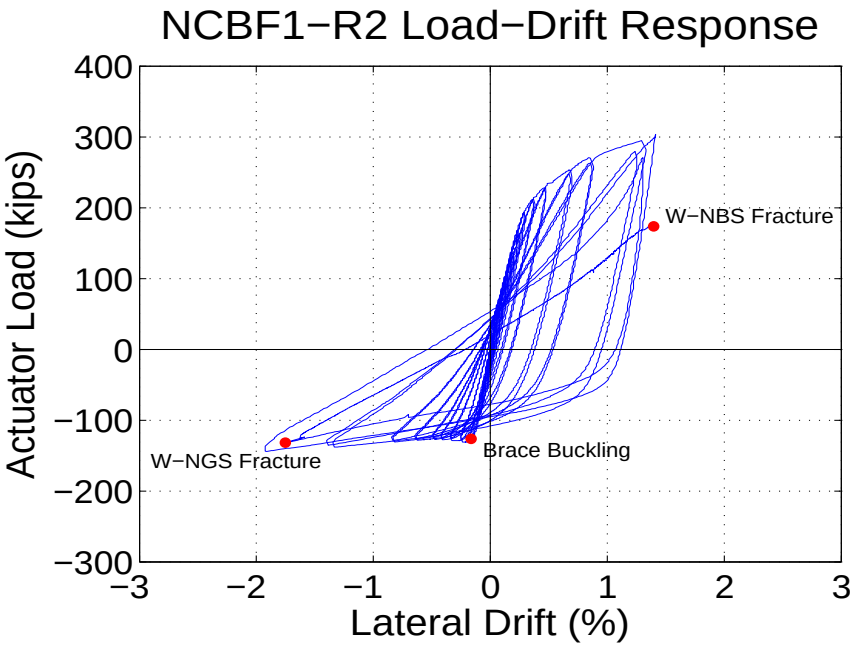

Figure 6.42 NCBF1-R2 Load-Drift History

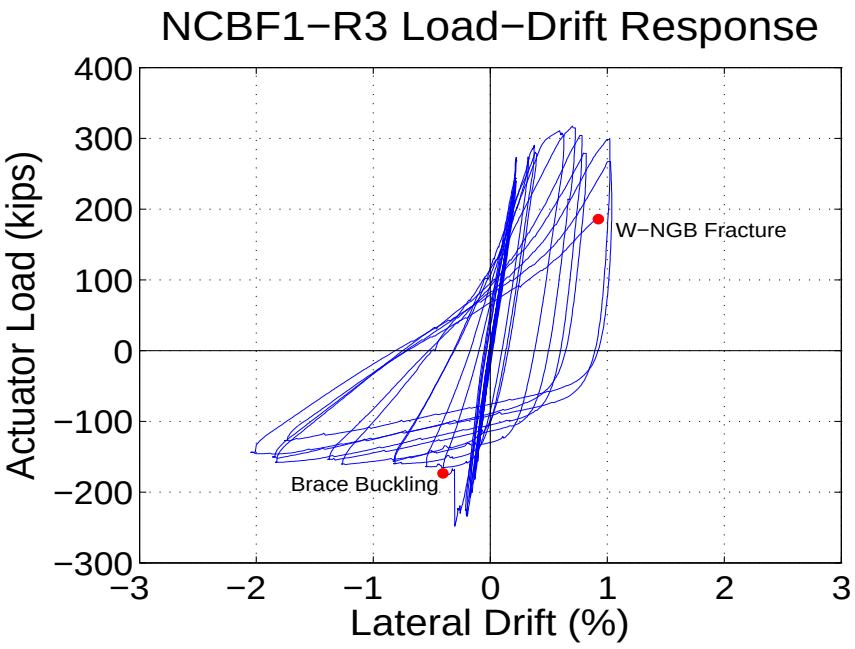

Figure 6.43 NCBF1-R3 Load-Drift History

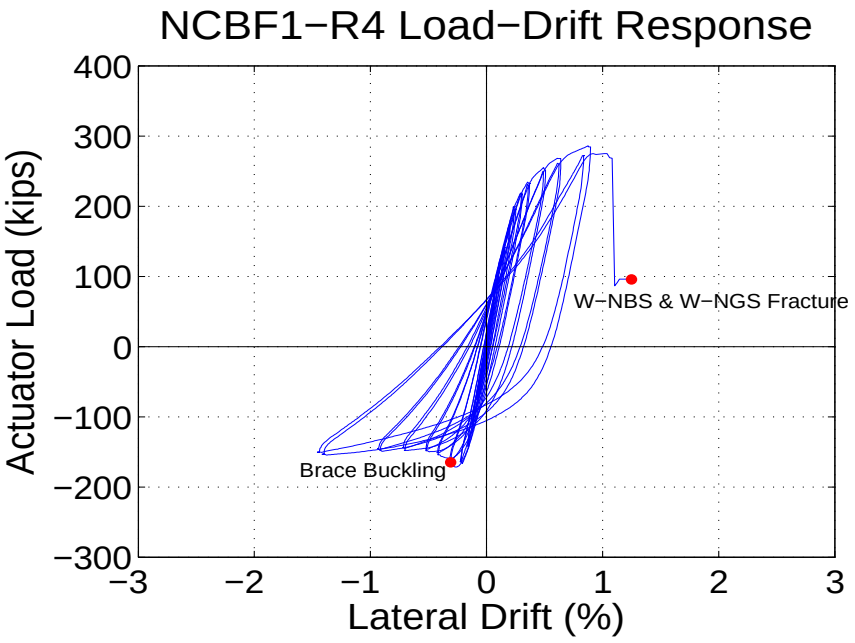

Figure 6.44 NCBF1-R4 Load-Drift History

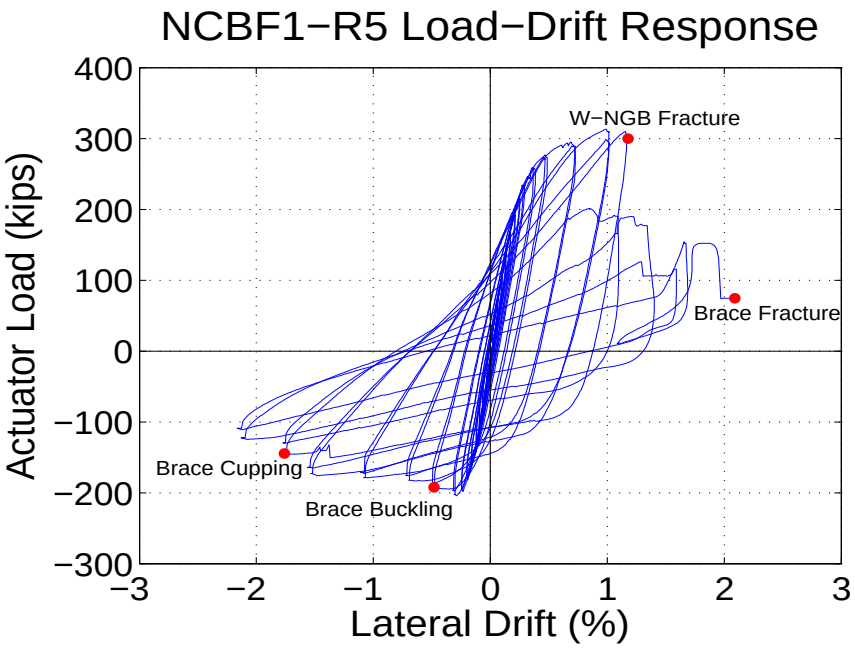

Figure 6.45 NCBF1-R5 Load-Drift History

From the load-drift history for each specimen, the peak values of each cycle were plotted to create a load-drift envelope, as shown in Figure 6.47. Also shown in Figure 6.47 are linear fits to the load-drift envelopes. Each fit is comprised of three line segments that estimate the envelope. These segments estimate behavior in the elastic drift range, the post-yield tensile drift range, and the post-buckling compressive drift range, as shown in Figure 6.46. Each of the three lines was fitted using a square root sum of squares best fit to the data points in that region of the load-drift envelope.

The intersection points of these lines are used to determine estimates of the yield and buckling displacement (Δ_y and Δ_c) and the yield and buckling load (R_y and R_c). The slopes of the lines are the elastic, post-yield, and post-buckling stiffnesses (K_e, K_y, and K_c). The computed values for each of the specimens are given Table 6.6.

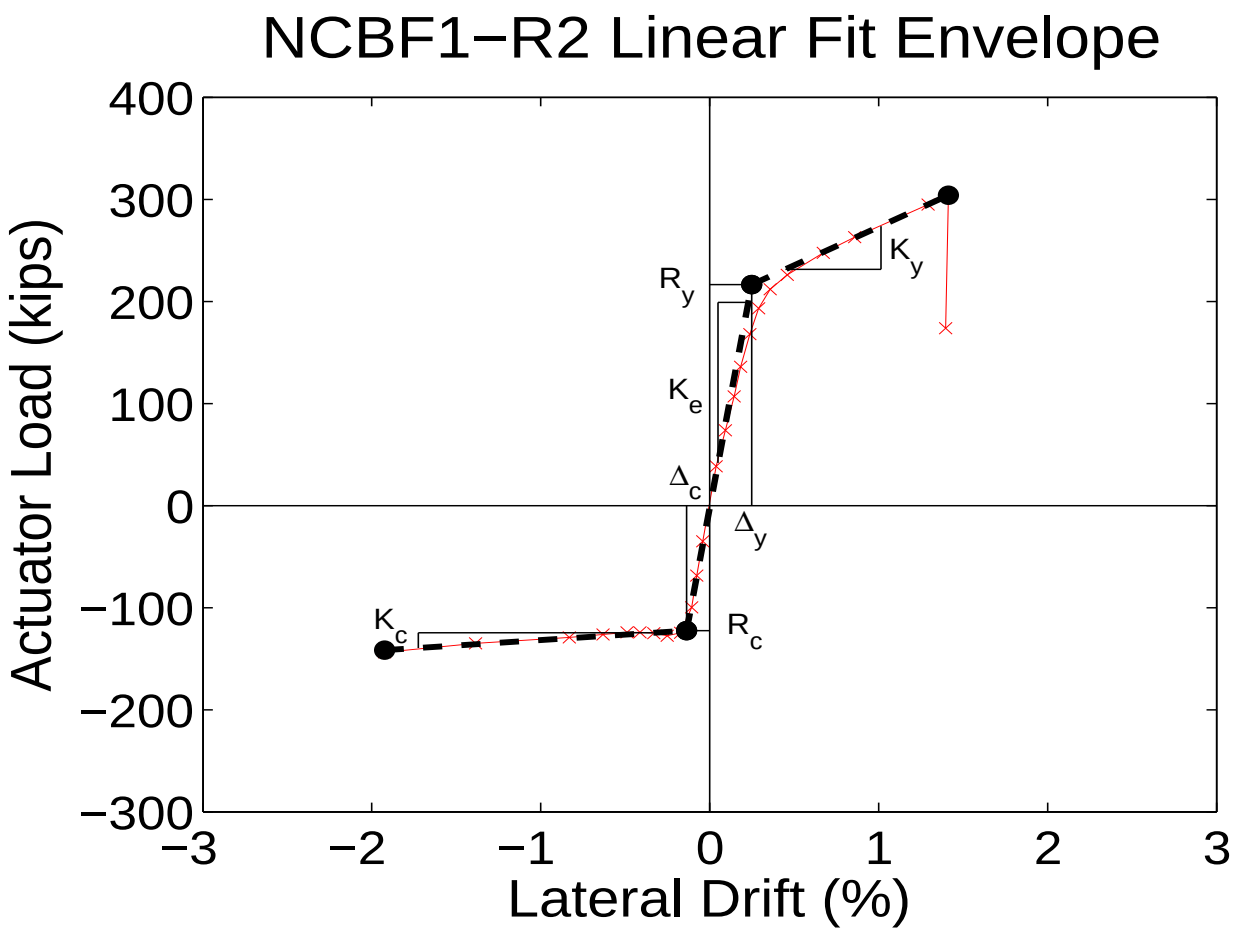

Figure 6.46 Quantities Derived from Envelope Linear Fit

Specimen	Load-Drift Envelope	Linear Fit to Load-Drift Envelope
NCBF1	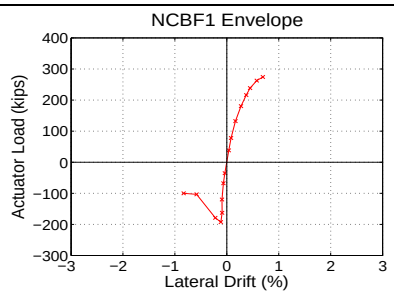	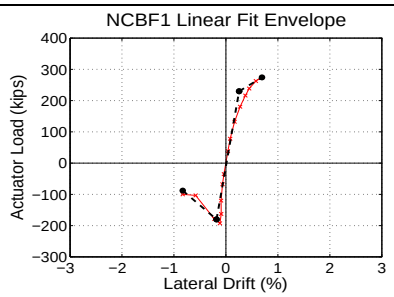
NCBF1-R2	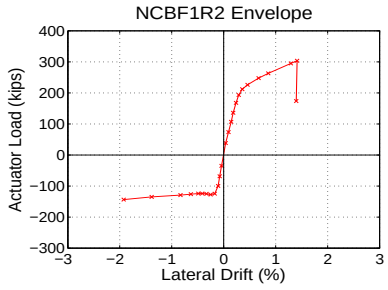	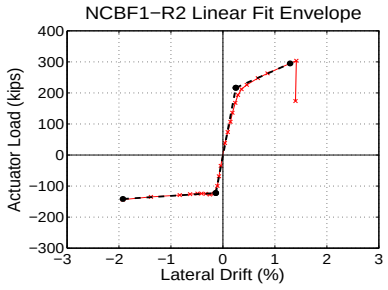
NCBF1-R3	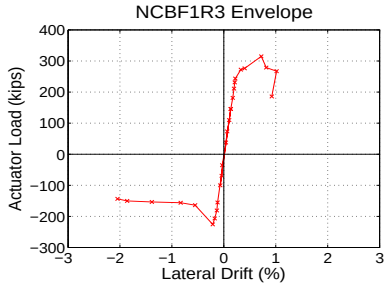	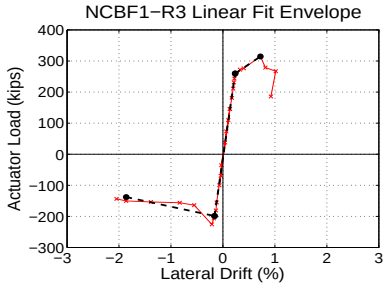
NCBF1-R4	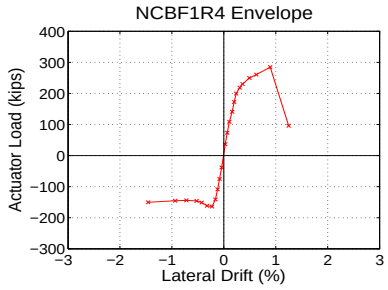	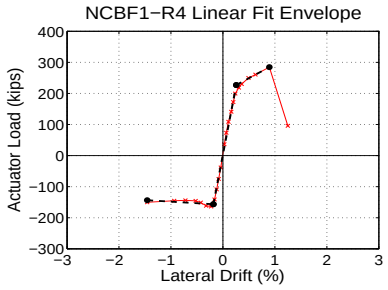
NCBF1-R5	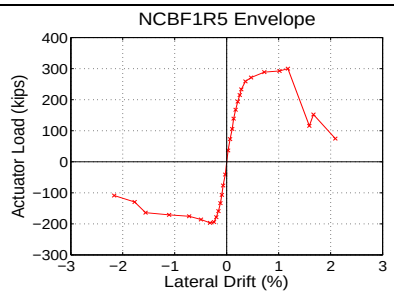	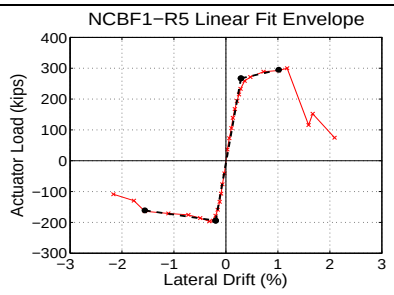

Figure 6.47 Load-Drift Envelopes and Linear Fits

Table 6.6 Frame Properties Derived from Linear Fits

Specimen	Elastic Stiffness (K/in)	Post-Yield Stiffness (K/in)	Post-Buckling Stiffness (K/in)	Yield Force (K)	Buckling Force (K)
NCBF1	657	70	-99	230	-180
NCBF1-R1	x	x	x	x	x
NCBF1-R2	611	37	3	228	-125
NCBF1-R3	802	78	-25	260	-199
NCBF1-R4	608	38	-7	241	-157
NCBF1-R5	655	27	-17	267	-194

Elastic stiffness was reasonably consistent for all specimens except NCBF1-R3. The higher stiffness of NCBF1-R3 may have been associated with the restraint of the brace midspan, which delayed buckling of the brace. Specimen NCBF1 had a large, negative post-buckling stiffness, which is an undesirable behavior for global performance, as it can lead to rapid system collapse. The retrofitted specimens utilized compact braces, which lose compressive strength less rapidly after buckling. As a result, their post-buckling stiffnesses are more stable, creating a system with less severe softening behavior. Post-yield stiffnesses were approximately 5%-10% of the elastic system stiffness, and the yield forces for all of the specimens fell within the 230-270 kip range.

6.4.2 Energy Dissipation

Energy dissipated by the frame is another valuable measure of system performance, as systems that dissipate large amount of energy are more capable of enduring seismic events. The energy dissipated by the frame can be computed by the area within the hysteretic loops of the load-drift response. Work done on the system by the actuator load can be computed using Equation (6.2-4).

$$W = \int_{a}^{b} F * d\Delta \tag{6.2-4}$$

The energy dissipated by the system over a complete cycle, or multiple complete cycles, is equal to the net work done by the applied load, because little or no elastic energy should remain in the system when it returns to its initial state. To compute the energy dissipation, or work, trapezoidal summation was used over the discrete displacement increments, per Equation (6.2-5).

$$W = \sum_{\mathrm{i}=1}^{\mathrm{n}} \frac{\mathrm{F}_i + F_{i-1}}{2} (\Delta_{\mathrm{i}} - \Delta_{\mathrm{i}-1}) \tag{6.2-5}$$

Figure 6.48 shows the cumulative energy dissipated versus total drift range for each of the specimens. The energy dissipated in each cycle typically increases as the test progresses. Cycles that reach larger displacements have more substantial inelastic action, which is the source of energy dissipation for the frame.

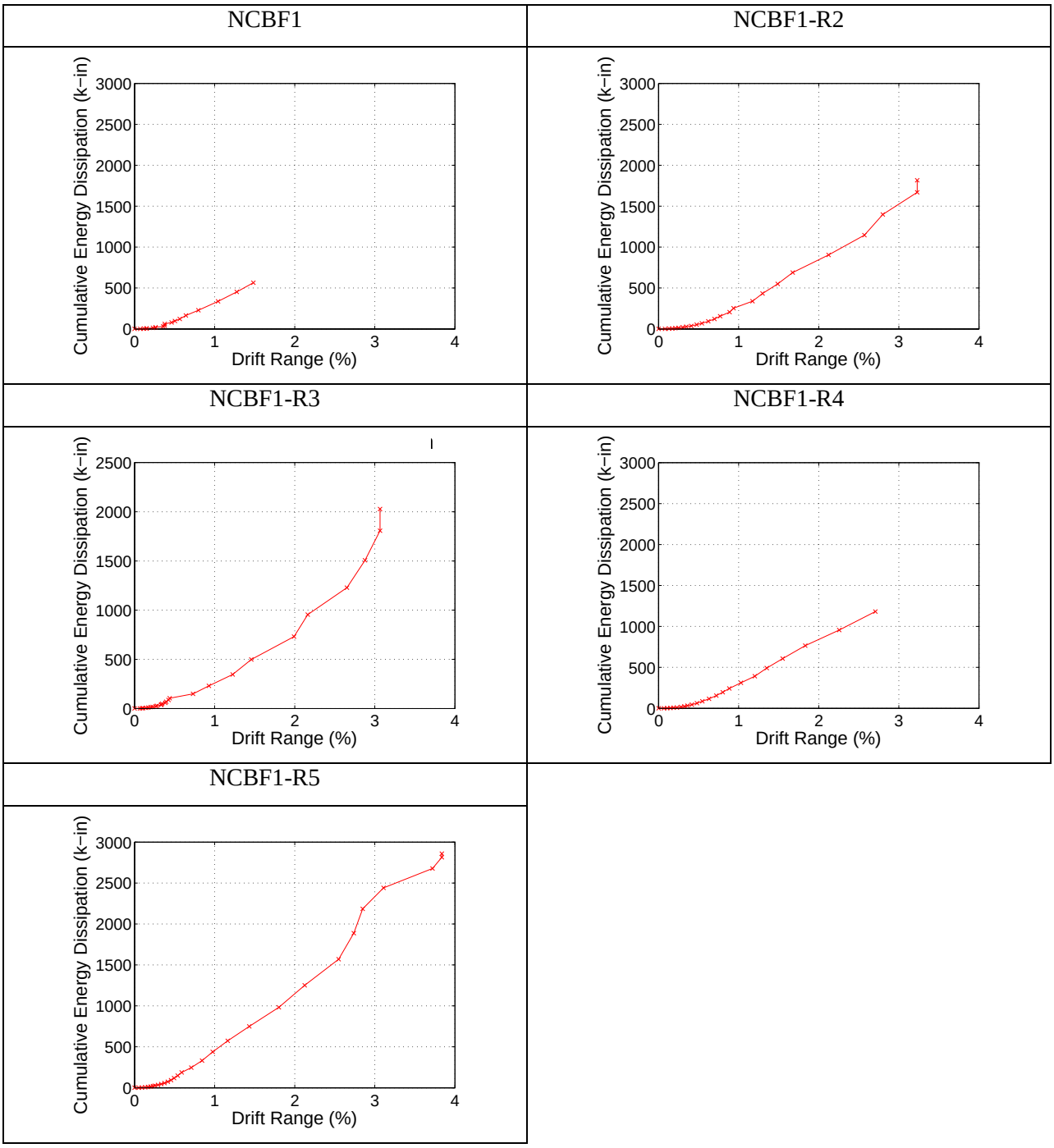

Figure 6.48 Cumulative Energy Dissipation

Figure 6.49 shows the cumulative energy dissipation for all of the specimens for comparison. The rate of energy dissipation is comparable for all tests except NCBF1-R5, which begins to dissipate energy more rapidly at the drift range associated with brace buckling. The primary source of this increased energy dissipation was the brace compressive capacity. NCBF1-R5 had one of the highest buckling loads of the

specimens tested, and it maintained most of its compressive resistance over subsequent cycles. This created a wider load-drift envelope and thus greater energy dissipation.

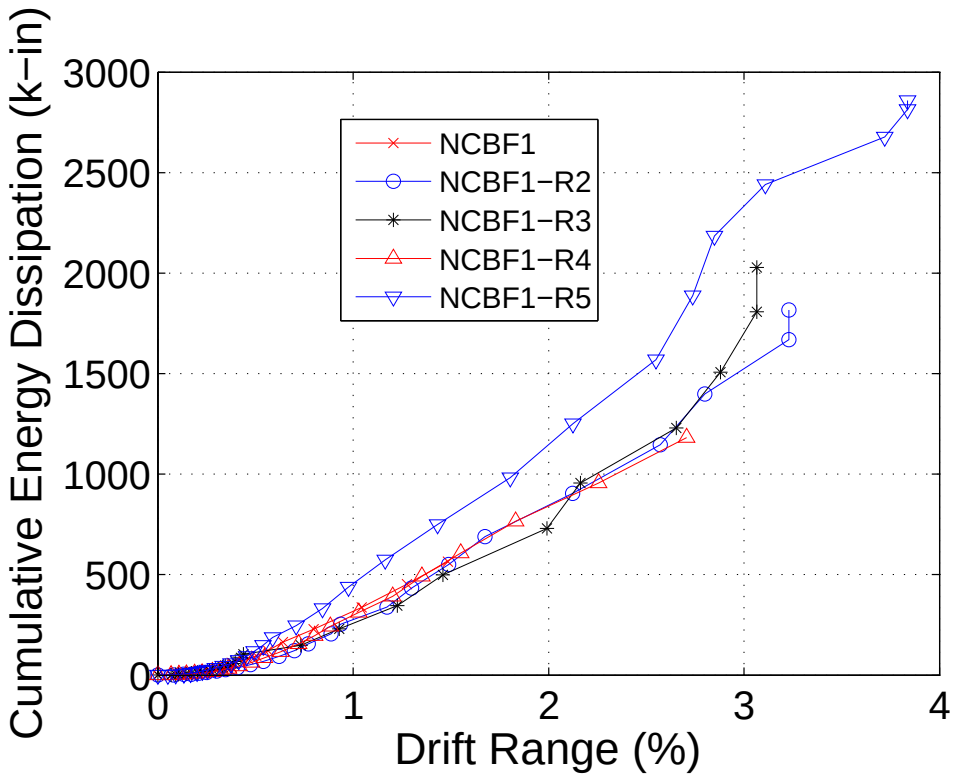

Figure 6.49 Cumulative Energy Dissipation - All Tests

6.4.3 Column Performance

Although the brace and gusset plate connections are the most critical aspects of the system performance, the behavior of the framing elements also contributes considerably to the overall system response. In an idealized braced frame, the connections act as perfect pins, so the beams and columns do not carry shear forces and bending moments. However, braced frame connections, particularly at the gusset plates, have a degree of flexural restraint, which causes the beams and columns to contribute to the lateral resistance of the system.

Figure 6.50 shows the process by which the shear forces and bending moments for the columns were calculated. Two sets of strain gauges were used to calculate the moment distribution and shear force for each column. The strain and stress were assumed to vary linearly over the cross section, which is a reasonable assumption for strains of this magnitude. Additionally, the shear force was assumed to be

constant between the connections, which is reasonable because no external force acts on the column in this region,

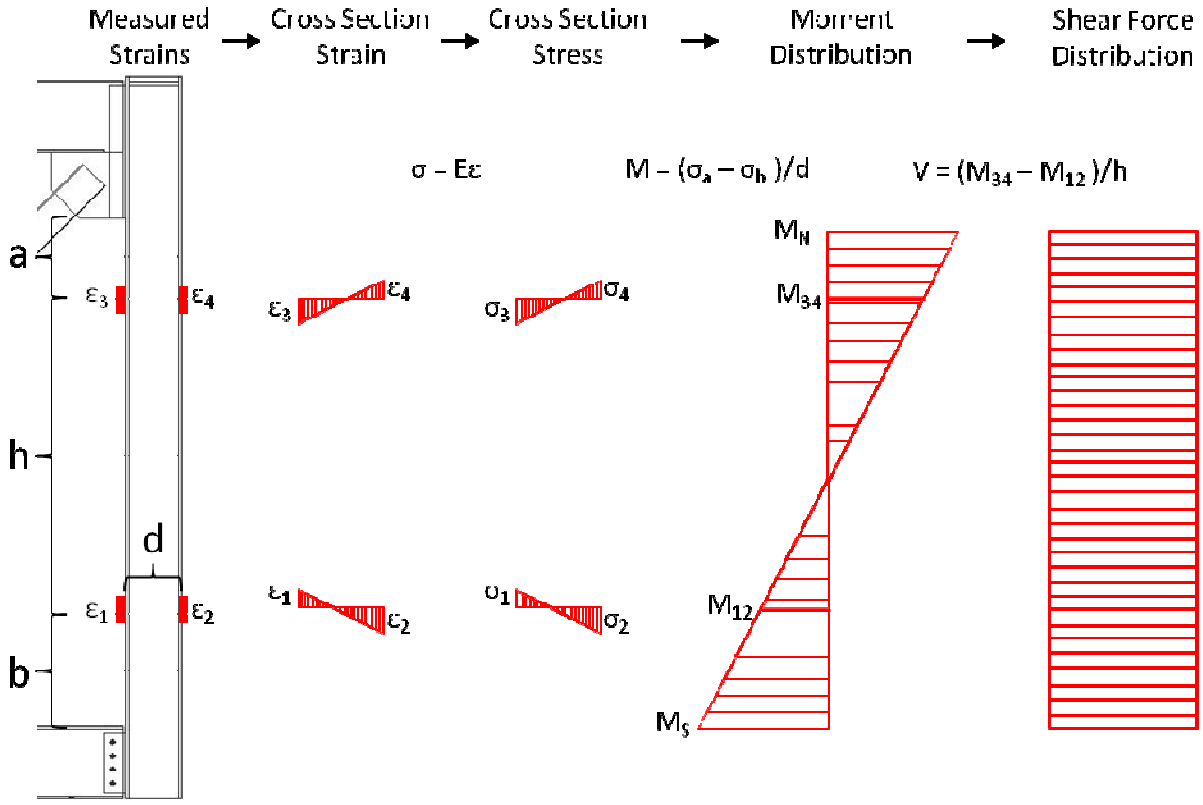

Figure 6.50 Computation of Column Shears and Moments

Unfortunately, strain gauge failures in a number of the specimens significantly limits the amount of data that can be derived for the columns. Column shears that were possible to compute are given in Figure 6.51. The shear force in the West column for NCBF1-R5 is higher than that for the East column. The likely cause of this is the additional restraint provided to the North end of the West column by the load beam. The rigidity of the load beam prevents the North end of the column from rotating, increasing restraint and thereby its force.

NCBF1 - East Column Shear	NCBF1-R3 West Column Shear Force
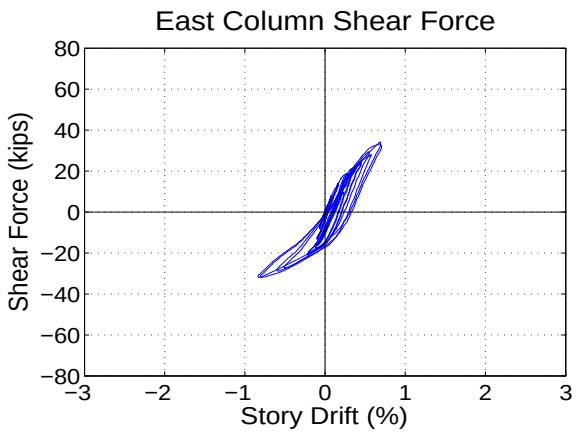	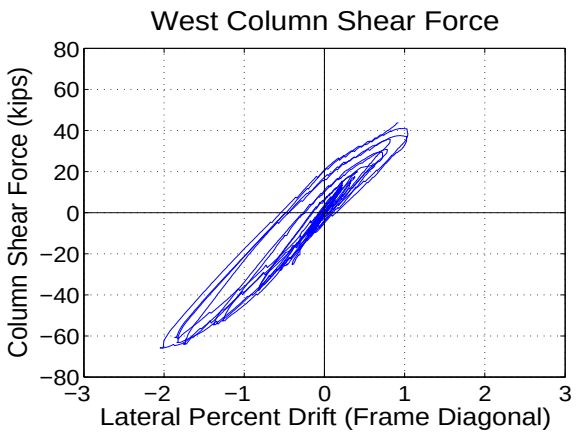
NCBF1-R5 East Column Shear Force	**NCBF1-R5 West Column Shear Force**
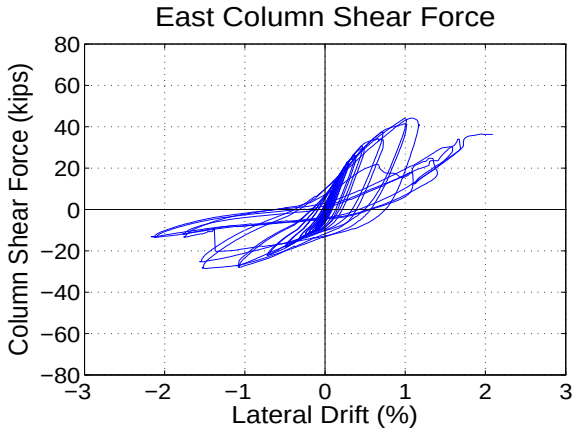	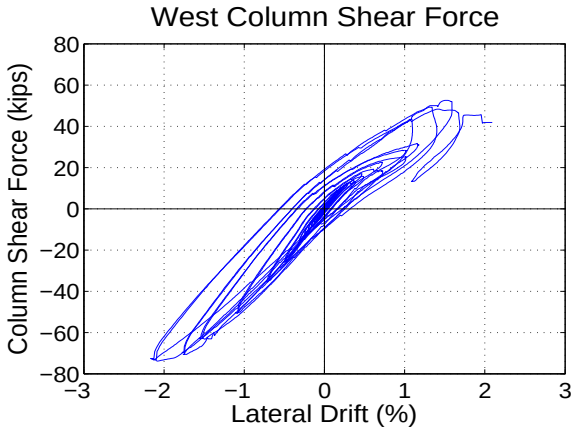

Figure 6.51 Column Shear Force

Since the bending moment is assumed to vary linearly along the height of the column, it is possible to compute the maximum flexural demands on the columns. The maximum flexural demand will occur at the edge of the connection at either end, because in the connection region, the connection contributes to the flexural strength of the column, thereby reducing stress. The moment at each of the two ends, labeled M_N and M_S in Figure 6.50, can be computed simply from a linear fit to the moments computed at the two strain gauge locations.

The computed moments are shown for the East Column in Figure 6.52 and for the West column in Figure 6.53. Moments for NCBF1 were small, which is reasonable given the small drift level that was reached. The East column of NCBF1-R5 underwent a substantial change in behavior at the North end at -1.5%

drift. This was a result of the fracture of the North gusset-beam weld. The fracture of this weld reduced the height of the beam-column connection by 50%, thereby substantially decreasing the end restraint. The column moment decreased to near 0 as a result of this change. This is also reflected in the East column shear force, which dropped significantly at the same point.

In both NCBF1-R3 and NCBF1-R5, the West column reached flexural demands near the plastic moment capacity of the section at the South connection. This was the location of the highest flexural demands of any of the calculated values. Observations from the tests showed that the most significant yielding in the columns occurred at this location, which is consistent. It is likely that the yield capacity of the steel exceeds the 50ksi design strength, meaning that the moment demand in the column is actually somewhat less than the plastic moment capacity.

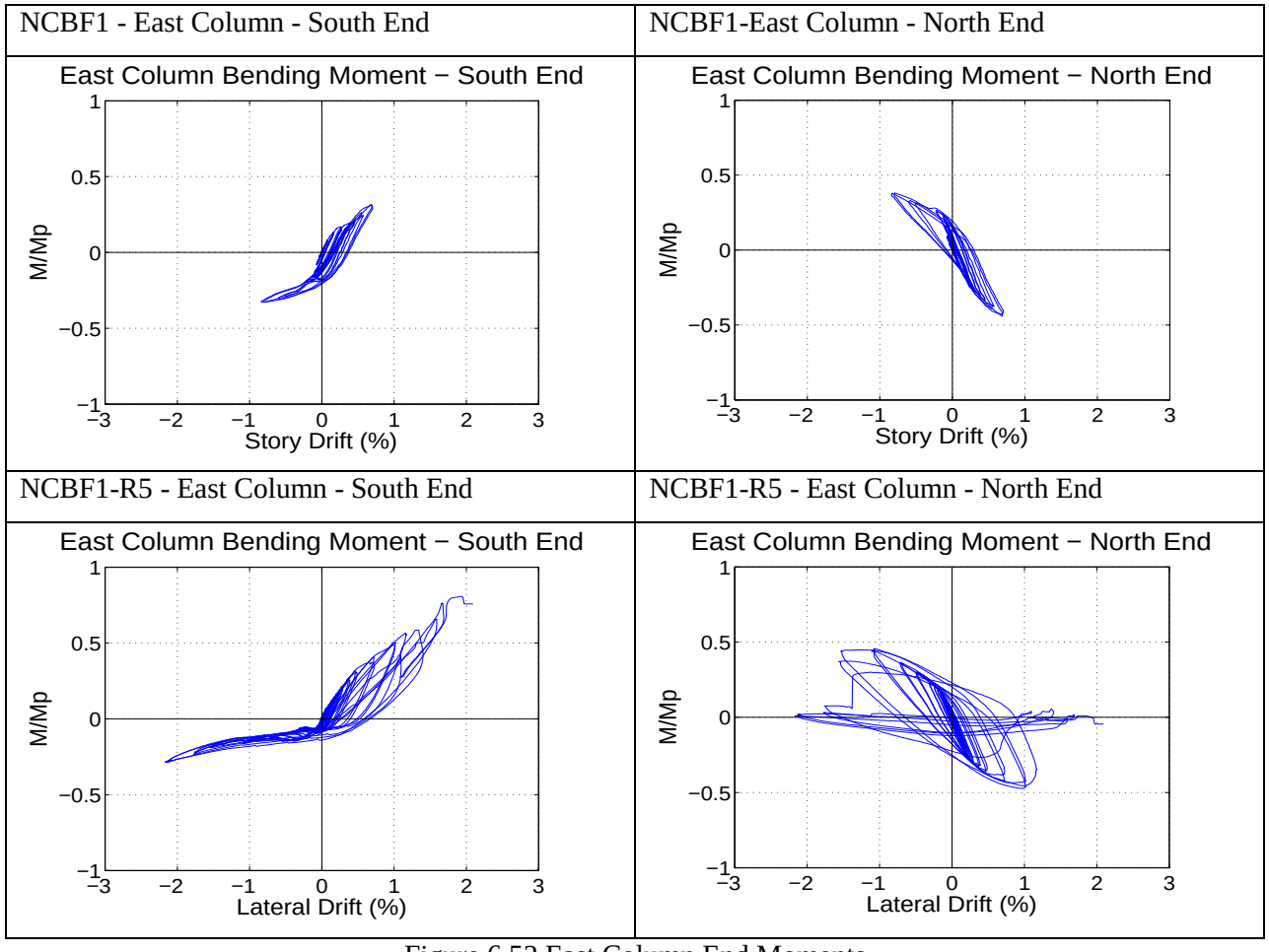

Figure 6.52 East Column End Moments

NCBF1-R3 - West Column - South End	NCBF1-R3 - West Column - North End
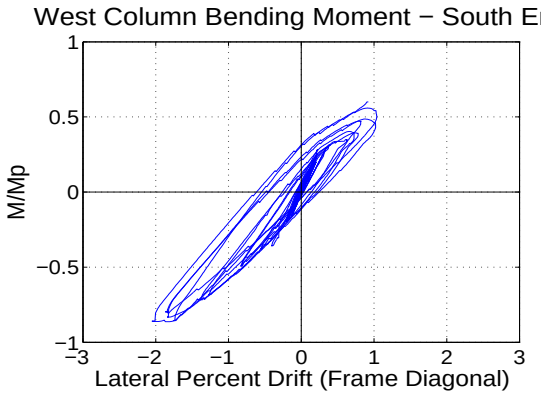	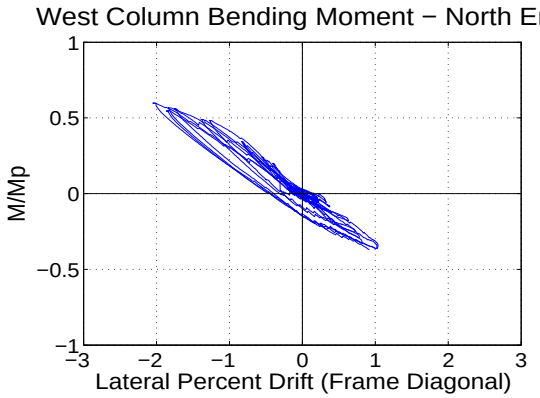
NCBF1-R5 - West Column - South End	NCBF1-R5 - West Column - North End
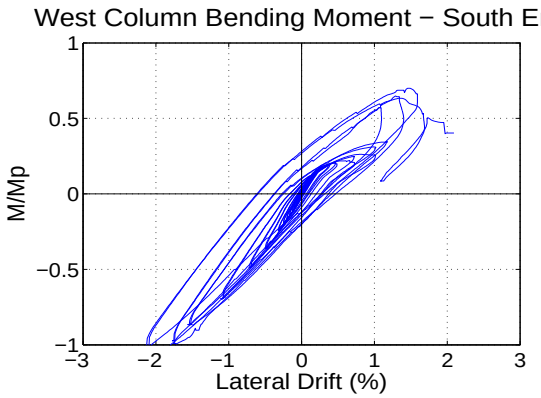	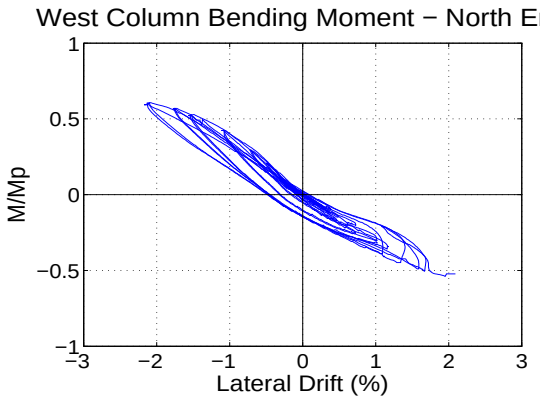

Figure 6.53 West Column End Moments

Chapter 7: Evaluation and Retrofit

7.1 Introduction

Seismic evaluation and Retrofit of existing structures in the US is typically accomplished using the procedures from ASCE 41. This document provides procedures for evaluating the capacity and expected seismic performance of existing structures. It also describes protocols for the retrofit of structures that are deemed deficient. This chapter builds on existing framework within ASCE 41 to provide procedures for the evaluation and retrofit of NCBFs based on the results presented in previous chapters. Section 7.2 describes the basis for the proposed evaluation procedure and its relation to the protocol from ASCE 41. Section 7.3 describes the results of this evaluation for each of the specimens tested. Section 7.4 summarizes these results and discusses the outcomes of the various retrofit procedures.

7.2 Evaluation Procedure

The current ASCE 41 procedure utilizes a component-based evaluation method. Components are described as either force-controlled or deformation controlled. The diagonal braces are the deformation-controlled elements within a braced frame system. They are expected to yield and to undergo substantial inelastic deformations. The other system components are force-controlled elements, which are required to withstand the demands placed on them by the deformation-controlled elements. Deformation-controlled elements are considered deficient if they are incapable if sustaining the required deformations or resisting the necessary seismic loads. Force-controlled elements are considered deficient if they are incapable of resisting the force demands placed on them by the deformation controlled elements.

Components that are not capable of resisting the necessary forces and deformations outlined in ASCE 41 must be retrofitted per modern governing design standards. Because none of the connections in the infrastructure review were capable of developing the brace capacity, they would likely require retrofit under the provisions of ASCE 41. For NCBF1, as well as the majority of the connections in the infrastructure review (Chapter 2), this would require the replacement of the brace, gusset plate, and potentially the beam-to-column connection. The retrofits tested in this experimental program were intended to demonstrate retrofit alternatives that substantially improve system performance without requiring extensive modifications to meet modern design standards. The emphasis of this chapter is on the categorization of the performance of the systems tested and the evaluation of the effectiveness of the tested retrofit procedures.

ASCE 41provides categorizes the performance of steel components with a backbone curve, which is shown in Figure 7.1. This curve describes the expected load-displacement or moment-rotation behavior of the component during a seismic event. The points A,B,C,D,E are defined by the specific properties of each component.

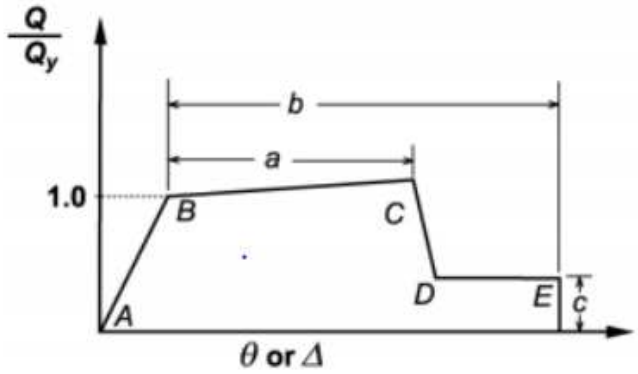

Figure 7.1 ASCE 41 Steel Component Backbone Curve

The results presented in the previous chapters of this thesis have demonstrated that there is substantial interdependency between the behavior of the brace, connections, and framing members. In light of this, the proposed NCBF evaluation procedure develops backbone curves at the subsystem level, rather than the component level. This allows the evaluation to more effectively capture these interdependencies, thus providing a more accurate and comprehensive prediction of system performance.

The subsystem tested was a single bay containing a single concentric diagonal brace. This system exhibits different behavior in the directions of brace tension and compression, which provides a challenge in establishing a backbone curve, which assumes symmetric system behavior. In order to achieve a symmetric response, a larger subsystem was analyzed. Because the behavior of single concentric braces is asymmetrical, structures typically have a mirrored brace in an adjacent bay, so that one brace will be in tension while the other is in compression, as shown in Figure 7.2. This subsystem has symmetric load-displacement behavior, making it a more viable candidate for developing backbone curves.

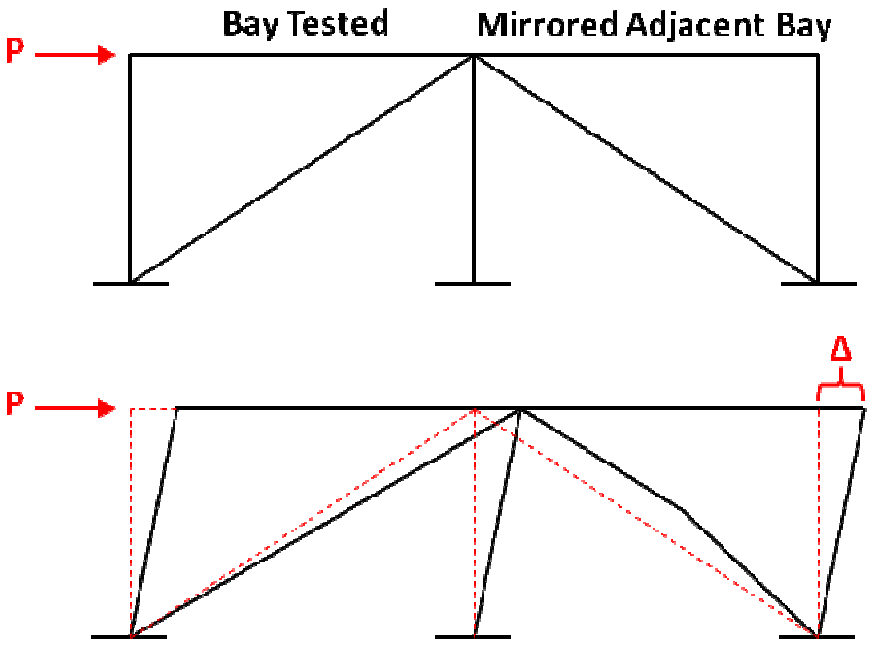

Figure 7.2 Two Bay Braced Frame Subassembly

To estimate the behavior of this two-bay subsystem, the tensile and compressive load-drift behavior of each specimen was superimposed to create a single curve. In an idealized case, this can be accomplished by the following procedure. For each displacement, the corresponding lateral resistance can be found for the tensile portion of the load-drift envelope, shown in Figure 7.3, and for the compressive portion of the load-drift envelope, shown in Figure 7.4. The difference between these two resistances, P_t and P_c, is the expected lateral resistance of the sub-assembly for the prescribed displacement, as shown in Figure 7.5. By applying this summation for each displacement increment, a complete load-drift envelope for the subsystem can be created. In order to achieve this, the tensile and compressive portions of the original load-drift envelope must have equal displacement increments, which is difficult to achieve experimentally.

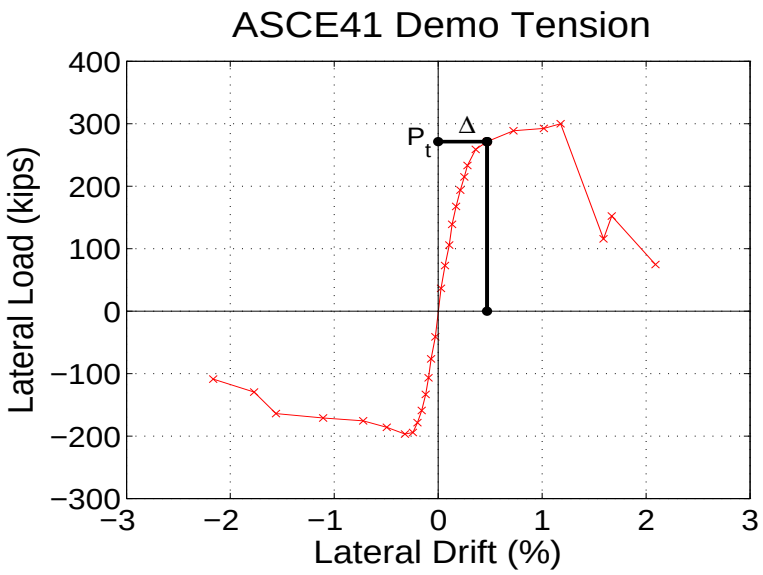

Figure 7.3 Tension Brace Lateral Load at Prescribed Displacement

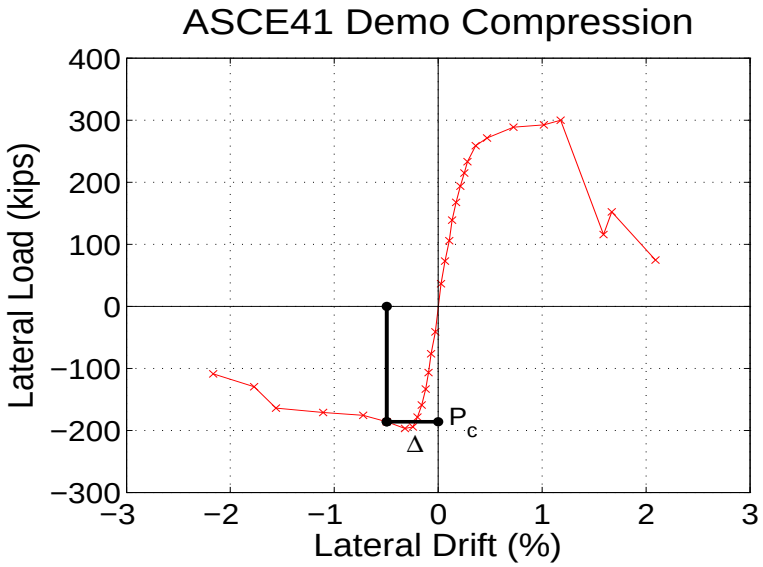

Figure 7.4 Compression Brace Lateral Load at Prescribed Displacement

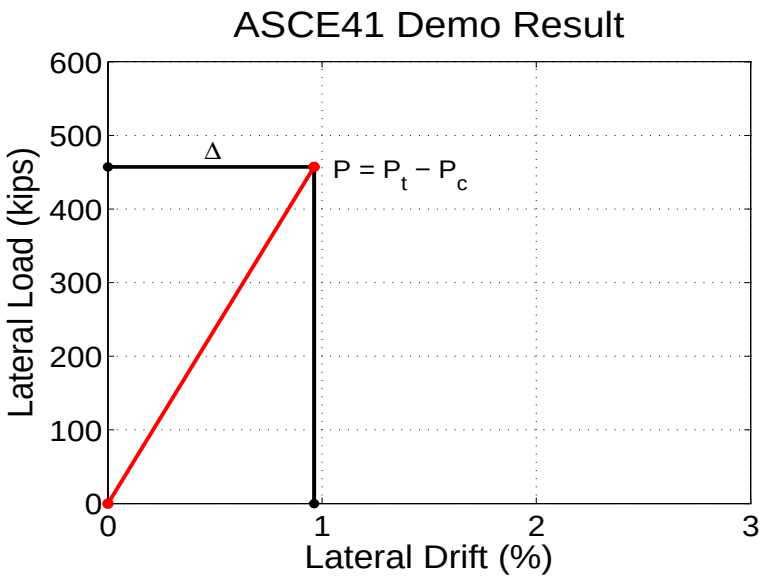

Figure 7.5 Sample Computation of a Point on Subsystem Load-Drift Curve

In order to create a single envelope curve from experimental data, a modified version of the above approach was necssary. Due to slip of components in the experimental setup, the drift values achieved at the tensile and compressive drifts for a given cycle were typically different, sometimes dramatically. Figure 7.6 demonstrates this asymmetry, as compressive drifts reach 2%, while tensile drifts only reach 1.4%. This makes it impossible to construct some portions of the combined load-drift curve, because for some displacements, there may be no corresponding data in one direction to match the data for opposing direction.

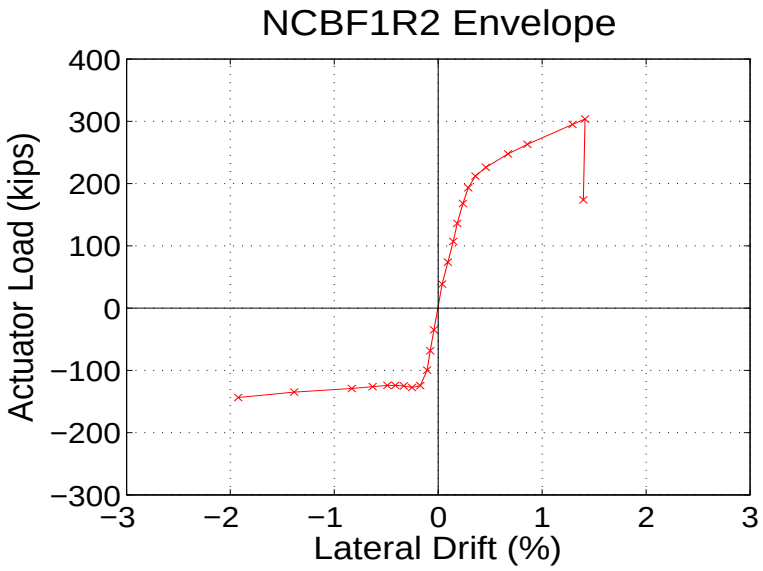

Figure 7.6 Asymmetric Experimental Load-Drift History (NCBF1-R2)

To address this issue, displacement values were computed from the difference between successive tensile and compressive peaks, as shown in Figure 7.7. Because the positive and negative displacements were not always of the same magnitude, the average of the magnitudes was used as the assumed lateral displacement for the two-bay subsystem.

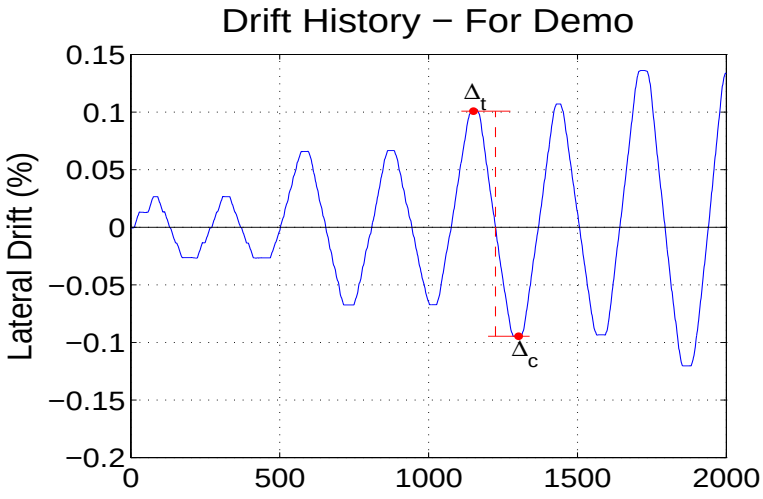

Figure 7.7 Experimental Displacements at Successive Peaks

The corresponding lateral load was computed as the sum of the magnitudes of the tension and compression resistances at the given displacement peaks, as shown in Figure 7.8. The average drift and total load at each cycle constitute a point on the combined load-drift envelope, as shown in Figure 7.9. Computing the averaged displacement and combined load for each successive cycle provides a complete load-displacement curve for the combined subsystem, as shown in Figure 7.10. This figure also shows the contributions to the total lateral resistance from the compressive brace and the tensile brace. All of the load curves are plotted against the averaged displacement estimate.

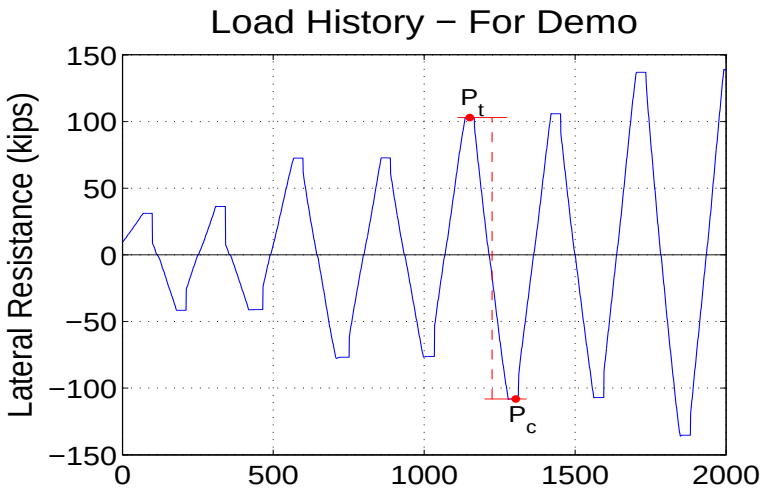

Figure 7.8 Experimental Loads at Successive Peaks

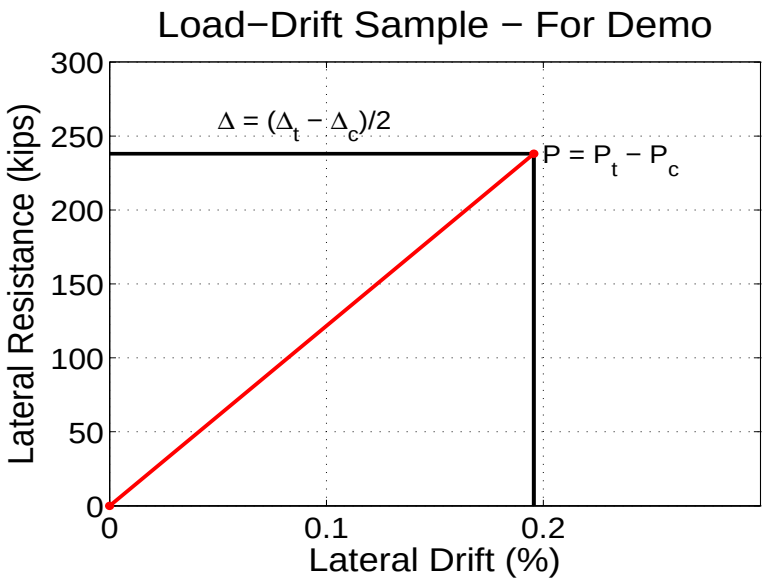

Figure 7.9 Sample Computation of a Point on Subsystem Load-Drift Curve

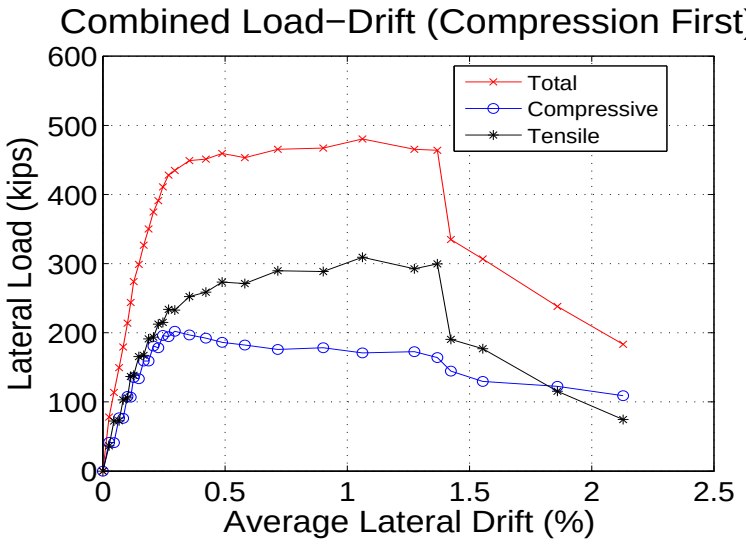

Figure 7.10 Load-Drift Curve for Two Bay Subsystem

Once the load-drift curve for the subsystem was created, the points for the backbone curve was fitted. The curve consists of five points, which are described in Table 7.1. In some cases, specimens progressed through multiple points simultaneously, as is the case for sudden failures.

Table 7.1 Key Points for ASCE 41 Backbone Curve

Point	Name	Description
A	Initial Resting State	Zero Load and Zero Displacement
B	Yield	Substantial Decrease in Stiffness - Typically Corresponds to Brace Buckling
C	Loss-of-Strength	Substantial Negative Stiffness - Typically Corresponds to Tearing of Brace or Fracture of Connection Components
D	Loss of Brace Strength	Complete Brace or Connection Fracture - Moment Frame Action Only Beyond this Point
E	Ultimate Failure	Fracture of Beam-to-Column Connection - Potential System Collapse

7.3 Results

Backbone curves are presented in this section in both normalized and standard formats. For the normalized curves, the displacement was normalized to the yield displacement Δ_y (point B on the backbone curve). The force was normalized to the expected lateral load capacity of the subsystem, P_y, as calculated from Equation (7.3-1), where P_t is the brace expected yield capacity and P_c is the brace expected compressive capacity, as calculated in Chapter 2.

$$P_y = \frac{P_t + P_c}{\sqrt{2}} \tag{7.3-1}$$

Table 7.2 gives the DCRs for each of the specimens tested for reference.

Table 7.2 Specimen DCRs

Limit State	NCBF1	NCBF1-R1	NCBF1-R2	NCBF1-R3	NCBF1-R4	NCBF1-R5
Brace Net Section Fracture	1.26	1.15	1.15	1.21	1.16	1.26
Brace-Gusset Plate Weld Fracture	0.92	0.92	0.92	0.92	0.92	0.92
Brace Block Shear	1.14	0.76	0.76	0.76	0.76	1.14
Gusset Plate Block Shear	1.16	1.33	1.33	1.22	1.78	1.16
Gusset Plate Whitmore Yielding	1.33	1.50	1.50	1.28	1.89	1.33
Gusset Plate Buckling	0.74	0.84	0.84	0.70	1.03	0.74
Gusset Plate Shear Yielding at Beam	1.16	1.16	1.16	1.16	1.16	1.16
Beam-Gusset Weld Fracture	1.55	1.55	1.55	1.55	1.55	1.55
Shear Tab to Gusset/Beam Weld Fracture	1.08	1.08	1.08	1.08	1.08	1.08
Shear Tab to Column Weld Fracture	0.65	0.65	0.65	0.65	0.65	0.65
Brace Width-to-Thickness Ratio	2.00	0.84	0.84	0.84	1.00	2.00

The behavior of NCBF1, the unretrofitted braced frame, is shown in the backbone curve in Figure 7.11 and normalized backbone curve in Figure 7.12. These figures demonstrate the effect of the non-compact brace on the system performance. NCBF1 had a negative post-yield stiffness due to the rapid loss of brace compressive strength after buckling.. Additionally, brace fracture occurred at less than $3\Delta_y$, which indicates that the system has very post-yield deformation capacity, in addition to the softening post-yield behavior. It is also notable that the frame achieved only 80% of the design lateral load resistance prior to yielding. In part, this results from brace buckling occurring at a smaller drift level than brace yielding. This was typical of most of the specimens tested, as shown throughout in this section.

Despite substantial strength deficiencies in the connections, almost no connection damage was observed prior to brace fracture. Because the connections were largely intact after brace fracture, some very small post-fracture cycles were completed. The dashed line with the arrow on the backbone curves indicates the

probable direction of the post-brace fracture behavior of the frame based on the post-brace fracture resistance of the frame.

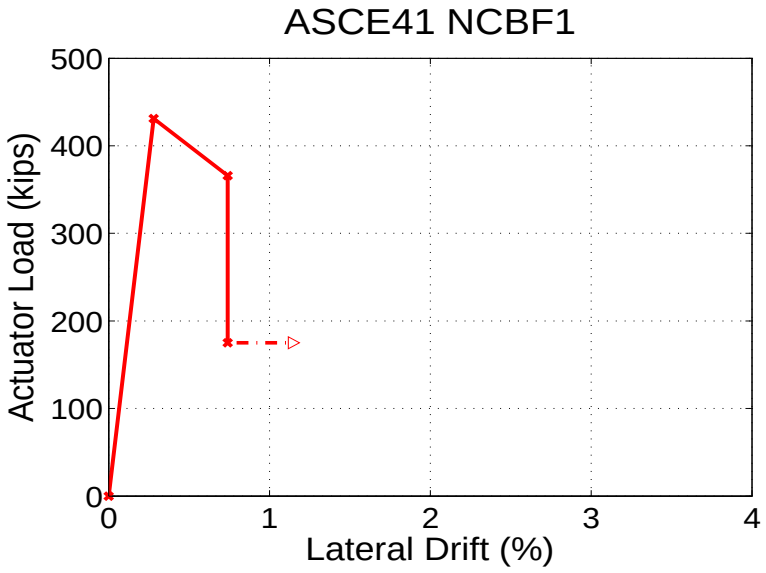

Figure 7.11 Backbone Curve - NCBF1

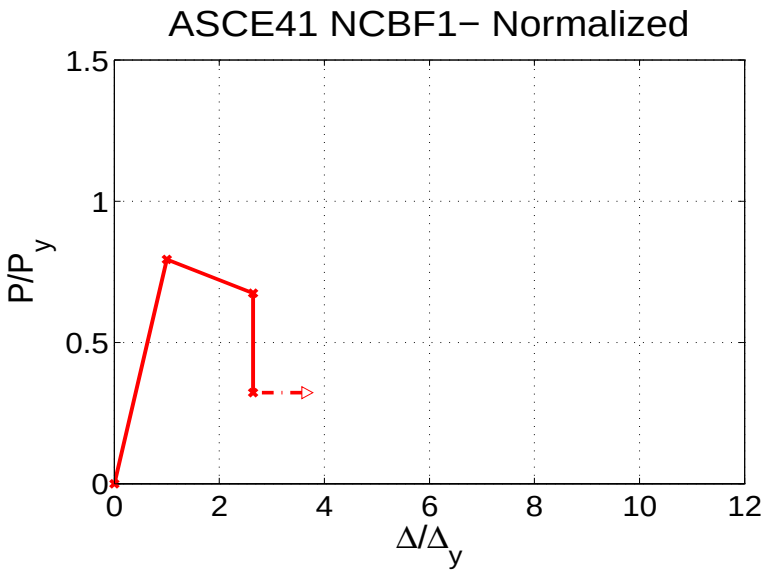

Figure 7.12 Normalized Backbone Curve - NCBF1

NCBF1-R2 replaced the non-compact brace used in NCBF1 with a compact section with similar cross-sectional area. The backbones for the two specimens are compared normalized in Figure 7.13 and non-normalized in Figure 7.14. Unlike NCBF1, NCBF1-R2 exhibited a positive post-yield stiffness, which is

desirable because the system continues to gain strength as it deforms inelastically. NCBF1-R2 was able to reach deformations of $5\Delta_y$ before the system began to lose strength. This is a substantial improvement over NCBF1 resulting from the use of a compact brace instead of a non-compact one.

However, NCBF1-R2 suffered a rapid failure at a displacement of $6\Delta_y$. Improving the brace performance caused concentration of damage in the connections, which failed suddenly as a result of the deficiency of the shear tab weld. This is undesirable behavior, as the beam-to-column and brace-to-frame connections failed simultaneously, potentially resulting in a partial system collapse.

NCBF1-R2 had a smaller design lateral load than NCBF1 because NCBF1-R2 used a compact brace, which had a lower buckling capacity. NCBF1-R1 achieved only 75% of its design strength at yield. However, it achieved nearly the full design strength prior to failure, unlike NCBF1, which achieved only 80% of its design strength. Using a compact brace theoretically results in a loss of lateral load capacity, but these plots show that the improvement in post-buckling brace strength and system ductility actually results in a slight net gain of lateral load capacity.

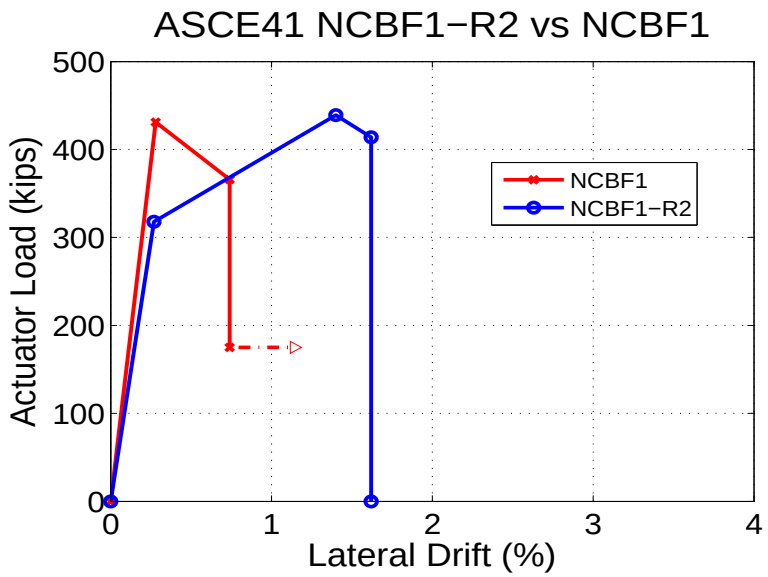

Figure 7.13 Normalized Backbone Curves - NCBF1 and NCBF1-R2

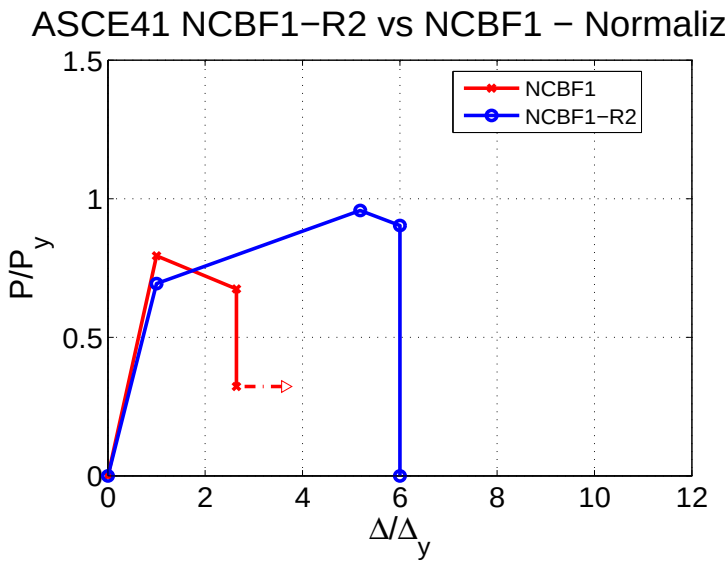

Figure 7.14 Backbone Curves - NCBF1 and NCBF1-R2

NCBF1-R3 utilized an in-plane brace buckling retrofit using the same brace shape as NCBF1-R2. The behavior of NCBF1-R3 is compared with NCBF1 in Figure 7.15 and Figure 7.16. The behavior of NCBF1-R3 was influenced by the restraint of the brace mid-span against downward buckling. This resulted in an unusually high buckling capacity and a negative post-yield stiffness. The influences of these factors makes it difficult to draw valuable information about the performance from the backbone curves. NCBF1-R3, like NCBF1-R2, suffered a sudden connection fracture which disconnected the beam from the column, which could lead to a partial collapse in a structure. This failure further emphasized the vulnerability of the deficient welds in the connections.

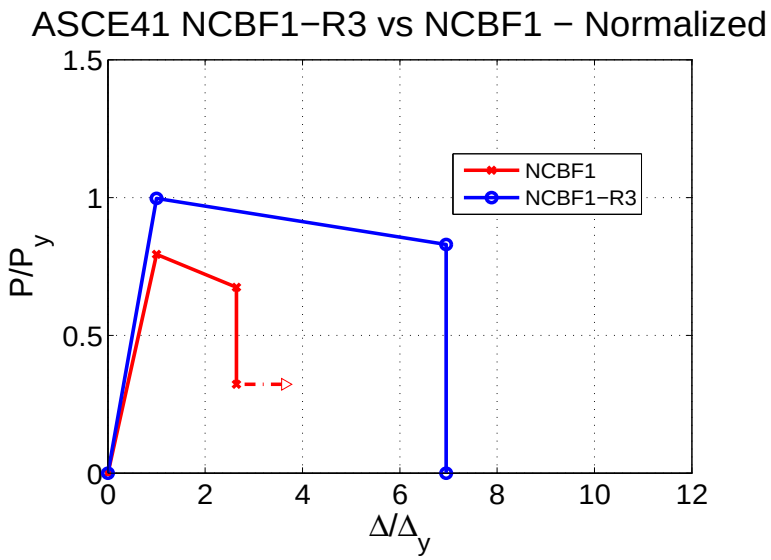

Figure 7.15 Normalized Backbone Curves - NCBF1 and NCBF1-R3

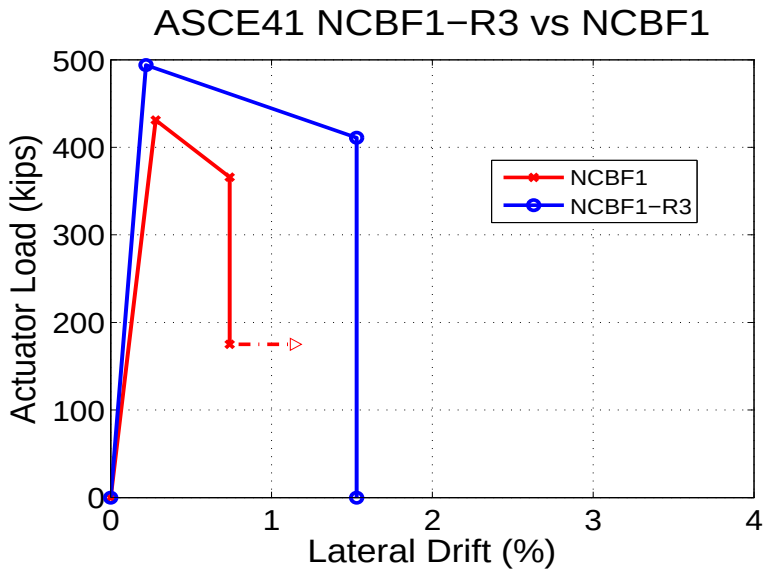

Figure 7.16 Backbone Curves - NCBF1 and NCBF1-R3

NCBF1-R4 also utilized an in-plane brace buckling retrofit but used a rectangular, rather than square, brace cross section. The behavior is compared with NCBF1 in Figure 7.17 and Figure 7.18. NCBF1-R4 exhibited positive stiffness after yielding until a displacement of $5\Delta_y$.However, after this point, the system suffered a sudden failure of the beam-column connection, again showing that the deficiency of the shear tab weld was critical to performance.

Like previous retrofits, NCBF1-R4 improved the post-yield drift range and stiffness of the system, but it suffered a less desirable failure. NCBF1-R4 achieved 80% of its expected capacity prior to yielding, similar to NCBF1. However, like NCBF1-R2, NCBF1-R4 achieved close to the full expected capacity after yield, while NCBF1 did not, as shown in Figure 7.18.

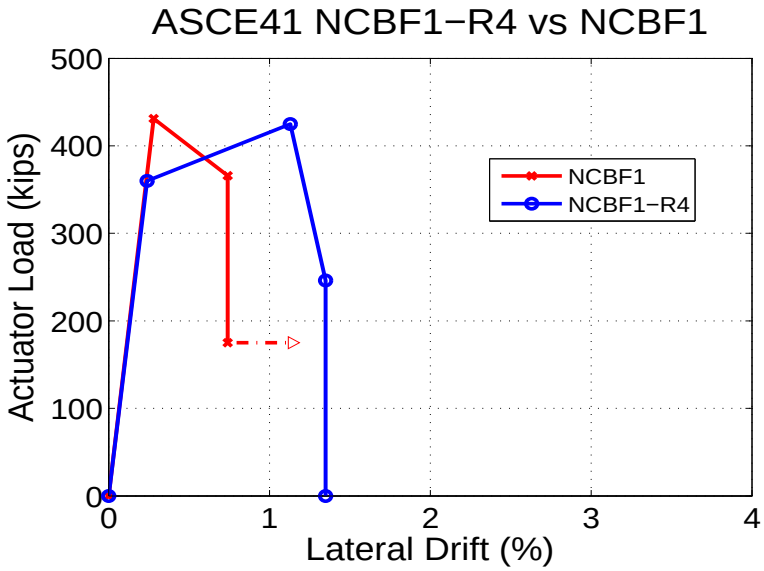

Figure 7.17 Normalized Backbone Curves - NCBF1 and NCBF1-R4

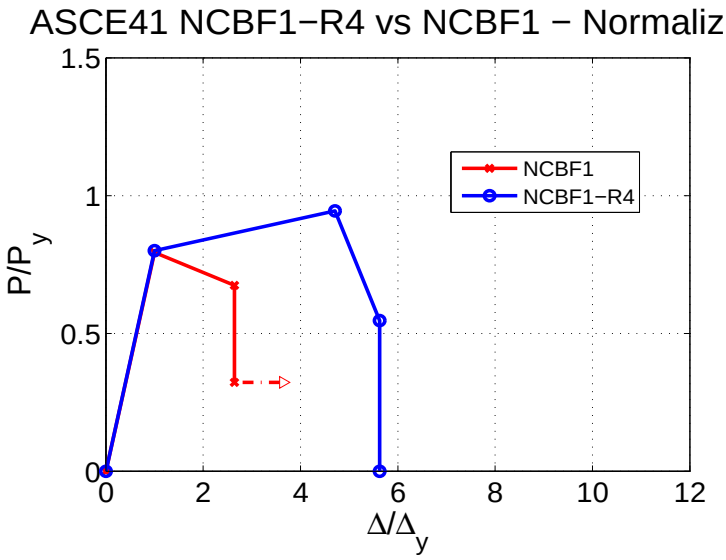

Figure 7.18 Backbone Curves - NCBF1 and NCBF1-R4

NCBF1-R5 retrofitted NCBF1 by filling the non-compact brace with concrete and adding bolts to reinforce the shear tab connection. The behavior of NCBF1-R5 and NCBF1 are compared in Figure 7.19 and Figure 7.20. NCBF1-R5 did achieve a positive post-yield stiffness and reached a displacement of $5\Delta_y$ prior to fracture of the North gusset-beam weld. NCBF1-R5 the same expected lateral load capacity as NCBF1, and attained a similar yield load. However, NCBF1-R5 had a positive post-yield stiffness, so it attained 85% of the expected strength prior to gusset-to-beam weld fracture, whereas NCBF1 began to lose strength after yield. NCBF1-R5 system then had negative stiffness until a displacement of $8\Delta_y$, when brace fracture occurred. Unlike previous retrofits, NCBF1 did not suffer a complete connection failure. This was likely due to the bolt reinforcement to the shear tab weld, which extended the connection life, even after fracture of the deficient gusset-to-beam weld.

After brace fracture, monotonically increasing cyclic displacement was applied to the specimen to evaluate the residual lateral load capacity of the frame. The lateral load resistance of the frame was consistent across a large range of displacement cycles. The test was terminated when the frame was at a total displacement range of $12.5\Delta_y$, although failure of the beam-column connections had not occurred and did not appear to be imminent. The post fracture behavior for NCBF1-R5 is signified with the dashed line and arrow on the figures below.

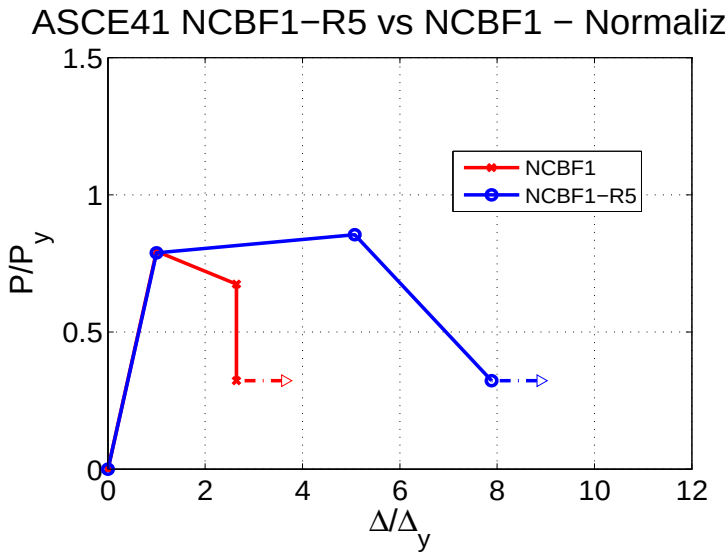

Figure 7.19 Normalized Backbone Curves - NCBF1 and NCBF1-R5

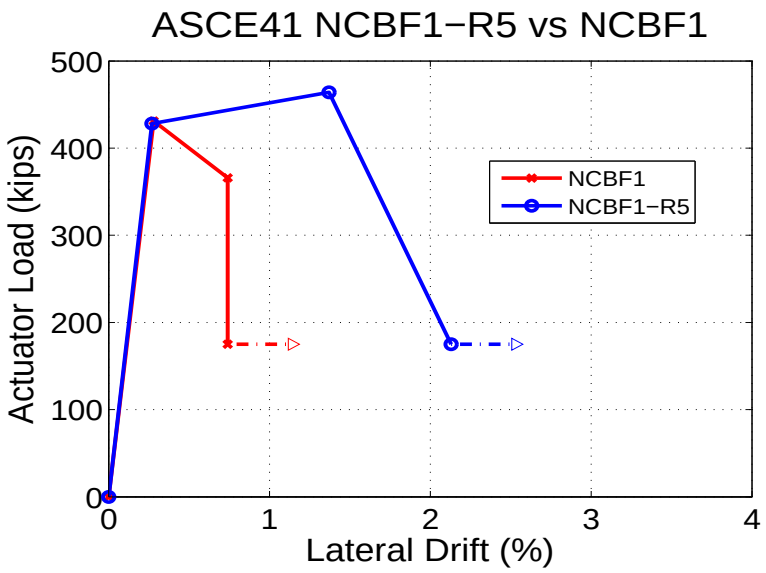

Figure 7.20 Backbone Curves - NCBF1 and NCBF1-R5

In addition to the six specimens tested for this thesis, backbone curves were constructed for two previous UW tests. Figure 7.21 and Figure 7.22 show NCBF0 and HSS08 alongside NCBF1. NCBF0 was a prototype NCBF test, as described in Chapter 2. It had a bolted double angle gusset-beam connection and suffered fracture of the brace-gusset weld at a very low drift level. Prying of the angles did allow the frame to reach large displacements after brace fracture. Like NCBF1, NCBF0 attained less than 1% drift prior to failure, further demonstrating the inadequacy of NCBF performance.

By contrast, HSS08, a typical SCBF designed to modern standards, has a positive post-yield stiffness and achieved a large displacement before brace failure. A connection detail for HSS08 is shown in Figure 7.23. The contrast between the behavior of HSS08 and the two NCBF specimens demonstrates the effectiveness of SCBF design requirements at ensuring ductile system performance, while simultaneously highlighting the vulnerability of NCBFs.

It is also notable that all three specimens achieved approximately 80% of their design lateral load capacity at yield. This consistency between NCBFs and SCBFs is informative, because it indicates that the frames behave similarly prior to brace buckling. However, the post-yield performance of the systems differs substantially.

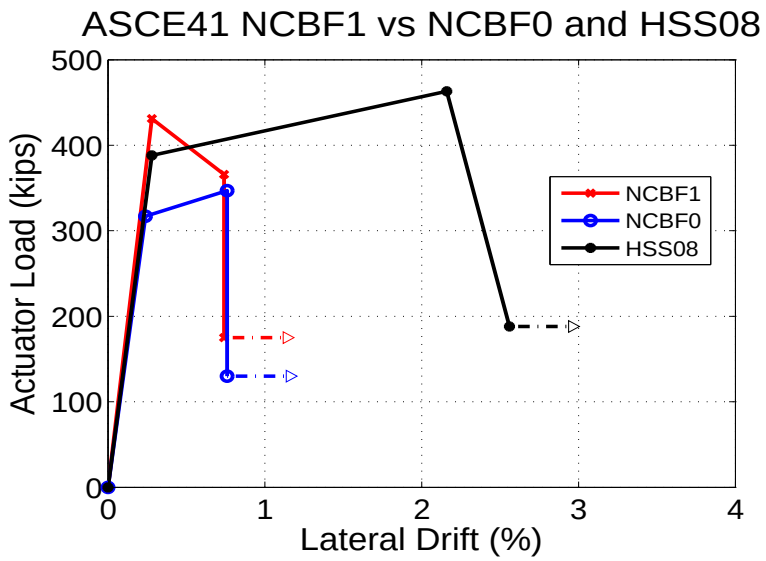

Figure 7.21 Backbone Curves - Comparison of NCBF and SCBF

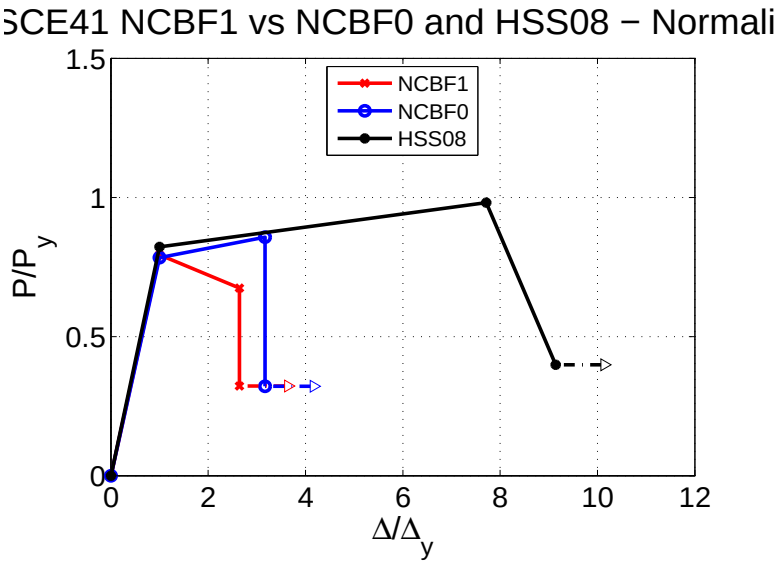

Figure 7.22 Normalized Backbone Curves - Comparison of NCBF and SCBF

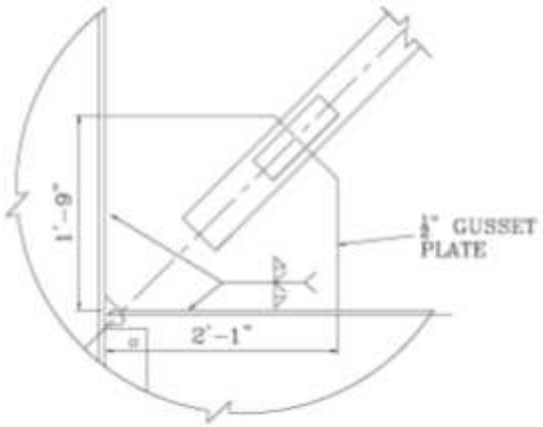

Figure 7.23 HSS08 Connection Detail

Figure 7.24 and Figure 7.25 compare NCBF1-R5, the most successful retrofit of NCBF1, with HSS08. NCBF1-R5 exhibits clear improvements in performance over NCBF1, and mirrors the behavior of HSS08 to a certain extent. Both specimens have positive post-yield stiffness and achieved large deformations before loss of strength occurred. These plots demonstrate the effectiveness of the bolt reinforcement and concrete fill used to address the shear tab weld and brace compactness deficiencies of NCBF1. While NCBF1-R5 falls short of SCBF performance, it represents a substantial improvement.

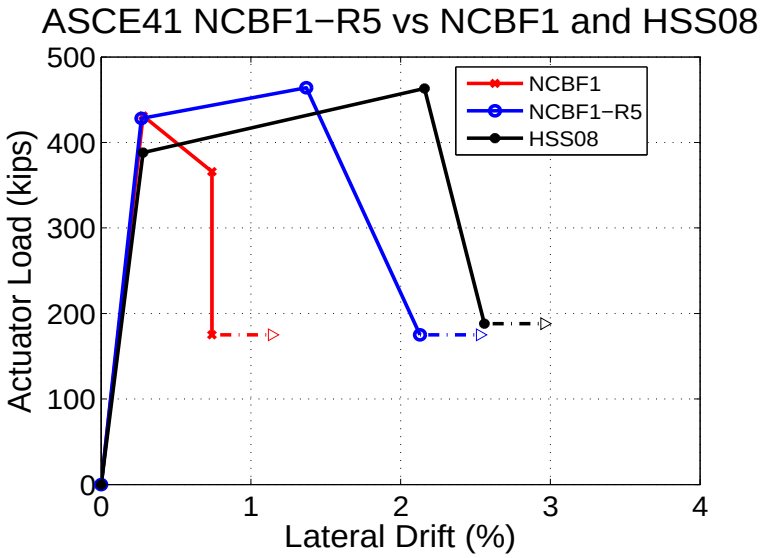

Figure 7.24 Backbone Curves - Comparison of NCBF1-R5 to SCBF

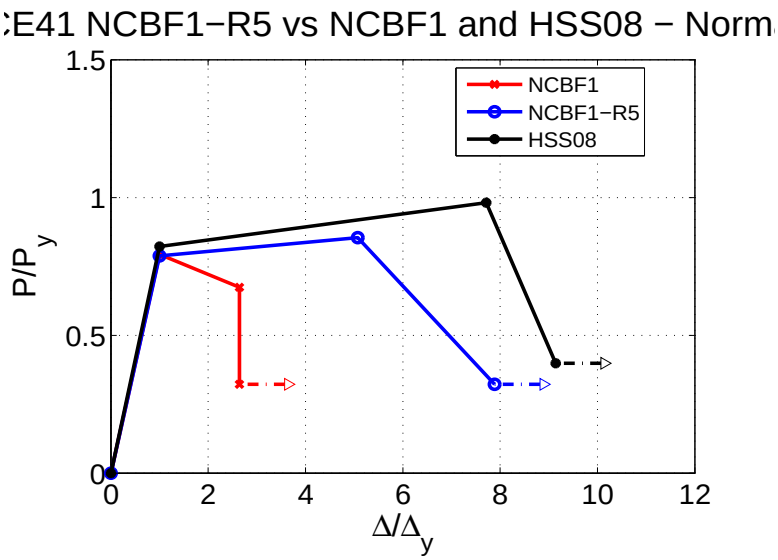

Figure 7.25 Normalized Backbone Curves - Comparison of NCBF1-R5 to SCBF

7.4 Implications for Evaluation and Retrofit

The results presented in Section 7.3 can be utilized to establish some guidelines for evaluating NCBFs. NCBF1 had numerous deficiencies which affected performance to varying degrees, as summarized in Table 7.3. Despite the weld and plate capacity deficiencies in the connection, the controlling aspect of the behavior of NCBF1 was the brace compactness. Subsequent retrofit specimens revealed additional deficiencies that adversely affected the system performance, particularly the beam-to-gusset weld and the gusset/beam to shear tab weld, both of which failed in several of the specimens. The retrofit specimens also identified successful methods for addressing each of the critical deficiencies of NCBF1, as presented in the remainder of this section

Table 7.3 NCBF1 Deficiencies

Limit State	DCR	Negative Impact on Performance
Brace Local Slenderness	2.04	Severe
Beam-Gusset Weld Fracture	1.55	Severe
Shear Tab to Gusset/Beam Weld Fracture	1.08	Severe
Gusset Plate Whitmore Yielding	1.33	Moderate
Gusset Plate Block Shear	1.16	Moderate
Gusset Plate Shear Yielding at Beam	1.16	Moderate
Brace Net Section Fracture	1.26	Low
Brace Block Shear	1.14	Low
Brace-Gusset Plate Weld Fracture	0.92	Low
Shear Tab to Column Weld Fracture	0.65	Low
Gusset Plate Buckling	0.74	Low

7.4.1 Brace Compactness

NCBF1 had a brace with a width-to-thickness ratio of twice the modern limit. This resulted in a rapid loss of brace compressive strength after buckling, cupping of the brace at a small drift level relative to specimens with code-compliant braces, and brace fracture at a small total drift range. The brace compactness had a significant adverse impact on the performance to the extent that damage to other deficient components was not observed. Thus, the brace compactness was the deficiency with the most substantial adverse impact on performance.

Replacing a non-compact brace with a compact section was effective at addressing the negative aspects of the non-compact brace performance. The compact braces used for retrofits retained more of their

compressive resistance, as shown in Figure 6.10. They also attained significantly larger mid-span displacements, as shown in Figure 6.11 and Figure 6.12.

However, the brace replacement strategy requires some sacrifices with respect to system lateral load resistance. For the retrofits tested in this thesis, a brace was selected which had the same tensile capacity as the original brace. A compact brace with the same cross-sectional area as a non-compact brace will have a lower buckling capacity, because it necessarily has a smaller radius of gyration, as demonstrated in Table 7.4. This is a concern for system behavior, as it reduces the lateral load capacity of the system. Additionally, NCBF1-R1 and NCBF1-R2 demonstrated that a more compact brace section is capable of subjecting the connections to larger demands, which in those specimens resulted in connection fracture. The alternative is to select a brace section that maintains the brace compressive resistance, but increases the tensile resistance, also shown in Table 7.4. This method can maintain the lateral load capacity of the system, but it may put much higher demands on the connections due to the brace compactness and the increased brace tensile strength. Given the apparent connection vulnerabilities in many NCBFs, increasing the brace strength may not be a tenable option.

Table 7.4 Brace Replacement Options

Section	HSS7x7x1/4	HSS5x5x3/8	HSS6x6x3/8
Width-to-Thickness Ratio	27.0	11.3	14.2
Area (in^2)	**6.17**	**6.18**	7.58
Radius of Gyration (in)	2.75	1.87	2.28
Tensile Capacity (kips)	**432**	**433**	531
Compressive Capacity (kips)	**-336**	-216	**-347**

A second retrofit option for a non-compact brace is to fill it with concrete. NCBF1-R5 demonstrated that replacing the brace with concrete prevented rapid loss of brace compressive capacity after buckling, as shown in Figure 6.13. Also, the concrete fill delayed local buckling, thus extending the brace life, also shown in Figure 6.13. Unlike brace replacement, filling the brace with concrete retains both the original tensile and compressive capacity of the brace, which is desirable for system performance. In order to avoid an increase in compressive capacity from the concrete, a gap must be provided between the concrete fill and the gusset plate edge at both ends, as was done for NCBF1-R5. This prevents contact force from developing between the gusset plate and the concrete, so the concrete carries minimal axial

load. Like the compact brace replacement, filling the brace with concrete increases demands on the connections, as it extends the brace life.

7.4.2 Beam-to-Gusset Weld

The beam-to-gusset weld had a DCR of 1.55 for all of the specimens tested. This weld fractured in NCBF1-R1, NCBF1-R3, and NCBF1-R5, leading immediately to connection failure in the first two of those specimens. This demonstrates that a high DCR for the beam-to-gusset weld is a critical performance issue for NCBF systems.

The lack of end rotational clearance for the brace also likely contributed to the vulnerability of the gusset-to-beam weld. NCBF1 and the various retrofits all lacked end rotational clearance for the brace. As discussed in Section 6.3, when the brace buckles out of plane, the lack of brace end clearance may cause substantial rotational demands on the gusset-to-beam weld, which may contribute to tearing and fracture. Improving the brace performance can extend its life, thereby putting larger rotational demands on the connection, and potentially contributing further to weld damage.

As described in Chapter 2, many NCBFs have short gusset-to-brace splice lengths and relatively thin gusset plates relative to the brace size. As a result, it is often not possible to retain the existing gusset plate for an NCBF and achieve an acceptable level of brace end clearance, which was the case for NCBF1. An in-plane buckling brace is a possible alternative to protect the gusset plate-to-beam weld without replacing the gusset plate. By forcing the brace to buckle in-plane, the out-of-plane rotational demands on the welds are substantially reduced. NCBF1-R4 demonstrated the effectiveness of this method, as its gusset plate-to-beam welds remained intact through the duration of the test. Alternatively, additional weld could be applied to increase the weld size, or the gusset plate could be replaced to address the vulnerability of this weld.

In order to achieve in-plane buckling, it was necessary to utilize a rectangular HSS section. With a knife plate retrofit, the effective length of the brace is larger for in-plane buckling than for out-of-plane buckling. This is based off of effective length factors of 1 in both directions, which was found to be reasonably accurate for the retrofits tested. The brace length for out-of-plane buckling extends to the end of each knife plate in the connection, as the knife plates deflect out-of-plane with the brace. For in-plane buckling, the knife plates hinge in the free region between the brace end and the gusset plate, so the effective length is the actual brace length. Due to the difference in brace effective lengths, it is necessary to select a brace cross-section that has a smaller radius of gyration for in-plane buckling than for out-of-

plane buckling. A section was selected for NCBF1-R4 that produced a lower expected in-plane buckling load than out-of-plane buckling load, using the assumptions above. This was effective in ensuring that in-plane buckling occurred. By contrast, using a square brace section resulted in substantial out-of-plane buckling.

7.4.3 Shear Tab Weld

The shear tab weld, which connects the gusset plate and the beam web to the shear tab, had a DCR of 1.08 for all specimens tested. Fracture of this weld contributed to the failure of all of the retrofit specimens except NCBF1-R5. In each of those cases, the weld fracture resulted in failure of the beam-to-column connection, which could lead to a partial collapse in a structure. This not only limits pre-fracture performance, but it also eliminates any residual lateral load capacity after fracture.

The shear tab weld began tearing at approximately 3% drift in all specimens, resulting in fracture within two cycles in each case except NCBF1-R5. This demonstrates that the shear tab weld puts a significant and quantifiable limitation on the achievable drift range for this system. It is initially surprising that this impacted performance so significantly, as the DCR for the weld was lower than many others for components of the connection. However, the weld was likely impacted not only by demands from the brace axial force, but also from in-plane rotational demands due to the lateral deformation of the frame, as discussed in Section 6.3.

The effective retrofit of the shear tab weld was the addition of bolts in the shear tab as reinforcement. Sufficient bolts were added to carry the entirety of the vertical component of the brace force, so that the bolts could, in principal, function adequately even in the event of complete weld fracture. While the bolts were not effective at delaying tearing of the shear tab weld, they drastically reduced the rate of tearing, preventing connection failure.

7.4.4 Gusset Plate and Shear Tab

The gusset plates for all of the specimens tested were deficient for Whitmore Yielding, block shear at the gusset-to-brace connection, and shear yielding at the beam-to-gusset weld. Yielding of the gusset plates was extensive in all of the specimens, demonstrating the effect of the gusset plate strength deficiency. However, none of the gusset plates tore or fractured, indicating that the deficiency of the gusset plates was not severe enough to cause connection failure. It is possible that the extensive yielding in the gusset plates caused high strain concentrations around the welds, which could have contributed to weld tearing.

However, it generally appears that gusset plates with the level of deficiency seen in these specimens are not critical.

The shear tabs in most specimens also yielded extensively. This was likely due to a combination of brace axial force and flexural demands from the relative rotation of the beam and column. As with the gusset plate yielding, there does not to appear to be any direct concern associated with the weakness of the shear tab, apart from the potential of tearing of the welds resulting from strain concentrations.

Due to the lack of end clearance and the severity of the deficiency of the gusset plate, the only effective way to reduce the DCRs for the plate would be to replace it with a larger one. The shear tab could potentially be reinforced by adding a second shear tab on the opposite side of the beam and gusset plate, but this could be difficult to construct. The other alternative is to replace the shear tab, which would require an extensive retrofit operation.

7.4.5 Brace Net Section

All of the braces tested had DCRs for brace net section fracture greater than 1.0, but almost no tearing of the brace net section was observed in the tests. This indicates that deficiency of the brace net section may not be as serious of an issue as some of the weld deficiencies. However, research by Powell (2010) suggested that the occurrence of net section tearing and fracture was strongly dependent on the load history applied. Specifically, two similar specimens were tested under different loading histories: one under the cyclic load protocol used for the NCBF specimens, and the second under a simulated near-fault ground motion loading. The specimen tested under near-fault loading suffered net section fracture, while the other specimen did not.

It is reasonable to expect that a similar result would be obtained for the NCBF specimens, because the experimental setup used is the same. Given that the addition of net section reinforcing plates is a quick and inexpensive retrofit measure, it seems reasonable to address the net section deficiencies by adding reinforcing plates to the brace net section.

Chapter 8: Summary and Conclusions

8.1 Summary

The research presented in this thesis began with a literature review and infrastructure survey, which established the level of deficiency of NCBF systems and provided direction for an experimental program. The experimental program consisted of 1 NCBF, 1 repair, and 4 retrofits, which were tested in the UW structures lab. Data analysis of the results from these specimens was conducted to quantify critical aspects of the system performance. Based on this analysis, preliminary guidelines for evaluation and retrofit were created based on the existing code framework, and a specific set of recommendations for evaluation and retrofit for the connection investigated were provided.

8.2 Conclusions

The research presented in this thesis has demonstrated that NCBF systems, which are common in the US, may perform poorly in seismic events, but that some effective retrofit methods are available to address NCBF deficiencies.

None of the connections evaluated in the infrastructure review were capable of developing the brace capacity, which emphasizes that NCBFs are susceptible to connection failures. NCBF1 verified that the deficiencies of NCBFs, particularly severe brace local slenderness, can cause premature failure and non-ductile system response. Table 8.1 shows the critical NCBF1 deficiencies and effective retrofits. Retrofits of NCBF1 demonstrated that the brace local slenderness could be effectively addressed by replacing the brace with a compact section or by filling the brace with concrete to delay local buckling.

However, these retrofits also demonstrated additional vulnerabilities to the NCBF connection. The gusset plate to beam weld, which had a high DCR for all specimens, was particularly vulnerable due in part to brace end out-of-plane rotations and the lack of brace end clearance on the gusset plate. This weld can be effectively protected by using an in-plane buckling brace with a knife plate retrofit, for which specific design recommendations were provided. The gusset plate/beam to shear tab weld also failed consistently, and clearly limited the achievable drift range of the specimens despite being only slightly deficient. This weld can be effectively protected by reinforcing it with bolts using the provided recommendations.

Table 8.1 NCBF1 Critical Deficiencies

Deficiency	DCR	Retrofit
Brace Local Slenderness	2.04	Brace Replacement, Concrete Fill
Gusset-to-Beam Weld	1.55	In-Plane Buckling Brace
Shear Tab to Gusset/Beam Weld	1.08	Bolt Reinforcement

The NCBF also had a range of deficiencies that did not adversely affect the system performance, shown in Table 8.2. In particular, the gusset plate strength deficiencies resulted in extensive gusset plate yielding, but did not directly lead to connection failures. Strength deficiencies in the shear tab and the brace net section also had minimal negative impact on the system performance. This result is valuable for evaluation, because it demonstrates that deficiencies in ductile limit states, such as gusset plate yielding, may not need to be addressed to achieve substantially improved system performance, as demonstrated by specimen NCBF1-R5.

Table 8.2 NCBF1 Non-Critical Deficiencies

Deficiency	DCR
Gusset Plate Whitmore Yielding	1.33
Gusset Plate Block Shear	1.16
Gusset Plate Shear Yielding at Beam	1.16
Brace Net Section Fracture	1.26
Brace Block Shear	1.14

Finally, based on the results from these specimens, preliminary procedures for construction of backbone curves to model subsystem performance were provided utilizing the existing framework from ASCE 41.

8.3 Future Work

Ongoing work on this project at UW and its partner laboratories will continue to evaluate vulnerabilities and retrofits of NCBFs. Below is a list of areas of possible topics of future investigation:

- Evaluation of other common connection details from the infrastructure review and retrofits to address their deficiencies.

- Investigation of further retrofits to NCBF1 or other connections with similar characteristics.
- Evaluation of larger subsystem deficiencies, including weak and non-compact beams, and undersized columns.
- Investigation of the implications of NCBF deficiencies on the performance of structures containing NCBFs using analytical modeling.
- Development of specific recommendations for evaluation and retrofit of NCBFs.

Appendix A: Infrastructure Review Supplements

A.1. List of Surveyed Buildings

Building	Date	State	Type	Floors	Braces	Configurations	Connection Types
83CA3A	Oct-83	CA	Corporate HQ	3	HSS, W	Single Diagonal, Chevron	Bolted Shear Tab
82TN4A	Nov-82	TN	Corporate HQ	3,5	HSS, Pipe	Single Diagonal, Chevron	Shared Gusset
88CA3A	Jan-88	CA	Research	2,3	HSS, Pipe	Single Diagonal, Chevron	Shared Gusset
80CA4A	Sep-80	CA	Office	4	HSS, W	Chevron, Single Diagonal	Beam Only
80WA8A	Jun-80	WA	Hospital	8	Angles	X-Bracing, Single Diagonal	Fully Welded, Bolted Shear Tab, Bolted End Plate
86WA3A	Apr-86	WA	Hospital	3	HSS	Chevron, Single Diagonal	Welded Shear Tab
88UT1A	Oct-88	UT	Retail	1	Angles	X-Bracing	Bolted End Plate
83CA2A	May-83	CA	Office	2	HSS	Chevron	Fully Welded
74CA6A	Jul-74	CA	Hospital	6	W	X-Bracing, Single Diagonal	Double Gusset Plate
82OR9A	Jun-82	OR	Hospital	9	W	Single Diagonal, Multi-Story X	Double Gusset Plate
92WA2A	Feb-92	WA	School	2,3	HSS	Chevron	Welded Shear Tab
86CA4A	Aug-86	CA	Office	4	HSS	Chevron	Bolted Double Angle

A.2. Connection and Frame Drawings and DCRs

For each of the connections from the survey, the drawings and DCRs for the connections and frames are given in this section. The images presented are excerpts from the drawings collected for the survey. The DCRs for the connections are given for each connection within the braced frame bay. For single concentric braces, this is each of the two corners. For chevron braces, this is the two corners and the one mid-span connection. The DCRs for the frame are the largest values from the four load cases investigated (see Chapter 2). The DCRs for the various components do not necessarily all come from the same load case. All of the values presented for the beams are assuming no composite action, with the exception of the combined compression and bending calculation that is explicitly labeled as composite.

A.2.1. 82TN4A--113-ZZ1A-2

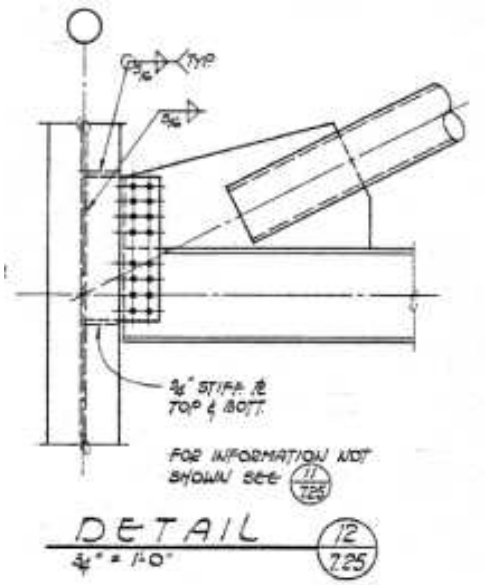

Figure A.1 Top and Bottom Connection Detail (82TN4A--113-ZZ1A-2)

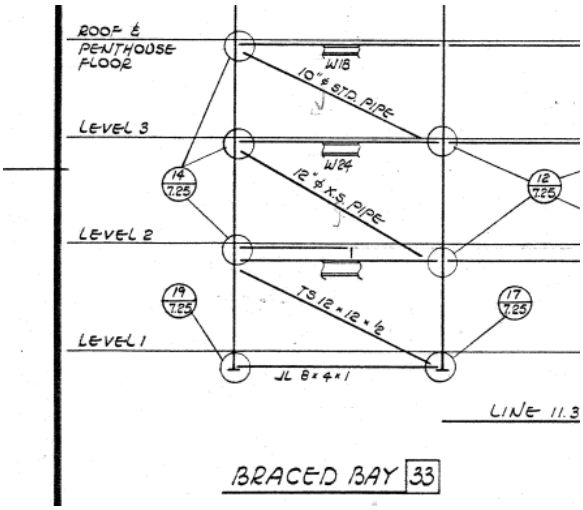

Figure A.2 Frame Elevation (82TN4A--113-ZZ1A-2)

Table A.1 Connection DCRs (82TN4A--113-ZZ1A-2)

Limit State	Top-Left	Bottom-Right
Net Section Fracture	0.84	0.84
Brace Block Shear	0.62	0.62
Plate Block Shear	0.45	0.45
Whitmore Yielding	0.83	0.85
Whitmore Fracture	0.51	0.52
Plate Buckling	0.49	0.51
Brace-Gusset Weld Fracture	1.13	1.13
Brace-Gusset Bolt Shear	NA	NA
Gusset Plate Shear at Beam-Gusset	0.72	0.72
Beam-Gusset Weld Fracture	0.94	1.04
Beam-Gusset Bolt Shear	NA	NA
Beam-Gusset Bolt Bearing	NA	NA
Beam-Gusset Block Shear	NA	NA
Gusset Plate Shear at Column-Gusset	NA	NA
Column-Gusset Bolt Shear	0.87	0.89
Column-Gusset Bolt Bearing	0.23	0.27
Column-Gusset Weld Fracture	1.08	1.06
Column-Gusset Block Shear	1.28	1.34

Table A.2 Frame DCRs (82TN4A--113-ZZ1A-2)

	Story 1	Story 2	Story 3
Right Column Compressive	0.56	0.25	0.06
Right Column Tensile	0.29	0.04	-0.06
Left Column Compressive	1.23	0.68	0.24
Left Column Tensile	0.40	0.19	0.04
Beam Compressive	1.17	0.78	0.55
Beam Tensile	0.57	0.28	0.00
Beam Bending	0.43	0.32	0.43
Beam Compression and Bending	1.55	1.06	0.94
Beam Comp+Bending (Compsite)	0.90	0.62	0.53

A.2.2. 83CA3A--14-LK-2

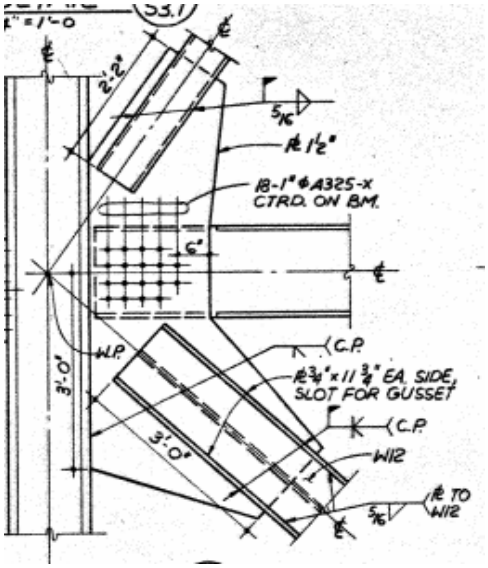

Figure A.3 Bottom Connection Detail (83CA3A--14-LK-2)

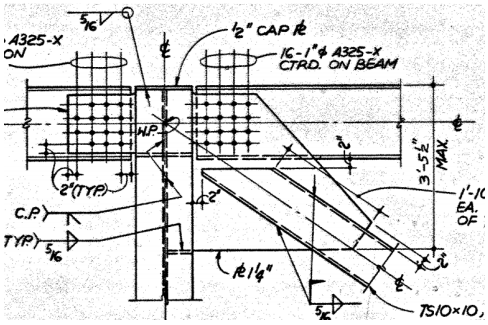

Figure A.4 Top Connection Detail (83CA3A--14-LK-2)

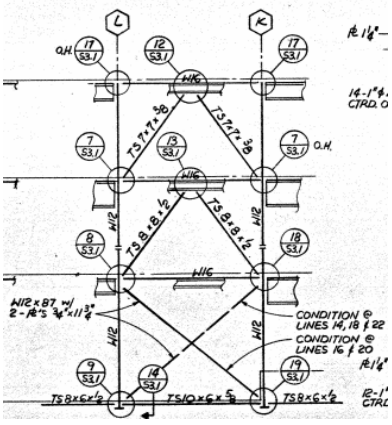

Figure A.5 Frame Elevation (83CA3A--14-LK-2)

Table A.3 Connection DCRs (83CA3A--14-LK-2)

Limit State	Top-Left	Bottom-Right
Net Section Fracture	1.10	1.10
Brace Block Shear	0.72	0.72
Plate Block Shear	0.37	0.37
Whitmore Yielding	0.45	0.45
Whitmore Fracture	0.28	0.28
Plate Buckling	0.54	0.54
Brace-Gusset Weld Fracture	0.88	0.88
Brace-Gusset Bolt Shear	NA	NA
Gusset Plate Shear at Beam-Gusset	NA	NA
Beam-Gusset Weld Fracture	NA	NA
Beam-Gusset Bolt Shear	0.99	0.99
Beam-Gusset Bolt Bearing	0.12	0.12
Beam-Gusset Block Shear	NA	NA
Gusset Plate Shear at Column-Gusset	0.35	0.35
Column-Gusset Bolt Shear	NA	NA
Column-Gusset Bolt Bearing	NA	NA
Column-Gusset Weld Fracture	NA	NA
Column-Gusset Block Shear	NA	NA

Table A.4 Frame DCRs (83CA3A--14-LK-2)

	Story 1	Story 2	Story 3
Right Column Compressive	0.97	0.57	0.21
Right Column Tensile	0.57	0.16	-0.09
Left Column Compressive	0.57	0.58	0.21
Left Column Tensile	0.32	0.16	-0.09
Beam Compressive	0.63	1.46	1.29
Beam Tensile	0.54	0.55	0.00
Beam Bending	0.24	5.75	4.08
Beam Compression and Bending	0.84	6.32	4.52
Beam Comp+Bending (Compsite)	0.60	3.49	2.50

A.2.3. 83CA3A--P-1415-3

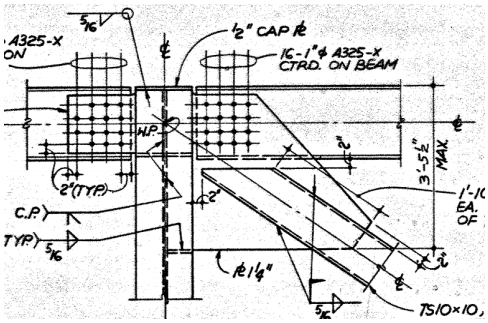

Figure A.6 Bottom Connection Detail (83CA3A--P-1415-3)

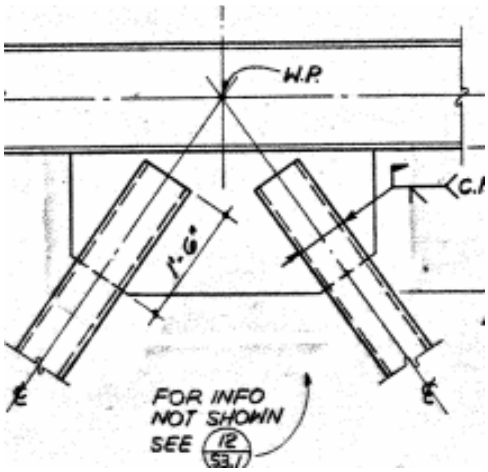

Figure A.7 Top Connection Detail (83CA3A--P-1415-3)

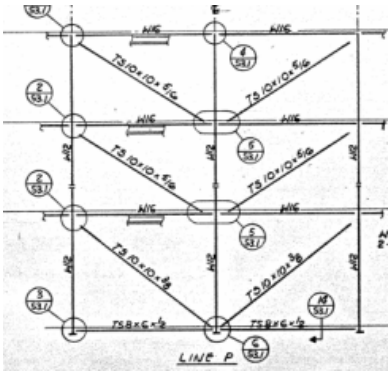

Figure A.8 Frame Elevation (83CA3A--P-1415-3)

Table A.5 Connection DCRs (83CA3A--P-1415-3)

Limit State	Bottom-Left	Top-Center	Bottom-Right
Net Section Fracture	1.09	1.11	1.04
Brace Block Shear	0.43	0.63	0.43
Plate Block Shear	0.53	0.70	0.76
Whitmore Yielding	0.64	1.00	0.97
Whitmore Fracture	0.40	0.61	0.60
Plate Buckling	0.59	0.79	0.88
Brace-Gusset Weld Fracture	0.90	1.30	0.90
Brace-Gusset Bolt Shear	NA	NA	NA
Gusset Plate Shear at Beam-Gusset	NA	0.56	NA
Beam-Gusset Weld Fracture	NA	1.58	NA
Beam-Gusset Bolt Shear	0.74	NA	0.74
Beam-Gusset Bolt Bearing	0.17	NA	0.26
Beam-Gusset Block Shear	NA	NA	NA
Gusset Plate Shear at Column-Gusset	0.74	NA	1.11
Column-Gusset Bolt Shear	NA	NA	NA
Column-Gusset Bolt Bearing	NA	NA	NA
Column-Gusset Weld Fracture	NA	NA	NA
Column-Gusset Block Shear	NA	NA	NA

Table A.6 Frame DCRs (83CA3A--P-1415-3)

	Story 1	Story 2	Story 3
Right Column Compressive	-0.13	-0.07	0.04
Right Column Tensile	0.51	0.37	-0.04
Left Column Compressive	0.86	0.94	0.48
Left Column Tensile	0.49	0.53	0.27
Beam Compressive	0.45	0.38	0.38
Beam Tensile	0.22	0.28	-0.37
Beam Bending	0.07	0.07	0.07
Beam Compression and Bending	0.51	0.45	0.44
Beam Comp+Bending (Compsite)	0.38	0.32	0.32

A.2.4. 88CA3A--1-CD-2

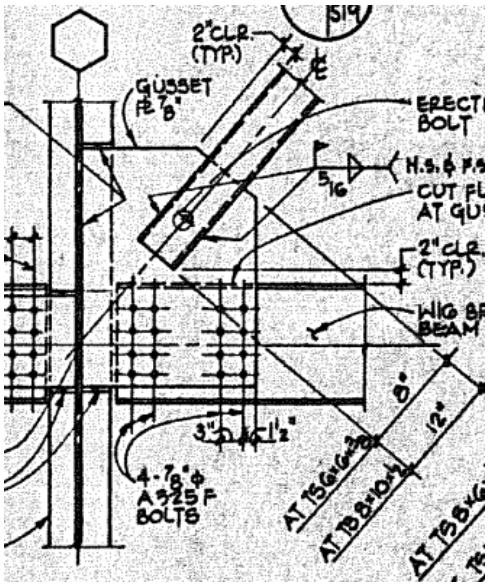

Figure A.9 Bottom Connection Detail (88CA3A--1-CD-2)

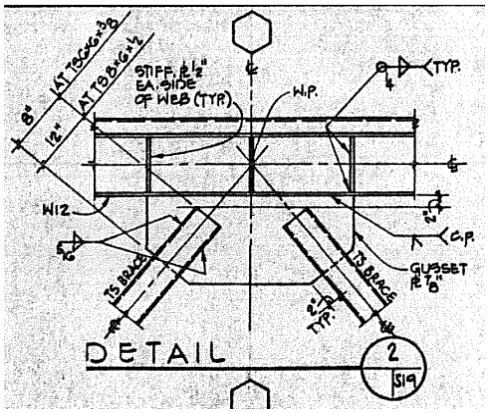

Figure A.10 Top Connection Detail (88CA3A--1-CD-2)

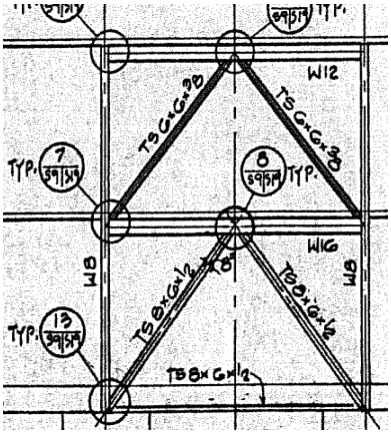

Figure A.11 Frame Elevation (88CA3A--1-CD-2)

Table A.7 Connection DCRs (88CA3A--1-CD-2)

Limit State	Bottom-Left	Top-Center	Bottom-Right
Net Section Fracture	1.30	1.30	1.30
Brace Block Shear	1.05	1.05	1.05
Plate Block Shear	0.80	0.80	0.80
Whitmore Yielding	1.02	1.08	1.02
Whitmore Fracture	0.63	0.66	0.63
Plate Buckling	0.53	0.55	0.53
Brace-Gusset Weld Fracture	1.64	1.64	1.64
Brace-Gusset Bolt Shear	NA	NA	NA
Gusset Plate Shear at Beam-Gusset	NA	0.48	NA
Beam-Gusset Weld Fracture	NA	NA	NA
Beam-Gusset Bolt Shear	0.63	NA	NA
Beam-Gusset Bolt Bearing	0.18	NA	0.18
Beam-Gusset Block Shear	NA	NA	NA
Gusset Plate Shear at Column-Gusset	1.00	NA	1.00
Column-Gusset Bolt Shear	NA	NA	NA
Column-Gusset Bolt Bearing	NA	NA	NA
Column-Gusset Weld Fracture	NA	NA	NA
Column-Gusset Block Shear	NA	NA	NA

Table A.8 Frame DCRs (88CA3A--1-CD-2)

	Story 1	Story 2
Right Column Compressive	1.30	0.49
Right Column Tensile	0.15	-0.22
Left Column Compressive	1.30	0.49
Left Column Tensile	0.15	-0.22
Beam Compressive	0.92	0.70
Beam Tensile	0.25	0.00
Beam Bending	9.03	6.89
Beam Compression and Bending	8.84	6.66
Beam Comp+Bending (Compsite)	4.13	3.03

A.2.5. 80CA4A--2-AB-2

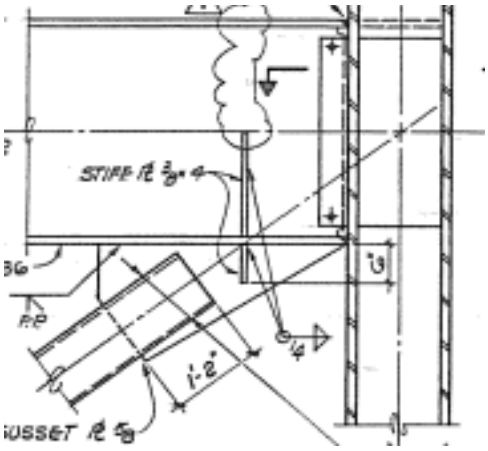

Figure A.12 Top Connection Detail (80CA4A--2-AB-2)

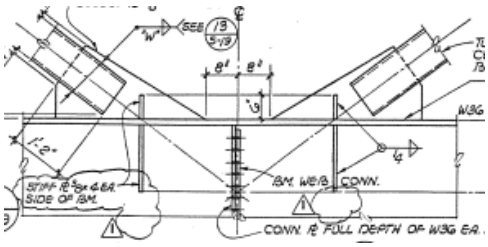

Figure A.13 Bottom Connection Detail (80CA4A--2-AB-2)

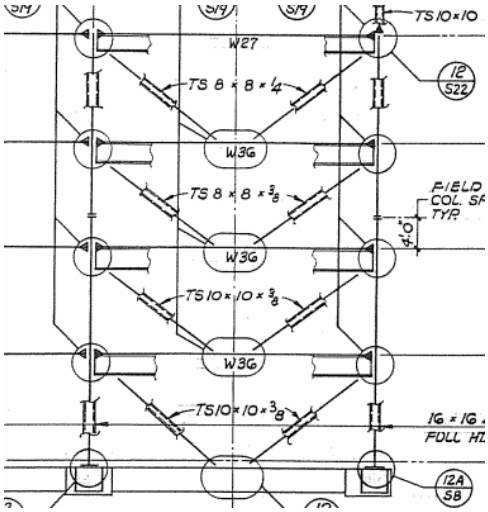

Figure A.14 Frame Elevation (80CA4A--2-AB-2)

Table A.9 Connection DCRs (80CA4A--2-AB-2)

Limit State	Top-Left	Bottom-Center	Top-Right
Net Section Fracture	1.21	1.21	1.21
Brace Block Shear	1.05	1.05	1.05
Plate Block Shear	1.15	1.15	1.15
Whitmore Yielding	2.75	2.70	2.75
Whitmore Fracture	1.63	1.59	1.63
Plate Buckling	NA	NA	NA
Brace-Gusset Weld Fracture	1.36	1.36	1.36
Brace-Gusset Bolt Shear	NA	NA	NA
Gusset Plate Shear at Beam-Gusset	1.30	1.29	1.30
Beam-Gusset Weld Fracture	NA	NA	NA
Beam-Gusset Bolt Shear	NA	NA	NA
Beam-Gusset Bolt Bearing	NA	NA	NA
Beam-Gusset Block Shear	NA	NA	NA
Gusset Plate Shear at Column-Gusset	NA	NA	NA
Column-Gusset Bolt Shear	NA	NA	NA
Column-Gusset Bolt Bearing	NA	NA	NA
Column-Gusset Weld Fracture	NA	NA	NA
Column-Gusset Block Shear	NA	NA	NA

Table A.10 Frame DCRs (80CA4A--2-AB-2)

	Story 1	Story 2	Story 3	Story 4
Right Column Compressive	3.65	2.50	1.40	0.57
Right Column Tensile	0.74	0.46	0.21	0.10
Left Column Compressive	3.65	2.50	1.40	0.57
Left Column Tensile	0.74	0.46	0.21	0.10
Beam Compressive	0.21	0.21	0.17	0.11
Beam Tensile	0.16	0.06	0.00	-0.10
Beam Bending	1.71	1.47	1.06	0.32
Beam Compression and Bending	1.73	1.53	1.14	0.38
Beam Comp+Bending (Compsite)	1.00	0.93	0.63	0.20

A.2.6. 86WA3A--10-HF-1

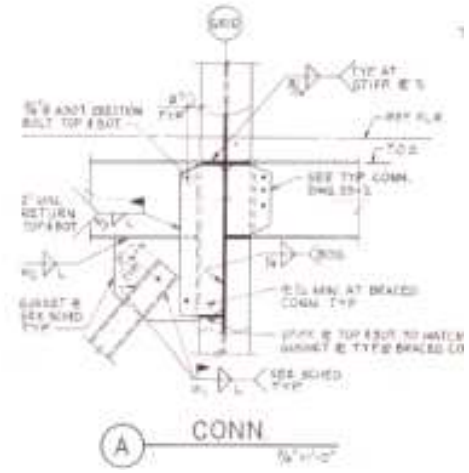

Figure A.15 Top Connection Detail (86WA3A--10-HF-1)

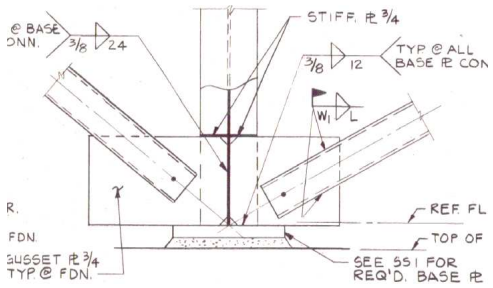

Figure A.16 Bottom Connection Detail (86WA3A--10-HF-1)

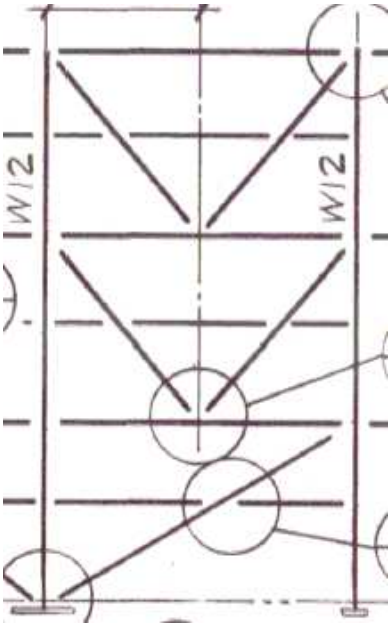

Figure A.17 Frame Elevation (86WA3A--10-HF-1)

Table A.11 Connection DCRs (86WA3A--10-HF-1)

Limit State	Bottom-Left	Top-Right
Net Section Fracture	1.07	1.07
Brace Block Shear	0.64	0.64
Plate Block Shear	0.86	0.86
Whitmore Yielding	1.24	1.17
Whitmore Fracture	0.77	0.71
Plate Buckling	1.11	0.92
Brace-Gusset Weld Fracture	1.25	1.25
Brace-Gusset Bolt Shear	NA	NA
Gusset Plate Shear at Beam-Gusset	1.77	1.77
Beam-Gusset Weld Fracture	1.61	1.61
Beam-Gusset Bolt Shear	NA	NA
Beam-Gusset Bolt Bearing	NA	NA
Beam-Gusset Block Shear	NA	NA
Gusset Plate Shear at Column-Gusset	1.10	0.95
Column-Gusset Bolt Shear	NA	NA
Column-Gusset Bolt Bearing	NA	NA
Column-Gusset Weld Fracture	1.35	0.95
Column-Gusset Block Shear	NA	NA

Table A.12 Frame DCRs (86WA3A--10-HF-1)

	Story 1	Story 2	Story 3
Right Column Compressive	2.21	1.40	0.44
Right Column Tensile	1.33	0.95	0.30
Left Column Compressive	1.85	1.55	0.49
Left Column Tensile	1.02	1.05	0.33
Beam Compressive	0.63	0.38	0.19
Beam Tensile	0.92	-0.01	-0.19
Beam Bending	3.52	1.39	0.18
Beam Compression and Bending	3.76	1.61	0.27
Beam Comp+Bending (Compsite)	1.96	0.89	0.16

A.2.7. 88UT1A--A-1516-1

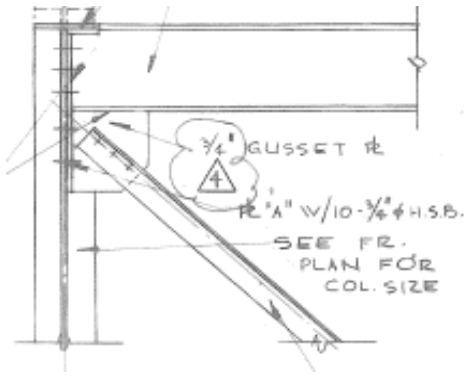

Figure A.18 Top Connection Detail (88UT1A--A-1516-1)

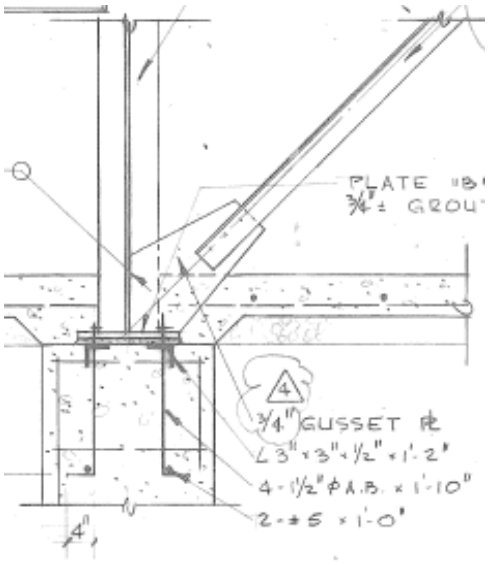

Figure A.19 Bottom Connection Detail (88UT1A--A-1516-1)

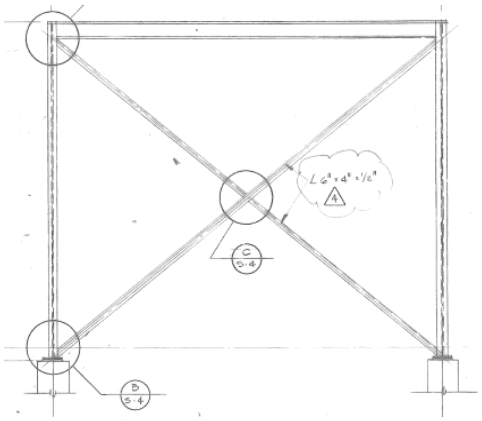

Figure A.20 Frame Elevation (88UT1A--A-1516-1)

Table A.13 Connection DCRs (88UT1A--A-1516-1)

Limit State	Top-Left	Bottom-Right
Net Section Fracture	1.05	1.05
Brace Block Shear	1.17	1.17
Plate Block Shear	0.48	0.88
Whitmore Yielding	1.57	1.57
Whitmore Fracture	0.97	0.97
Plate Buckling	0.45	0.46
Brace-Gusset Weld Fracture	NA	NA
Brace-Gusset Bolt Shear	2.96	2.96
Gusset Plate Shear at Beam-Gusset	1.01	1.20
Beam-Gusset Weld Fracture	1.00	1.05
Beam-Gusset Bolt Shear	NA	NA
Beam-Gusset Bolt Bearing	NA	NA
Beam-Gusset Block Shear		
Gusset Plate Shear at Column-Gusset	0.53	1.03
Column-Gusset Bolt Shear	0.39	NA
Column-Gusset Bolt Bearing	NA	NA
Column-Gusset Weld Fracture	0.46	0.90
Column-Gusset Block Shear	0.39	NA

Table A.14 Frame DCRs (88UT1A--A-1516-1)

	Story 1
Right Column Compressive	1.26
Right Column Tensile	0.04
Left Column Compressive	3.85
Left Column Tensile	0.07
Beam Compressive	0.51
Beam Tensile	-0.43
Beam Bending	2.69
Beam Compression and Bending	2.90
Beam Comp+Bending (Compsite)	NA

A.2.8. 74CA6A--10-MN-1

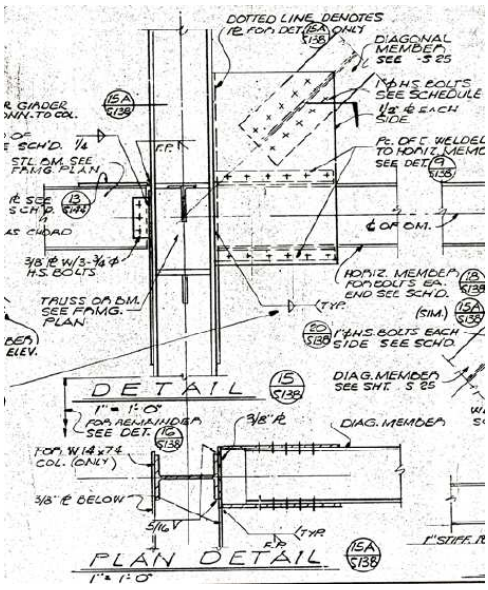

Figure A.21 Top and Bottom Connection Detail (74CA6A--10-MN-1)

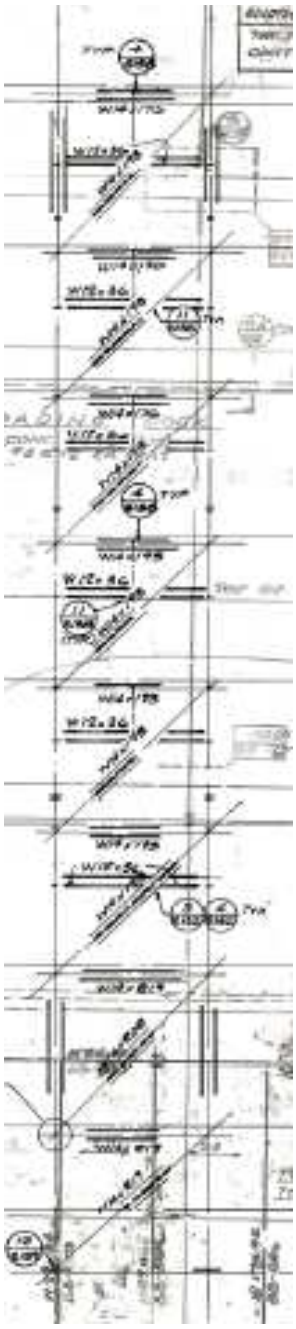

Figure A.22 Frame Elevation (74CA6A--10-MN-1)

Table A.15 Connection DCRs (74CA6A--10-MN-1)

Limit State	Bottom-Left	Top-Right
Net Section Fracture	1.05	1.05
Brace Block Shear	0.45	0.45
Plate Block Shear	1.61	1.61
Whitmore Yielding	2.07	2.11
Whitmore Fracture	1.25	1.28
Plate Buckling	1.88	1.88
Brace-Gusset Weld Fracture	NA	NA
Brace-Gusset Bolt Shear	1.36	1.36
Gusset Plate Shear at Beam-Gusset	2.85	2.85
Beam-Gusset Weld Fracture	1.38	1.38
Beam-Gusset Bolt Shear	1.68	1.68
Beam-Gusset Bolt Bearing	NA	NA
Beam-Gusset Block Shear	NA	NA
Gusset Plate Shear at Column-Gusset	2.73	2.73
Column-Gusset Bolt Shear	NA	NA
Column-Gusset Bolt Bearing	NA	NA
Column-Gusset Weld Fracture	0.99	0.99
Column-Gusset Block Shear	NA	NA

Table A.16 Frame DCRs (74CA6A--10-MN-1)

	Story B1	Story B2	Story 1	Story 2	Story 3	Story 4	Story 5	Story 6
Right Column Compressive	2.98	2.56	2.49	2.08	2.69	2.03	2.02	1.02
Right Column Tensile	2.40	2.06	2.09	1.75	2.24	1.68	1.66	0.83
Left Column Compressive	2.98	2.53	2.46	1.97	2.39	1.60	1.20	0.02
Left Column Tensile	2.12	1.77	1.79	1.43	1.72	1.14	1.20	-0.02
Beam Compressive	0.53	0.53	0.57	0.57	0.57	0.63	0.63	0.62
Beam Tensile	0.47	0.47	0.53	0.52	0.53	0.58	0.58	0.57
Beam Bending	0.06	0.06	0.07	0.07	0.07	0.08	0.08	0.08
Beam Compression and Bending	0.59	0.59	0.63	0.63	0.64	0.69	0.69	0.69
Beam Comp+Bending (Compsite)	0.50	0.50	0.54	0.53	0.54	0.59	0.59	0.58

A.2.9. 82OR9A--H-1719-2

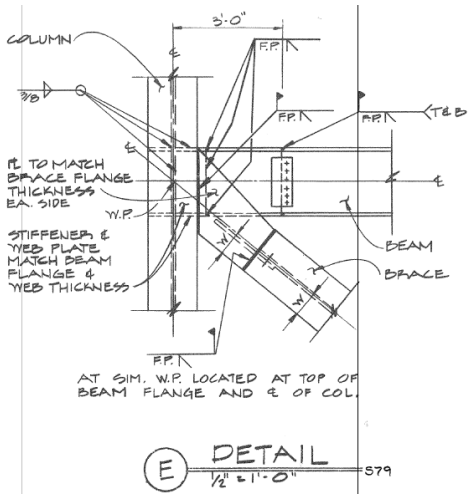

Figure A.23 Top and Bottom Connection Detail (82OR9A--H-1719-2)

Figure A.24 Frame Elevation (82OR9A--H-1719-2)

Table A.17 Connection DCRs (82OR9A--H-1719-2)

Limit State	Top-Left	Bottom-Right
Net Section Fracture	NA	NA
Brace Block Shear	NA	NA
Plate Block Shear	NA	NA
Whitmore Yielding	1.93	1.93
Whitmore Fracture	1.20	1.20
Plate Buckling	2.56	1.95
Brace-Gusset Weld Fracture	NA	NA
Brace-Gusset Bolt Shear	NA	NA
Gusset Plate Shear at Beam-Gusset	NA	NA
Beam-Gusset Weld Fracture	NA	NA
Beam-Gusset Bolt Shear	NA	NA
Beam-Gusset Bolt Bearing	NA	NA
Beam-Gusset Block Shear	NA	NA
Gusset Plate Shear at Column-Gusset	NA	NA
Column-Gusset Bolt Shear	NA	NA
Column-Gusset Bolt Bearing	NA	NA
Column-Gusset Weld Fracture	NA	NA
Column-Gusset Block Shear	NA	NA

Table A.18 Frame DCRs (82OR9A--H-1719-2)

	Story 1	Story 2	Story 3	Story 4	Story 5	Story 6	Story 7	Story 8	Story 9
Right Column Compressive	1.09	1.07	1.04	1.03	1.06	0.99	0.55	0.31	-0.09
Right Column Tensile	1.36	1.37	1.36	1.36	1.44	1.40	0.89	0.57	0.07
Left Column Compressive	1.48	1.61	1.54	1.43	1.42	1.34	0.95	0.86	0.46
Left Column Tensile	1.52	1.68	1.62	1.51	1.51	1.42	1.03	0.92	0.47
Beam Compressive	0.62	0.77	0.86	0.86	0.86	0.62	0.62	0.65	0.52
Beam Tensile	0.56	0.70	0.77	0.77	0.77	0.56	0.42	0.57	0.00
Beam Bending	0.12	0.20	0.32	0.31	0.37	0.23	0.27	0.34	0.27
Beam Compression and Bending	0.52	0.60	0.57	0.58	0.53	0.42	0.38	0.35	0.28
Beam Comp+Bending (Compsite)	0.36	0.39	0.36	0.36	0.33	0.30	0.28	0.22	0.20

A.2.10. 80WA8A--E201-S46S72-1

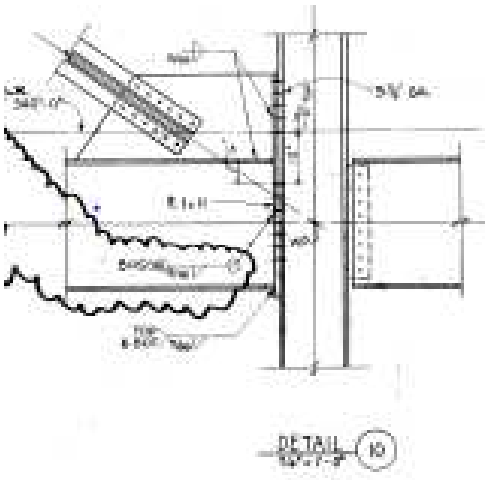

Figure A.25 Top and Bottom Connection Detail (80WA8A--E201-S46S72-1)

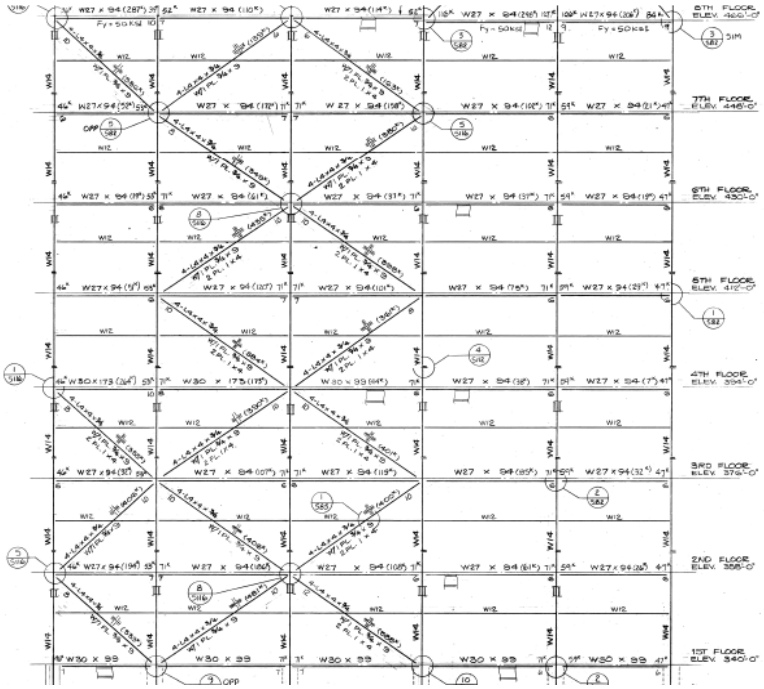

Figure A.26 Frame Elevation (80WA8A--E201-S46S72-1)

Table A.19 Connection DCRs (80WA8A--E201-S46S72-1)

Limit State	Top-Left	Bottom-Right
Net Section Fracture	1.08	1.08
Brace Block Shear	0.79	0.79
Plate Block Shear	1.08	1.08
Whitmore Yielding	1.23	1.23
Whitmore Fracture	0.91	0.91
Plate Buckling	0.89	0.89
Brace-Gusset Weld Fracture	NA	NA
Brace-Gusset Bolt Shear	1.68	1.68
Gusset Plate Shear at Beam-Gusset	0.65	0.65
Beam-Gusset Weld Fracture	1.05	1.05
Beam-Gusset Bolt Shear	NA	NA
Beam-Gusset Bolt Bearing	NA	NA
Beam-Gusset Block Shear	NA	NA
Gusset Plate Shear at Column-Gusset	0.45	0.45
Column-Gusset Bolt Shear	0.48	0.48
Column-Gusset Bolt Bearing	NA	NA
Column-Gusset Weld Fracture	0.72	0.72
Column-Gusset Block Shear	NA	NA

A.2.11. 83CA2A--D-45-2

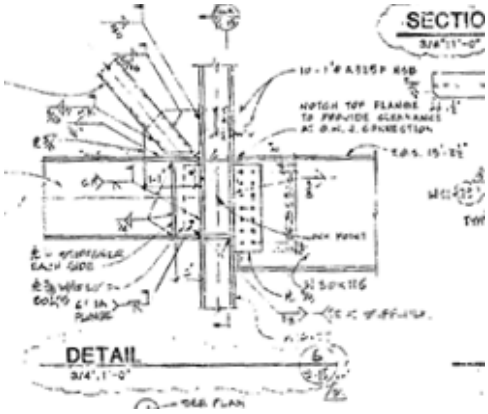

Figure A.27 Bottom Connection Detail (83CA2A--D-45-2)

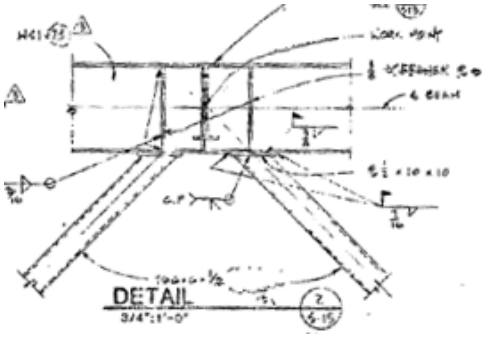

Figure A.28 Top Connection Detail (83CA2A--D-45-2)

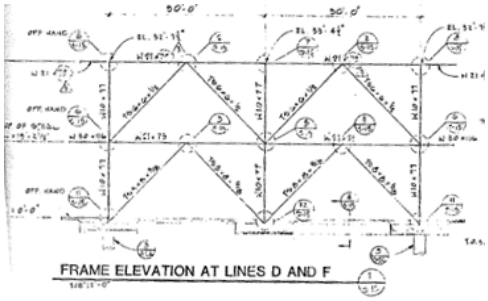

Figure A.29 Frame Elevation (83CA2A--D-45-2)

Table A.20 Connection DCRs (83CA2A--D-45-2)

Limit State	Bottom-Left	Top-Center	Bottom-Right
Net Section Fracture	1.14	NA	1.14
Brace Block Shear	0.71	NA	0.71
Plate Block Shear	1.19	NA	1.19
Whitmore Yielding	1.62	NA	1.62
Whitmore Fracture	0.97	NA	0.97
Plate Buckling	0.78	NA	0.78
Brace-Gusset Weld Fracture	1.48	NA	1.48
Brace-Gusset Bolt Shear	NA	NA	NA
Gusset Plate Shear at Beam-Gusset	2.02	NA	2.02
Beam-Gusset Weld Fracture	0.68	NA	0.68
Beam-Gusset Bolt Shear	NA	NA	NA
Beam-Gusset Bolt Bearing	NA	NA	NA
Beam-Gusset Block Shear	NA	NA	NA
Gusset Plate Shear at Column-Gusset	0.73	NA	0.73
Column-Gusset Bolt Shear	NA	NA	NA
Column-Gusset Bolt Bearing	NA	NA	NA
Column-Gusset Weld Fracture	1.13	NA	1.13
Column-Gusset Block Shear	NA	NA	NA

Table A.21 Connection DCRs (83CA2A--D-45-2)

	Story 1	Story 2
Right Column Compressive	1.00	0.66
Right Column Tensile	-0.52	-0.32
Left Column Compressive	0.98	0.43
Left Column Tensile	-0.11	-0.23
Beam Compressive	1.45	1.12
Beam Tensile	1.42	1.08
Beam Bending	3.70	2.79
Beam Compression and Bending	4.35	3.32
Beam Comp+Bending (Compsite)	2.62	2.00

A.2.12. 86CA4A--D-45-2

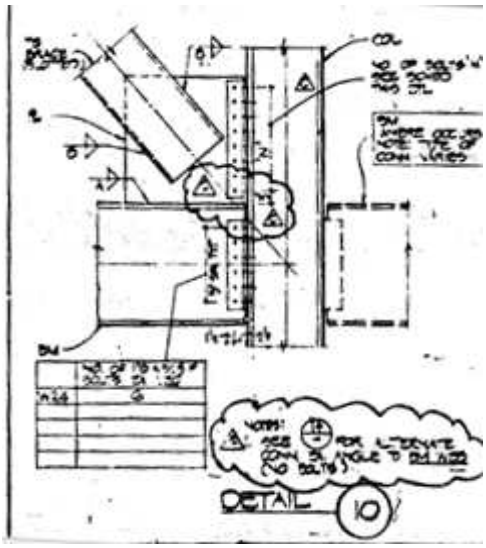

Figure A.30 Bottom Connection (86CA4A--D-45-2)

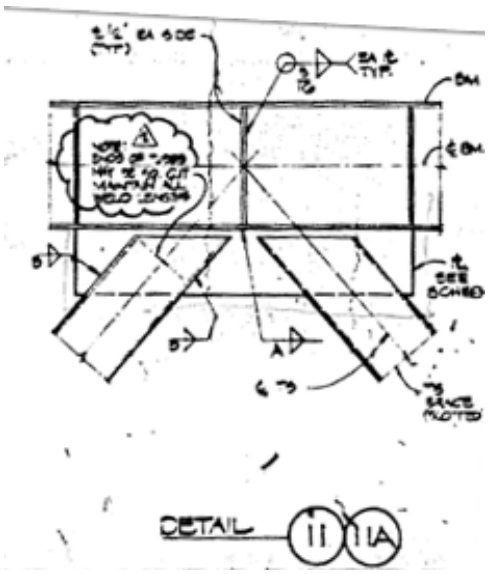

Figure A.31 Top Connection (86CA4A--D-45-2)

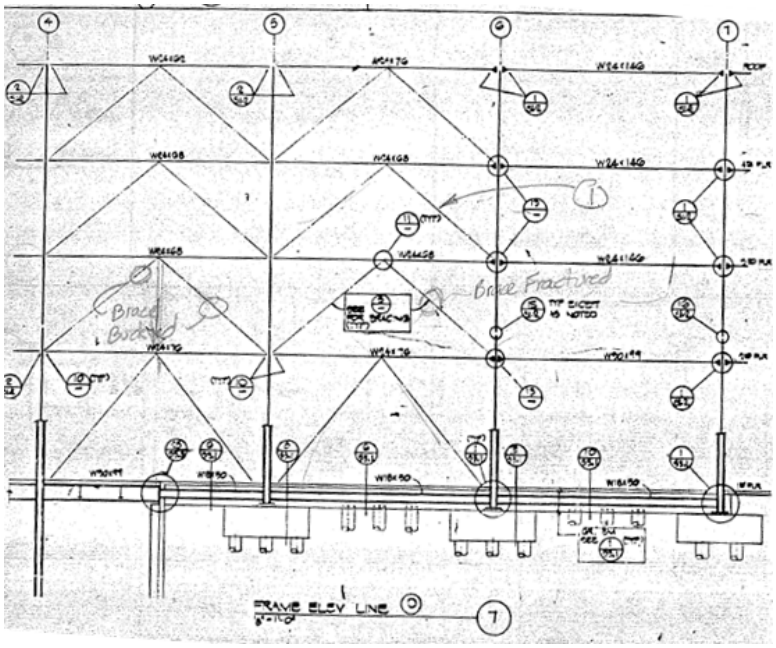

Figure A.32 Frame Elevation (86CA4A--D-45-2)

Table A.22 Connection DCRs (86CA4A--D-45-2)

Limit State	Bottom-Left	Top-Center	Bottom-Right
Net Section Fracture	1.14	1.14	1.14
Brace Block Shear	0.89	0.89	0.89
Plate Block Shear	0.88	0.88	0.88
Whitmore Yielding	1.25	1.50	1.25
Whitmore Fracture	0.76	0.89	0.76
Plate Buckling	1.02	1.04	1.02
Brace-Gusset Weld Fracture	0.87	0.87	0.87
Brace-Gusset Bolt Shear	NA	NA	NA
Gusset Plate Shear at Beam-Gusset	0.78	0.61	0.81
Beam-Gusset Weld Fracture	0.63	0.63	0.63
Beam-Gusset Bolt Shear	NA	NA	NA
Beam-Gusset Bolt Bearing	NA	NA	NA
Beam-Gusset Block Shear	0.81	NA	0.81
Gusset Plate Shear at Column-Gusset	NA	NA	NA
Column-Gusset Bolt Shear	1.30	NA	1.32
Column-Gusset Bolt Bearing	NA	NA	NA
Column-Gusset Weld Fracture	NA	NA	NA
Column-Gusset Block Shear	0.81	NA	0.81

Table A.23 Frame DCRs (86CA4A--D-45-2)

	Story 1	Story 2	Story 3	Story 4
Right Column Compressive	0.80	0.60	0.53	0.34
Right Column Tensile	-0.50	-0.38	-0.32	-0.20
Left Column Compressive	0.86	0.84	0.48	0.19
Left Column Tensile	0.29	0.23	0.00	-0.12
Beam Compressive	2.12	0.92	1.20	1.42
Beam Tensile	2.08	0.90	1.18	1.39
Beam Bending	4.84	2.94	2.94	2.45
Beam Compression and Bending	5.91	3.30	3.52	3.25
Beam Comp+Bending (Compsite)	3.13	1.77	1.90	1.73

A.2.13. 92WA2A--ZZ-79-2

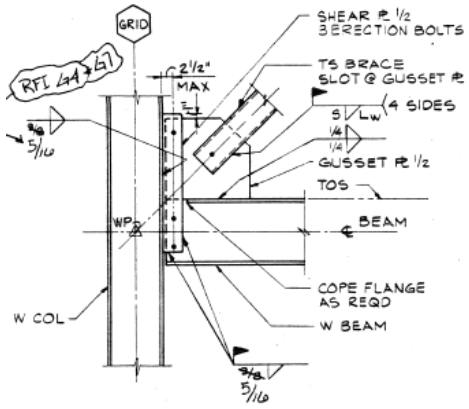

Figure A.33 Bottom Connection Detail (92WA2A--ZZ-79-2)

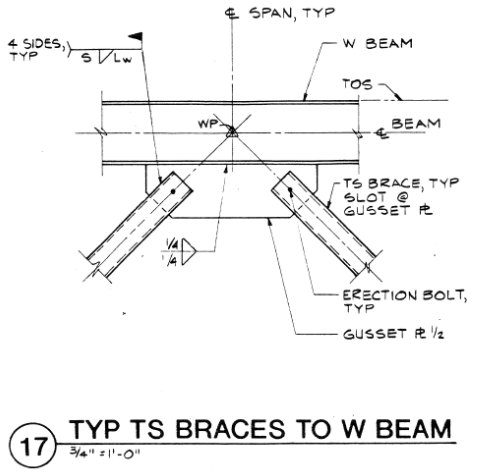

Figure A.34 Top Connection Detail (92WA2A--ZZ-79-2)

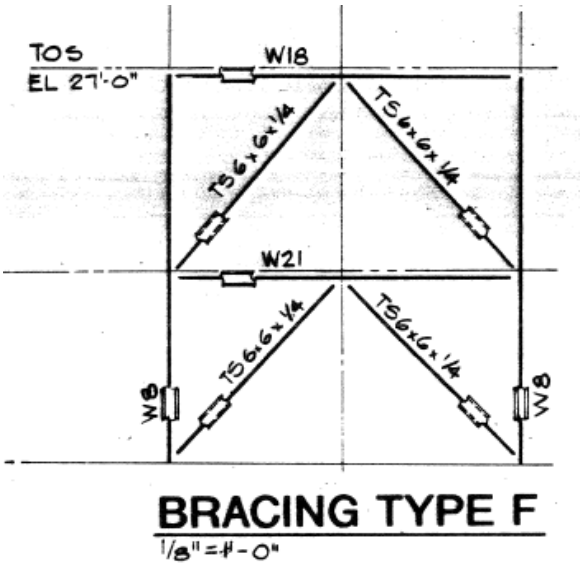

Figure A.35 Frame Elevation (92WA2A--ZZ-79-2)

Table A.24 Connection DCRs (92WA2A--ZZ-79-2)

Limit State	Bottom-Left	Top-Center	Bottom-Right
Net Section Fracture	1.28	1.28	1.28
Brace Block Shear	1.09	1.09	1.09
Plate Block Shear	0.65	0.65	0.65
Whitmore Yielding	0.89	0.90	0.89
Whitmore Fracture	0.55	0.55	0.55
Plate Buckling	0.40	0.12	0.40
Brace-Gusset Weld Fracture	1.42	1.42	1.42
Brace-Gusset Bolt Shear	NA	NA	NA
Gusset Plate Shear at Beam-Gusset	0.78	0.29	0.78
Beam-Gusset Weld Fracture	0.68	0.42	0.68
Beam-Gusset Bolt Shear	NA	NA	NA
Beam-Gusset Bolt Bearing	NA	NA	NA
Beam-Gusset Block Shear	NA	NA	NA
Gusset Plate Shear at Column-Gusset	0.95	NA	0.95
Column-Gusset Bolt Shear	NA	NA	NA
Column-Gusset Bolt Bearing	NA	NA	NA
Column-Gusset Weld Fracture	0.83	NA	0.83
Column-Gusset Block Shear	NA	NA	NA

Table A.25 Frame DCRs (92WA2A--ZZ-79-2)

	Story 1	Story 2
Right Column Compressive	1.21	0.65
Right Column Tensile	0.03	-0.31
Left Column Compressive	1.21	0.65
Left Column Tensile	0.03	-0.31
Beam Compressive	0.67	0.97
Beam Tensile	0.27	0.00
Beam Bending	3.60	4.89
Beam Compression and Bending	3.84	5.09
Beam Comp+Bending (Compsite)	1.93	2.55

A.3. Sample Evaluation Calculations

This section provides an example of how DCRs were calculated for the infrastructure review. The sample structure, shown in Figure A.36, is 92WA2A--ZZ-79-A. Only one of the corner connections will be demonstrated in this section.

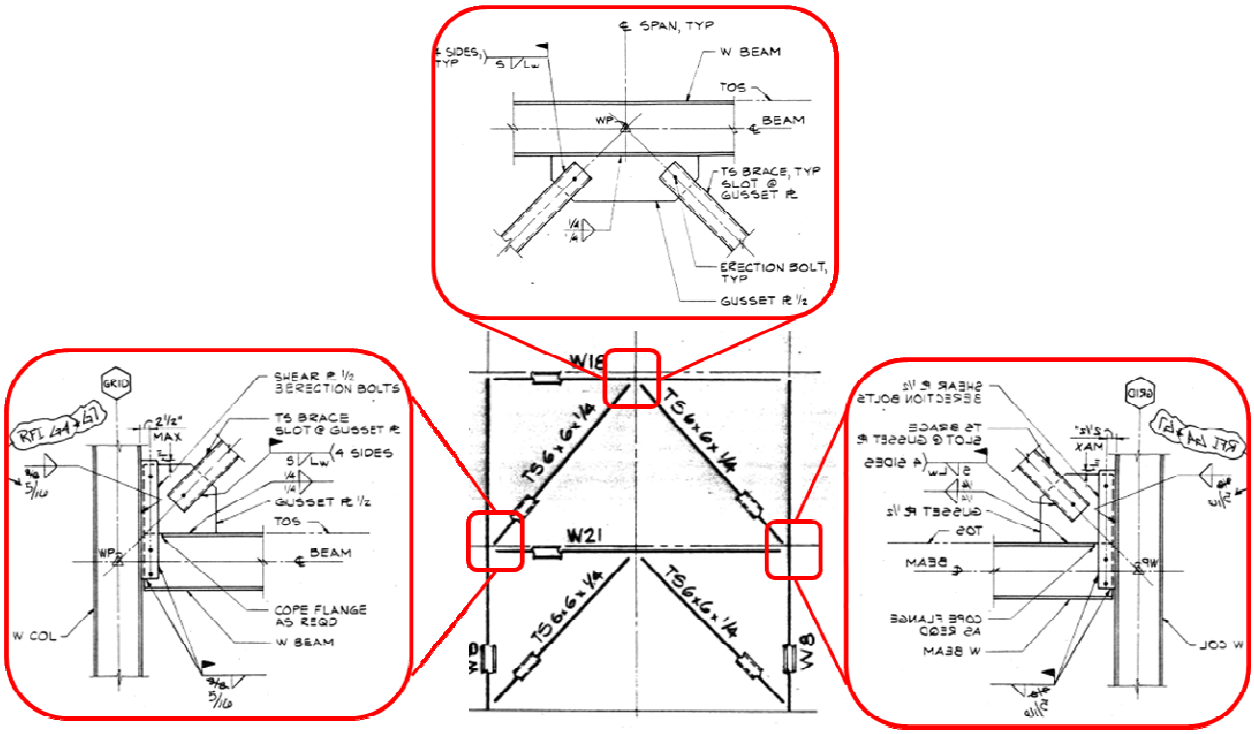

Figure A.36 Sample Frame Layout

Table A.26 Brace Properties

	Brace	HSS6x6x1/4	
L_b	Length of Brace	260.66	in
θ_2	Brace-Beam Angle	37.2	degrees
R_y	Ratio of Expected to Design Yield Strength	1.4	
R_t	Ratio of Expected to Design Ultimate Strength	1.3	
A_b	Gross Area of Brace	5.24	in^2
t_b	Brace Wall Thickness	0.25	in
h_{br}	Brace Cross-Sectional Width	6	in
F_{yb}	Brace Yield Strength	46	ksi
F_{ub}	Brace Ultimate Strength	58	ksi

K_b	Brace Effective Length Factor	1	
r_b	Brace Radius of Gyration	2.34	in

First, we compute the demands the brace will place on the system. The capacities of the various connection limit states will be evaluated against these demands computed for the brace.

The expected brace tensile capacity is:

$$P_t = R_y F_y A_g = 1.4 * 46ksi * 5.24in^2 = \mathbf{337.5\ kips}$$

The expected brace compressive capacity is computed as follows:

$$Euler\ Buckling\ Stess:\ F_e = \frac{\pi^2 E}{\left(\frac{KL}{r}\right)^2} = \frac{\pi^2 * 29000ksi}{\left(\frac{1 * 260.7in}{2.34in}\right)^2} = 23.1ksi$$

$$Slenderness\ Ratio:\ \frac{KL}{r} = 111.4 > 4.71\sqrt{\frac{E}{R_y F_y}} = 100$$

$$Critical\ Buckling\ Stress:\ F_{cr} = 0.877F_e\ = 0.877 * 23.1ksi = 20.0ksi$$

$$P_c = 1.1F_{cr}A_g = 1.1 * 20.0ksi * 5.24in = \mathbf{161.1kips}$$

Table A.27 Brace-Gusset Connection Properties

Fyp	Gusset Plate Yield Strength	36	ksi
Fup	Gusset Plate Ultimate Strength	58	ksi
Kp	Gusset Plate Effective Length Factor	0.65	
tp	Gusset Plate Thickness	0.5	in
wt	Gusset-Brace Weld Type	Fillet	
Nw	Gusset-Brace Number of Welds	4	
w2	Gusset-Brace Weld Size	0.25	in
Lc	Length of Gusset-Brace Connection	8	in

Brace Net Section Capacity:

$$\bar{x} = \frac{B^2 + 2BH}{4(B+H)} = \frac{6in^2 + 2 * 6in * 6in}{4(6in + 6in)} = 2.25in$$

$$Shear\ Lag\ Factor:\ U = 1 - \frac{\bar{x}}{L_c} = \frac{2.25in}{8in} = 0.72$$

$$Net\ Area:\ A_n = A_g - A_{slots} = 5.24in^2 - 2 * 0.25in * 0.75in = 4.87in^2$$

$$Effective\ Net\ Area:\ A_e = UA_n = 0.72 * 4.87in^2 = 3.50in^2$$

$$Net\ Section\ Capacity: R = R_t F_u A_e = 1.3 * 58ksi * 3.50in^2 = \mathbf{263.7kips}$$

$$Net\ Section\ DCR:\ DCR = \frac{P_t}{R} = \frac{337.5kips}{263.7kips} = \mathbf{1.28}$$

Brace Block Shear Capacity

$$Net\ Shear\ Area:\ A_{nv} = 4t_b L_c = 4 * 0.25in * 8in = 8in^2$$

$$Gross\ Shear\ Area:\ A_{gv} = 4t_b L_c = 4 * 0.25in * 8in = 8in^2$$

$$Net\ Tension\ Area:\ A_{nt} = 0in^2$$

$$Block\ Shear\ Capacity: R = U_{bs} A_{nt} R_t F_u + 0.6 * \min\left(A_{nv} R_t F_u\ , A_{gv} R_y F_y\right)$$

$$R = 1 * 0in^2 * 1.3 * 58ksi + 0.6 * \min(8in^2 * 1.3 * 58ksi\ , 8in^2 * 1.4 * 46ksi) = \mathbf{309.1kips}$$

$$Block\ Shear\ DCR = \frac{P_t}{R} = \frac{337.5kips}{309.1kips} = \mathbf{1.09}$$

Gusset Plate Block Shear Capacity

$$Net\ Shear\ Area:\ A_{nv} = 2t_p L_c = 2 * 0.5in * 8in = 8in^2$$

$$Gross\ Shear\ Area:\ A_{gv} = 2t_p L_c = 2 * 0.5in * 8in = 8in^2$$

$$Net\ Tension\ Area:\ A_{nt} = t_p h_{br} = 6in * 0.5in = 3in^2$$

$$Block\ Shear\ Capacity: R = U_{bs} A_{nt} F_u + 0.6 * \min\left(A_{nv} F_u\ , A_{gv} F_y\right)$$

$$R = 1 * 4.5in^2 * 58ksi + 0.6 * \min(12in^2 * 58ksi\ , 12in^2 * 46ksi) = \mathbf{346.8kips}$$

$$Block\ Shear\ DCR = \frac{P_t}{R} = \frac{337.5kips}{346.8kips} = \mathbf{0.97}$$

Gusset Plate Whitmore Yielding

$$Whitmore\ Area:\ A_w = h_{br} + 2L_c \tan(30) = 6in + 2 * 8in * \tan(30) = 7.38in^2$$

$$Whitmore\ Yielding\ Capacity:\ R = A_w F_y = 7.38in^2 * 36ksi = \mathbf{266.1kips}$$

$$Whitmore\ Yelding\ DCR = \frac{P_t}{R} = \frac{337.5kips}{266.1kips} = \mathbf{1.62}$$

Brace-to-Gusset Plate Weld

$$Weld\ Capacity:\ R = 0.6F_{EXX}(0.707w_2)L_w N_w = 0.6 * 70ksi * (0.707 * .25) * 8in * 4 = \mathbf{237.6kips}$$

$$Weld\ \ DCR = \frac{P_t}{R} = \frac{337.5kips}{237.6kips} = \mathbf{1.27}$$

Gusset Plate Buckling

$$Clear\ Length\ for\ Buckling:\ L = \frac{L_1 + L_2 + L_3}{3} = \frac{9in + 1in + (-1in)}{3} = 3in$$

$$Radius\ of\ Gyration:\ r = \sqrt{\frac{I}{A}} = \sqrt{\frac{\left(\frac{bh^3}{12}\right)}{bh}} = \sqrt{\frac{\left(\frac{15.25 * 0.5^3}{12}\right)}{15.25 * 0.5}} = 0.15in$$

$$Euler\ Buckling\ Stess:\ F_e = \frac{\pi^2 E}{\left(\frac{KL}{r}\right)^2} = \frac{\pi^2 * 29000ksi}{\left(\frac{1 * 3in}{0.15in}\right)^2} = 1618ksi$$

$$Slenderness\ Ratio:\ \frac{KL}{r} = 13.3 < 4.71\sqrt{\frac{E}{F_y}} = 100$$

$$Critical\ Buckling\ Stress:\ F_{cr} = 0.658^{\frac{F_y}{F_e}} F_y = 0.658^{\frac{36}{1618}} 36 = \mathbf{35.7ksi}$$

$$Gusset\ Plate\ Buckling\ Capacity:\ R = F_{cr} A_w = 35.7ksi * 7.38in^2 = \mathbf{263.7kips}$$

Moment Due to Load Eccentricity

Figure A.37 shows the force equilibrium on the gusset plate. The loads on the gusset plate result in an unbalanced moment on the gusset plate. This moment is divided evenly between the gusset-to-beam weld and the gusset-to-shear tab weld.

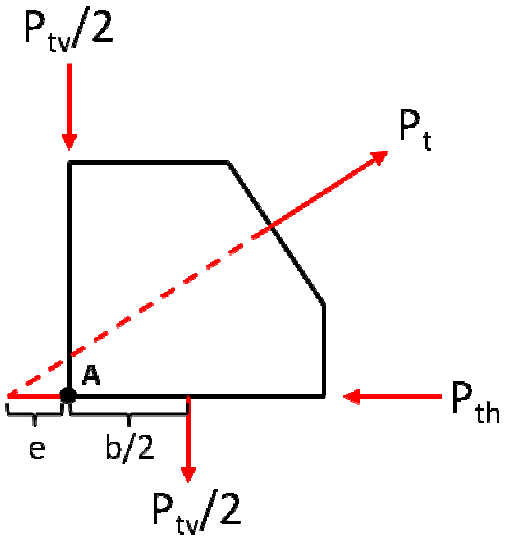

Figure A.37 Force Equilibrium on Gusset Plate

Gusset-to-Beam Weld

$$Stress\ on\ Weld:\ \sigma_{yf} = \frac{P_y}{A_w} = 0ksi$$

$$Force\ Parallel\ to\ Weld:\ P_x = P_t \sin(\theta_{br}) = 154kips$$

$$Stress\ on\ Weld:\ \sigma_{xf} = \frac{P_x}{A_w} = \frac{P_x}{0.707 w_2 L_w N_w} = \frac{154kips}{0.707 * 0.313in * 31.7in * 1} = 22.0ksi$$

$$Moment\ on\ Weld:\ M = \frac{M_w}{2} = 1736k - in$$

$$Max\ \sigma\ on\ Weld:\ \sigma_{ym} = \frac{M * y}{I_w} = \frac{M * \frac{L_w}{2}}{\frac{1}{12} 0.707 N_w w_2 L_w^3} = \frac{1736k - in * \frac{31.7in}{2}}{\frac{1}{12} 0.707 * 1 * 0.313in * (31.7in)^3} = 47.0ksi$$

$$Total\ Stress\ on\ Weld:\ \sigma_{tot} = \sqrt{(\sigma_{xf})^2 + (\sigma_{yf} + \sigma_{ym})^2} = 51.9ksi$$

$$Angle\ of\ Stress\ on\ Weld:\ \theta_{tot} = \text{atan}\left(\frac{\sigma_{yf} + \sigma_{ym}}{\sigma_{xf}}\right) = 1.13\ radians$$

$$Weld\ \sigma\ Capacity:\ \sigma_{all} = 0.6 F_{EXX}(1 + 0.5 \sin(\theta_{tot})^{1.5}) = 0.6 * 70(1 + 0.5 \sin(1.13)^{1.5}) = \mathbf{60.1ksi}$$

$$Weld\ DCR:\ \frac{\sigma_{tot}}{\sigma_{all}} = \frac{85.9ksi}{60ksi} = \mathbf{1.83}$$

Gusset Plate Shear Yielding at Beam

$$Capacity:\ R = 0.6 F_y A_p = 0.6 * 36ksi * 21.4in * 0.5in = \mathbf{405kips}$$

$$DCR:\ \frac{P_x}{R} = \frac{270kips}{405kips} = \mathbf{0.78}$$

Gusset Plate and Beam to Shear Tab Weld

$$Force\ Perpendicular\ to\ Weld:\ P_y = \frac{P_t \sin(\theta_{br})}{2} = 102kips$$

$$Stress\ on\ Weld:\ \sigma_{yf} = \frac{P_y}{A_w} = \frac{P_y}{0.707 w_2 L_w N_w} = \frac{102kips}{0.707 * 0.25in * 21.4in * 2} = 13.5ksi$$

$$Force\ Parallel\ to\ Weld:\ P_x = P_t \cos(\theta_{br}) = 270kips$$

$$Stress\ on\ Weld:\ \sigma_{xf} = \frac{P_x}{A_w} = \frac{P_x}{0.707 w_2 L_w N_w} = \frac{270kips}{0.707 * 0.25in * 21.4in * 2} = 35.7ksi$$

$$Moment\ on\ Weld:\ M = \frac{M_w}{2} = 1736k - in$$

$$Max\ \sigma\ on\ Weld:\ \sigma_{ym} = \frac{M * y}{I_w} = \frac{M * \frac{L_w}{2}}{\frac{1}{12} 0.707 N_w w_2 L_w^3} = \frac{1736k - in * \frac{21.4in}{2}}{\frac{1}{12} 0.707 * 2 * 0.25in * (21.4in)^3} = 64.7ksi$$

$$Total\ Stress\ on\ Weld:\ \sigma_{tot} = \sqrt{(\sigma_{xf})^2 + (\sigma_{yf} + \sigma_{ym})^2} = 85.9ksi$$

$$Angle\ of\ Stress\ on\ Weld:\ \theta_{tot} = \text{atan}\left(\frac{\sigma_{yf} + \sigma_{ym}}{\sigma_{xf}}\right) = 1.14\ radians$$

$$Weld\ \sigma\ Capacity:\ \sigma_{all} = 0.6 F_{EXX}(1 + 0.5 \sin(\theta_{tot})^{1.5}) = 0.6 * 70(1 + 0.5 \sin(1.14)^{1.5}) = \mathbf{60ksi}$$

$$Weld\ DCR:\ \frac{\sigma_{tot}}{\sigma_{all}} = \frac{85.9ksi}{60ksi} = \mathbf{0.86}$$

Appendix B: Instrumentation Layouts

B.1. NCBF1

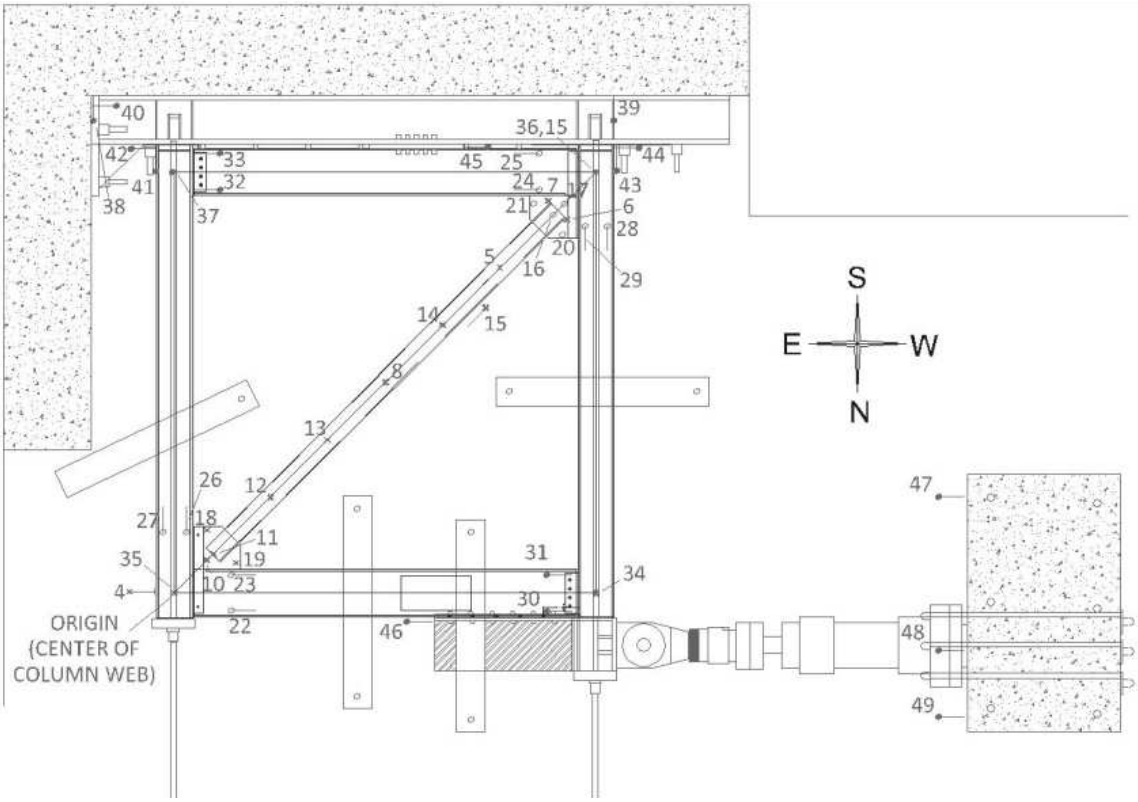

Figure B.8.1 NCBF1 Potentiometer Layout

Table B.1. NCBF1 Potentiometer Locatons

Ch #	Name	Type	X (in)	Y (in)	Z (in)	Axis	L (in)	Purpose	Location
0	0	NA	x	x	x	x	x	Terminal Resistor	x
1	MTS 500 Kips Load	Load Cell	x	x	x	x	x	Actuator Load	Actuator
2	2 MTS 1_1 LDVT	LDVT	x	x	x	x	x	Actuator Displacement	Actuator
3	3 terminator resistor	NA	x	x	x	x	x	Terminator resistor 3	x
4	4 ColLatNE	D9600	-6	0	0	X+	12	Lateral Frame Displacement	NW Corner of Frame
5	5 BrVert6thSW	P510	111	111	-4	Z+	14	Elongation of Brace	Brace
6	6 BrExt	P510	134	128	3.5	X-Y-	167	Brace Out of Plane Displacement	SW Brace 5/6 Point
7	7 Br3Pin	P510	128	134	3.5	X-Y-	167	Brace Out of Plane Displacement	Brace
8	8 BrVertMid	P510	72	72	-4	Z+	14	Brace Out of Plane Displacement	Brace Center
9	9 Null	Not Used	x	x	x	x	x	round duncan cable	
10	10 GusNECL	P510	11	11	-0	Z+	17	Gusset Plate Out of Plane Displacement	NE Gusset Plate
11	11 BrVertEndNE	P510	13	13	-4	Z+	14	Brace Out of Plane Displacement	NE End of Brace
12	12 BrVert6thNE	P510	33	33	-4	Z+	14	Brace Out of Plane Displacement	NE Brace 1/6 Point
13	13 BrVert3rdNE	P510	52	52	-4	Z+	14	Brace Out of Plane Displacement	NE Brace 1/3 point
14	14 BrVert3rdSW	P510	72	72	-4	Z+	14	Brace Out of Plane Displacement	SW Brace 2/3 Point
15	15 FrDiag	P510	144	144	30	X-Y-	204	Elongation of Frame Diagonal	Work Points
16	16 BrVertEndSW	D9600	131	131	-4	Z+	14	Brace Out of Plane Displacement	SW End of Brace
17	17 GusSWCL	D9600	133	133	-0	Z+	17	Gusset Plate Out of Plane Displacement	SW Gusset Plate
18	18 GusNES	P510	11	21	-0	Z+	17	Gusset Plate Out of Plane Displacement	NE Gusset Plate
19	19 GusNEW	P510	21	11	-0	Z+	17	Gusset Plate Out of Plane Displacement	NE Gusset Plate
20	20 GusSWN	D9600	133	123	-0	Z+	17	Gusset Plate Out of Plane Displacement	SW Gusset Plate
21	21 GusSWE	D9600	123	133	-0	Z+	17	Gusset Plate Out of Plane Displacement	SW Gusset Plate
22	22 NBmHngN	D9600	19	-7	2	X+	16	Beam Plastic Hinge Rotation	North Beam at NW Gusset
23	23 NBmHngS	D9600	19	6.8	2	X+	16	Beam Plastic Hinge Rotation	North Beam at NW Gusset
24	24 SBmHngN	D9600	125	137	2	X-	16	Beam Plastic Hinge Rotation	South Beam at SE Gusset
25	25 SBmHngS	D9600	125	151	2	X-	16	Beam Plastic Hinge Rotation	North Beam at NW Gusset
26	26 WColHngE	D9600	140	125	4	Y-	13	Column Plastic Hinge Rotation	West Column at NW Gusset
27	27 WColHngW	D9600	149	125	4	Y-	13	Column Plastic Hinge Rotation	North Beam at NW Gusset
28	28 EColHngE	D9600	4.5	19	4	Y+	13	Column Plastic Hinge Rotation	East Column at SE Gusset
29	29 EColHngW	D9600	14	19	4	Y+	13	Column Plastic Hinge Rotation	East Column at SE Gusset
30	30 STNWN	D600	136	-8	2	X+	2	Shear Tab Connection Rotation	NE Shear Tab
31	31 STNWS	D600	136	7.5	2	X+	2	Shear Tab Connection Rotation	NE Shear Tab
32	32 STSEN	D600	8	137	2	X-	2	Shear Tab Connection Rotation	SW Shear Tab
33	33 STSES	D600	8	152	2	X-	2	Shear Tab Connection Rotation	SW Shear Tab
34	34 NEWPVert	P510	0	0	0	Z+	12	Vertical Displacement of Work Point	NE Work Point
35	35 NWWPVert	P510	144	0	0	Z+	12	Vertical Displacement of Work Point	NW Work Point
36	36 SEWPVert	D600	0	144	0	Z+	12	Vertical Displacement of Work Point	SE Work Point
37	37 SWWPVert	D600	144	144	0	Z+	12	Vertical Displacement of Work Point	SW Work Point
38	38 ChanLiftSW	D600	150	170	7	Y+	2	Uplift of Channel Assembly	Near SW Corner of Frame
39	39 ChanLiftSE	D600	-27	170	9	Y+	2	Uplift of Channel Assembly	Near SE Corner of Frame
40	40 ChanSlip	D600	-27	172	9	X-	2	Shear Slip of Channel Assembly	SW Corner of Strong Wall
41	41 ColLiftSW	D600	150	151	0	Y+	2	Uplift of Column	SW Corner of Frame
42	42 ColSlipSW	D600	152	153	1	X-	2	Column Shear Slip	SW Corner of Frame
43	43 ColLiftSE	D600	-7	151	0	Y+	2	Uplift of Column	SE Corner of Frame
44	44 ColSlipSE	D600	-9	153	1	X-	2	Column Shear Slip	SE Corner of Frame
45	45 SBmSlip	D600	99	152	0	X-	2	Shear Slip of Beam	South Beam
46	46 NBmSlip	D600	87	-9	0	X+	2	Shear Slip of Load Beam	North Beam at Load Beam
47	47 SBlkSlip	D600	269	44	-17	X+	2	Slip of Reaction Block	SW Corner of Reaction Block
48	48 CBlkSlip	D600	269	-2	-17	X+	2	Slip of Reaction Block	W Side of Reaction Block
49	49 NBlkSlip	D600	269	-43	-17	X+	2	Slip of Reaction Block	NW Corner of Reaction Block
50	50 res 2_18	NA	x	x	x	x	x	Terminator resistor	x

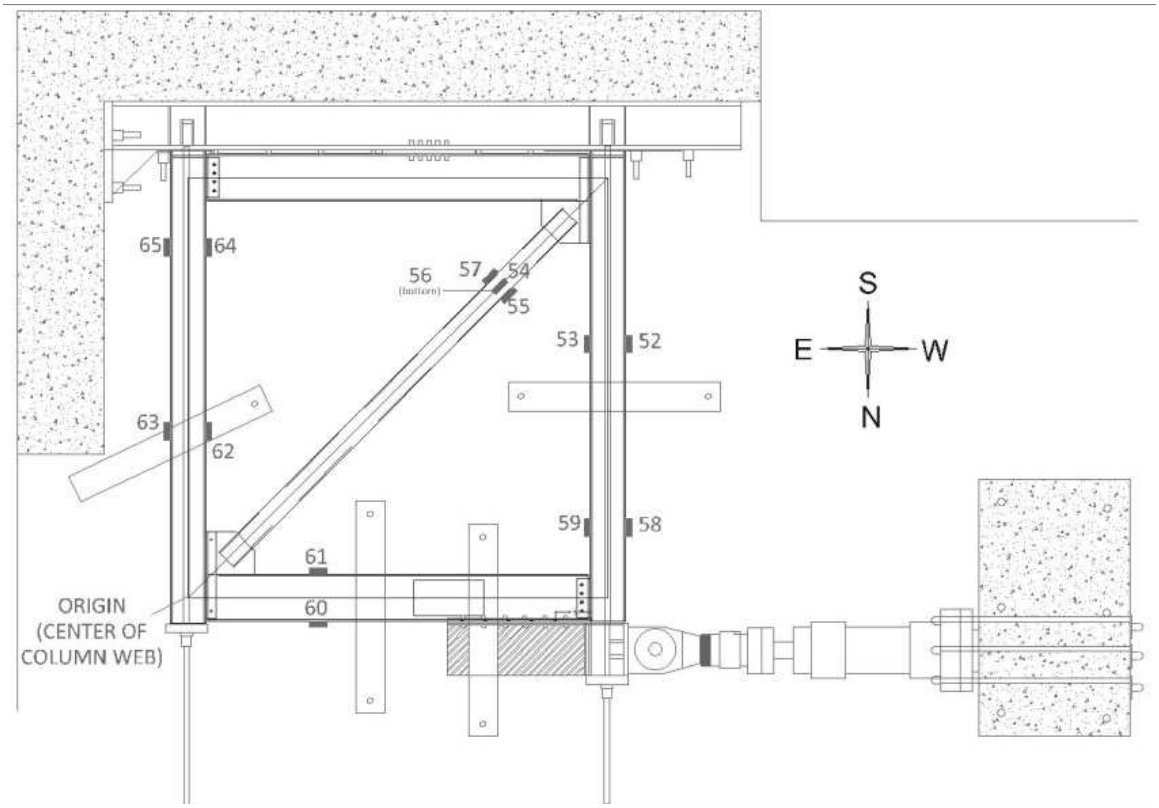

Figure B.8.2 NCBF1 Strain Gauge Layout

Table B.2. NCBF1 Strain Gauge Locatons

Ch #	Name	Type	X (in)	Y (in)	Z (in)	Axis	Length	Purpose	Location
51	Strain Res 3_0	NA	x	x	x	x		Terminal Resistor	x
52	Strn 3_1	Str Gauge	107	107	3.5	X+Y+	NA	Column Forces	W Column, S End, W Side
53	Strn 3_2	Str Gauge	105	109	0	X+Y+	NA	Column Forces	W Column, S End, E Side
54	Strn 3_3	Str Gauge	107	107	-4	X+Y+	NA	Brace Forces	Brace Top
55	Strn 3_4	Str Gauge	110	104	0	X+Y+	NA	Brace Forces	Brace, N Side
56	Strn 3_5	Str Gauge	150	87	0	Y+	NA	Brace Forces	Brace Bottom
57	Strn 3_6	Str Gauge	138	87	0	Y+	NA	Brace Forces	Brace, S Side
58	Strn 3_7	Str Gauge	150	24	0	Y+	NA	Column Forces	W Column, N End, W Side
59	Strn 3_8	Str Gauge	138	24	0	Y+	NA	Column Forces	W Column, N End, E Side
60	Strn 3_9	Str Gauge	6.2	120	0	Y+	NA	Beam Forces	N Beam, N Side
61	Strn 3_10	Str Gauge	-6	120	0	Y+	NA	Beam Forces	N Beam, S Side
62	Strn 3_11	Str Gauge	6.2	57	0	Y+	NA	Column Forces	E Column, N End, W Side
63	Strn 3_12	Str Gauge	-6	57	0	Y+	NA	Column Forces	E Column, N End, E Side
64	Strn 3_13	Str Gauge	45	-8	0	X+	NA	Column Forces	E Dolumn, S End, W Side
65	Strn 3_14	Str Gauge	45	7.9	0	X+	NA	Column Forces	E Column, S End, E Side
66	res 3_15	NA	x	x	x	x	x	Terminal Resistor	x

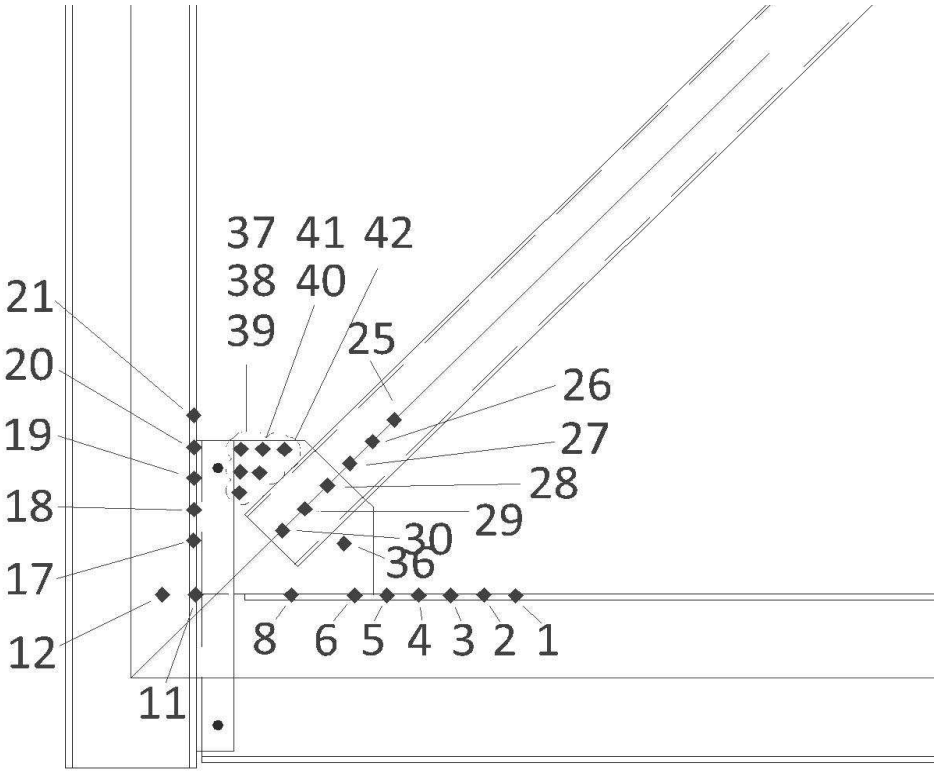

Figure B.8.3 NCBF1 Optotrak Layout

Table B.3. NCBF1 Optotrak Locatons

Marker	X	Y	Z	Location
1	35.95	7.86	3.34	North Beam Flange
2	32.99	7.93	3.37	North Beam Flange
3	29.89	7.88	3.35	North Beam Flange
4	26.89	7.91	3.36	North Beam Flange
5	23.93	7.88	3.36	North Beam Flange
6	20.92	7.90	3.36	North Beam Flange
7	-21.68	24.65	-48.51	Malfunctioned
8	14.98	7.94	3.36	North Beam Flange
9	-21.68	24.65	-48.51	Malfunctioned
10	-21.68	24.65	-48.51	Malfunctioned
11	6.03	7.96	3.35	East Column Flange
12	2.93	7.97	3.34	East Column Web
13	-21.68	24.65	-48.51	Malfunctioned
14	-21.68	24.65	-48.51	Malfunctioned
15	-21.68	24.65	-48.51	Malfunctioned
16	-21.68	24.65	-48.51	Malfunctioned
17	5.86	13.14	6.11	East Column Flange
18	5.90	16.07	6.10	East Column Flange
19	5.91	19.09	6.10	East Column Flange
20	5.90	22.05	6.11	East Column Flange
21	5.88	25.11	6.11	East Column Flange
22	-21.68	24.65	-48.51	Malfunctioned
23	-21.68	24.65	-48.51	Malfunctioned
24	-21.68	24.65	-48.51	Malfunctioned
25	22.72	26.41	5.82	Brace
26	20.67	24.34	5.81	Brace
27	18.56	22.24	5.82	Brace
28	16.49	20.13	5.83	Brace
29	14.36	17.89	5.84	Brace
30	12.28	15.84	5.84	Brace
31	-21.68	24.65	-48.51	Malfunctioned
32	-21.68	24.65	-48.51	Malfunctioned
33	-21.68	24.65	-48.51	Malfunctioned
34	-21.68	24.65	-48.51	Malfunctioned
35	-21.68	24.65	-48.51	Malfunctioned
36	19.92	12.85	9.42	NE Gusst Plate
37	8.23	19.46	9.56	NE Gusset Plate
38	8.34	21.43	9.56	NE Shear Tab
39	8.38	23.62	9.57	NE Shear Tab
40	10.13	21.35	9.59	NE Gusset Plate
41	12.47	23.58	9.61	NE Gusset Plate
42	10.44	23.60	9.60	NE Gusset Plate

B.2. NCBF1-R1

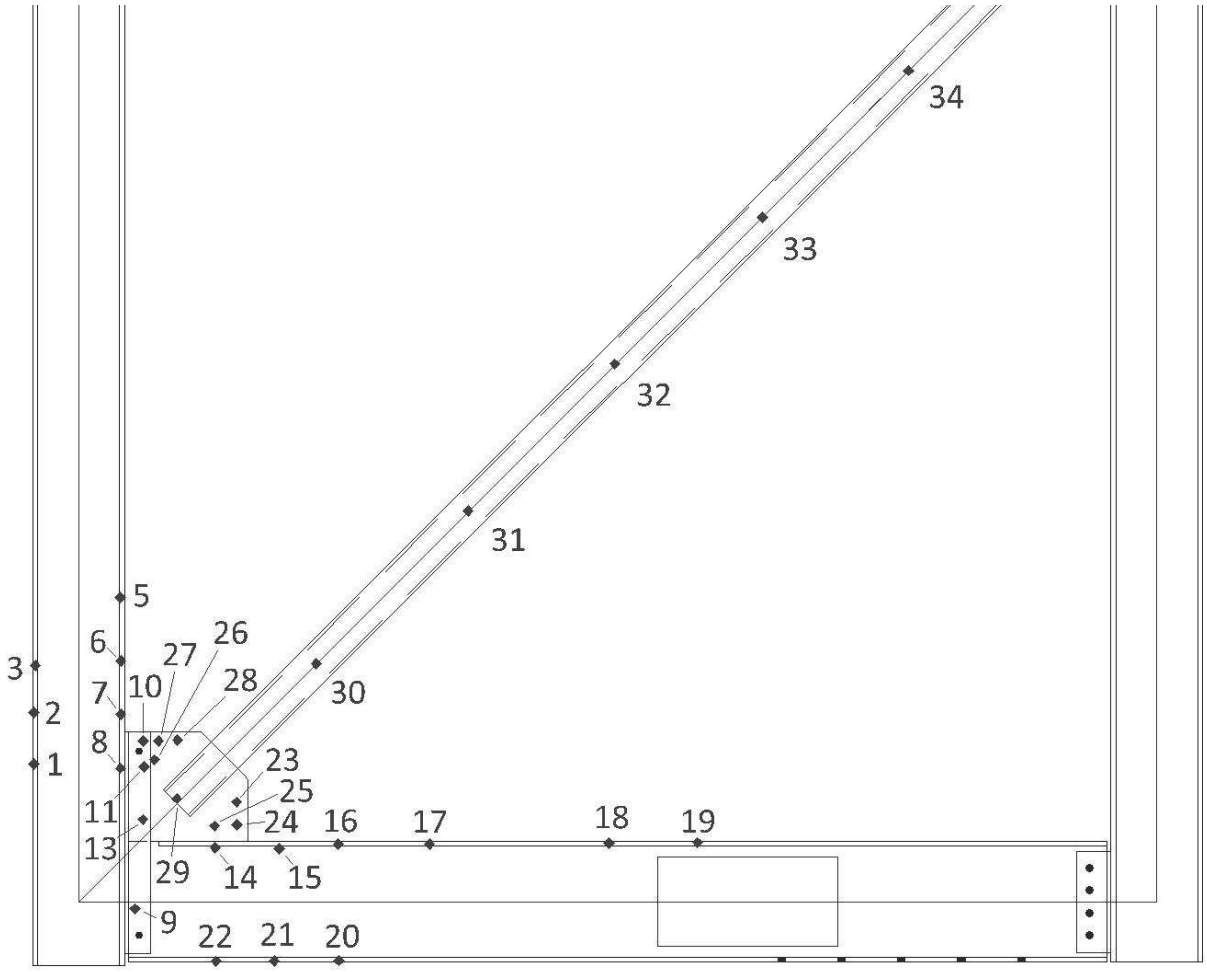

Figure B.8.4 NCBF1-R1 Optotrak Layout

Table B.4. NCBF1-R1 Optotrak Locations

Marker	X	Y	Z	Location
1	-6.02	18.37	5.91	East Column Flange
2	-6.00	25.23	5.94	East Column Flange
3	-3.73	29.56	-44.87	East Column Web
4	71.09	69.37	6.79	Malfunctioned
5	8.27	40.58	-53.18	East Column Flange
6	5.62	32.12	6.11	East Column Flange
7	5.62	25.00	6.12	East Column Flange
8	5.59	17.77	6.10	East Column Flange
9	7.54	-0.96	-39.38	NE Shear Tab
10	8.62	21.41	11.72	NE Shear Tab
11	8.70	17.96	11.80	NE Shear Tab
12	71.09	69.37	6.79	Malfunctioned
13	8.58	10.93	11.84	NE Shear Tab
14	18.22	7.15	1.25	North Beam Web
15	26.75	7.03	-0.09	North Beam Web
16	34.67	7.64	8.86	North Beam Flange
17	46.85	7.70	8.85	North Beam Flange
18	70.82	7.79	8.85	North Beam Flange
19	82.68	7.86	8.84	North Beam Flange
20	34.76	-7.88	8.84	North Beam Flange
21	26.11	-7.93	8.78	North Beam Flange
22	18.35	-7.95	8.71	North Beam Flange
23	21.08	13.27	12.28	NE Gusset Plate
24	21.15	10.26	12.24	NE Gusset Plate
25	18.13	10.07	12.31	NE Gusset Plate
26	10.14	18.92	17.59	NE Gusset Plate
27	10.64	21.44	12.04	NE Gusset Plate
28	13.21	21.52	12.03	NE Gusset Plate
29	13.10	13.75	9.59	Brace
30	35.41	28.03	-61.51	Brace
31	52.01	52.12	9.54	Brace
32	71.62	71.69	9.67	Brace
33	91.30	91.29	9.31	Brace
34	110.87	110.82	9.36	Brace
35	71.09	69.37	6.79	Malfunctioned
36	71.09	69.37	6.79	Malfunctioned
37	71.09	69.37	6.79	Malfunctioned
38	71.09	69.37	6.79	Malfunctioned
39	71.09	69.37	6.79	Malfunctioned
40	71.09	69.37	6.79	Malfunctioned
41	71.09	69.37	6.79	Malfunctioned
42	71.09	69.37	6.79	Malfunctioned
43	71.09	69.37	6.79	Malfunctioned
44	71.09	69.37	6.79	Malfunctioned
45	71.09	69.37	6.79	Malfunctioned
46	71.09	69.37	6.79	Malfunctioned
47	71.09	69.37	6.79	Malfunctioned
48	71.09	69.37	6.79	Malfunctioned
49	71.09	69.37	6.79	Malfunctioned
50	71.09	69.37	6.79	Malfunctioned
51	71.09	69.37	6.79	Malfunctioned

B.3. NCBF1-R2

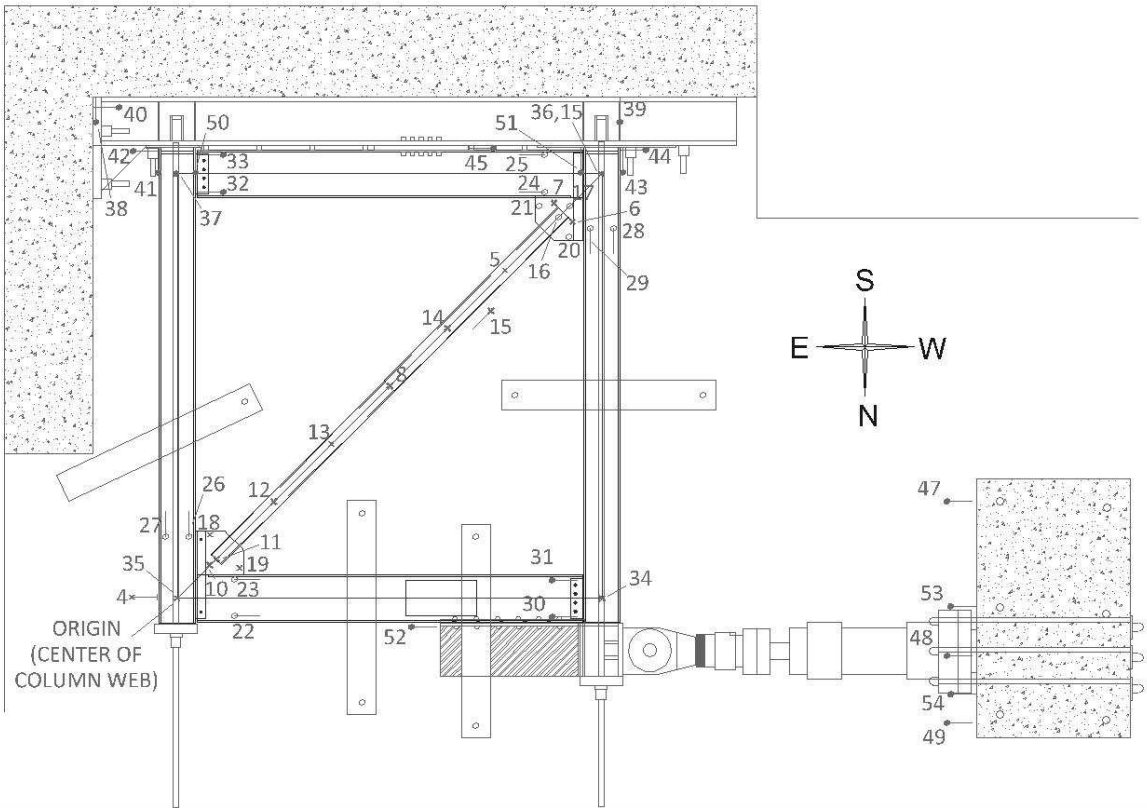

Figure B.8.5 NCBF1-R2 Potentiometer Layout

Table B.5. NCBF1-R2 Potentiometer Locations

Ch #	Name	Type	X (in)	Y (in)	Z (in)	Axis	Length	Purpose	Location
0	0	NA	x	x	x	x	x	x	x
1	1 MTS 500 Kips Load	Load Cell	x	x	x	x	x	MTS 500 kips Load cell	Actuator
2	2 MTS 1_1 LDVT	LDVT	x	x	x	x	x	Actuator LDVT	Actuator
3	3 terminator resistor	NA	x	x	x	x	x	Terminator resistor 3	x
4	4 ColLatNE	D9600	-6	0	0	X+	12	Lateral Frame Displacement	NW Corner of Frame
5	5 BrVert6thSW	P510	111	111	-4	Z+	14	Elongation of Brace	Brace
6	6 BrExt	P510	134	128	3.5	X-Y-	167	Brace Out of Plane Displacement	SW Brace 5/6 Point
7	7 Br3Pin	P510	128	134	3.5	X-Y-	167	Brace Out of Plane Displacement	Brace
8	8 BrVertMid	P510	72	72	-4	Z+	14	Brace Out of Plane Displacement	Brace Center
9	9 Null	Not Used	x	x	x	x	x	Not used	x
10	10 BusNECL	P510	11	11	-0	Z+	17	Gusset Plate Out of Plane Displacement	NE Gusset Plate
11	11 BrVertEndNE	P510	13	13	-4	Z+	14	Brace Out of Plane Displacement	NE End of Brace
12	12 BrVert6thNE	P510	33	33	-4	Z+	14	Brace Out of Plane Displacement	NE Brace 1/6 Point
13	13 BrVert3rdNE	P510	52	52	-4	Z+	14	Brace Out of Plane Displacement	NE Brace 1/3 point
14	14 BrVert3rdSW	P510	72	72	-4	Z+	14	Brace Out of Plane Displacement	SW Brace 2/3 Point
15	15 FrDiag	P510	144	144	30	X-Y-	204	Elongation of Frame Diagonal	Work Points
16	16 BrVertEndSW	D9600	131	131	-4	Z+	14	Brace Out of Plane Displacement	SW End of Brace
17	17 GusSWCL	D9600	133	133	-0	Z+	17	Gusset Plate Out of Plane Displacement	SW Gusset Plate
18	18 GusNES	P510	11	21	-0	Z+	17	Gusset Plate Out of Plane Displacement	NE Gusset Plate
19	19 GusNEW	P510	21	11	-0	Z+	17	Gusset Plate Out of Plane Displacement	NE Gusset Plate
20	20 GusSWN	D9600	133	123	-0	Z+	17	Gusset Plate Out of Plane Displacement	SW Gusset Plate
21	21 GusSWE	D9600	123	133	-0	Z+	17	Gusset Plate Out of Plane Displacement	SW Gusset Plate
22	22 NBmHngN	D9600	19	-7	2	X+	16	Beam Plastic Hinge Rotation	North Beam at NE Gusset
23	23 NBmHngS	D9600	19	6.8	2	X+	16	Beam Plastic Hinge Rotation	North Beam at NE Gusset
24	24 SBmHngN	D9600	125	137	2	X-	16	Beam Plastic Hinge Rotation	South Beam at SE Gusset
25	25 SBmHngS	D9600	125	151	2	X-	16	Beam Plastic Hinge Rotation	South Beam at SE Gusset
26	26 WColHngE	D9600	140	125	4	Y-	13	Column Plastic Hinge Rotation	West Column at NE Gusset
27	27 WColHngW	D9600	149	125	4	Y-	13	Column Plastic Hinge Rotation	West Column at NE Gusset
28	28 EColHngE	D9600	4.5	19	4	Y+	13	Column Plastic Hinge Rotation	East Column at SE Gusset
29	29 EColHngW	D9600	14	19	4	Y+	13	Column Plastic Hinge Rotation	East Column at SE Gusset
30	30 STNWN	D600	136	-8	2	X+	2	Shear Tab Connection Rotation	NW Shear Tab
31	31 STNWS	D600	136	7.5	2	X+	2	Shear Tab Connection Rotation	NW Shear Tab
32	32 STSEN	D600	8	137	2	X-	2	Shear Tab Connection Rotation	SE Shear Tab
33	33 STSES	D600	8	152	2	X-	2	Shear Tab Connection Rotation	SE Shear Tab
34	34 NEWPVert	P510	0	0	0	Z+	12	Vertical Displacement of Work Point	NE Work Point
35	35 NWWPVert	P510	144	0	0	Z+	12	Vertical Displacement of Work Point	NW Work Point
36	36 SWWPVert	D600	0	144	0	Z+	12	Vertical Displacement of Work Point	SW Work Point
37	37 SEWPVert	D600	144	144	0	Z+	12	Vertical Displacement of Work Point	SE Work Point
38	38 ChanLiftSE	D600	150	170	7	Y+	2	Uplift of Channel Assembly	Near SE Corner of Frame
39	39 ChanLiftSW	D600	-27	170	9	Y+	2	Uplift of Channel Assembly	Near SW Corner of Frame
40	40 ChanSlip	D600	-27	172	9	X-	2	Shear Slip of Channel Assembly	SW Corner of Strong Wall
41	41 ColLiftSW	D600	150	151	0	Y+	2	Uplift of West Column, West Flange	SW Corner of Frame
42	42 ColSlipSW	D600	152	153	1	X-	2	Column Shear Slip	SW Corner of Frame
43	43 ColLiftSE	D600	-7	151	0	Y+	2	Uplift of East Column, East Flange	SE Corner of Frame
44	44 ColSlipSE	D600	-9	153	1	X-	2	Column Shear Slip	SE Corner of Frame
45	45 SBmSlip	D600	99	152	0	X-	2	Shear Slip of Beam	South Beam
46	46 NBmSlip	Not Used	x	x	x	x	x	Shear Slip of Load Beam - Now Ch#52	North Beam at Load Beam
47	47 SBlkSlip	D600	269	44	-17	X+	2	Slip of Reaction Block	SW Corner of Reaction Block
48	48 CBlkSlip	D600	269	-2	-17	X+	2	Slip of Reaction Block	W Side of Reaction Block
49	49 NBlkSlip	D600	269	-43	-17	X+	2	Slip of Reaction Block	NW Corner of Reaction Block
50	50 GSTNES	D600	6.5	151	0	Y+	2	Uplift East Column, west flange	E Column Base, W Flange
51	51 STNWS	D600	137	151	0	Y+	2	Uplift West Column, east flange	W Column Base, E Flange
52	52 BSTNEN	D600	87	-9	0	X+	2	Shear Slip of Load Beam	North Beam at Load Beam
53	53 BSTSlipNE	D600	269	-32	0	X+	2	Actuator base south side	Actuator Base Movement
54	54 GSTNEN	D600	269	-3	0	X+	2	Actuator base north side	Actuator Base Movement
55	55 GSTSlipNE	D600	x	x	x	x	x	Not used	x
56	56 Res 2-24	Resistor	x	x	x	x	x	Terminator resistor	x

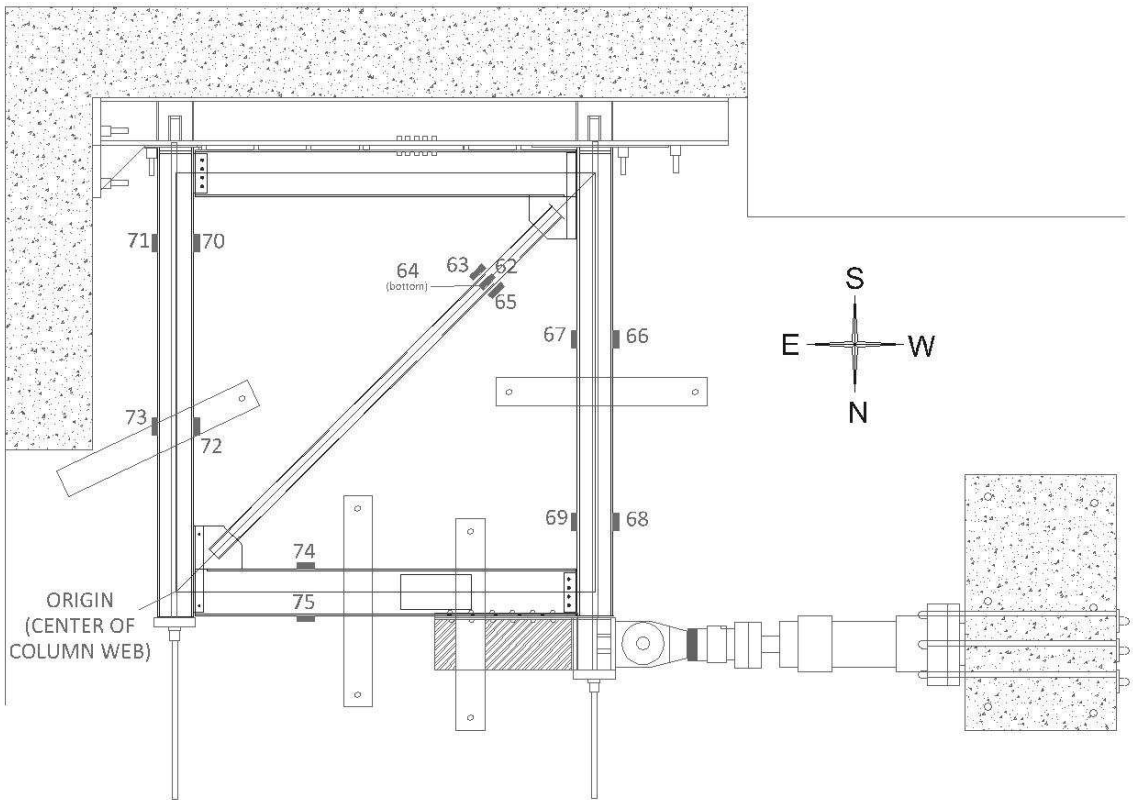

Figure B.8.6 NCBF1-R2 Strain Gauge Layout

Table B.6. NCBF1-R2 Strain Gauge Locations

Ch #	Name	Type	X (in)	Y (in)	Z (in)	Axis	Length	Purpose	Location
57	57 strn 3_0	Resistor	x	x	x	x	x	Terminator resistor	x
58	58 strn 3_1	Not Used	x	x	x	x	x	NA	NA
59	59 strn 3_2	Not Used	x	x	x	x	x	NA	NA
60	60 strn 3_3	Not Used	x	x	x	x	x	NA	NA
61	61 strn 3_4	Not Used	x	x	x	x	x	NA	NA
62	62 strn 1	Str Gauge	107	107	-4	X+Y+	NA	Brace Forces	Brace Top
63	63 strn 2	Str Gauge	110	104	0	X+Y+	NA	Brace Forces	Brace, S Side
64	64 strn 3	Str Gauge	107	107	3.5	X+Y+	NA	Brace Forces	Brace Bottom
65	65 strn 4	Str Gauge	105	109	0	X+Y+	NA	Brace Forces	Brace, N Side
66	66 strn 5	Str Gauge	150	87	0	Y+	NA	Column Forces	W Column, S End, W Side
67	67 strn 6	Str Gauge	138	87	0	Y+	NA	Column Forces	W Column, S End, E Side
68	68 strn 7	Str Gauge	150	24	0	Y+	NA	Column Forces	W Column, N End, W Side
69	69 strn 8	Str Gauge	138	24	0	Y+	NA	Column Forces	W Column, N End, E Side
70	70 strn 9	Str Gauge	6.2	57	0	Y+	NA	Column Forces	E Dolumn, S End, W Side
71	71 strn 10	Str Gauge	-6	57	0	Y+	NA	Column Forces	E Column, S End, E Side
72	72 strn 11	Str Gauge	6.2	120	0	Y+	NA	Column Forces	E Column, N End, W Side
73	73 strn 12	Str Gauge	-6	120	0	Y+	NA	Column Forces	E Column, N End, E Side
74	74 strn 13	Str Gauge	45	-8	0	X+	NA	Beam Forces	N Beam S Side
75	75 strn 14	Str Gauge	45	7.9	0	X+	NA	Beam Forces	N Beam N Side
76	76 Strain term	Resistor	x	x	x	x	x	Terminator resistor	x

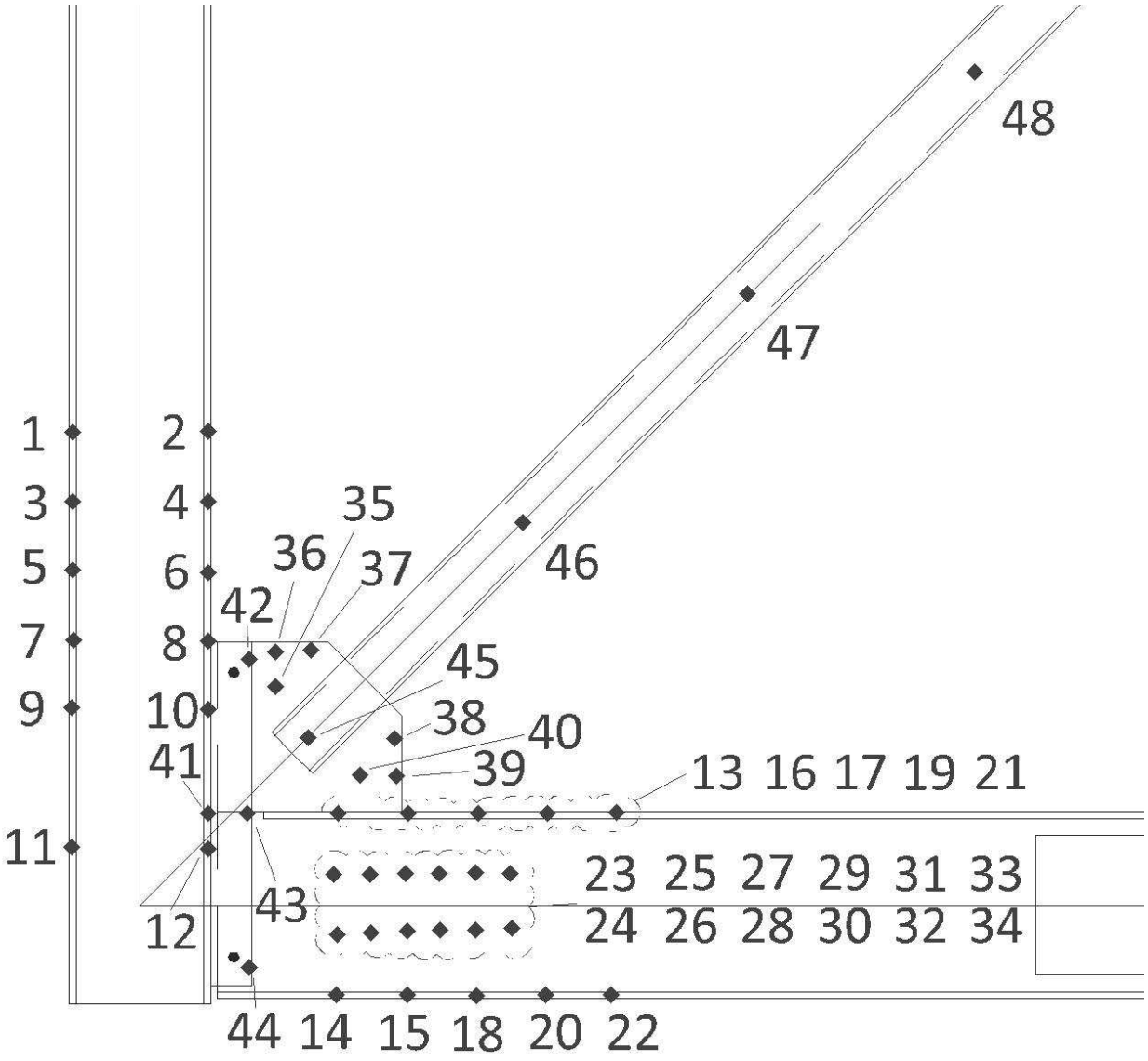

Figure B.8.7 NCBF1-R2 Optotrak Layout

Table B.7. NCBF1-R2 Optotrak Locations

Marker	X	Y	Z	Location
1	-5.79	40.79	6.11	East Column Flange
2	5.88	40.84	6.10	East Column Flange
3	-5.82	34.83	6.12	East Column Flange
4	5.88	34.80	6.09	East Column Flange
5	-5.82	28.93	6.30	East Column Flange
6	5.89	28.69	6.10	East Column Flange
7	-5.77	22.84	6.32	East Column Flange
8	5.90	22.77	6.10	East Column Flange
9	-5.87	17.01	6.30	East Column Flange
10	5.88	16.86	6.10	East Column Flange
11	-5.94	4.97	6.33	East Column Flange
12	5.88	4.88	6.11	East Column Flange
13	17.12	7.95	3.51	North Beam Flange
14	16.96	-7.74	3.44	North Beam Flange
15	23.08	-7.73	3.47	North Beam Flange
16	23.14	7.88	3.51	North Beam Flange
17	29.18	7.92	3.52	North Beam Flange
18	29.09	-7.77	3.52	North Beam Flange
19	35.19	7.91	3.52	North Beam Flange
20	35.06	-7.74	3.52	North Beam Flange
21	41.15	7.96	3.51	North Beam Flange
22	40.73	-7.73	3.53	North Beam Flange
23	16.75	2.67	0.06	North Beam Web
24	17.03	-2.57	0.03	North Beam Web
25	19.86	2.69	0.03	North Beam Web
26	19.92	-2.42	0.04	North Beam Web
27	22.93	2.76	0.03	North Beam Web
28	23.12	-2.23	0.04	North Beam Web
29	25.83	2.75	0.02	North Beam Web
30	25.92	-2.11	0.04	North Beam Web
31	28.99	2.78	0.03	North Beam Web
32	28.96	-2.17	0.03	North Beam Web
33	31.98	2.70	0.04	North Beam Web
34	32.13	-1.96	0.04	North Beam Web
35	11.70	18.81	0.02	NE Gusset Plate
36	11.73	21.82	0.04	NE Gusset Plate
37	14.73	21.95	-0.01	NE Gusset Plate
38	22.00	14.33	0.03	NE Gusset Plate
39	22.18	11.12	0.05	NE Gusset Plate
40	18.97	11.19	0.04	NE Gusset Plate
41	5.86	7.88	6.12	East Column Flange
42	9.39	21.19	0.46	Northeast Shear Tab
43	9.29	7.88	0.53	NE Shear Tab
44	9.43	-5.36	0.43	NE Shear Tab
45	14.49	14.47	2.52	Brace
46	33.07	33.02	2.59	Brace
47	52.48	52.75	2.57	Brace
48	72.11	71.78	2.56	Brace

B.4. NCBF1-R3

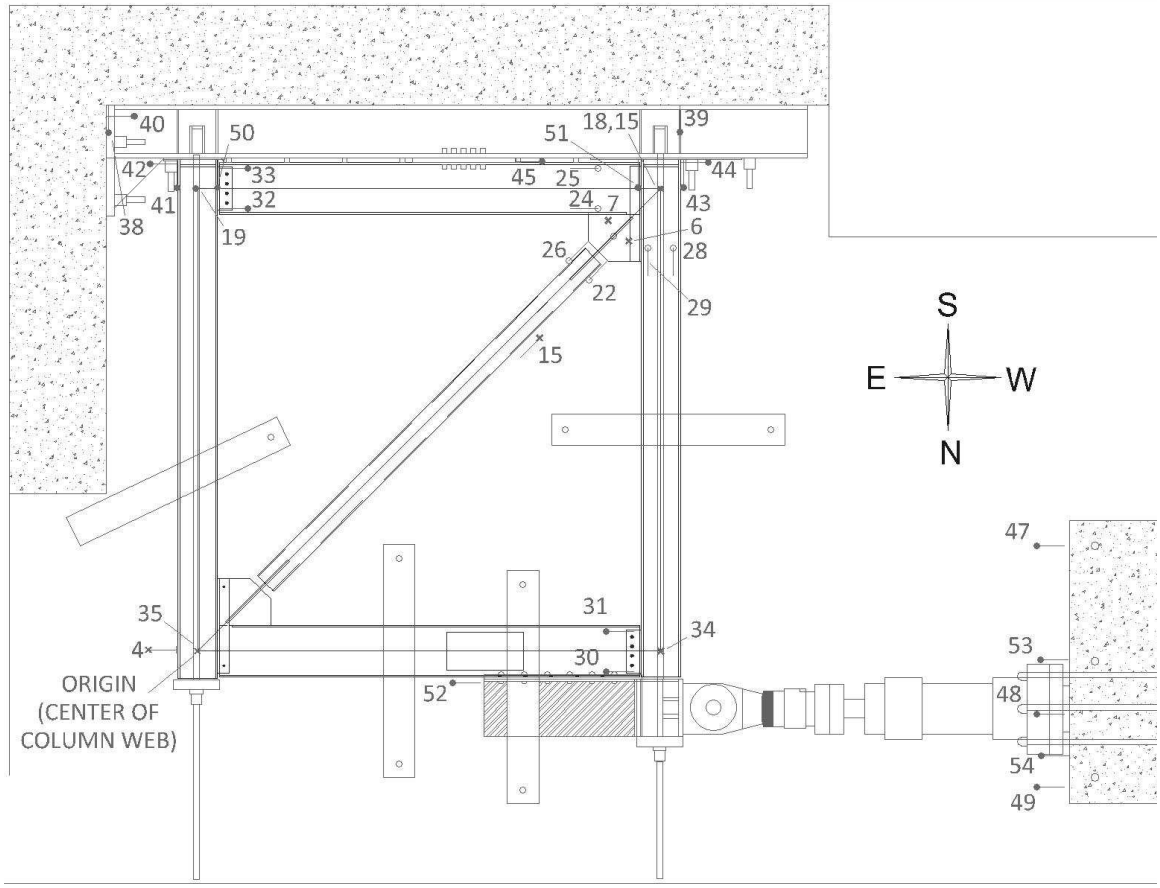

Figure B.8.8 NCBF1-R3 Potentiometer Layout

Table B.8 NCBF1-R3 Potentiometer Locations

Ch #	Name	Type	X (in)	Y (in)	Z (in)	Axis	Length	Purpose	Location
0	0	NA	x	x	x	x	x	x	x
1	1 MTS 500 Kips Load	Load Cell	x	x	x	x	x	MTS 500 kips Load cell	Actuator
2	2 MTS 1_1 LDVT	LDVT	x	x	x	x	x	Actuator LDVT	Actuator
3	3 Terminal Resistor	NA	x	x	x	x	x	Terminator resistor 3	x
4	4 ColLatNE	D9600	-6	0	0	X+	12	Lateral Frame Displacement - NE Corner	NW Corner of Frame
5	5 BrVert6thSW	P510	x	x	x	x	x	Elongation of Brace	Brace
6	6 BrExt	P510	134	128	3.5	X-Y-	167	Brace Out of Plane Displacement	SW Brace 5/6 Point
7	7 Br3PinNull	P510	111	111	-4	Z+	14	Brace Diagonal Elongation (end to end)	Brace
8	8 BrVertMid	P510	x	x	x	x	x	Brace Out of Plane Displacement	Brace Center
9	9 Null	Not Used	x	x	x	x	x	Not used	
10	10 BusNECL	P510	x	x	x	x	x	Gusset Plate Out of Plane Displacement	NE Gusset Plate
11	11 BrVertEndNE	P510	x	x	x	x	x	Brace Out of Plane Displacement	NE End of Brace
12	12 BrVert6thNE	P510	x	x	x	x	x	Brace Out of Plane Displacement	NE Brace 1/6 Point
13	13 BrVert3rdNE	P510	x	x	x	x	x	Brace Out of Plane Displacement	NE Brace 1/3 point
14	14 BrVert3rdSW	P510	x	x	x	x	x	Brace Out of Plane Displacement	SW Brace 2/3 Point
15	15 FrDiag	P510	144	144	30	X-Y-	204	Frame Diagonal Elongation	Work Points
16	16 Null	D9600	x	x	x	x	x	Brace Out of Plane Displacement	Null
17	17 Null	D9600	x	x	x	x	x	Gusset Plate Out of Plane Displacement	Null
18	18 GusNES	P510	0	144	0	Z+	12	Southwest Work Point Vertical	SW Work Point
19	19 GusNEW	P510	144	144	0	Z+	12	SE Work Point Vertical	SE Work Point
20	20 GusSWN_Null	D9600	x	x	x	x	x	Gusset Plate Out of Plane Displacement	Null
21	21 GusSWE_null	D9600	x	x	x	x	x	Gusset Plate Out of Plane Displacement	Null
22	22 NBmHngN_null	D9600	124	120	1	X+Y+	6	SW Knife Plate Rotation North Side	SW Knife Plate, North Side
23	23 NBmHngS_null	D9600	x	x	x	x	x	North Beam Plastic Hinge	Null
24	24 SBmHngN	D9600	125	137	2	X-	16	South Beam Plastic Hinge North	South Beam at SE Gusset
25	25 SBmHngS	D9600	125	151	2	X-	16	Beam Plastic Hinge Rotation	South Beam at SE Gusset
26	26 WColHngE_null	D9600	119	125	1	X+Y+	6	SW Knife Plate Rotation South Side	SW Knife Plate, South Side
27	27 WColHngW_null	D9600	x	x	x	x	x	Column Plastic Hinge Rotation	Null
28	28 EColHngE	D9600	140	125	4	Y-	13	West Column Plastic Hinge West	West Column at SW Gusset
29	29 EColHngW	D9600	149	125	4	Y-	13	West Column Plastic Hinge East	West Column at SW Gusset
30	30 STNWN	D600	136	-8	2	X+	2	NW Shear Tab Rotation South Flange	NW Shear Tab
31	31 STNWS	D600	136	7.5	2	X+	2	NW Shear Tab Rotation North Flange	NW Shear Tab
32	32 STSEN	D600	8	137	2	X-	2	SE Shear Tab Rotation North Flange	SE Shear Tab
33	33 STSES	D600	8	152	2	X-	2	SE Shear Tab Rotation South Flange	SE Shear Tab
34	34 NEWPVert	P510	144	0	0	Z+	12	NW Work Point Vertical	NE Work Point
35	35 NWWPVert	P510	0	0	0	Z+	12	NE Work Point Vertical	NW Work Point
36	36 SWWPVert_null	D600	x	x	x	x	x	Not used	SW Work Point
37	37 SEWPVert	D600	6.5	151	0	Y+	2	E Column Uplift West Flange	East Column, W Flange, South End
38	38 ChanLiftSE	D600	150	170	7	Y+	2	Uplift of Channel Assembly	Near SE Corner of Frame
39	39 ChanLiftSW	D600	-27	170	9	Y+	2	Uplift of Channel Assembly (SW)	Near SW Corner of Frame
40	40 ChanSlip	D600	-27	172	9	X-	2	Shear Slip of Channel Assembly	SW Corner of Strong Wall
41	41 ColLiftSW	D600	150	151	0	Y+	2	E Column Uplift East Flange	SW Corner of Frame
42	42 ColSlipSW	D600	152	153	1	X-	2	E Column Lateral Slip (E Flange)	SW Corner of Frame
43	43 ColLiftSE	D600	-7	151	0	Y+	2	W Column Uplift West Flange	SE Corner of Frame
44	44 ColSlipSE	D600	-9	153	1	X-	2	W Column Lateral Slip (W Flange)	SE Corner of Frame
45	45 SBmSlip	D600	99	152	0	X-	2	Slip Between S Beam and Channel Assembly	South Beam
46	46 NBmSlip_null	Not Used	x	x	x	x	x	BROKEN - Not Used	North Beam at Load Beam
47	47 SBlkSlip	D600	269	44	-17	X+	2	Slip of Reaction Block	SW Corner of Reaction Block
48	48 CBlkSlip	D600	269	-2	-17	X+	2	Slip of Reaction Block	W Side of Reaction Block
49	49 NBlkSlip	D600	269	-43	-17	X+	2	Slip of Reaction Block	NW Corner of Reaction Block
50	50 null	D600	6.5	151	0	Y+	2	Uplift of East Column, west flange	E Column Base, W Flange
51	51 WColLiftEFlange	D600	137	151	0	Y+	2	Uplift West Column, east flange	W Column Base, E Flange
52	52 NBeamSlip	D600	87	-9	0	X+	2	Slip Between Load Beam and North Beam	North Beam at Load Beam
53	53 null	D600	269	-32	0	X+	2	Actuator-Reaction Block Slip (S)	Actuator Base Movement
54	54 null	D600	269	-3	0	X+	2	Actuator-Reaction Block Slip (N)	Actuator Base Movement
55	55 null	D600	x	x	x	x	x	Not used	x
56	56 Null	Resistor	x	x	x	x	x	Terminator resistor	x

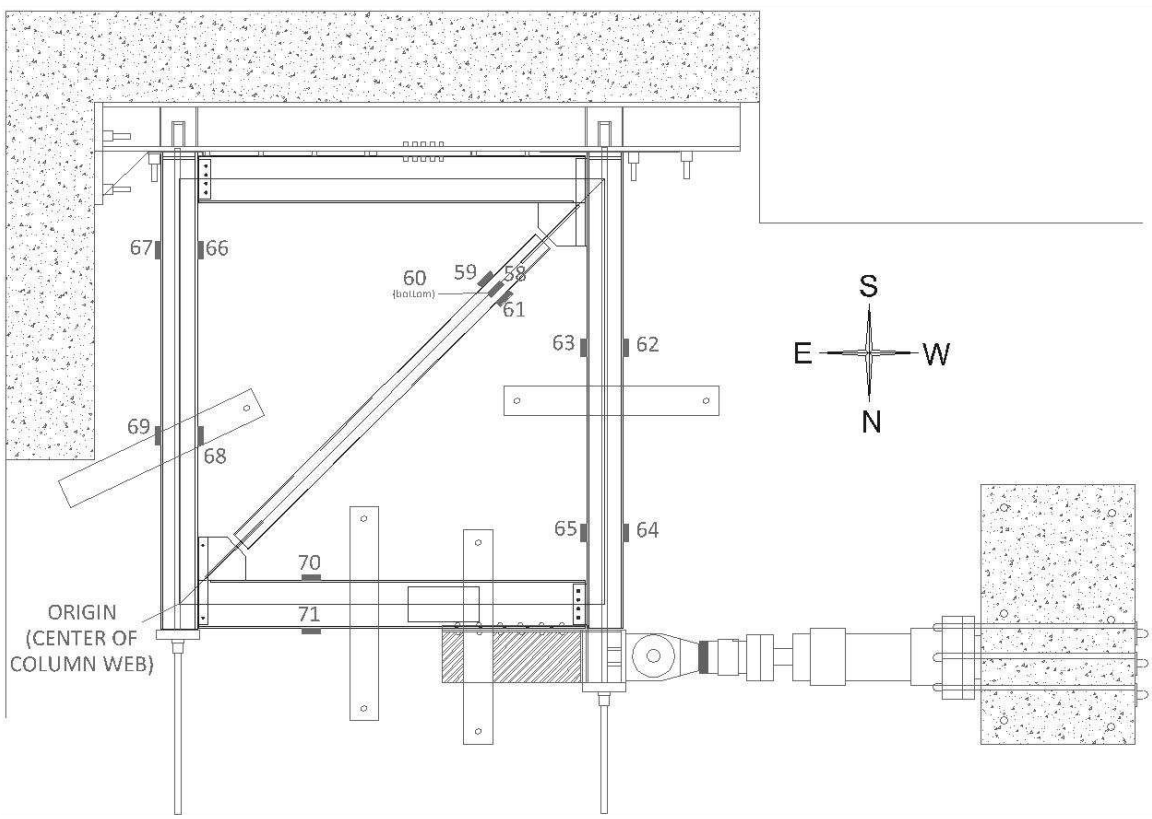

Figure B.8.9 NCBF1-R3 Strain Gauge Layout

Table B.9. NCBF1-R2 Strain Gauge Locations

Ch #	Name	Type	X (in)	Y (in)	Z (in)	Axis	Length	Purpose	Location
57	57 strn 3_0	Resistor	x	x	x	x	x	Terminator resistor	x
58	58 strn 1 3_1	Str Gauge	107	107	-4	X+Y+	NA	Brace Forces	Brace Top
59	59 strn 2 3_2	Str Gauge	110	104	0	X+Y+	NA	Brace Forces	Brace, S Side
60	60 strn3 3_3	Str Gauge	107	107	3.5	X+Y+	NA	Brace Forces	Brace Bottom
61	61 strn 4 3_4	Str Gauge	105	109	0	X+Y+	NA	Brace Forces	Brace, N Side
62	62 strn 5 3_5	Str Gauge	150	87	0	Y+	NA	Column Forces	W Column, S End, W Side
63	63 strn 6 3_6	Str Gauge	138	87	0	Y+	NA	Column Forces	W Column, S End, E Side
64	64 strn 7 3_7	Str Gauge	150	24	0	Y+	NA	Column Forces	W Column, N End, W Side
65	65 strn 8 3_8	Str Gauge	138	24	0	Y+	NA	Column Forces	W Column, N End, E Side
66	66 strn 9 3_9	Str Gauge	6.2	57	0	Y+	NA	Column Forces	E Dolumn, S End, W Side
67	67 strn 10 3_10	Str Gauge	-6	57	0	Y+	NA	Column Forces	E Column, S End, E Side
68	68 strn 11 3_11	Str Gauge	6.2	120	0	Y+	NA	Column Forces	E Column, N End, W Side
69	69 strn 12 3_12	Str Gauge	-6	120	0	Y+	NA	Column Forces	E Column, N End, E Side
70	70 strn 13 3_13	Str Gauge	45	-8	0	X+	NA	Beam Forces	N Beam S Side
71	71 strn 14 3_14	Str Gauge	45	7.9	0	X+	NA	Beam Forces	N Beam N Side
72	72 Terminal Resistor	Resistor	x	x	x	x	x	Terminator resistor	x

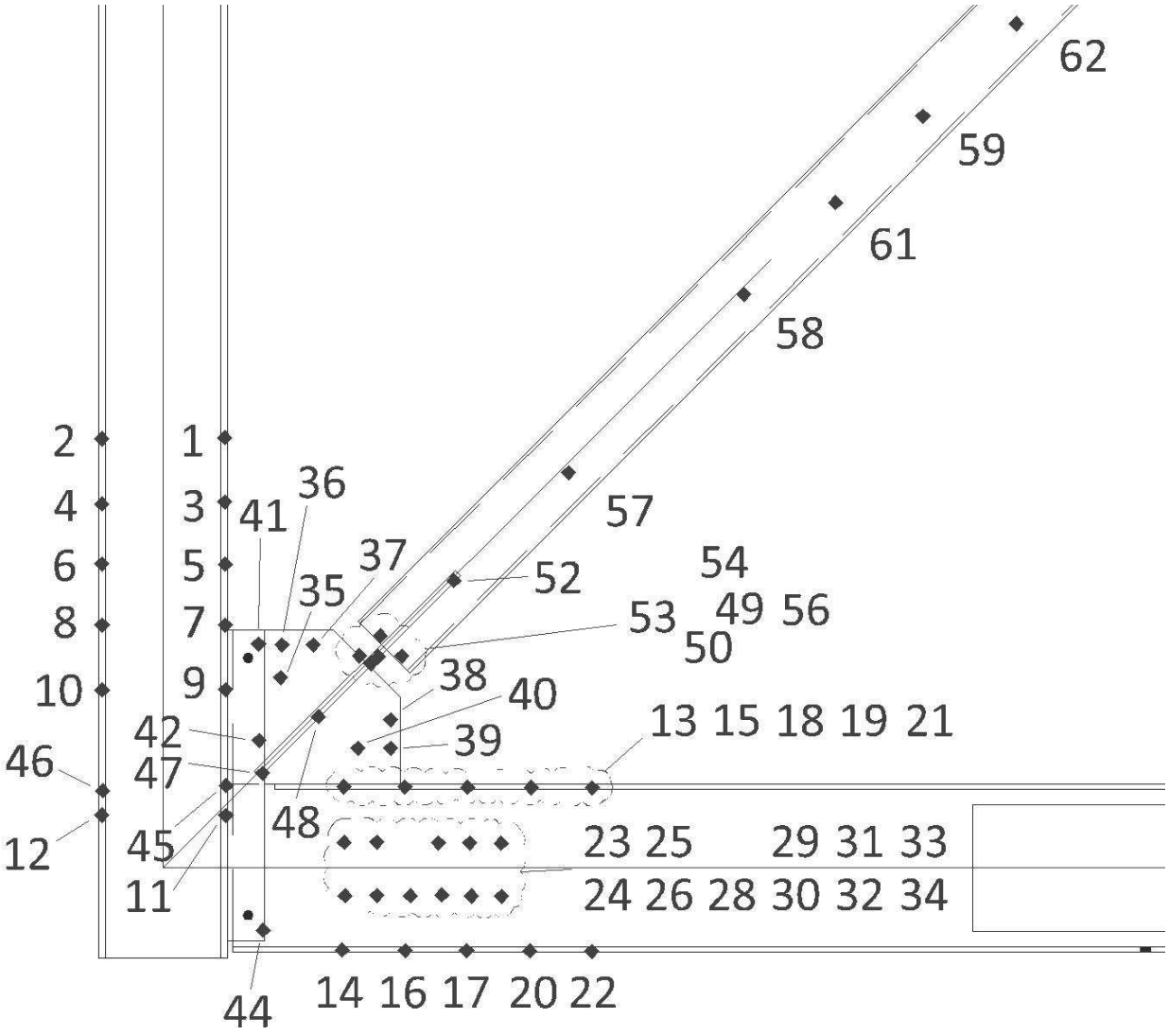

Figure B.8.10 NCBF1-R3 Optotrak Layout

Table B.10. NCBF1-R3 Optotrak Locations

Marker	X	Y	Z	Location
1	5.88	41.07	6.09	East Column Flange
2	-5.89	40.96	5.90	East Column Flange
3	5.87	34.94	6.08	East Column Flange
4	-5.88	34.75	5.88	East Column Flange
5	5.93	28.99	6.09	East Column Flange
6	-5.87	29.01	5.87	East Column Flange
7	5.93	23.20	6.09	East Column Flange
8	-5.85	23.18	5.82	East Column Flange
9	5.95	17.04	6.09	East Column Flange
10	-5.85	16.99	5.81	East Column Flange
11	5.98	5.04	6.06	East Column Flange
12	-5.87	5.05	5.81	East Column Flange
13	17.25	7.77	8.69	North Beam Flange
14	17.09	-7.84	8.68	North Beam Flange
15	23.10	7.74	8.69	North Beam Flange
16	23.12	-7.86	8.70	North Beam Flange
17	28.99	-7.87	8.69	North Beam Flange
18	29.09	7.71	8.68	North Beam Flange
19	35.16	7.68	8.67	North Beam Flange
20	35.05	-7.90	8.68	North Beam Flange
21	41.01	7.67	8.68	North Beam Flange
22	40.95	-7.97	8.68	North Beam Flange
23	17.30	2.45	12.10	North Beam Web
24	17.38	-2.65	12.08	North Beam Web
25	20.42	2.47	12.05	North Beam Web
26	20.43	-2.61	12.08	North Beam Web
27	98.63	30.12	28.55	Malfunctioned
28	23.64	-2.65	12.09	North Beam Web
29	26.32	2.40	12.05	North Beam Web
30	26.62	-2.56	12.09	North Beam Web
31	29.28	2.41	12.04	North Beam Web
32	29.47	-2.67	12.09	North Beam Web
33	32.29	2.37	12.05	North Beam Web
34	32.32	-2.69	12.09	North Beam Web
35	11.21	18.19	12.13	NE Gusset Plate
36	11.34	21.29	12.13	NE Gusset Plate
37	14.32	21.30	12.26	NE Gusset Plate
38	21.74	14.16	12.26	NE Gusset Plate
39	21.72	11.45	12.17	NE Gusset Plate
40	18.62	11.45	12.17	NE Gusset Plate
41	9.10	21.39	11.59	NE Shear Tab
42	9.17	12.19	11.62	NE Shear Tab
43	98.63	30.12	28.55	Malfunctioned
44	9.53	-5.93	11.60	NE Shear Tab
45	6.02	7.87	6.08	East Column Flange
46	-5.81	7.37	5.78	East Column Flange
47	9.49	9.04	7.12	NE Shear Tab
48	14.84	14.43	7.32	NE Knife Plate
49	20.54	20.17	7.55	NE Knife Plate
50	19.85	19.52	7.53	NE Knife Plate
51	98.63	30.12	28.55	Malfunctioned
52	27.78	27.41	7.87	NE Knife Plate
53	18.74	20.26	12.37	NE Gusset Plate
54	20.75	22.18	10.06	Brace
55	98.63	30.12	28.55	Malfunctioned
56	22.79	20.23	10.08	Brace
57	38.73	37.74	10.32	Brace
58	55.51	54.72	10.59	Brace
59	72.62	71.74	10.72	Brace
60	98.63	30.12	28.55	Malfunctioned
61	64.27	63.52	10.66	Brace
62	81.53	80.57	10.76	Brace

B.5. NCBF1-R4

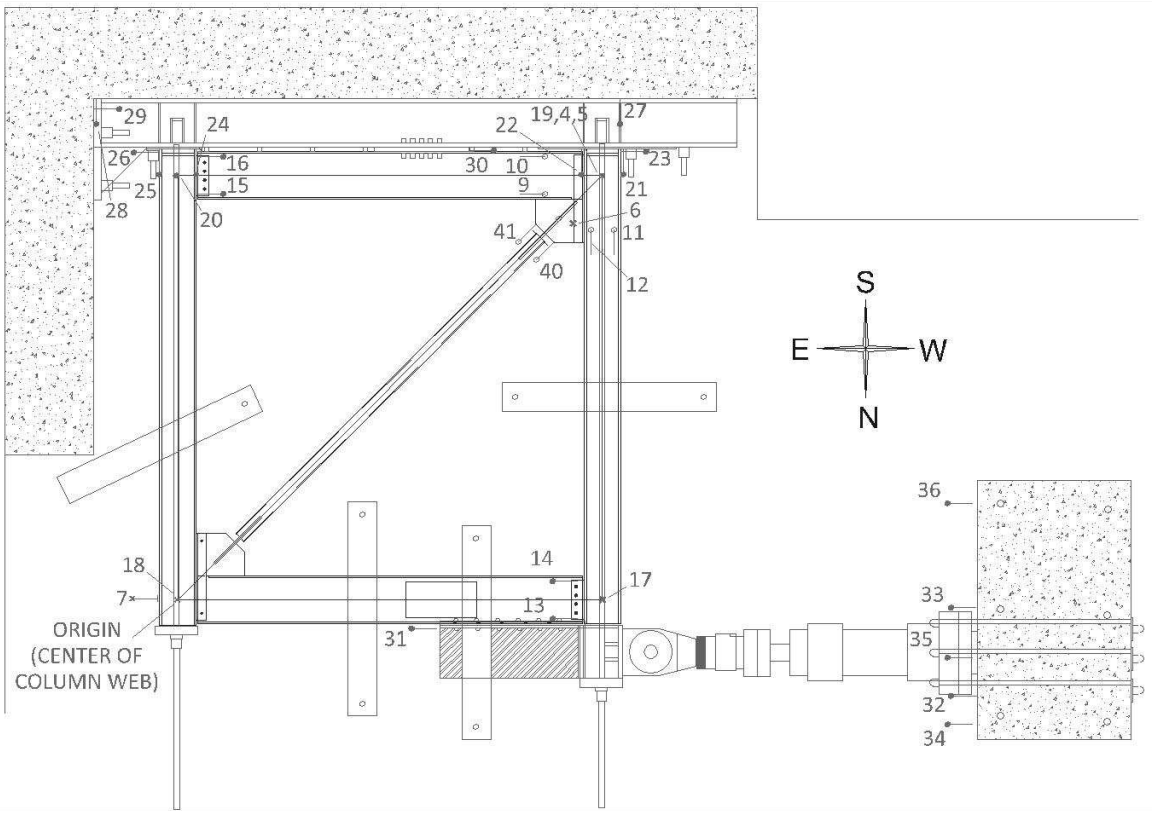

Figure B.8.11 NCBF1-R4 Potentiometer Layout

Table B.11 NCBF1-R4 Potentiometer Locations

Ch #	Name	Type	X (in)	Y (in)	Z (in)	Axis	Length	Purpose	Location
0	0	NA	x	x	x	x	x	x	x
1	1 MTS 500 Kips Load	Load Cell	x	x	x	x	x	MTS 500 kips Load cell	Actuator
2	2 MTS 1_1 LVDT	LDVT	x	x	x	x	x	Actuator LDVT	Actuator
3	3 terminator resistor	Resistor	x	x	x	x	x	Terminator resistor 3	x
4	4 FrDiagTop	P510	144	144	30	X-Y-	204	Frame Diagonal Elongation	NE,SW Work Points
5	5 FrDiagBot	P510	144	144	24	X-Y-	204	Frame Diagonal Elongation	NE,SW Work Points
6	6 BrElong	P510	111	111	-4	Z+	14	Brace Elongation	Brace Ends
7	7 FrLateral	P510	-6	0	0	X+	12	Lateral Frame Displacement	NE Corner of Frame
8	8 BrMid	P510	x	x	x	x	x	NOT USED	Brace Center
9	9 SBmHngN	D9600	125	137	2	X-	16	South Beam Plastic Hinge North	South Beam at SE Gusset
10	10 SBmHngS	D9600	125	151	2	X-	16	Beam Plastic Hinge Rotation	South Beam at SE Gusset
11	11 WColHngW	D9600	140	125	4	Y-	13	West Column Plastic Hinge West	West Column at SW Gusset
12	12 WColHngE	D9600	149	125	4	Y-	13	West Column Plastic Hinge East	West Column at SW Gusset
13	13 NWShearTabN	D600	136	-8	2	X+	2	NW Shear Tab Rotation South Flange	NW Shear Tab
14	14NWShearTabS	D600	136	7.5	2	X+	2	NW Shear Tab Rotation North Flange	NW Shear Tab
15	15 SEShearTabN	D600	8	137	2	X-	2	SE Shear Tab Rotation North Flange	SE Shear Tab
16	16 SEShearTabS	D600	8	152	2	X-	2	SE Shear Tab Rotation South Flange	SE Shear Tab
17	17 NWWPVert	P510	0	0	0	Z+	12	Vertical Displacement of Work Point	NE Work Point
18	18 NEWPVert	P510	144	0	0	Z+	12	Vertical Displacement of Work Point	NW Work Point
19	19 SWWPVert	P510	0	144	0	Z+	12	Vertical Displacement of Work Point	SE Work Point
20	20 SEWPVert	P510	144	144	0	Z+	12	Vertical Displacement of Work Point	SW Work Point
21	21 WColUpliftW	D600	150	151	0	Y+	2	W Column Uplift West Flange	SW Corner of Frame
22	22 WColUpliftE	D600	137	151	0	Y+	2	Uplift West Column, east flange	W Column Base, E Flange
23	23 WColSlip	D600	152	153	1	X-	2	W Column Lateral Slip (W Flange)	SW Corner of Frame
24	24 EColUpliftW	D600	6.5	151	0	Y+	2	E Column Uplift West Flange	SE Corner of Frame
25	25 EColUpliftE	D600	-7	151	0	Y+	2	E Column Uplift East Flange	SE Corner of Frame
26	26 EColSlip	D600	-9	153	1	X-	2	E Column Lateral Slip (E Flange)	SE Corner of Frame
27	27 ChanUpliftW	D600	150	170	7	Y+	2	Uplift of Channel Assembly	Near SE Corner of Frame
28	28 ChanUpliftE	D600	-27	170	9	Y+	2	Uplift of Channel Assembly (SW)	Near SW Corner of Frame
29	29 ChanSlip	D600	-27	172	9	X-	2	Shear Slip of Channel Assembly	SW Corner of Strong Wall
30	30 SBeamSlip	D600	99	152	0	X-	2	Slip Between S Beam and Channel Assembly	South Beam
31	31 NBeamSlip	D600	87	-9	0	X+	2	Slip Between Load Beam and North Beam	North Beam at Load Beam
32	32 ActBaseN	D600	269	-32	0	X+	2	Actuator-Reaction Block Slip (N)	Actuator Base Movement
33	33 ActBaseS	D600	269	-3	0	X+	2	Actuator-Reaction Block Slip (S)	Actuator Base Movement
34	34 RxnBlkN	D600	269	-43	-17	X+	2	Slip of Reaction Block	NW Corner of Reaction Block
35	35 RxnBlkC	D600	269	-2	-17	X+	2	Slip of Reaction Block	W Side of Reaction Block
36	36 RxnBlkS	D600	269	44	-17	X+	2	Slip of Reaction Block	SW Corner of Reaction Block
37	37 Terminal	Not Used	x	x	x	x	x	x	x
38	38 Null	D600	x	x	x	x	x	x	x
39	39 Null	D600	x	x	x	x	x	x	x
40	40 KPSWN	D9600	124	120	1	X+Y+	6	SW Knife Plate Rotation North Side	SW Knife Plate, North Side
41	41 KPSWS	D9600	119	125	1	X+Y+	6	SW Knife Plate Rotation South Side	SW Knife Plate, South Side
42	42 Term Resistor	Resistor	x	x	x	x	x	Terminal resistor	x

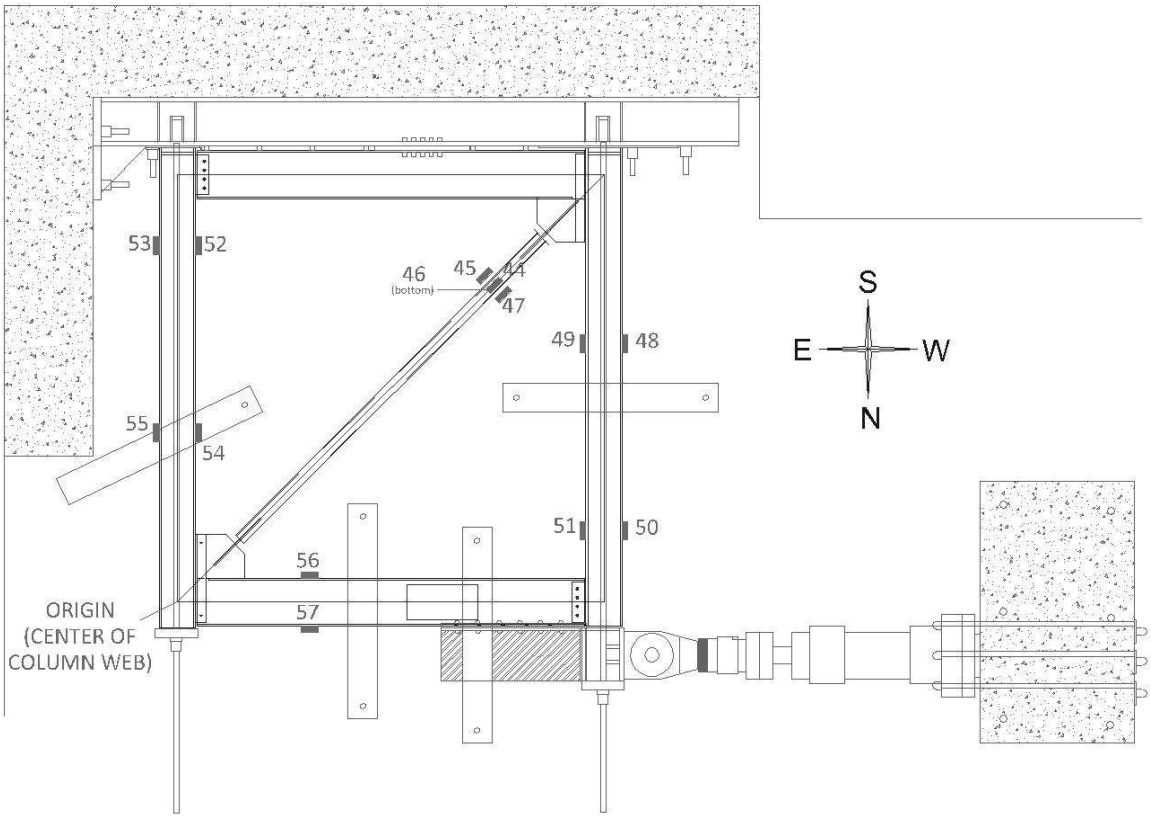

Figure B.8.12 NCBF1-R4 Strain Gauge Layout

Table B.12 NCBF1-R4 Strain Gauge Locations

Ch #	Name	Type	X (in)	Y (in)	Z (in)	Axis	Length	Purpose	Location
43	43 Str Term Resistor	Resistor	x	x	x	x	x	Terminator resistor	x
44	44 Str1	Str Gauge	107	107	-4	X+Y+	NA	Brace Forces	Brace Top
45	45 Str2	Str Gauge	110	104	0	X+Y+	NA	Brace Forces	Brace, S Side
46	46 Str3	Str Gauge	107	107	3.5	X+Y+	NA	Brace Forces	Brace Bottom
47	47 Str4	Str Gauge	105	109	0	X+Y+	NA	Brace Forces	Brace, N Side
48	48 Str5	Str Gauge	150	87	0	Y+	NA	Column Forces	W Column, S End, W Side
49	49 Str6	Str Gauge	138	87	0	Y+	NA	Column Forces	W Column, S End, E Side
50	50 Str7	Str Gauge	150	24	0	Y+	NA	Column Forces	W Column, N End, W Side
51	51 Str8	Str Gauge	138	24	0	Y+	NA	Column Forces	W Column, N End, E Side
52	52 Str9	Str Gauge	6.2	57	0	Y+	NA	Column Forces	E Dolumn, S End, W Side
53	53 Str10	Str Gauge	-6	57	0	Y+	NA	Column Forces	E Column, S End, E Side
54	54 Str11	Str Gauge	6.2	120	0	Y+	NA	Column Forces	E Column, N End, W Side
55	55 Str12	Str Gauge	-6	120	0	Y+	NA	Column Forces	E Column, N End, E Side
56	56 Str13	Str Gauge	45	-8	0	X+	NA	Beam Forces	N Beam S Side
57	57 Str14	Str Gauge	45	7.9	0	X+	NA	Beam Forces	N Beam N Side
58	58 Str Resitor	Resistor	x	x	x	x	x	Terminator resistor	x

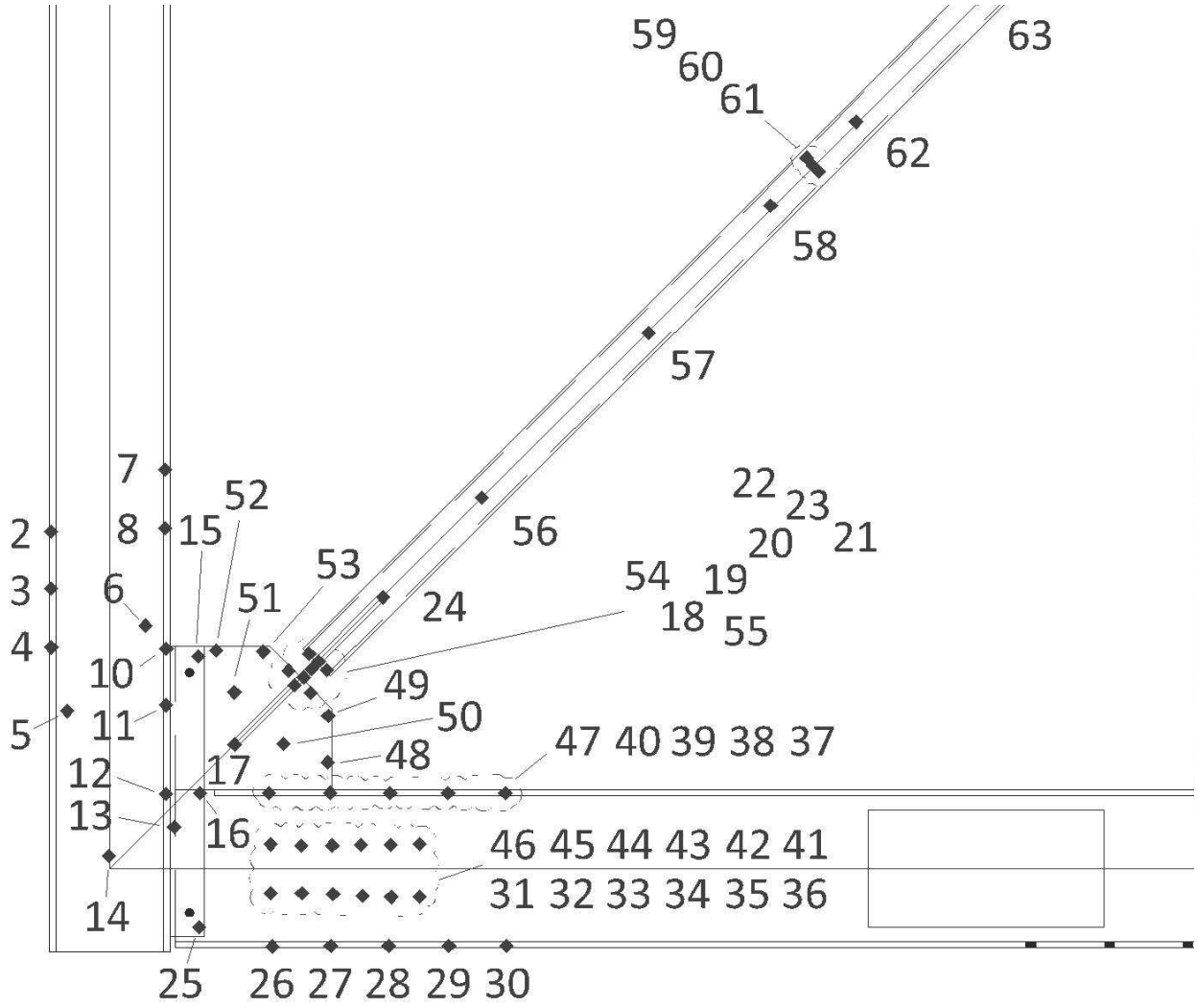

Figure B.8.13 NCBF1-R4 Optotrak Layout

Table B.13. NCBF1-R4 Optotrak Locations

Marker	X	Y	Z	Location
1	-28.84	-17.50	63.39	Malfunctioned
2	-6.00	34.47	6.00	East Column Flange
3	-5.97	28.61	6.02	East Column Flange
4	-5.96	22.60	6.01	East Column Flange
5	-4.33	16.08	10.39	East Column Web
6	3.67	24.84	-5.27	East Column Web
7	5.61	40.75	6.09	East Column Flange
8	5.64	34.78	6.09	East Column Flange
9	98.42	32.15	27.37	Malfunctioned
10	5.76	22.47	6.10	East Column Flange
11	5.74	16.70	6.09	East Column Flange
12	5.72	7.59	6.10	East Column Flange
13	6.55	4.22	8.79	NE Shear Tab
14	-0.12	1.28	-14.72	East Column Web
15	9.02	21.67	11.56	NE Shear Tab
16	9.19	7.70	11.58	NE Shear Tab
17	12.72	12.69	7.28	NE Shear Tab
18	18.84	18.71	7.32	NE Knife Plate
19	19.81	19.55	7.32	NE Knife Plate
20	20.55	20.40	7.32	NE Knife Plate
21	22.14	20.26	9.35	Brace
22	20.33	21.97	9.31	Brace
23	21.29	21.16	7.33	NE Knife Plate
24	27.85	27.72	7.36	NE Knife Plate
25	9.09	-6.00	11.59	NE Shear Tab
26	16.56	-7.97	8.54	North Beam Flange
27	22.52	-7.91	8.54	North Beam Flange
28	28.42	-7.94	8.53	North Beam Flange
29	34.57	-7.91	8.50	North Beam Flange
30	40.44	-7.93	8.51	North Beam Flange
31	16.42	-2.53	11.97	North Beam Web
32	19.57	-2.54	11.96	North Beam Web
33	22.76	-2.60	11.95	North Beam Web
34	25.78	-2.80	11.96	North Beam Web
35	28.68	-2.91	11.95	North Beam Web
36	31.60	-2.90	11.94	North Beam Web
37	40.31	7.73	8.63	North Beam Flange
38	34.49	7.70	8.63	North Beam Flange
39	28.58	7.73	8.63	North Beam Flange
40	22.48	7.74	8.63	North Beam Flange
41	31.60	2.47	11.97	North Beam Web
42	28.63	2.39	11.98	North Beam Web
43	25.58	2.39	11.98	North Beam Web
44	22.69	2.36	11.97	North Beam Web
45	19.51	2.32	11.98	North Beam Web
46	16.39	2.46	11.98	North Beam Web
47	16.25	7.72	8.63	North Beam Flange
48	22.20	10.87	12.05	NE Gusset Plate
49	22.26	15.59	12.17	NE Gusset Plate
50	17.71	12.73	12.05	NE Gusset Plate
51	12.70	18.00	12.03	NE Gusset Plate
52	10.87	22.31	11.99	NE Gusset Plate
53	15.65	22.16	12.06	NE Gusset Plate
54	18.19	20.24	12.09	NE Gusset Plate
55	20.47	17.93	12.17	NE Gusset Plate
56	37.89	37.91	9.37	Brace
57	54.95	54.77	9.36	Brace
58	67.38	67.76	9.37	Brace
59	71.04	72.67	9.37	Brace
60	71.66	71.87	9.38	Brace
61	72.29	71.23	9.36	Brace
62	76.06	76.32	9.37	Brace
63	88.48	88.99	9.38	Brace

B.6. NCBF1-R5

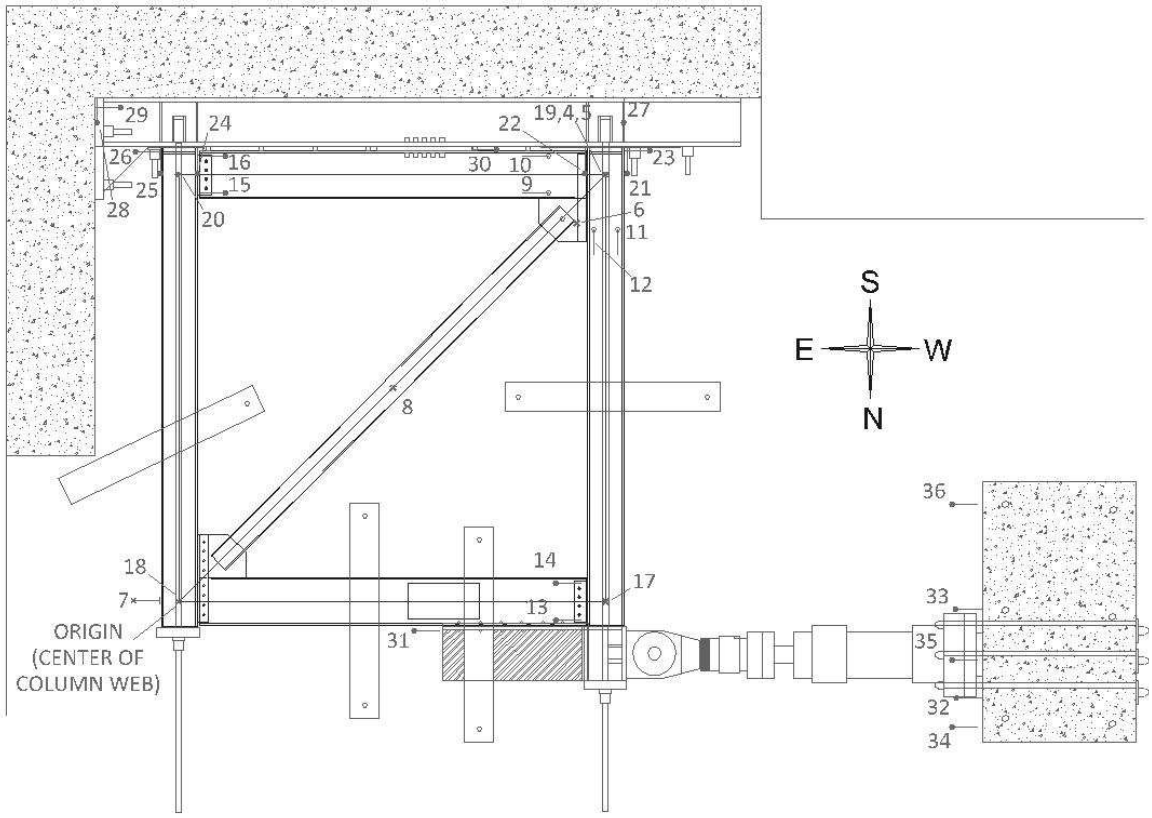

Figure B.8.14 NCBF1-R5 Potentiometer Layout

Table B.14 NCBF1-R5 Potentiometer Locations

Ch #	Name	Type	X (in)	Y (in)	Z (in)	Axis	Length	Purpose	Location
0	0	NA	x	x	x	x	x	x	x
1	1 MTS 500 Kips Load	Load Cell	x	x	x	x	x	MTS 500 kips Load cell	Actuator
2	2 MTS 1_1 LVDT	LDVT	x	x	x	x	x	Actuator LDVT	Actuator
3	3 terminator resistor	Resistor	x	x	x	x	x	Terminator resistor 3	x
4	4 FrDiagTop	P510	144	144	30	X-Y-	204	Frame Diagonal Elongation	NE,SW Work Points
5	5 FrDiagBot	P510	144	144	24	X-Y-	204	Frame Diagonal Elongation	NE,SW Work Points
6	6 BrElong	P510	111	111	-4	Z+	14	Brace Elongation	Brace Ends
7	7 FrLateral	P510	-6	0	0	X+	12	Lateral Frame Displacement	NE Corner of Frame
8	8 BrMid	P510	72	72	-4	Z+	14	NOT USED	Brace Center
9	9 SBmHngN	D9600	125	137	2	X-	16	South Beam Plastic Hinge North	South Beam at SE Gusset
10	10 SBmHngS	D9600	125	151	2	X-	16	Beam Plastic Hinge Rotation	South Beam at SE Gusset
11	11 WColHngW	D9600	140	125	4	Y-	13	West Column Plastic Hinge West	West Column at SW Gusset
12	12 WColHngE	D9600	149	125	4	Y-	13	West Column Plastic Hinge East	West Column at SW Gusset
13	13 NWShearTabN	D600	136	-8	2	X+	2	NW Shear Tab Rotation South Flange	NW Shear Tab
14	14NWShearTabS	D600	136	7.5	2	X+	2	NW Shear Tab Rotation North Flange	NW Shear Tab
15	15 SEShearTabN	D600	8	137	2	X-	2	SE Shear Tab Rotation North Flange	SE Shear Tab
16	16 SEShearTabS	D600	8	152	2	X-	2	SE Shear Tab Rotation South Flange	SE Shear Tab
17	17 NWWPVert	P510	0	0	0	Z+	12	Vertical Displacement of Work Point	NE Work Point
18	18 NEWPVert	P510	144	0	0	Z+	12	Vertical Displacement of Work Point	NW Work Point
19	19 SWWPVert	P510	0	144	0	Z+	12	Vertical Displacement of Work Point	SE Work Point
20	20 SEWPVert	P510	144	144	0	Z+	12	Vertical Displacement of Work Point	SW Work Point
21	21 WColUpliftW	D600	150	151	0	Y+	2	W Column Uplift West Flange	SW Corner of Frame
22	22 WColUpliftE	D600	137	151	0	Y+	2	Uplift West Column, east flange	W Column Base, E Flange
23	23 WColSlip	D600	152	153	1	X-	2	W Column Lateral Slip (W Flange)	SW Corner of Frame
24	24 EColUpliftW	D600	6.5	151	0	Y+	2	E Column Uplift West Flange	SE Corner of Frame
25	25 EColUpliftE	D600	-7	151	0	Y+	2	E Column Uplift East Flange	SE Corner of Frame
26	26 EColSlip	D600	-9	153	1	X-	2	E Column Lateral Slip (E Flange)	SE Corner of Frame
27	27 ChanUpliftW	D600	150	170	7	Y+	2	Uplift of Channel Assembly	Near SE Corner of Frame
28	28 ChanUpliftE	D600	-27	170	9	Y+	2	Uplift of Channel Assembly (SW)	Near SW Corner of Frame
29	29 ChanSlip	D600	-27	172	9	X-	2	Shear Slip of Channel Assembly	SW Corner of Strong Wall
30	30 SBeamSlip	D600	99	152	0	X-	2	Slip Between S Beam and Channel Assembly	South Beam
31	31 NBeamSlip	D600	87	-9	0	X+	2	Slip Between Load Beam and North Beam	North Beam at Load Beam
32	32 ActBaseN	D600	269	-32	0	X+	2	Actuator-Reaction Block Slip (N)	Actuator Base Movement
33	33 ActBaseS	D600	269	-3	0	X+	2	Actuator-Reaction Block Slip (S)	Actuator Base Movement
34	34 RxnBlkN	D600	269	-43	-17	X+	2	Slip of Reaction Block	NW Corner of Reaction Block
35	35 RxnBlkC	D600	269	-2	-17	X+	2	Slip of Reaction Block	W Side of Reaction Block
36	36 RxnBlkS	D600	269	44	-17	X+	2	Slip of Reaction Block	SW Corner of Reaction Block
37	37 Terminal	Not Used	x	x	x	x	x	x	x
38	38 Null	D600	x	x	x	x	x	x	x
39	39 Null	D600	x	x	x	x	x	x	x
40	40 KPSWN	D9600	x	x	x	x	x	SW Knife Plate Rotation North Side	SW Knife Plate, North Side
41	41 KPSWS	D9600	x	x	x	x	x	SW Knife Plate Rotation South Side	SW Knife Plate, South Side
42	42 Term Resistor	Resistor	x	x	x	x	x	Terminal resistor	x

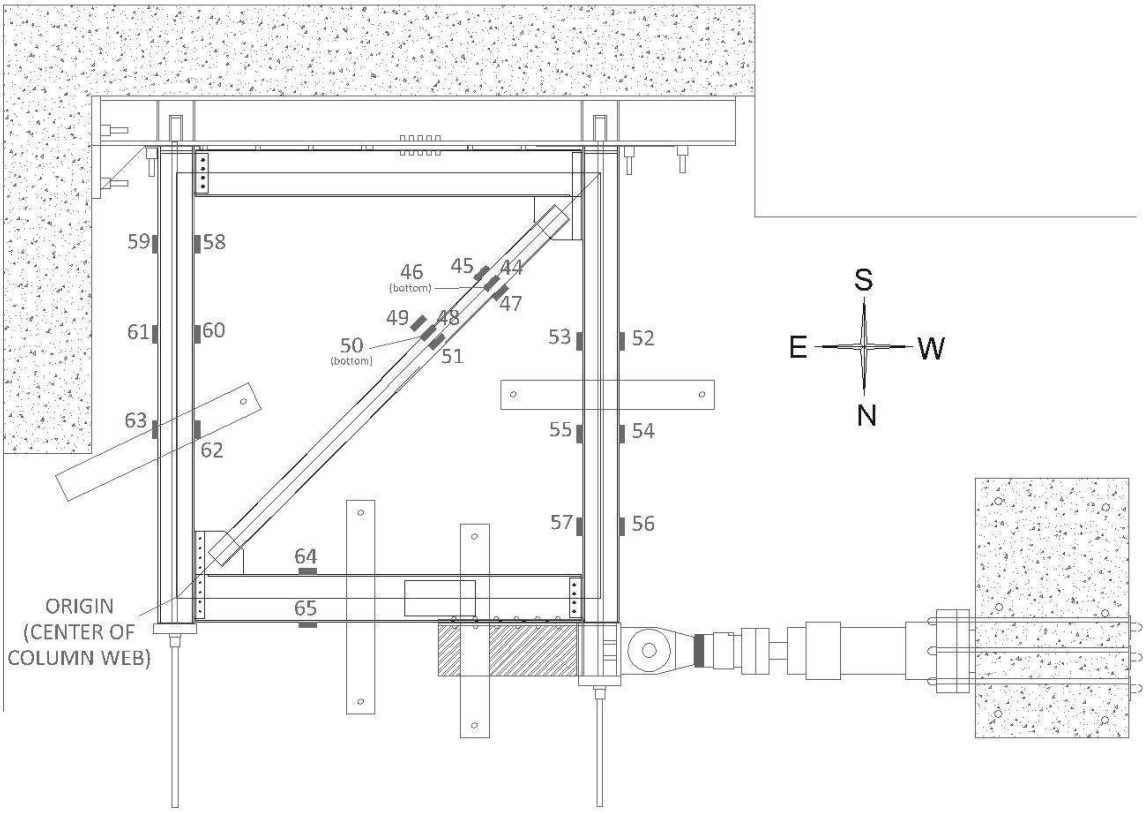

Figure B.8.15 NCBF1-R5 Stain Gauge Layout

Table B.15 NCBF1-R5 Strain Gauge Locations

Ch #	Name	Type	X (in)	Y (in)	Z (in)	Axis	Length	Purpose	Location
43	43 Str Term Resistor	Resistor	x	x	x	x	x	Terminator resistor	x
44	44 Str1	Str Gauge	107	107	-4	X+Y+	NA	Brace Forces	Brace Top, 6th Point
45	45 Str2	Str Gauge	110	104	0	X+Y+	NA	Brace Forces	Brace, S Side, 6th Point
46	46 Str3	Str Gauge	107	107	3.5	X+Y+	NA	Brace Forces	Brace Bottom, 6th Point
47	47 Str4	Str Gauge	105	109	0	X+Y+	NA	Brace Forces	Brace, N Side, 6th Point
48	48 Str5	Str Gauge	87	87	-4	X+Y+	NA	Brace Forces	Brace Top, 3rd Point
49	49 Str6	Str Gauge	90	84	0	X+Y+	NA	Brace Forces	Brace, S Side, 3rd Point
50	50 Str7	Str Gauge	87	87	3.5	X+Y+	NA	Brace Forces	Brace Bottom, 3rd Point
51	51 Str8	Str Gauge	85	90	0	X+Y+	NA	Brace Forces	Brace, N Side, 3rd Point
52	52 Str9	Str Gauge	150	87	0	Y+	NA	Column Forces	W Column, S End, W Side
53	53 Str10	Str Gauge	138	87	0	Y+	NA	Column Forces	W Column, S End, E Side
54	54 Str11	Str Gauge	150	55	0	Y+	NA	Column Forces	W Column, Center, W Side
55	55 Str12	Str Gauge	138	55	0	Y+	NA	Column Forces	W Column, Center, E Side
56	56 Str13	Str Gauge	150	24	0	Y+	NA	Column Forces	W Column, N End, W Side
57	57 Str14	Str Gauge	138	24	0	Y+	NA	Column Forces	W Column, N End, E Side
58	58 Str15	Str Gauge	6.2	57	0	Y+	NA	Column Forces	E Dolumn, S End, W Side
59	59 Str16	Str Gauge	-6	57	0	Y+	NA	Column Forces	E Column, S End, E Side
60	60 Str17	Str Gauge	6.2	24	0	Y+	NA	Column Forces	E Dolumn, Center, W Side
61	61 Str18	Str Gauge	-6	32	0	Y+	NA	Column Forces	E Column, Center, E Side
62	62 Str19	Str Gauge	6.2	120	0	Y+	NA	Column Forces	E Column, N End, W Side
63	63 Str20	Str Gauge	-6	120	0	Y+	NA	Column Forces	E Column, N End, E Side
64	64 Str21	Str Gauge	45	-8	0	X+	NA	Beam Forces	N Beam S Side
65	65 Str 22	Str Gauge	45	7.9	0	X+	NA	Beam Forces	N Beam N Side
66	58 Str Resitor	Resistor	x	x	x	x	x	Terminator resistor	x

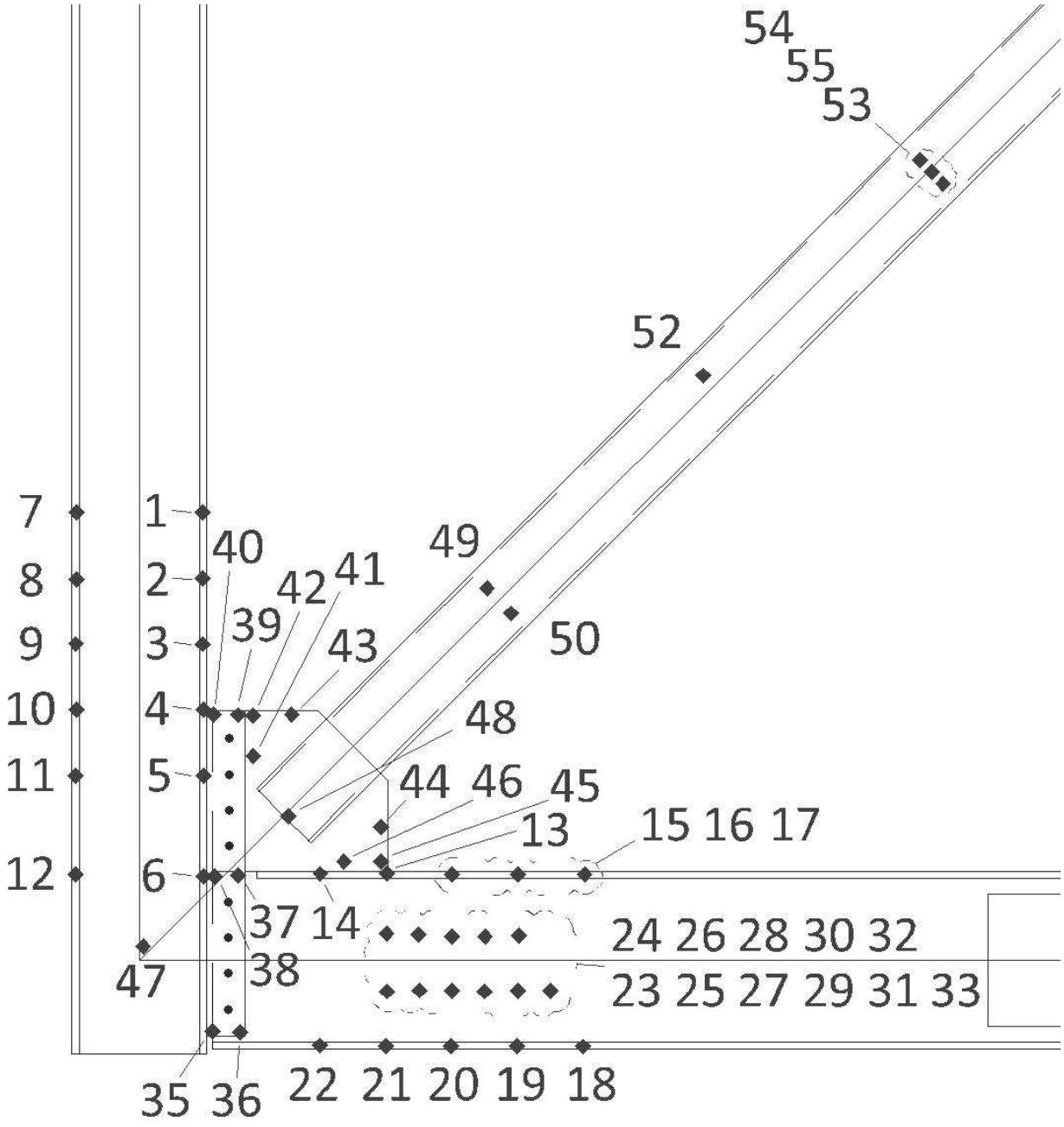

Figure B.8.16 NCBF1-R5 Optotrak Layout

Table B.16 NCBF1-R5 Optotrak Locations

Marker	X	Y	Z	Location
1	5.77	40.79	6.09	East Column Flange
2	5.77	34.75	6.10	East Column Flange
3	5.71	28.78	6.11	East Column Flange
4	5.84	22.81	6.11	East Column Flange
5	5.82	16.77	6.09	East Column Flange
6	5.82	7.65	6.08	East Column Flange
7	-5.73	40.76	6.14	East Column Flange
8	-5.76	34.69	6.13	East Column Flange
9	-5.80	28.79	6.12	East Column Flange
10	-5.75	22.83	6.11	East Column Flange
11	-5.81	16.80	6.11	East Column Flange
12	-5.83	7.84	6.09	East Column Flange
13	22.57	7.88	3.59	North Beam Flange
14	16.46	7.86	3.58	North Beam Flange
15	28.47	7.80	3.58	North Beam Flange
16	34.49	7.79	3.57	North Beam Flange
17	40.55	7.80	3.58	North Beam Flange
18	40.43	-7.85	3.66	North Beam Flange
19	34.40	-7.81	3.63	North Beam Flange
20	28.38	-7.83	3.61	North Beam Flange
21	22.44	-7.79	3.58	North Beam Flange
22	16.41	-7.77	3.56	North Beam Flange
23	22.52	-2.84	0.25	North Beam Web
24	22.49	2.41	0.21	North Beam Web
25	25.49	-2.75	0.24	North Beam Web
26	25.42	2.32	0.19	North Beam Web
27	28.49	-2.78	0.25	North Beam Web
28	28.49	2.19	0.20	North Beam Web
29	31.43	-2.83	0.25	North Beam Web
30	31.47	2.16	0.20	North Beam Web
31	34.47	-2.82	0.26	North Beam Web
32	34.58	2.24	0.19	North Beam Web
33	37.45	-2.78	0.25	North Beam Web
34	99.38	30.99	-15.68	Malfunctioned
35	6.67	-6.46	0.56	NE Shear Tab
36	9.12	-6.58	0.56	NE Shear Tab
37	8.96	7.75	0.55	NE Shear Tab
38	6.85	7.66	0.56	NE Shear Tab
39	9.01	22.33	0.48	NE Shear Tab
40	6.72	22.35	0.51	NE Shear Tab
41	10.36	18.62	0.14	NE Gusset Plate
42	10.35	22.25	0.08	NE Gusset Plate
43	13.86	22.34	0.18	NE Gusset Plate
44	21.98	12.14	0.19	NE Gusset Plate
45	21.99	9.00	0.12	NE Gusset Plate
46	18.63	8.98	0.14	NE Gusset Plate
47	0.32	1.29	26.78	East Column Web
48	13.52	13.11	5.74	Brace
49	31.66	33.84	3.86	Brace
50	33.85	31.57	3.88	Brace
51	99.38	30.99	-15.68	Malfunctioned
52	51.40	53.22	3.77	Brace
53	73.23	70.70	3.71	Brace
54	71.14	72.82	3.69	Brace
55	72.20	71.75	3.70	Brace
56	99.38	30.99	-15.68	Malfunctioned
57	65.99	37.50	-17.67	Malfunctioned
58	54.80	34.27	-5.35	Malfunctioned

Appendix C: Experimental Setup

C.1. Strong Floor and Strong Wall

The strong floor and strong wall are permanent fixtures in the University of Washington structural engineering lab. The strong floor consists of a 30 inch thick prestressed concrete floor with embedded threaded rod tie downs. The tie downs are arranged in a 36 inch grid, except in the area near the strong wall, where they are spaced at 18 inches for greater flexibility in experimental setups. The strong wall is 13 feet 6 inches tall and attached to the southeast corner of the strong wall in an L-shaped configuration. The wall consists of 30 inch thick prestressed concrete with an 18 inch grid of conduits for anchoring components. Both the strong wall and the strong floor can reasonably be considered rigid supports during experiments, given the high level of strength and stiffness they provide.

C.2. Reaction Block and Actuator

An MTS hydraulic actuator was used to apply load to the specimen and was controlled using an MTS controller. The actuator runs at 3000 psi hydraulic pressure and has a maximum load capacity of 470 kips when pushing and 330 kips when pulling. Actuator pushing coincides with brace tension, when the lateral resistance of the frame is higher, thus allowing the testing of stronger specimens. The actuator stroke range is ±10 inches.

The head of the actuator was attached to a swivel, which prevents transverse loads from being carried by the actuator. This protects the actuator from damage and ensures that only lateral load is applied to the specimen. The swivel was attached to the loading beam with four 1 inch diameter hex bolts. Actuator load was recorded using the actuator load cell, positioned behind the swivel. This load cell and the onboard LDVT provided continuous feedback to the controller to allow for accurate displacement control of the specimen. At its base, the actuator was bolted to a 4 inch thick steel adaptor plate. The actuator was attached to the reaction block using six 1 1/8 inch diameter B-7 threaded rods, each stressed to 60 kips. Between the adapter plate and the reaction block was an elastomeric bearing pad, which provides rotational freedom for the actuator at its base. This serves to reduce moments carried by the actuator, and to accommodate the small lateral movement of the actuator due to displacements of the frame.
The reaction block consists of a 6’x8’x4’ reinforced concrete block with horizontal conduits configured for mounting actuators and 6 vertical conduits for anchoring the block. The reaction block was anchored to the strong floor using 6 Williams rods 2 inches in diameter and stressed to 220 kips each. Hydro-Stone

was poured between the reaction block and the strong floor and between the steel washer plates and the reaction block. This provided a uniform contact surface, increasing the fixity of the reaction block.

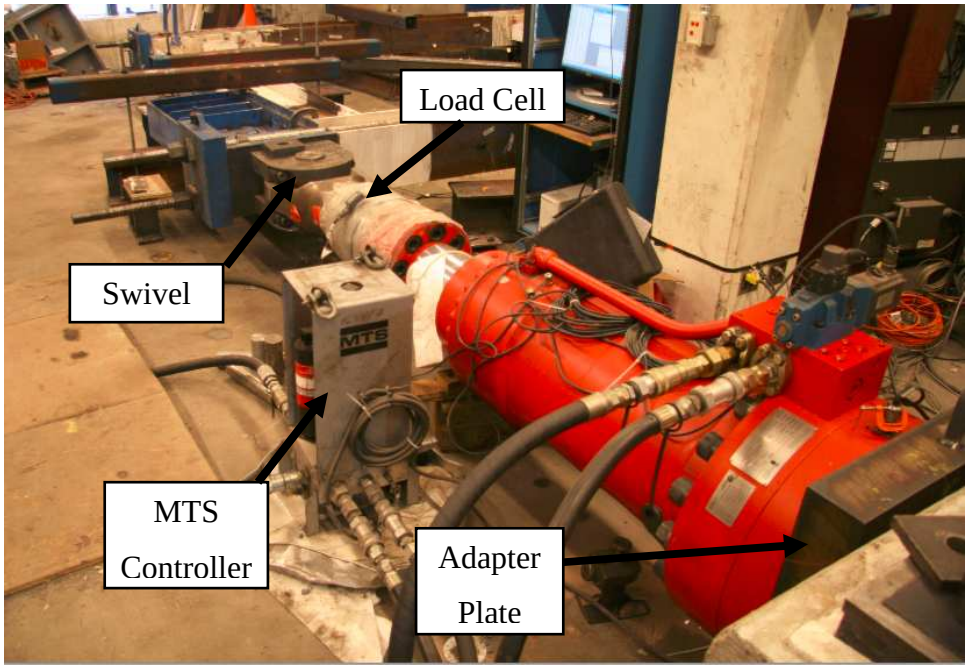

Figure C.1: Photograph of MTS Actuator

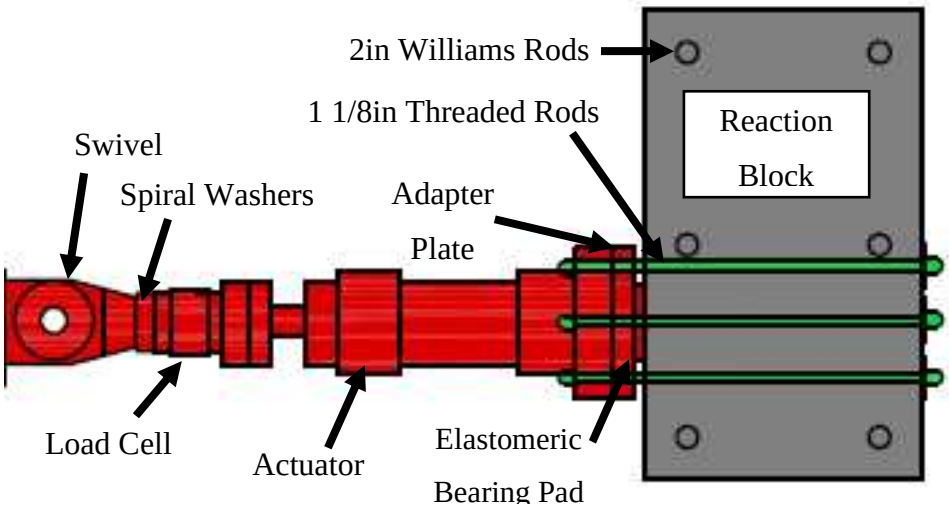

Figure C.2: Schematic of Actuator and Reaction Block

C.3. Load Beam

Load was transferred between the actuator head swivel and the North beam of the specimen through a built-up W21x62 section. The load beam was bolted to the actuator head swivel using hex head bolts and

to the North flange of the North beam of each specimen using 10-1 inch diameter A490 bolts. The beam is strengthened with several plates to prevent damage and distribute load. A 2 inch end plate provides a contact surface for the actuator head. In conjunction with a second 2 inch plate, it provides continuity of the column flanges to the cap plate where axial prestressing load is applied. This prevents local buckling of the load beam, which must carry the full column axial load through its depth in this region. 4 additional stiffener plates are provided at the opposite end of the load beam to prevent local buckling of the load beam flanges.

The eccentricity between the line of action of the actuator force and the center of the beam depth causes a moment to develop in the load beam. This moment results in a compressive force at the leading edge of the load beam where it contacts the flange of the North beam of the specimen. This compressive force causes local buckling of the web and beam of the specimen. Because this damage is a result of the loading conditions and not reflective of performance of a real system, a web double plate is provided for the beam to reduce the severity of this damage.

The positioning of the load beam is intended to be reflective of loading conditions in a structure, where lateral load typically enters the frame through a shear connection between the floor slab and the beam. Providing a full-length shear connection would increase the stiffness of the beam by an unacceptable margin, so load is instead applied over only 40% of the length.

Figure C.3: Load Beam

C.4. Channel Reaction Assembly

The channel assembly was designed by Shawn Johnson for the first series of SCBF tests (Johnson 2005). It has been used for all subsequent braced frame experiments, including the current test series.. The assembly consists of two C15x50 channel sections built up with steel plates. The assembly was post-tensioned to the strong wall to provide resistance to shear and overturning loads from the specimen.

The assembly connection has a nominal shear capacity of 589 kips, which is designed to resist the maximum horizontal force that the actuator can apply, 470 kips. Ten 1 inch diameter bolts connect the South beam of the specimen to the channel assembly to provide shear transfer. The assembly was tensioned to the strong wall with five 1 3/4 inch diameter Williams rods tensioned to 220 kips and seven 1 inch diameter threaded rods tensioned to 60 kips. The contact surface between the assembly and the strong wall was filled with Hydro-Stone to create a smoother contact surface.
In 2007, repairs and modifications were made to the channel assembly. The bearing plates at the bases of the columns were replaced due to local deformations from a total of 23 frame tests. Additional 1/2 inch bearing plates were added at the locations of the Williams rods to better distribute the load to the assembly.

C.5. Axial Load System

Axial load was applied to each of the columns to simulate gravity loads from the structure. Two 1 3/4 inch diameter Williams rods were tensioned in each column, with one on each side of the web. Each rod was tensioned to 225 kips, providing an axial load of 450 kips to each column. The axial load was applied using a short-stroke hydraulic ram. 4 inch thick cap plates provided a bearing surface for the nuts on the rods to transfer the axial load to the column. At the column bases, the rods pass through HSS4x4x1/2 tubes welded to the channel reaction assembly. The ends of the rods were fastened with Williams spherical hex nuts and dish plates. The interface surface between the nuts and plates was cated with machine grease. This system allowed the rods to rotate freely at the ends, preventing bending moments from developing when lateral drift was applied to the frame.

Figure C.4: East Column Cap Plate and Axial Load Rods

Figure C.5: Axial Load Rod Anchor for East Column

C.6. Out-of-Plane Restraints

Out-of-Plane (OOP) restraints were used to prevent the specimen from moving excessively out of plane while not restricting in-plane motion. Figures 4.3.6.1 through 4.3.6.4 show images of the out of plane

restraints used, and figure 4.3.6.5 shows a schematic of the out of plane restraints. Two restraints were applied on the North beam of the specimen along its length. These simulate the restraint that would be imposed by the floor slab in a structure. One restraint was applied to each column at mid-height. These simulate the fixity of columns coming from beams in both orthogonal directions, as well as continuity with columns in floors above and below. The layout of the testing area did not permit the restraint of the corners of the frame, so the columns are braced at mid-height as an approximation. The North Beam was braced at 2 points along its length, simulating the lateral restraint provided by a floor slab in a typical structure. The South Beam was effectively restrained by the bolts fastening it to the reaction assembly.

The base of the OOPs were wide flange sections, which were tensioned to the strong floor with 1 inch diameter threaded rods. The top of the restraints were HSS5x5x3/8. Which were tensioned with ¾" threaded rods to the wide flange restraints. Sliding interface was created by affixing slotted nylon rods to the flanges of the beams and columns, which slid on greased stainless steel plates attached to the restraints. This created a low-friction interface, minimizing restrain to in-plane movement.

Figure C.6: Out-of-Plane Restraint for East Column

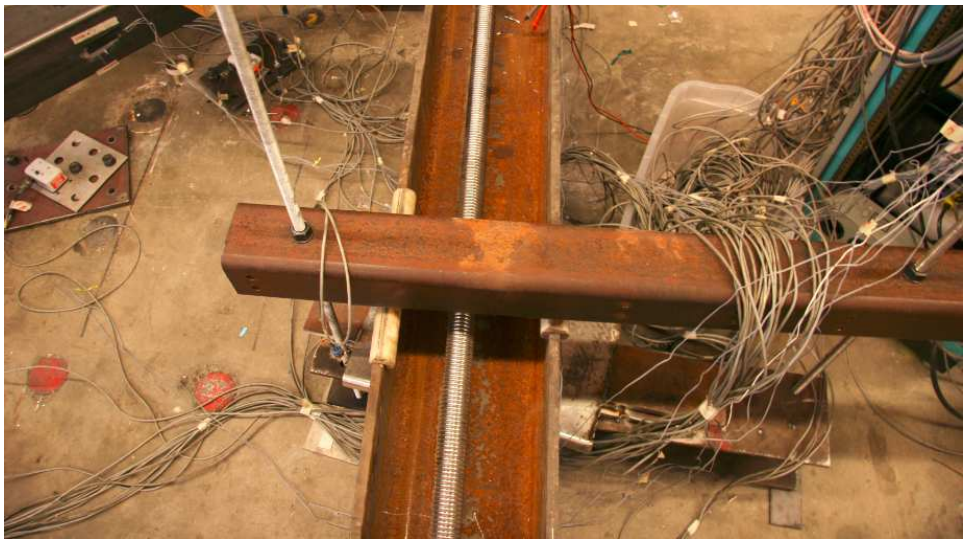

Figure C.7: Out-of-Plane Restraint for West Column

Figure C.8: Out-of-Plane Restraint Load Beam

Figure C.9: Out-of-Plane Restraint for North Beam

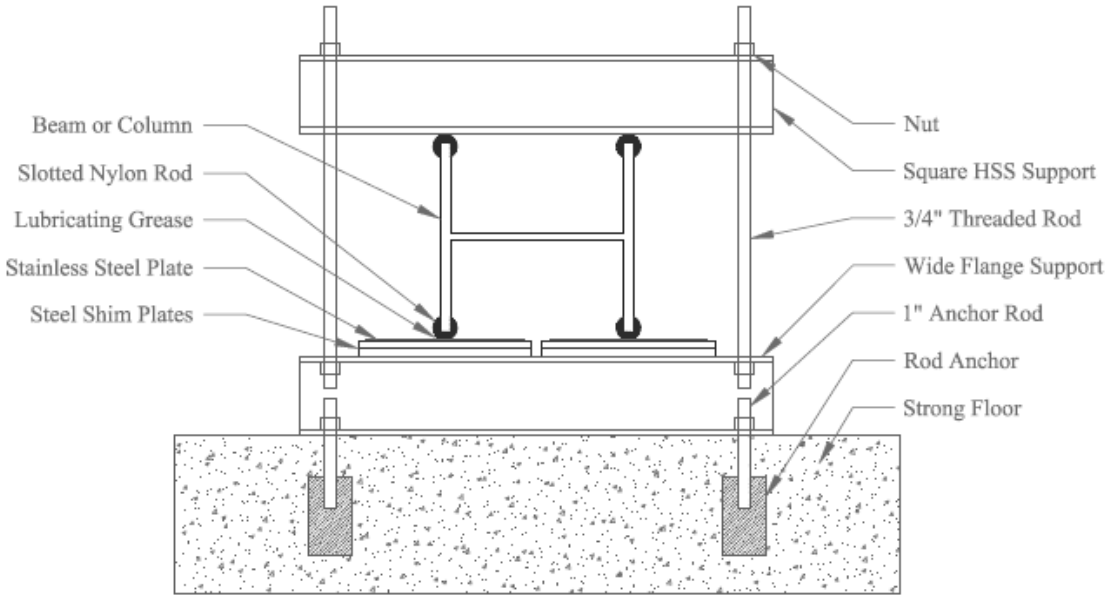

Figure C.10: Schematic for Out-of-Plane Restraints

Appendix D: Data Analysis Plots

D.1. Brace Elongation

The axial elongation of the brace is of interest because this elongation comprises the majority of lateral deformation of a typical braced frame. It was measured using a potentiometer attached to each end of the brace. This measurement requires correction to remove the artificial elongation induced by the brace end rotation. Figure D.1 shows the induced error in the brace elongation for one end of the brace. δ_m is the measured elongation, and δ_t is the true brace elongation. When making the correction, the error, which is the difference between the two values, must be doubled because this figure accounts for only one end of the brace. Equation (D.1-1) was used for the correction.

(D.1-1)

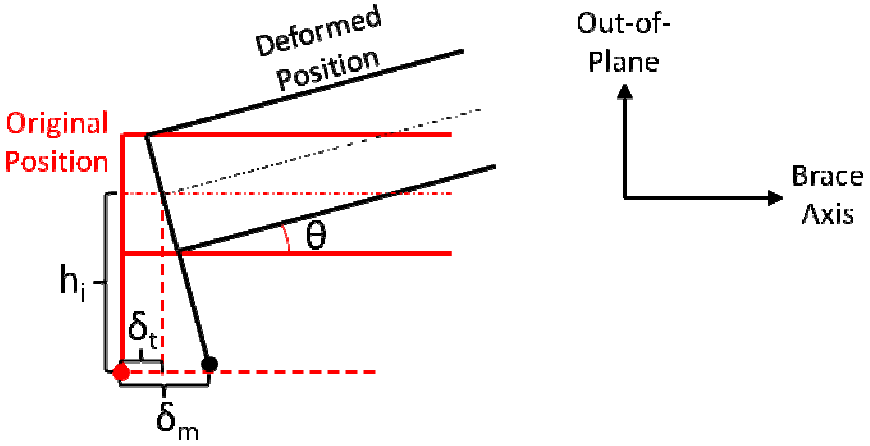

Figure D.1 Brace Elongation Correction

When the brace end rotations become large, the corrected values often differed from the measured values by more than 50%. Because such a large contribution to the behavior comes from error, the results become less reliable. Figure D.2 gives the brace elongation envelopes for the specimens for which a reasonable result could be obtained,

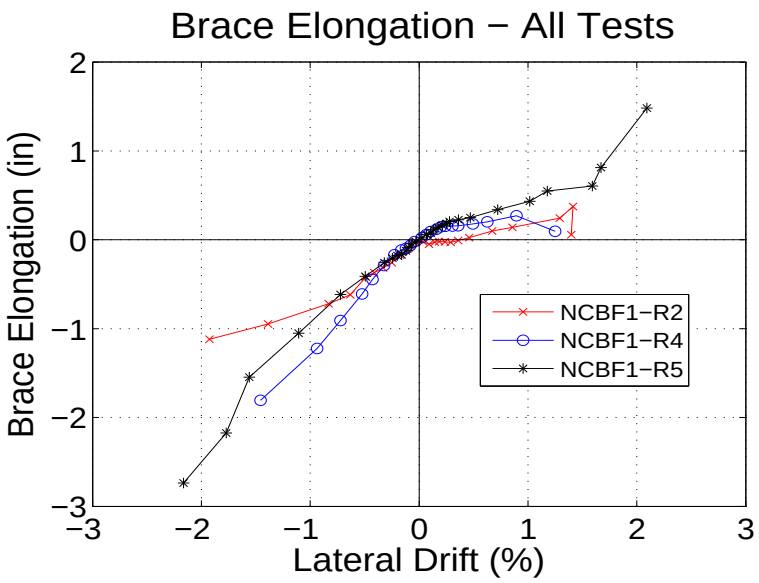

Figure D.2 Brace Elongation Envelopes

D.2. Connection Elongation

As mentioned in Section D.1, there is a difference between the measured values for brace elongation and frame diagonal elongation. The remaining elongation must occur in the region between the brace ends and the work points. This includes the gusset plates, shear tabs, and a portion of the column at each end of the brace, as shown in Figure D.3.

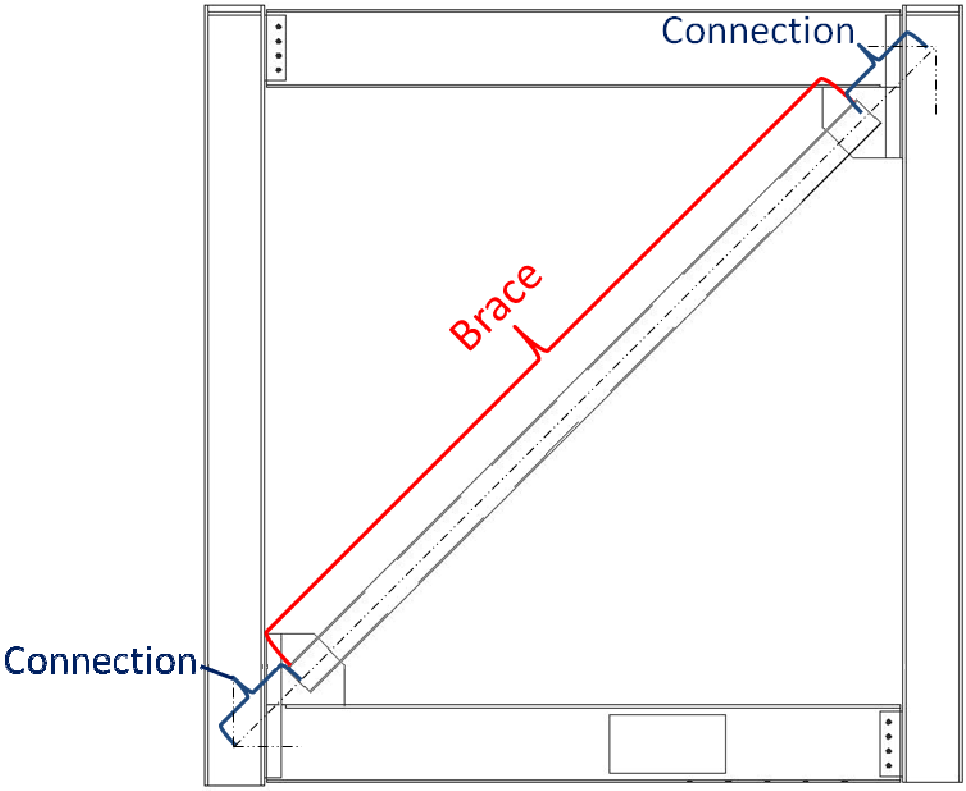

Figure D.3 Connection Elongation Schematic

Figure D.4 shows the connection elongation for the tests for which brace elongation data was available. There is strong consistency in the data when the brace is in tension. The combined elongation of the two connections reaches 1 inch for all three specimens. These elongation values were larger than those for the braces. Figure D.5, Figure D.6, and Figure D.7 give the brace elongation and connection elongation for each specimen normalized to the corresponding length.

Also of interest is the trend observed in compression in specimens NCBF1-R4 and NCBF1-R5. After brace buckling occurs, the elongation of the gusset plate becomes positive. What is likely occurring is residual tensile strain in the gusset plate. After brace buckling, the axial force in the brace is significantly higher in tension than in compression. As a result, the gusset plate is likely to go through large plastic deformations in the tensile direction. If these deformations are large enough, the connection might retain some residual positive elongation, even when the brace is in compression. This is an interesting phenomenon, and it emphasizes the degree to which the weakness of the connecting elements influences the frame behavior.

It should be noted that the connection elongation is derived from a combination of the brace elongation, brace end rotation, and frame diagonal elongation measurements. As such, there may be substantial error in the quantities reported here.

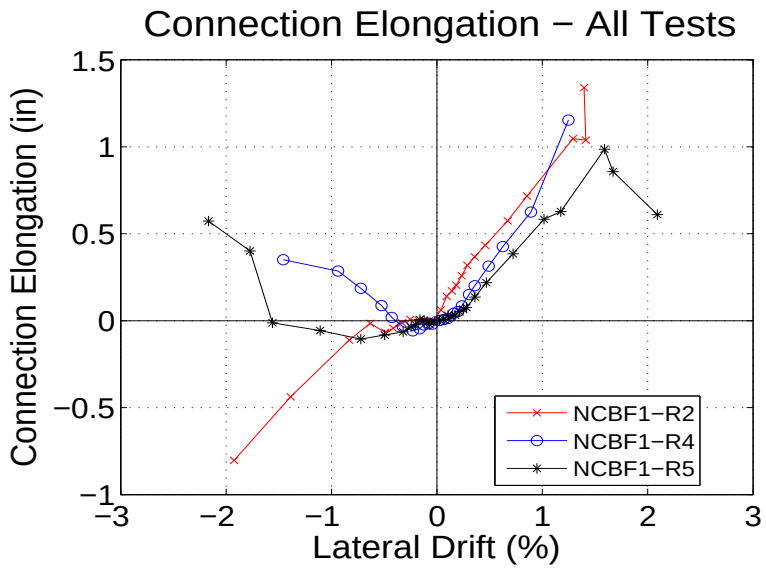

Figure D.4 Connection Elongation

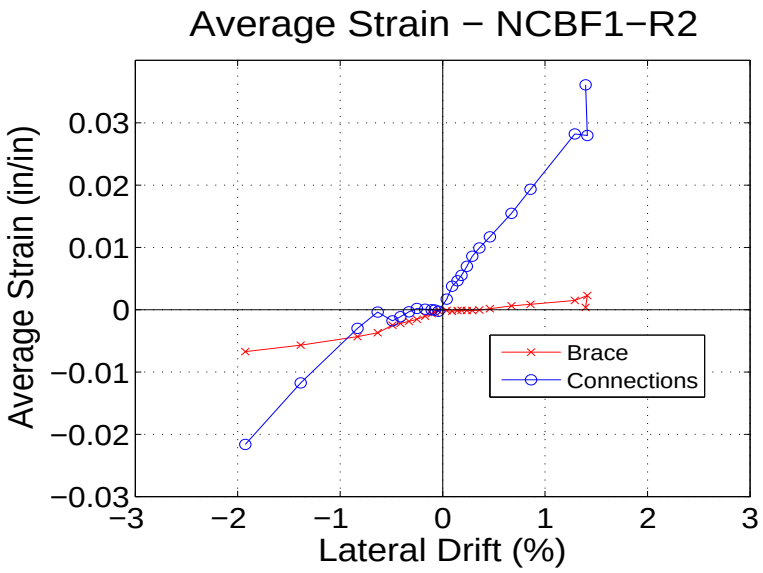

Figure D.5 NCBF1-R2 Average Strain

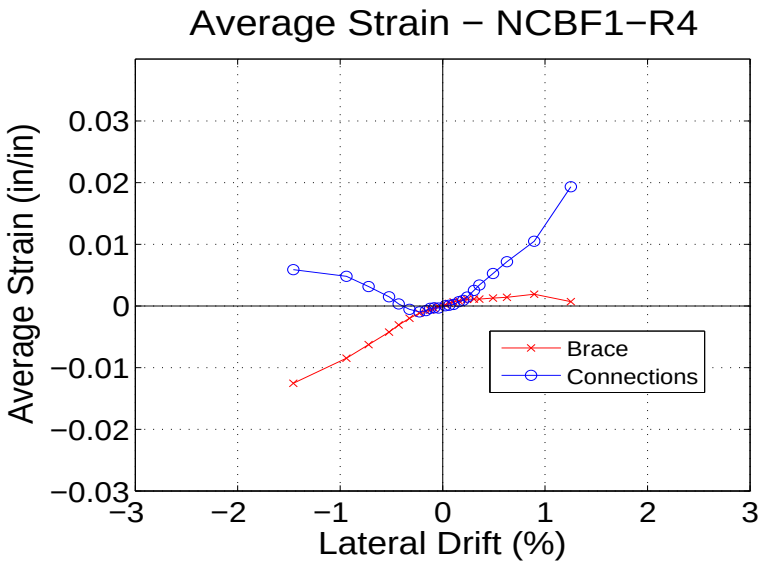

Figure D.6 NCBF1-R4 Average Strain

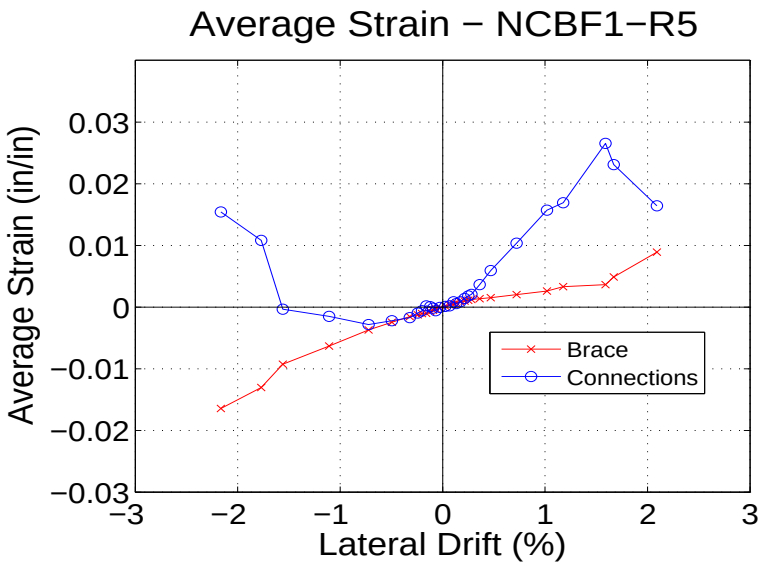

Figure D.7 NCBF1-R5 Average Strain

D.3. Construction of ASCE 41 Backbone Curves

When constructing the ASCE 41 backbone curves for the 2-bay braced frame subsystem, one procedural factor can impact the results. In Section 7.2, the methodology for creating the combined load-drift envelope is described. The successive peaks of the load and drift histories are used to create the points on the combined load-drift envelope. This is shown in Figure 7.7 amd Figure 7.8, which are shown below for reference as Figure D.8 and Figure D.9.

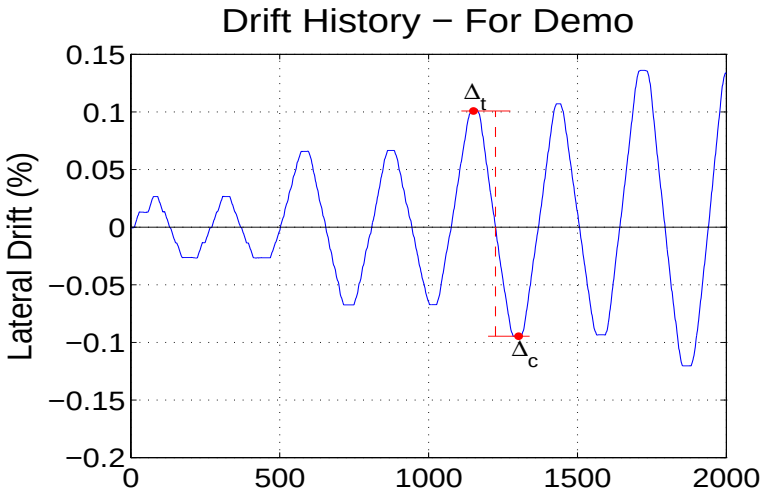

Figure D.8 Experimental Displacements at Successive Peaks

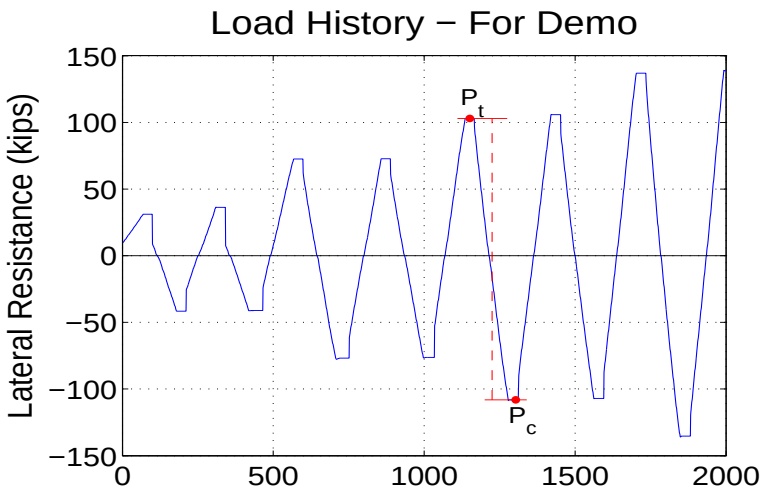

Figure D.9 Experimental Loads at Successive Peaks

Below are shown plots for each of the specimens which compare the combined load-drift envelope computed in two different ways. The first is to take each tension peak and the following compression peak to create each point on the envelope. This is called "Tension First" below. The second method is to take each compressive peak with the following tension peak, called "Compression First" below. As these plots demonstrate, the procedure used has a small impact on the shape of the envelope, particularly when the resistance of the system changes rapidly.

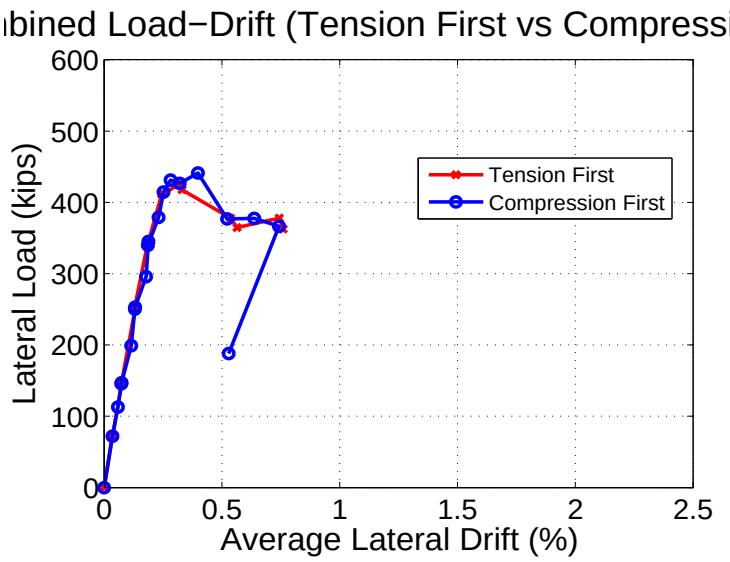

Figure D.10 Comparison of Load-Drift Envelope Methods - NCBF1

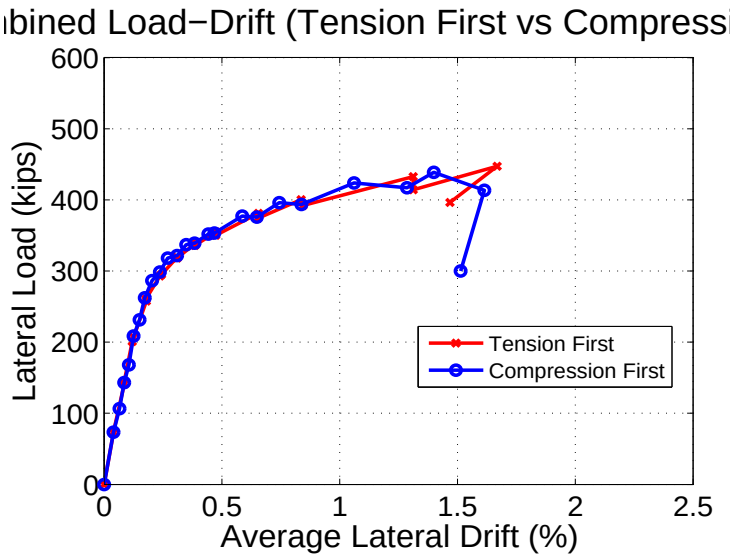

Figure D.11 Comparison of Load-Drift Envelope Methods - NCBF1-R2

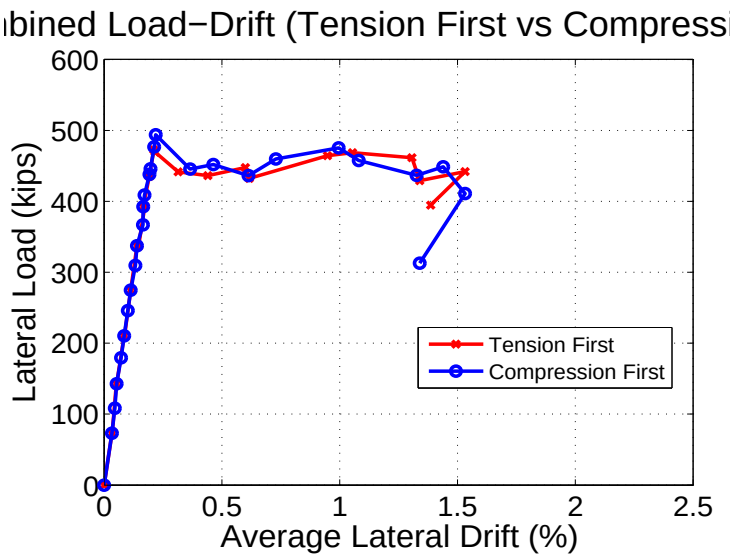

Figure D.12 Comparison of Load-Drift Envelope Methods - NCBF1-R3

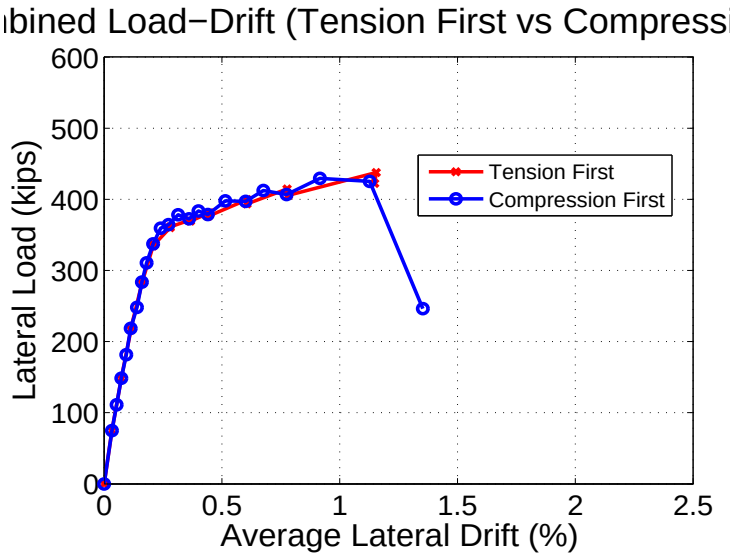

Figure D.13 Comparison of Load-Drift Envelope Methods - NCBF1-R4

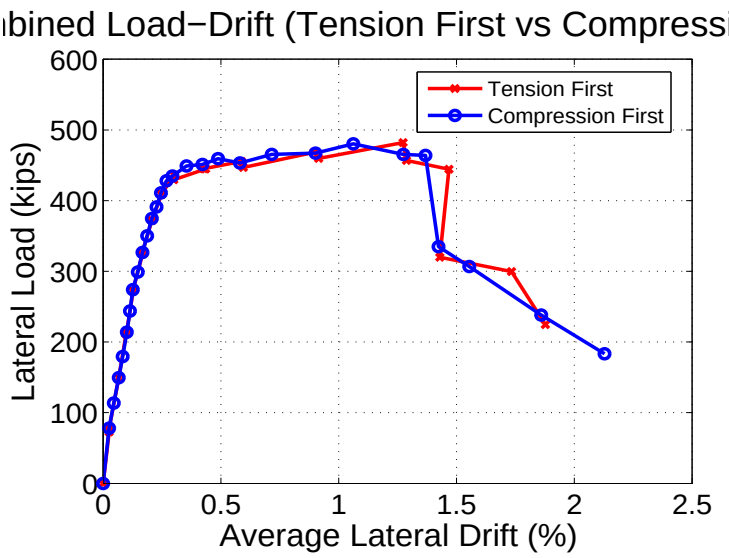

Figure D.14 Comparison of Load-Drift Envelope Methods - NCBF1-R5

D.4. Slip Losses

The lateral displacement measured using the frame diagonal elongation is typically substantially lower than the displacement applied by the actuator. This is largely a result of displacement losses within the system. Some of those losses were monitored during the tests.

The plots below show the total slip as a function of actuator load for each of the specimens. Note that for NCBF1, the North beam and actuator base measurements were not functional, so the actual losses were likely much greater. The losses at the channel assembly and reaction block base were typically negligible throughout the tests. The actuator base loses were highly load-proportional across all specimens. The slips at the North and South beams of the specimen (where load is transferred to and from the frame) were less predictable. Large slips occasionally occurred, likely due to exceeding the slip-critical load for some or all of the bolts. As a result, there are sometimes sudden jumps in the losses.

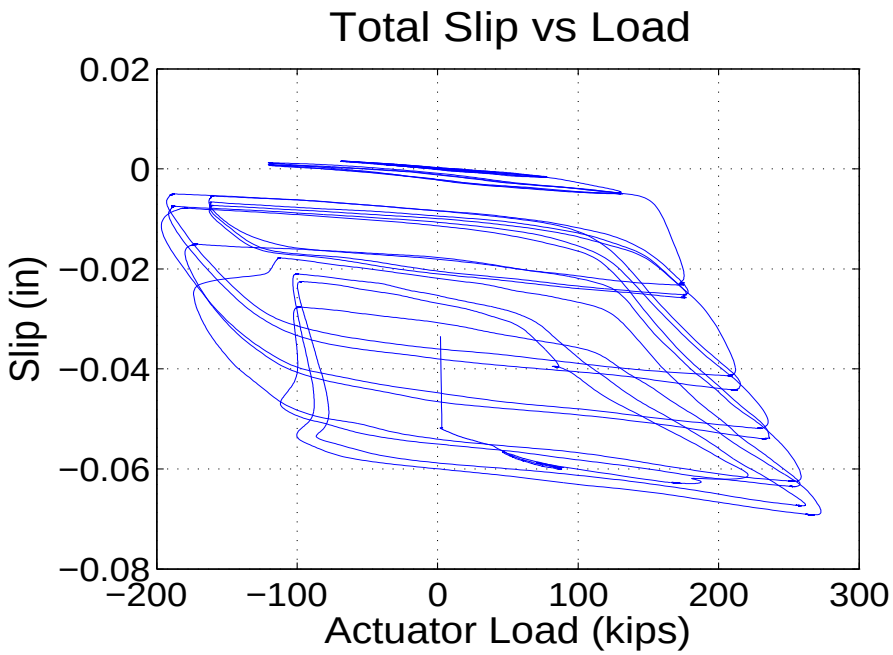

Figure D.14 Total Slip vs Load for NCBF1

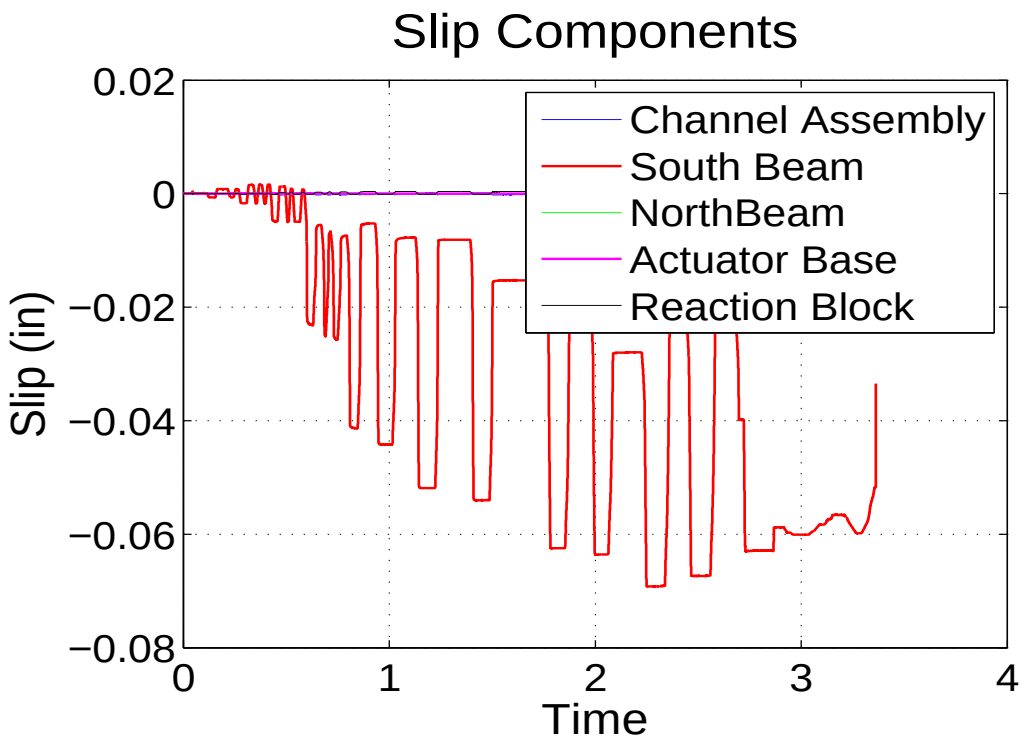

Figure D.15 Slip Components for NCBF1

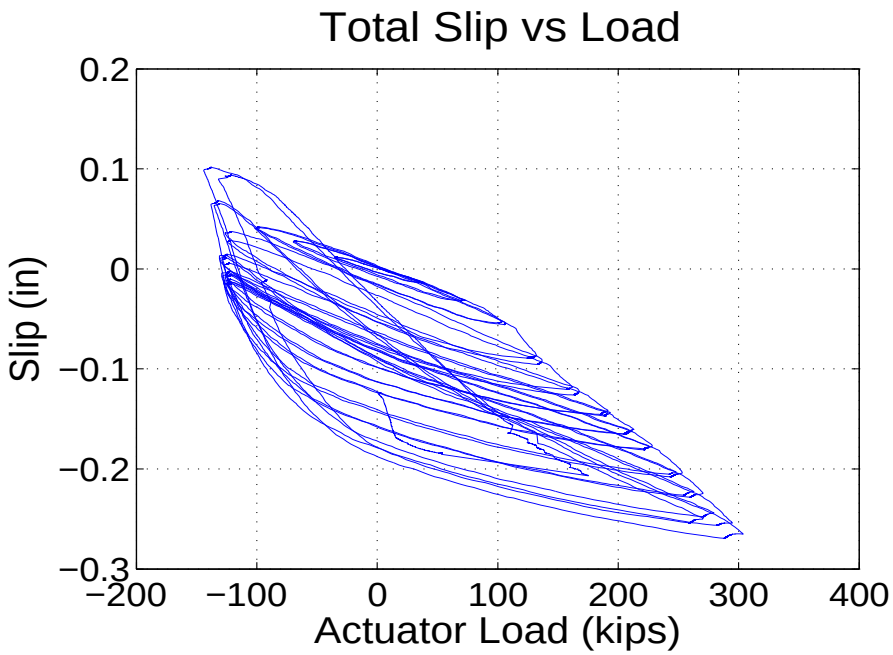

Figure D.16 Total Slip vs Load for NCBF1-R2

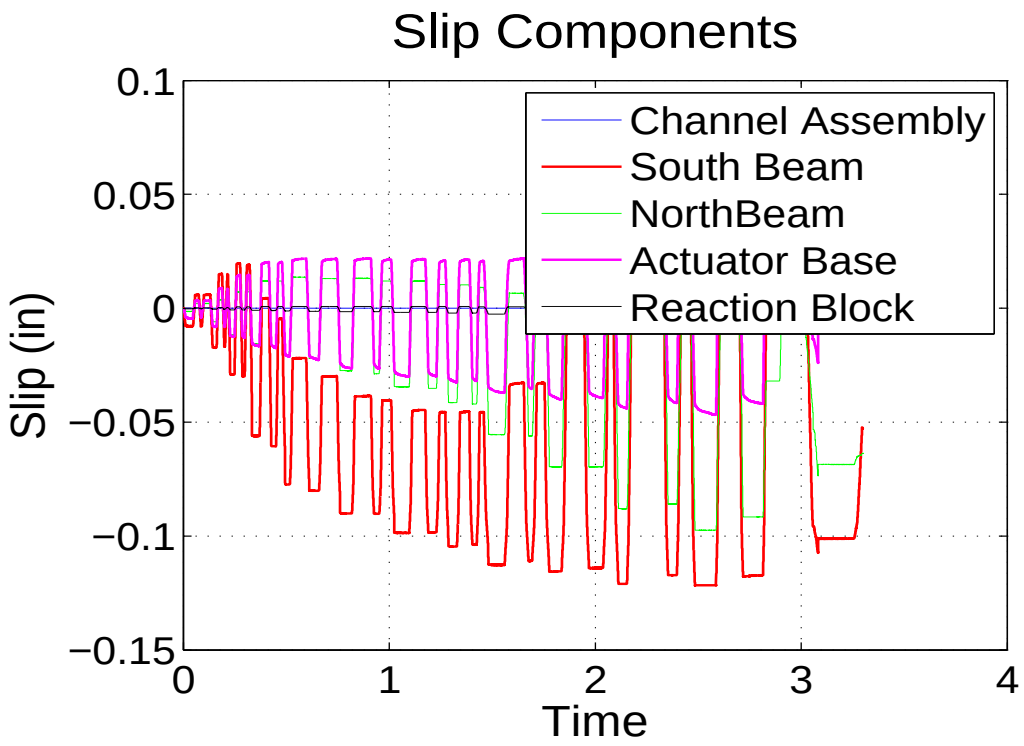

Figure D.17 Slip Components for NCBF1-R2

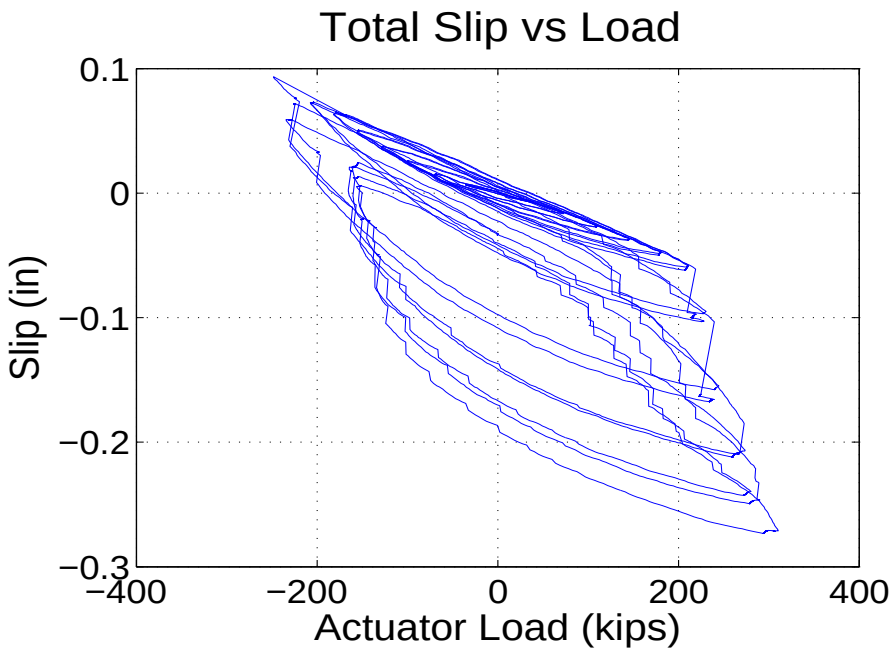

Figure D.18 Total Slip vs Load for NCBF1-R3

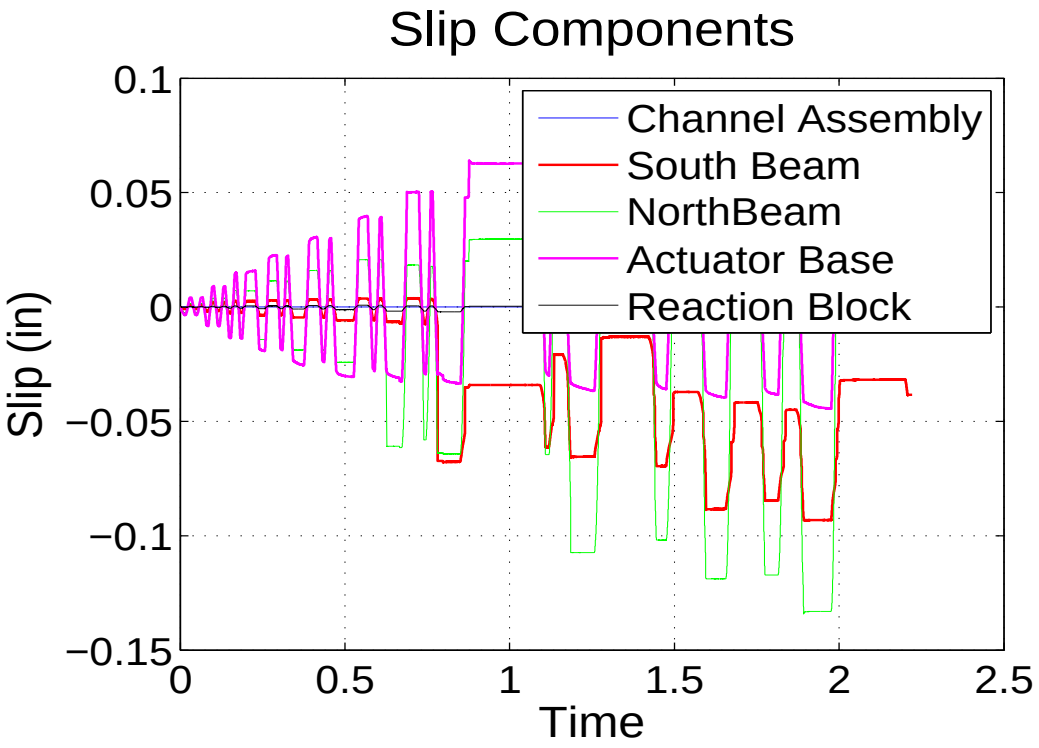

Figure D.19 Slip Components for NCBF1-R3

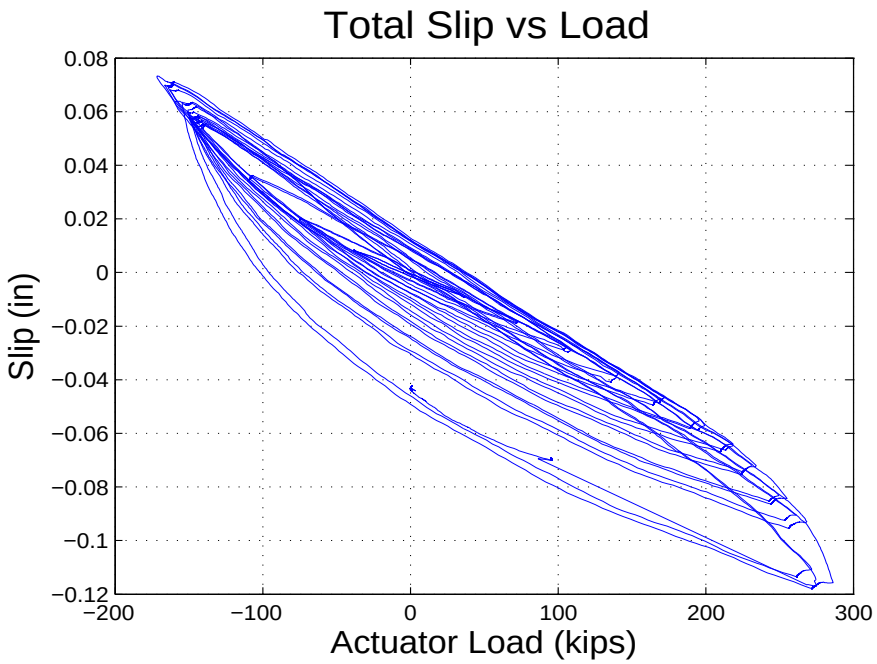

Figure D.20 Total Slip vs Load for NCBF1-R4

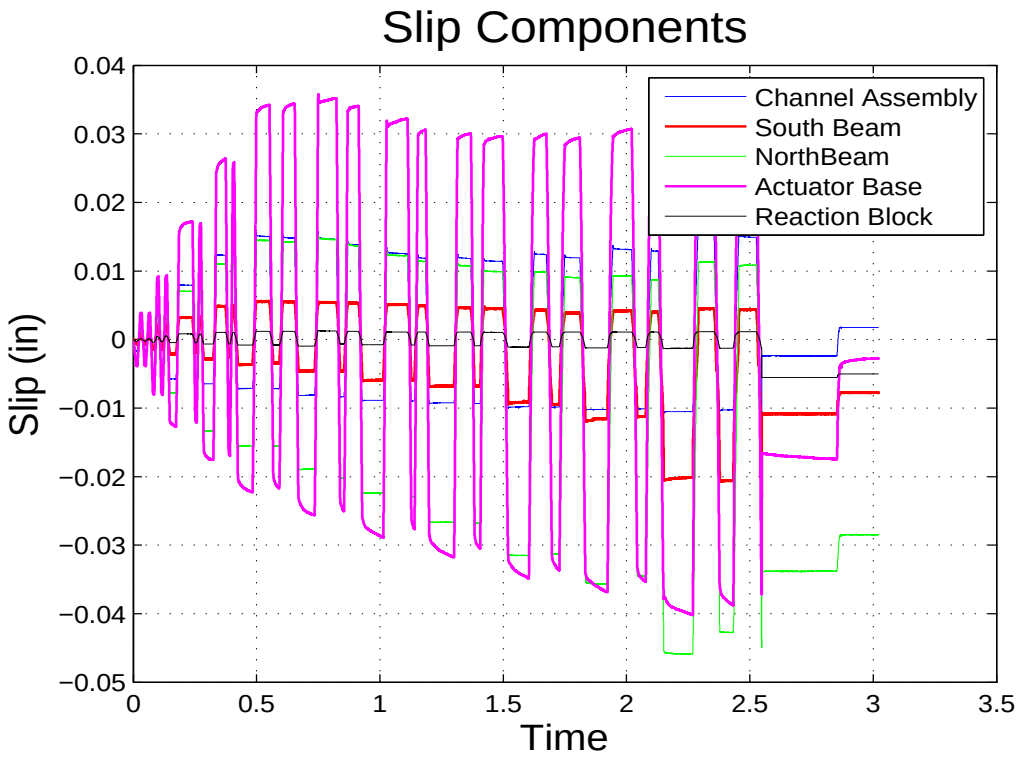

Figure D.21 Slip Components for NCBF1-R4

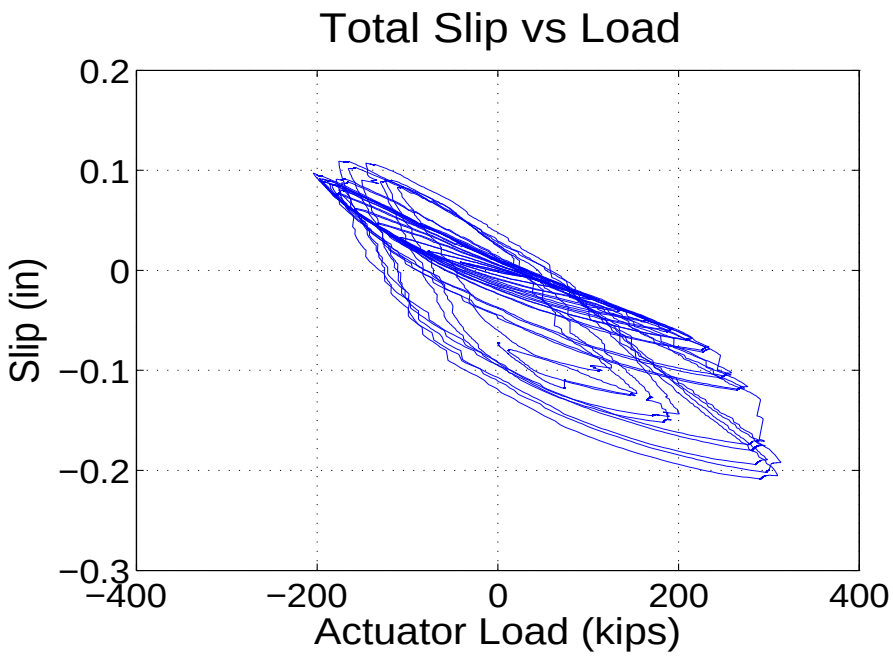

Figure D.22 Total Slip vs Load for NCBF1-R5

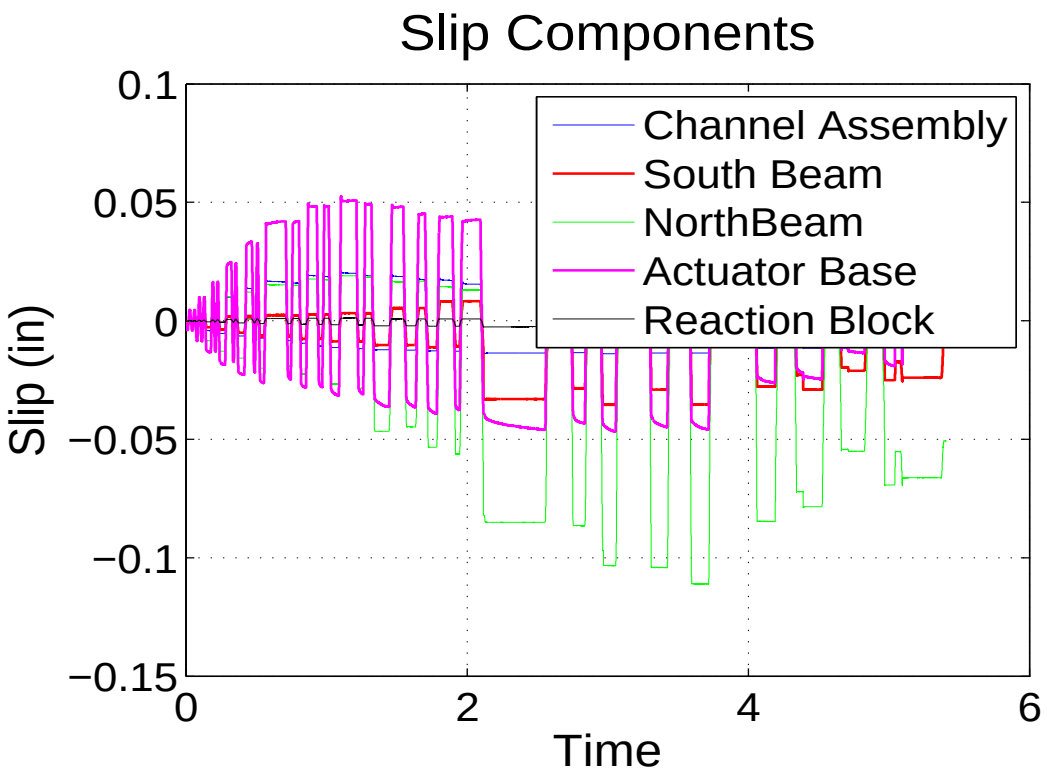

Figure D.23 Slip Components for NCBF1-R5

The figures below show the total eccentricity in the lateral drift for each specimen. Typically, drifts are larger in compression, as losses are somewhat proportional to load, and thus are larger in tension. Also shown are the maximum losses in each corresponding direction. The second plot has an "eccentricity" plotted. This is the "missing" tensile displacement required to make the hysteresis symmetric. This clearly demonstrates that the measured slip losses do not account for all of the eccentricity, though they do account for some of it. Other contributing factors include axial deformation within the test setup components, as well as column base uplift, and rotation of the towers holding the frame diagonal elongation potentiometer.

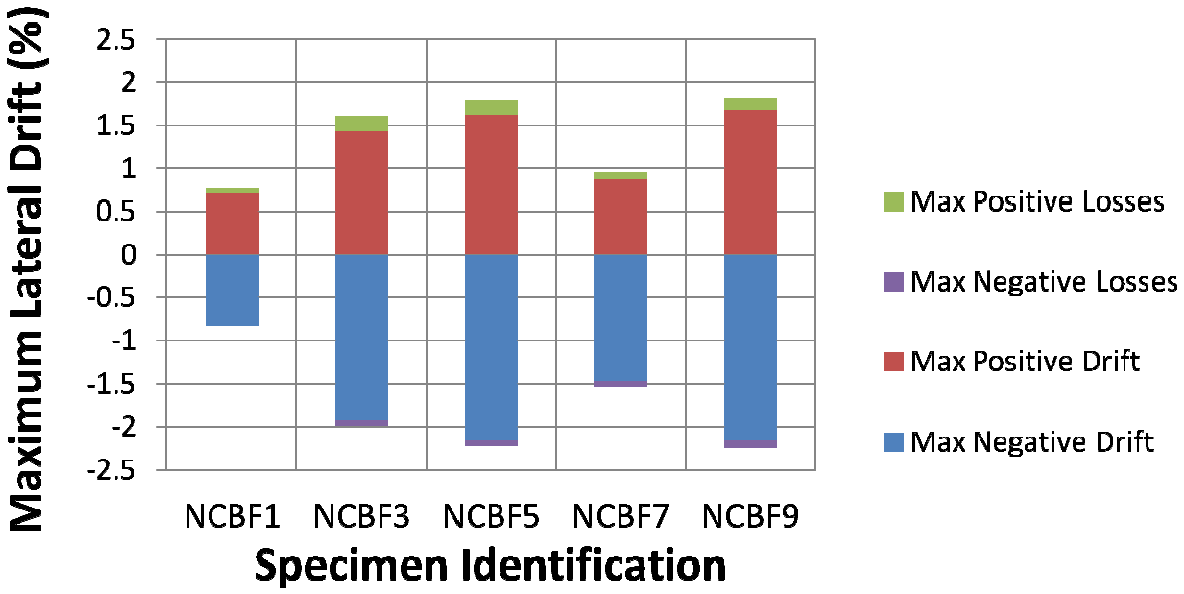

Figure D.24 Drift Eccentricity

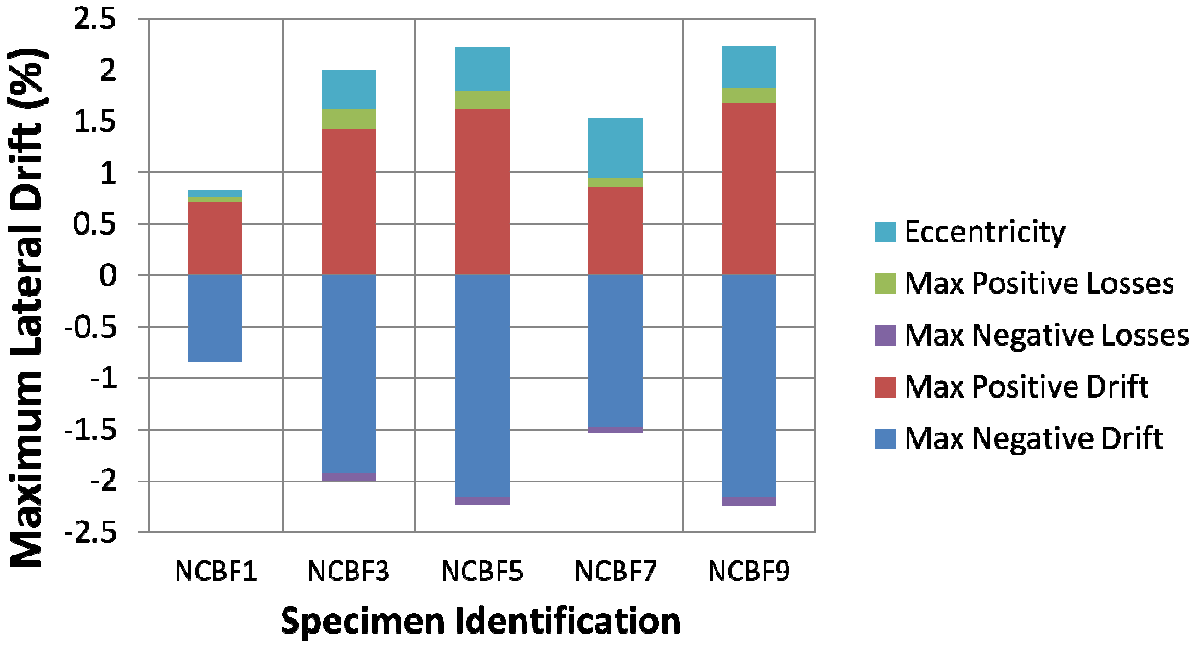

Figure D.25 Drift Eccentricity with all Losses

The plot below shows the drift eccentricity for each cycle of each test as a function of the load eccentricity for the corresponding cycle. Other than NCBF1-R2. which may have had instrumentation problems (as it was one of the first tests), there is a clear relationship between the load and displacement eccentricity. This appears to break down when connection damage starts to occur, particularly for NCBF1-R5.

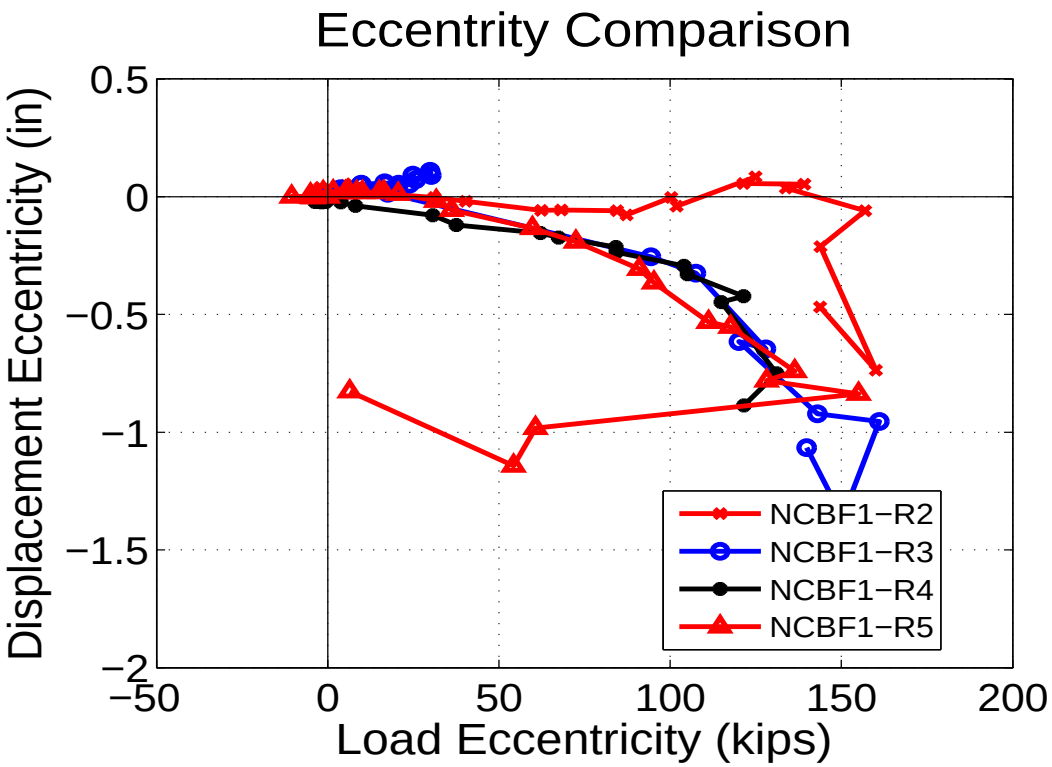

Figure D.23 Displacement Eccentricity for Each Cycle vs Load Eccentricity

References

1. AISC “Steel Construction Manual,” 14th Edition, American Institute of Steel Construction, Chicago, Illinois, 2010
2. AISC “Seismic Design Manual,” American Institute of Steel Construction, Chicago, Illinois, 2010
3. AISC “Seismic Provisions for Structural Steel Buildings,” American Institute of Steel Construction, Chicago, Illinois, 1997
4. Astaneh-Asl, A., "Seismic Behavior and Design of Gusset Plates," Steel TIPS, Structural Steel Educational Council, Moraga, California, December, 1998
5. Astaneh-Asl, A., Goel, S.C., and Hanson, R.D., “Cyclic Behavior of Double Angle Bracing Members with End Gusset Plates,” Research Report UMEE 82R7, Department of Civil Engineering, University of Michigan, Ann Arbor, Michigan, August, 1982
6. ATC 24, "Guidelines for Cyclic Seismic Testing of Components of Steel Structures," Applied Technology Council, 1992
7. Bjorhovde, R., Chakrabarti, S., "Tests of Full-Sized Gusset Plate Connections," Journal of Structural Engineering, ASCE, 111.3:667-684 (1985).
8. Fahnestock, L.A., Stoakes, C.D., “Cyclic Behavior and Perofrmance of Beam-Column Connections in Concentrically Braced Frames,” ASCE, Structures 2008: Crossing Borders, 2008
9. Herman, D.J., “Further Improvements on and Understanding of Special Concentrically Brace Frame Systems,” Department of Civil Engineering, University of Washington, Seattle, Washington, 2007
10. Hsiao, P., Lehman, D., Berman, D., Roeder, C., Powell, L., (2014). "Seismic Vulnerability of Older Braced Frames," Journal of Performance of Constructed Facilities 28, Special Section: Performance of Bridges under Critical Natural Hazards, 108-120.
11. Hsiao, P.C., “Simulation Methods for Special Concentrically Braced Frames”, General Examination, Department of Civil Engineering, University of Washington, Seattle, Washington, December 2009
12. ICBO "Uniform Building Code," International Conference of Building Officials, Whittier, CA, 1980.
13. ICBO "Uniform Building Code," International Conference of Building Officials, Whittier, CA, 1988.
14. ICBO "Uniform Building Code," International Conference of Building Officials, Whittier, CA, 1994.
15. Johnson, M. "Seismic Evaluation of Bolted Connections in Special and Non-Seismic Concentrically Braced Frames," Department of Civil Engineering, University of Washington, Seattle, Washington, 2014
16. Johnson, S.M., “Improved Seismic Performance of Special Concentrically Brace Frames,” Department of Civil Engineering, University of Washington, Seattle, WA, June 2005
17. Kotulka, BA. “Analysis for a design guide on gusset plates used in special concentrically braced frames.” Department of Civil Engineering, University of Washington, Seattle, WA, 2007
18. Liu, C., Goel, S.C., "Cyclic Load Behavior of Concrete-Filled Tubular Braces," Journal of Structural Engineering, American Society of Civil Engineers, 1988.114:1488-1506.

19. Lumpkin, E. "Enhanced Seismic Performance of Multi-Story Special Concentrically Braced Frames Using a Balanced Design Procedure," Department of Civil Engineering, University of Washington, Seattle, Washington, 2007
20. Powell, J.. "Evaluation of Special Concentrically Braced Frames for Improved Seismic Performance and Constructability," Department of Civil Engineering, University of Washington, Seattle, Washington, 2010
21. Rai, D.C., Goel, S.C., "Seismic Evaluation and Upgrading of Chevron Braced Frames," Journal of Constructional Steel Research, 59 (2003) 971-994.
22. Roeder, CW., Lumpkin, EJ., Lehman, DE., "A Balanced Design Procedure for Special Concentrically Braced Frame Connections," Journal of Constructional Steel Research, 67.11:1760-1772 (2011).
23. Segui, W.T., “Steel Design,” 4th Edition, Thomson Publishers, c2007
24. Sen, A.D., Sloat, D., Pan, L., Roeder, C.W., Lehman, D.E., and Berman, J.W. (2013). Evaluation of the Seismic Performance of Two-Story Concentrically Braced Frames with Weak Beams. *5th International Conference on Advances in Experimental Structural Engineering*. Taipei, Taiwan.
25. Shaback, B., Brown, T., "Behaviour of square hollow structural steel braces with end connections under reversed cyclic axial loading," Canadian Journal of Civil Engineering, v 30, n 4, p 745-753, August, 2003
26. Thornton, W.A., "Bracing Connections for Heavy Construction," Engineering Journal, AISC, Vol. 21, No. 3, pp. 139-148., 1984
27. Tremblay R., "Inelastic seismic response of steel bracing members," Journal of Constructional Steel Research, 58, 665-701, 2002
28. Whitmore, R.E., "Experimental Investigation of Stresses in Gusset Plates," Bulletin No. 16, Engineering Experiment Station, University of Tennessee, 1952
29. Zayas, VA., Popov, EP., Mahin, SA., "Cyclic Inelastic Buckling of Tubular Steel Braces," University of California Earthquake Engineering Research Center, 1980.